DATE DUE	DATE DUE	DATE DUE
OCT 0 9 2004		NOV 2 2 2004

MOLLING HEAT
IN F

MODELING HEAT TRANSFER FOR PARAMETER ESTIMATION IN FLASH DIFFUSIVTY EXPERIMENTS

By

Robert L. McMasters IV

A DISSERTATION

Submitted to

Michigan State University

in partial fulfillment of the requirements

for the degree of

DOCTOR OF PHILOSOPHY

Department of Mechanical Engineering

1997

MODELING HEAT
IN FL

Since the est
diffusivity measur
materials. Severa
been used in analy
levels of sophisti

This research
past beyond the
various heat tran
different assumpt
distribution insi
thermal conductio
assuming a semi-
An evaluation is
factors which may
is done in quanti
of the models in

Estimation of
developed as part
experimental data

ABSTRACT

MODELING HEAT TRANSFER FOR PARAMETER ESTIMATION IN FLASH DIFFUSIVTY EXPERIMENTS

By

Robert L. McMasters IV

Since the early 1960s, the laser flash method of diffusivity measurement has been used on a large variety of materials. Several parameter estimation methods have also been used in analyzing such experiments, employing various levels of sophistication.

This research investigates the penetration of the laser flash beyond the surface of the material being heated. Various heat transfer models are presented, each with different assumptions about the initial temperature distribution inside the material. Besides the mechanism of thermal conduction, radiation transport is also considered, assuming a semi-transparent emitting and scattering medium. An evaluation is made of the response of the methods to factors which may enter into the experimental process. This is done in quantitative terms so as to assess the adequacy of the models in comparison to one another.

Estimation of thermal parameters, using the models developed as part of this research, is performed on experimental data from 15 laboratories around the world,

involving a Vacuum

the experiments t

diffusivities var

terms.

When direct

parameters are use

ses in calculat

terms of regulari

theorem which imp

states method of

be otherwise obtai

implicitly in mat

involving a variety of materials. Ambient temperatures in the experiments range from 20°C to 2000°C and estimated diffusivities vary from 0.3 to nearly 80 square mm per second.

When direct solutions which have closely correlated parameters are used in parameter estimation, the equations used in calculating the parameters can be very unstable. A method of regularization is presented as part of this research which imparts stability to the ordinary least squares method of parameter estimation, where parameters may be otherwise unobtainable. This method is presented compactly in matrix format.

to the only God ...

who is, who was, and who is to come

The input

James Beck,

Norman Bell as

the special pr

communicable

scientific writ

The assis

laboratory pe

provided me wi

measurements

In order to fi

additional sam

Finally,

to my wife Mary

abbreviations w

program.

ACKNOWLEDGMENTS

The input and help of my Ph.D. guidance committee, James Beck, John Lloyd, Merle Potter, Indrek Wichman and Norman Bell is acknowledged. To my advisor James Beck, I owe special gratitude for helping me put my thoughts into communicable terminology so as to be presentable to the scientific world.

The assistance of the High Temperature Material Laboratory, part of the Oak Ridge National Laboratory, provided me with the opportunity to obtain most of the measurements utilized in this research. Special thanks are in order to Hsin Wang and Ralph Dinwiddie for the many additional samples they tested for me.

Finally, I owe thanks to my family for their support. To my wife MaryLynn, I am particularly grateful for her exhortations which initiated my application to the Ph.D. program.

TABLE OF CONTENTS

LIST OF TABLES

LIST OF FIGURES

Figure 4-12 V

Figure 4-13 V

Figure 4-14 V

Figure 4-15

Figure 4-16

Figure 4-17

a	Absor
b	Datum
B_i	Bott
c	Specif
e	Resid
$E_{x,x',t,t'}$	Co
f	Conver
$F_{t,\theta,\varepsilon}$	Radiat
G	Therma
G_1	Radiati
G_2	Radiati
h	Mean Fr
h_1	Spline
h_2	Spline
h_3	Composi
i	Number
j	Sample
$J_{\theta,\varphi}$	Phase F
k	Weighti
k_1	Magnitud
k_2	Square r
l	Internal

NOMENCLATURE

a	Absorption Coefficient
$\mathbf{b}$	Estimated Parameter Vector
Bi	Biot Number (hL/k)
c_p	Specific Heat
e_i	Residual
$G_{X33}(x,x',t,\tau)$	Green's Function for the X33 case
h	Convective Heat Transfer Coefficient
$I(\tau,\theta,\phi)$	Radiation Intensity
k	Thermal Conductivity
k_r	Radiative Conductivity
k_{ro}	Radiative Conductivity at Ambient Temperature
m	Mean Free Path of a Photon
m_i	Spline Conversion Coefficient
$\mathbf{M}_i$	Spline Conversion Coefficient Matrix
$\mathbf{M}_c$	Composite Spline Conversion Coefficient Matrix
n	Number of Measurements
L	Sample Thickness
$p(\theta,\phi)$	Phase Function
$p(I)$	Weighting Function for Mollification Method
q_o	Magnitude of the Laser Pulse (Joules per Square mm)
q_r	Internal Radiation Flux

$\mathbf{R}$	Pre-Conditioning Matrix
$S(\tau,\theta,\phi)$	Radiation Source Function
t	Time
t^*	Non-Dimensional Time ($\alpha t/L^2$)
$t_{1/2}$	Half-Rise Time
T	Temperature
$\mathbf{T}$	Calculated Temperature Vector
$\mathbf{T}^*$	Transformed Calculated Temperature Vector
T_∞	Experiment Ambient Absolute Temperature
T_∞^*	Non-Dimensional Absolute Temperature $T_\infty kL/q_o\alpha$
T_i	Temperature Calculated at node i
v	Variance
x	Spacial Dimension
X	Sensitivity Matrix
$\mathbf{X}^*$	Transformed Sensitivity Matrix
Y_i	Temperature Measured at Time Step i
$\underset{\sim}{Y}_i$	Spline Approximation of Temperature at Time Step i
$\mathbf{Y}$	Temperature Meaurement Vector
$\mathbf{Y}^*$	Transformed Temperature Meaurement Vector
α	Thermal Diffusivity
β	Parameter Vector - True but Unknown
β_m	Eigen Value
δ	Blurring Radius in Mollification Method
$\delta(t)$	Dirac Delta Function

ϵ	Emissivity
ϵ_i	Residuals $Y_i - T_i$
κ	Extinction Coefficient ($a + \sigma$)
μ	Cosine of ϕ
ρ	Density
σ	Scattering Coefficient
σ_b	Stefan-Boltzmann Constant (5.729×10^{-8} W/m^2K^4)
σ_r	Standard Deviation of Residuals
τ	Variable of Integration for Time in Convolution Integral
τ_L	Optical Thickness
ϕ	Polar Angle of Radiation
ψ	Constant Expressed as a Function of Albedo
θ	Azimuth Angle
Ω_o	Albedo (σ/κ)

CHAPTER 1

BACKGROUND

1.1 INTRODUCTION

Many new materials are being synthesized for various high temperature uses in the aerospace industry. Knowledge of the thermal diffusivity of these materials is extremely important in evaluating their appropriateness for particular applications. Because of the extreme high-temperature environments in which many of these materials are expected to perform, parameter estimation experiments must also be conducted at these temperatures in order to establish valid estimates of the thermal parameters of the materials in their intended working environments. At these extremely high temperatures, traditional methods of contact heating and temperature measurement become impossible. The flash method of diffusivity measurement has proven extremely useful for this application. The procedure for conducting flash diffusivity experiments is described in detail in Chapter 2.

Some of the objectives of the research conducted here are

1. To determine the thermal properties of the materials tested, specifically thermal diffusivity, from transient temperature measurements.

2. To investigate the possibility of internal radiation as an ancillary means of heat transfer to Fourier conduction and to investigate penetration of the laser flash beyond the surface of the specimen.

3. To investigate non-radiative effects which could be responsible for systematic disparities between measured data and the mathematical model.

The common underlying motivation behind each of the above objectives is to develop and utilize a heat transfer model for these experiments which will more accurately conform to the physical phenomenon observed, thereby giving greater confidence in the parameter values reported. In many cases, changing the mathematical model can change the estimated parameter values by as much as 20 percent. This in turn can have an impact in the design phase of the utilization of the material. For example, changes in the

properties of

to changes in

fuel require-

This chap

Section 1.1 as

and the direct

for refined mod

nitration for

derivative regi

radiation param

sensitivities of

1.6. Finally,

Section 1.7, brie

dissertation.

1.2 PREVIOUSLY PU

Prior to the

computers for use

methods were util

accurate computat

dissolvity measu

means by which di

principle of what

described in Part

properties of materials used in space vehicles can translate to changes in space vehicle weight, which in turn can affect fuel requirements and mission capability.

This chapter addresses Previously Used Methods in Section 1.2 as well as a brief description of the experiment and the direct problem solution in Section 1.3. The need for refined models is discussed in Section 1.4 which is the motivation for this research. Section 1.5 introduces derivative regularization as a tool necessary for extracting radiation parameters. Further work in exploring the sensitivities of the experiment are introduced in Section 1.6. Finally, the goal of the research is summarized in Section 1.7, including a summary of the remainder of the dissertation.

1.2 PREVIOUSLY USED METHODS

Prior to the widespread availability of high speed computers for use in parameter estimation, simplified methods were utilized to facilitate more rapid parameter estimate computation. When the procedure of laser flash diffusivity measurement was introduced in 1961, the primary means by which diffusivity was calculated involved the principle of "half rise time". This pioneering work is described in Parker et. al. [46]. Early models assumed a

pulse heat acc
insulated corr
rate in the per
$\sin\theta = \theta$ for
the non-dimens
measured surfa
half of its max
non-dimensional
relationship wa

where L is the s
corresponding to
half of the final

Numerous re
in the literature
accommodation for
surfaces. This
correction charts
temperature, maxi
emissivity. The
rise-time re
accounting for hea

pulse heat addition to the incident side of the sample, and insulated conditions otherwise. An additional assumption made in the development of this model is the approximation $\sin(\epsilon) = \epsilon$ for small values of ϵ. Using these assumptions, the non-dimensional time corresponding to the point where measured surface temperature on the non-heated side reaches half of its maximum, or equilibrium, temperature is 1.38 non-dimensional time units. Based on this correlation, the relationship was established

$$\alpha = \frac{1.38L^2}{\pi^2 t_{1/2}} \qquad (1\text{-}1)$$

where L is the sample thickness and $t_{1/2}$ is the time corresponding to that at which measured temperature reaches half of the final, or equilibrium, temperature.

Numerous revisions to this method have been presented in the literature in subsequent years. Cowan [43] provided accommodation for radiative heat losses from the sample surfaces. This modification required the analyst to enter correction charts with parameters such as ambient temperature, maximum sample temperature, and surface emissivity. The correction factors are then applied to the half-rise-time method described above. A similar method accounting for heat losses from the sample circumference is

emented by Cla

omparing this

Clark and Taylo

Later work

quares error a

loss coefficien

as performed b

onformance of

easured data.

athematical mod

surface heat los

This effect has

ncluding consid

nstantaneous.

n various experi

easured data and

Input from

ulated by the A

ASHV, as put forw

rovides a standa

eat loss factors

standardized meth

ise principle.

Further inve

examined by Clark and Taylor [44]. Several test cases comparing this method with the Cowan method are examined by Clark and Taylor as well.

Later work incorporated the minimization of least squares error as a means of estimating diffusivity and heat loss coefficient simultaneously. Early work in this area was performed by Koski [42] and includes discussion on the conformance of the mathematical model to the laboratory measured data. Taylor [47] also examines conformance of the mathematical model to the measured data for, not only surface heat loss, but for finite pulse length as well. This effect has to do with the time duration of the flash, including considerations for the flash being non-instantaneous. This paper by Taylor examines the residuals in various experiments, that is, the difference between the measured data and the mathematical model.

Input from many of the above contributions has been utilized by the American Society for Testing and Materials (ASTM) as put forth in 1992 [40]. This ASTM publication provides a standardized procedure for accounting for both heat loss factors and finite pulse duration factors. The standardized method is based on the time of half-temperature rise principle.

Further investigation into aspects of this experiment

is made by Bayl

of various mod-

amination of

estimates as we

are found is pr-

ecently, the ty

least squares ma

experiment by Be

advantage of al

various phenomena

parameters.

The standard

experiments note

the anticipated

unresolved inade

improvements have

simultaneous cal

characteristic s

experiments for s

iterated from in

decaying through

that predicted by

implies that anot

experiments, such

is made by Raynaud, et. al. [48] in regard to the adequacy of various models. This discussion not only includes an examination of the residuals, but of the sequential estimates as well. A discussion of how sequential estimates are found is presented in detail in Chapter 2. More recently, the method of non-linear regression using ordinary least squares has been applied to the flash diffusivity experiment by Beck and Dinwiddie [37]. This method has the advantage of allowing model flexibility to account for various phenomena by simultaneously calculating multiple parameters.

The standard deviation of the residuals in many of the experiments noted above is considerably higher than that of the anticipated measurement errors, pointing to some unresolved inadequacy in the models. Although large improvements have been made in model conformance through simultaneous calculation of heat loss and diffusivity, a characteristic signature is evident with the analysis of experiments for some materials. The shape of the signature generated from these models suggests that the "wave" of heat diffusing through the solid material arrives earlier than that predicted by conventional kinetic conduction. This implies that another mechanism is at work in these experiments, such as internal radiation or a penetration of

the laser flas

these phenomen

which consists

mechanisms at

1.3 [illegible]

Several re

order to deter

evaluate the re

primary method

standard deviati

deviation of the

important is the

the residuals,

the physical rea

A character

of continuous pos

behavior in the

with the measure

Another key indic

of the sequential

in detail in Chap

goals will be ex

characteristic sig

the laser flash beyond the surface of the material. Both of these phenomena are investigated as part of this research, which consists of a further examination of heat transfer mechanisms at work in various flash diffusivity experiments.

1.3 THE NEED FOR REFINED MODELS

Several means are used as part of this research in order to determine the adequacy of the models used and to evaluate the need for further refinement of the models. The primary method of evaluation is by comparison of the standard deviation of the residuals to the standard deviation of the expected measurement errors. Even more important is the emergence of a characteristic signature in the residuals, indicating that the model does not conform to the physical measurements.

A characteristic signature is exhibited by long periods of continuous positive or negative residuals. This type of behavior in the residuals can also be evidence of a problem with the measurements, specifically, correlated errors. Another key indication of model inadequacy is the stability of the sequential estimates. These phenomena are discussed in detail in Chapter 2. In the following chapters, various models will be examined in an effort to account for the characteristic signature in the residuals and the lack of

consistency in

1.1 DIRECT PRO

Typically,

experiments by

accomplished by

specifically in

shaped object in

the subsequent

following the

much larger than

it, heat losses

the temperature

of the disk from

In order to

experiment, a di

models were util

research. Later

early models at

The first a

through the samp

then experiments

temperatures, th

transparent to

consistency in the sequential parameter estimates.

1.4 DIRECT PROBLEM SOLUTION

Typically, specimen heating is accomplished in these experiments by laser flash. Temperature measurement is accomplished by infrared photometry. This research specifically investigates the heat transfer through a disk shaped object in one dimension from a flash heat source and the subsequent heat loss to the ambient surroundings following the flash. Since the diameter of the sample is much larger than the thickness, normally by a factor of 15-20, heat losses on the perimeter of the disk are neglected. The temperature measurements are made on the opposite side of the disk from the side exposed to the flash.

In order to estimate properties for a sample in an experiment, a direct solution must be obtained. Several models were utilized for direct solutions as part of this research. Later models are generally more rigorous than early models at the cost of increased complexity.

The first and most simple model assumes conduction through the sample and convection from the exposed surfaces. When experiments such as these are performed at very high temperatures, the materials may be likely to become more transparent to radiation of the frequencies emitted from

matter internally. Part of the objective of this research is to investigate the effects of combined conductive and radiative heat transfer inside the material. Several models are available to address this phenomenon. The most appropriate model for optically thick material utilizes a radiation coefficient which models the radiation as a diffusive phenomenon. This model is discussed in detail in Chapter 3. Other factors which are to be investigated include the penetration of the laser flash into the material at the instant the flash heating occurs. Additionally, there is an investigation into the reflection of the laser flash inside the furnace. These factors are discussed in detail in Chapter 4.

1.5 DERIVATIVE REGULARIZATION

When studying the subtle effect of a small contribution of heat transfer from a mechanism such as internal radiation, in addition to the dominant mechanism of conduction, the extraction of a parameter such as "radiative conductivity", becomes extremely difficult. This is because the sensitivity coefficients are closely correlated. When this occurs, the final set of equations used in solving for the parameters becomes nearly singular. Without being treated with some type of regularization or stabilizing

influence, the
solving simul
precision in p
measurement er
each iteration
increasingly wi
the development
parameters to c
assumptions as
is achieved by
first and secon
coefficients a
approximated b
respective curv
radiative con
model. This p

1.6 OPTIMIZ

Investig
calculations
an important
method of cal
as a parameter
measured at a

influence, the parameters cannot be found. Occasionally in solving singular sets of equations, the use of double precision in the computing method can improve results. With measurement errors in the data however, this is of no use; each iteration of the non-linear regression gives increasingly wild answers. A part of this research includes the development of a method of regularization which allows parameters to be calculated even with inaccurate initial assumptions as to the parameter values. The stabilization is achieved by incorporating information related to the first and second time-derivatives of the sensitivity coefficients and the measured data. The Derivatives are approximated by fitting parabolic splines through the respective curves. This method allows estimation of the "radiative conductivity" term in the internal radiation model. This procedure is explained in detail in Chapter 5.

1.6 OPTIMIZING THE ANALYSIS METHOD

Investigating methods which may simplify the calculations in this problem and provide better accuracy is an important part of this research. Variations of the method of calculation include the elimination of heat flux as a parameter by normalizing the solution to a temperature measured at a specific time in the experiment. Further

investigation
also made. Va
the establish
adequacy of va
undertaken to
calculating sen
parameters are
order to estab
dependence of
investigation
Chapter 6.

1.7 RESEARCH

The main
measure of con
diffusivity e
investigated
with the expe
of investigat
values can h
effectiveness
intended for

As an
Chapter 2 c

investigation into the optimum duration of the experiment is also made. Various criteria are investigated pursuant to the establishment of a systematic way of evaluating the adequacy of various competing models. An analysis is undertaken to determine the validity of the method used in calculating sensitivity coefficients. Finally, the parameters are estimated over sequential experiments in order to establish the functional form of the temperature dependence of the parameters. The results of the investigation into these issues is presented in detail in Chapter 6.

1.7 RESEARCH GOAL AND DISSERTATION OUTLINE

The main goal of the research is to obtain a greater measure of confidence in the results of the flash diffusivity experiments. Various physical phenomena are investigated as possible causes for model non-compatibility with the experimental measurements. This is a critical area of investigation since small changes in estimated parameter values can have a large impact on the cost and ultimate effectiveness of the devices in which the material is intended for use.

As an outline of the remainder of the dissertation, Chapter 2 describes the fundamentals of the experiment and

aspects of par

solving for p

internal radia

rock material

com simulated

are described

instantaneous p

the time of rea

replication

examining the

aspects of sens

presented in Ch

Chapter 7.

aspects of parameter estimation for a three-parameter model, solving for diffusivity, heat flux and Biot Number. Internal radiation as a diffusive mechanism for optically thick materials is discussed in Chapter 3 with analysis of both simulated and real measurements. Non-radiative models are described in Chapter 4, involving an effectively instantaneous penetration of the flash into the material at the time of heating. The concept of derivative regularization is discussed in detail in Chapter 5, examining the benefits and costs of the method. Various aspects of sensitivity analysis and method refinements are presented in Chapter 6 and the work is summarized in Chapter 7.

FLA

2.1 INTRODUCTI

The histo
diffusivity me
ume of the fi
since the proc
development, t
measurement ma
laboratories a

A sample
this area is a
investigation
tungsten and r
This type of m
industry. Thi
Reference [52]
transparent ma
tick. This wo
contribution s
an extrapolate
superposed o

CHAPTER 2

FLASH MEASUREMENT OF DIFFUSIVITY

2.1 INTRODUCTION

The historical discussion of the flash method of diffusivity measurement, featured in Chapter 1, highlights some of the milestones and significant refinements made since the procedure originated. During the course of this development, the flash method of thermal diffusivity measurement has been used many times in dozens of laboratories around the world.

A sample list of countries having made contributions in this area is as follows: Reference [54] presents an investigation of the thermal diffusivity of thin coatings of tungsten and molybdenum which are applied by plasma spray. This type of material application is in use in the nuclear industry. This work was performed by Canadian researchers. Reference [52] discusses experimental measurements of semi-transparent materials in the temperature range of 300 to 800K. This work was performed by researchers in France. A contribution from Germany was made in reference [36] where an extrapolated radiation heat transfer solution was superimposed on a kinetic conduction solution in order to

obtain more ac

climate. A c

reference pa

measurements

packaging sub

reference [10]

papers used

examines meas

layers. Pea

researchers

on dielectri

characteris

damage from

measurement

the USA.

measuremen

flash by t

The

non-contact

Contact t

solids

from sili

consistent

Researcher

obtain more accurate estimates of the thermal diffusivity of alumina. A contribution from Ireland is presented in reference [57] which explores thermal diffusivity measurements taken on alumina based ceramics used as packaging substrates. A contribution from Japan in reference [53] discusses measurements taken on casting powders used in the steel making industry. This method examines measurements of material consisting of multiple layers. Reference [56] is a paper written by Scottish researchers regarding flash diffusivity measurements taken on dielectric crystals which exhibit non-linear optical characteristics. The work specifically looks into crystal damage from absorbed laser radiation as a result of the measurement process. Many contributions have been made by the USA. Reference [40] presents a standardized method for measurement and calculation of thermal diffusivity by laser flash by the American Society for Testing and Materials.

The flash method of diffusivity measurement employs non-contact sample heating and temperature measurement. Contact methods of heating and temperature measurement of solids typically produce non-uniformities which come about from such factors as imperfect contact, serpentine heater construction and the additional thermal mass inherent in the heaters, thermocouples, adhesives and lubricants. The

effect of the

samples of pr

advantages of

nature of the

non-uniformit

This in turn

enclosures to

also allows t

changed quick

performed at

short amount

extreme high

nature of th

need be no c

measuring eq

environments

duration of

experiments

Once t

solution m

the parame

the dimens

coordinate

the sample

effect of these factors can be minimized by employing samples of physically large size. One of the prime advantages of the laser flash method is that the non-contact nature of the heating and temperature measurement eliminates non-uniformities which allows the use of small samples. This in turn allows small furnaces and other sample enclosures to be employed. The small size of the samples also allows the ambient temperature of the experiment to be changed quickly, so that successive experiments may be performed at varying ambient temperatures over a relatively short amount of time. The flash method can also be used in extreme high-temperature environments due to the non-contact nature of the heating and temperature measurement. There need be no concern for the degradation of the heating and measuring equipment from exposure to high-temperature environments. The small sample size typically allows the duration of the experiments to be quite short, with most experiments lasting less than one minute.

Once laboratory measurements have been taken, a direct solution must be computed for the problem in order to obtain the parameters. The model utilized in this chapter assumes one dimensional Fourier conduction in a rectangular coordinate system with convective heat loss on both sides of the sample, each side having the same heat transfer

coefficient.

with the thi

the sample a

Section

of samples

instrument

computation

2.4, assum

correction.

provided in

aspects of t

inadequacies

2.7, demonst

sophisticate

2.2 DESCRIPT

Data fr

analyzed as

the experimen

disk shaped s

thermal diffu

approximately

surfaces of

from near zer

coefficient. Due to the large sample diameter in comparison with the thickness, heat losses from the perimeter edge of the sample are neglected.

Section 2.2 provides a brief description of the types of samples used as part of this research. The measurement instrument used is described in Section 2.3. The Computation of the direct solution is presented in Section 2.4, assuming simple one dimensional conduction and convection. A finite difference version of this solution is provided in Section 2.5 with the parameter estimation aspects of the problem discussed in Section 2.6. The inadequacies of this simple model are discussed in Section 2.7, demonstrating a need for further research into more sophisticated modeling techniques.

2.2 DESCRIPTION OF SAMPLES

Data from fifteen laboratories around the world were analyzed as part of this research. Ambient temperatures for the experiments performed ranged from 20°C to 2000°C. The disk shaped samples ranged from 1mm to 18mm in thickness. Thermal diffusivity estimated from the data ranged from approximately 0.3 to 80 mm^2/sec. Heat loss from the surfaces of the samples following the pulse heating ranged from near zero to a Biot number of approximately 10.

The primary area of study for this research is centered on the Carbon Bonded Carbon Fiber (CBCF) material developed at Oak Ridge National Laboratory. This material is primarily intended as insulation for objects exposed to atmosphere re-entry conditions in space applications. The material is manufactured by Oak Ridge National Laboratory. CBCF insulation is vacuum molded from a slurry of chopped amorphous carbon fibers in a mixture of water and phenolic resin. The material is then dried and the resin, which accumulates where the fibers touch, is carbonized. This process results in an open structure where both the density of the solid fibers and the overall porosity are continuous throughout the material. One specific use of the material is as an insulator in radioisotope thermoelectric generators such as the General Purpose Heat Source used to supply power to deep space probes like Galileo.

2.3 ASPECTS OF MEASUREMENT

Since the flash method of thermal diffusivity measurement has been in use for several decades, equipment designed for conducting flash diffusivity experiments is available for purchase in the form of pre-manufactured systems. Two companies which sell such equipment are

Holometrix Inc.
25 Wiggins Ave.
Bedford, Mass. 01730-2323
(800) 688-6738

Anter Corp.
1700 Universal Rd., Dept. 10
Pittsburgh Pa. 15235-3998
(412) 795-6410
www.anter.com

Measurements were made as part of this research by equipment made from both these manufacturers. A majority of the sample measurements, however, were made using the Anter system at Oak Ridge National Laboratory. A schematic diagram of this system is shown in Figure 2-1. In this system, the sample is held horizontally and the laser flash is introduced vertically, incident on the top of the sample.

Figure 2-2 is a photograph of the Anter system at Oak Ridge National Laboratory. This system happens to be configured for four modules, but the systems are available with as few as one module, depending on the range of intended temperature applications. The four modules provided in the Oak Ridge machine include a low temperature aluminum block furnace for temperatures from -150°C to 500°C, a room temperature to 1700°C furnace, a 500°C to 2500°C graphite furnace and a room temperature to 1200°C quench furnace. The quench furnace is cooled by a blast of helium gas once the heat source is turned off. The

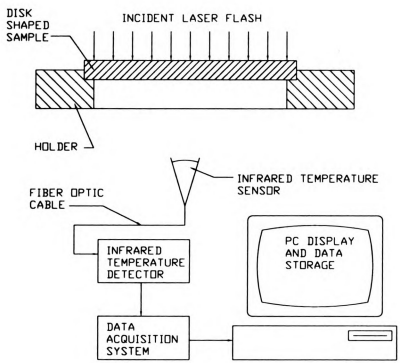

Figure 2-1 Schematic Diagram of a Typical Flash Diffusivity Measurement System

Figure 2-2 Photograph of the Anter System at the Oak Ridge National Laboratory

quenching pro

temperature c

Samples

are typically

furnace over

laser flash

passes throu

In order to

the laser fla

provide ever

of 35 double

established

Subsequent

through a tr

computer co

The

is also pr

takes read

window at

passed thr

unit. The

allows seve

temperature

additionall

quenching process is capable of reducing the sample temperature by approximately 200°C per second.

Samples held at high ambient temperatures in a furnace are typically in a vacuum or an inert gas in order to minimize chemical interaction with the surroundings. The laser flash is generated on the outside of the furnace and passes through a spectrally neutral neodymium-glass window in order to reach the sample. Since the sample is small, the laser flash is able to cover the entire surface to promote even heating. The laser has a maximum pulse energy of 35 joules. This pulse magnitude is adjustable and is established based on an initial operator-assigned maximum. Subsequent laser flashes for a given experiment are adjusted through a trial and error process, facilitated by the computer control system, after the initial flash.

The infrared temperature sensor used in the experiment is also physically located outside the sample furnace and takes readings through a spectrally non-interactive glass window at the bottom of the furnace. The measured signal is passed through a fiber optic cable to the actual detector unit. The detector unit includes a pre-amplifier, which allows several furnaces to be served by the same infrared temperature detector without moving the detector itself. Additionally, the sensitive electronic components of the

detector are p

fumace by the

ses two detec

temperature ap

ambient detec

The detec

at different te

a look-up table

intensity vers

stored in Read-

controller unit

actual practice

various values

calibration.

The outp

terms of volts

temperature.

ted for each

signal record

expression of

above ambient

The temp

letter in big

distinctive

detector are protected from the high temperatures of the furnace by the physical separation. The Oak Ridge machine uses two detectors: a silicon photodiode detector for high temperature applications and cryogenically cooled Indium-Antimony detector for low temperature applications.

The detector is calibrated using simulated black bodies at different temperatures. From this calibration procedure, a look-up table is generated which provides a mapping of intensity versus radiation wavelength. The lookup table is stored in Read-Only-Memory (ROM) in the detector's controller unit. Measurements taken using the instrument in actual practice are arrived at by interpolation of the various values which are stored in the lookup table during calibration.

The output of the detector is usually expressed in terms of volts, which are directly proportional to temperature. The detector is normally calibrated to read zero for each experiment at furnace temperature. The final signal recorded in the data acquisition equipment is an expression of a signal proportional to temperature rise above ambient temperature.

The temperature measuring instruments tend to perform better in higher temperature experiments due to the more distinctive spectral signal emitted at high temperatures.

An additional

that liquid n

environment f

minimize back

measurement p

the backgrou

below 600 deg

temperature.

2.1 DIRECT S

The Acte

provides time

self-rise tim

automatically

the methods o

[44], Koski

this informat

the informati

The resu

based on non-

[50]. This r

solution. Th

kinetic condi

solved analyt

An additional requirement for low temperature experiments is that liquid nitrogen must be used to provide a cryogenic environment for the detector. This is necessary so as to minimize background radiation not related to the temperature measurement of the sample. In spite of this precaution, more background noise typically exists in measurements taken below 600 degrees centigrade than is exhibited above that temperature.

2.4 DIRECT SOLUTION COMPUTATION

The Anter system described in the previous section provides immediate analysis of diffusivity by evaluating the half-rise time as described previously. The system automatically computes several diffusivities, each based on the methods of Parker [46], Cowan [43], Clark and Taylor [44], Koski [42], and Heckman [59]. The computer displays this information in tabular form and automatically stores the information in an individual file for each experiment.

The method of analysis used in the present research is based on non-linear regression, as described in reference [25]. This method requires the formulation of a direct solution. The most basic model, which assumes conventional kinetic conduction of heat through the material, can be solved analytically. In order to accomplish this, the

Green's func

dimensional

with convect

reference (s

conductivity

dimensional

The boundary

$$-q\frac{\partial}{\partial}$$

In these equ

heat, T is t

conductivity

typically ex

delta Dirac

is the sampl

ation to the

assured to

function. So

Green's function is used for the X33 case, that is one dimensional conduction in the Cartesian coordinate system with convection at both boundaries, as put forth in reference [51]. Assuming no internal radiation and constant conductivity with respect to temperature, the one dimensional differential equation for this problem is

$$\rho c_p \frac{\partial T}{\partial t} = k \frac{\partial^2 T}{\partial x^2} \tag{2-1}$$

The boundary conditions are

$$-k\left[\frac{\partial T}{\partial x}\right]_{x=0} = q_0 \delta(t) + h(T_\infty - T_{x=0}) \tag{2-2}$$

$$-k\left[\frac{\partial T}{\partial x}\right]_{x=L} = h(T_{x=L} - T_\infty) \tag{2-3}$$

In these equations, ρ is the density, c_p is the specific heat, T is temperature, t is time, k is thermal conductivity, q_0 is the magnitude of the heat pulse, typically expressed in joules per square mm, $\delta(t)$ is the Delta Dirac function, h is the heat transfer coefficient, L is the sample thickness and x is the spacial dimension. Prior to the initiation of the flash at t=0, the sample is assumed to be at ambient temperature, T_∞. The Green's Function Solution Equation given in reference [51] is

$$T(x,t) = T_0 +$$

where the dre

$$\beta_m(x) = \alpha_m x \quad \alpha, \beta$$

where

$$A_n = \frac{2}{}$$

$$B_n(x) = \beta_n$$

In these equa

the right and

Since the temp

diffusivity e

temperature r

it is convenie

bare medium e

approximately

Set $B_i = Bi_1$. T

$$T(x,t) = \frac{qg_0}{\kappa} \int$$

$$T(x,t)=T_\infty+\frac{\alpha}{k}\int_{\tau=0}^{t} G_{X33}(x,x'|t,\tau)\,q_0\delta(\tau)\,d\tau \qquad (2\text{-}4)$$

where the Green's function for X33 is given as

$$G_{X33}(x,x'|t,\tau)=\frac{2}{L}\sum_{m=1}^{\infty} e^{-\beta_m^2\alpha(t-\tau)/L^2}\,A_m(x)\;\eta_m(x') \qquad (2\text{-}5)$$

where

$$A_m(x)=\frac{\beta_m\cos(\beta_m\frac{x}{L})+Bi_1\sin(\beta_m\frac{x}{L})}{(\beta_m^2+Bi_1^2)\left[1+\frac{Bi_2}{\beta_m^2+Bi_2^2}\right]+Bi_1} \qquad (2\text{-}6)$$

$$\eta_m(x')=\beta_m\cos(\beta_m\frac{x'}{L})+Bi_1\sin(\beta_m\frac{x'}{L}) \qquad (2\text{-}7)$$

In these equations, Bi_1 and Bi_2 refer to the Biot numbers on the right and left hand sides of the specimen, respectively. Since the temperature measuring instrument used in the flash diffusivity experiments reports voltage proportional to temperature rise above the experimental ambient temperature, it is convenient to set $T_\infty=0$ in the solution. Since the same medium exists on both sides of the sample at approximately the same temperature, it is also reasonable to set $Bi_1=Bi_2$. The solution now becomes

$$T(L,t)=\frac{\alpha q_0}{k}\int_{\tau=0}^{t}\frac{2}{L}\sum_{m=1}^{\infty} e^{-\beta_m^2\alpha(t-\tau)/L^2}\;A_m\;\delta(\tau)\,d\tau \qquad (2\text{-}8)$$

rate

$$A_n = \frac{2}{\pi}$$

Integrating

$$T = L, \quad$$

In order to

equation

A rapid pr

method, wh

equation,

equation,

$$f = 3$$

Using this

the case o

than 6 dig

method pro

zero to ap

where

$$A_m = \frac{\beta_m [\beta_m \cos(\beta_m) + Bi \sin(\beta_m)]}{\beta_m^2 + Bi^2 + 2Bi} \qquad (2\text{-}9)$$

Integrating and non-dimensionalizing, we have

$$T^*(L,t) = \frac{T(L,t)kL}{\alpha q_0} = 2\sum_{m=1}^{\infty} e^{-\beta_m^2 \alpha t / L^2} A_m \qquad (2\text{-}10)$$

In order to compute the eigenvalues, the following eigen condition must be satisfied

$$\tan(\beta_m) = \frac{2\beta_m Bi}{\beta_m^2 - Bi^2} \qquad (2\text{-}11)$$

A rapid procedure for computing eigenvalues is Newton's method, which involves finding the roots of the following equation, which is simply a re-arrangement of the above equation, expressed as a function set equal to zero.

$$f(\beta_m) = \tan(\beta_m)(\beta_m^2 - Bi^2) - 2\beta_m Bi = 0 \qquad (2\text{-}12)$$

Using this method, an initial guess is made for β_m which, in the case of this research, was 2.5 for Biot numbers less than 6 and 3.5 for Biot numbers of 6 and greater. This method proved effective for Biot numbers ranging from near zero to approximately 30, well above any experimentally

observed val

A more re

equivalue ap

Both numbers

be used

$$\beta_1 = \frac{1}{}$$

where

f Bi =

For cases wh

following re

$$\beta_1 =$$

For values o

approximatio

As a more ge

for this pro

part of this

observed values.

A more refined method for arriving at an initial eigenvalue approximation is given in reference [51]. For Biot numbers less than 1.0, the following approximation may be used

$$\beta_1 \approx \left[\frac{-45-30Bi+[f(Bi)]^{1/2}}{4Bi} \right]^{1/2} \tag{2-13}$$

where

$$f(Bi)=225(3+2Bi)^2+360Bi(Bi^2+2Bi) \tag{2-14}$$

For cases where Biot number is between 1 and 4.85 the following relation may be used

$$\beta_1 \approx \frac{\frac{\pi}{2}+\left[\left(\frac{\pi}{2}\right)^{1/2}+(2Bi+1)\right]^{1/2}}{\frac{(2Bi+1)}{Bi}} \tag{2-15}$$

For values of Biot number greater than 4.85, the following approximation may be used

$$\beta_1 \approx \frac{Bi\pi}{2+Bi} \tag{2-16}$$

As a more general approximation of the initial eigenvalue for this problem, the following relation was arrived at as part of this research

The above exp

nigher with a

against the c

the residuals

using this re

This graph sh

using this re

combination

an equation o

eigenvalue eq

exponent in t

research by c

similar to th

conduction eq

After co

eigenvalue, s

period by add

$\Delta 3 = \frac{1}{}$

$$\beta_1 = \frac{\pi}{\left[1+\left(\frac{\pi}{\sqrt{2Bi}}\right)^{2.151}\right]^{1/2.151}} \qquad (2\text{-}17)$$

The above expression is valid for Biot Numbers from 0.2 and higher with an error of less than one percent when compared against the converged value. Figure 2-3 shows a graph of the residuals of the approximate eigenvalues arrived at using this method compared to the true converged values. This graph shows the very close approximations achieved using this method. Equation 2-17 was developed as a continuation of work initiated by Yovanovich [61] who used an equation of the same form for computing the first eigenvalue for the X23 case. The constant 2.151 in the exponent in this equation was arrived at as part of this research by ordinary least squares parameter estimation, similar to that used in estimating parameters in the heat conduction equations.

After computing the first approximation of the first eigenvalue, subsequent iterations are made using the Newton method by adding a correction value, $\Delta\beta$, computed as follows

$$\Delta\beta = \frac{-f(\beta)}{f'(\beta)} = \frac{-\tan(\beta)+\frac{Bi}{\beta^2}}{\frac{1}{\cos^2(\beta)}+\frac{Bi}{\beta}} \qquad (2\text{-}18)$$

Figur

With the LSL te
be calculated a

where the i sup
convergence.
research, eigen
figures.

Once the s
satisfactory de
subsequent eige
the previously

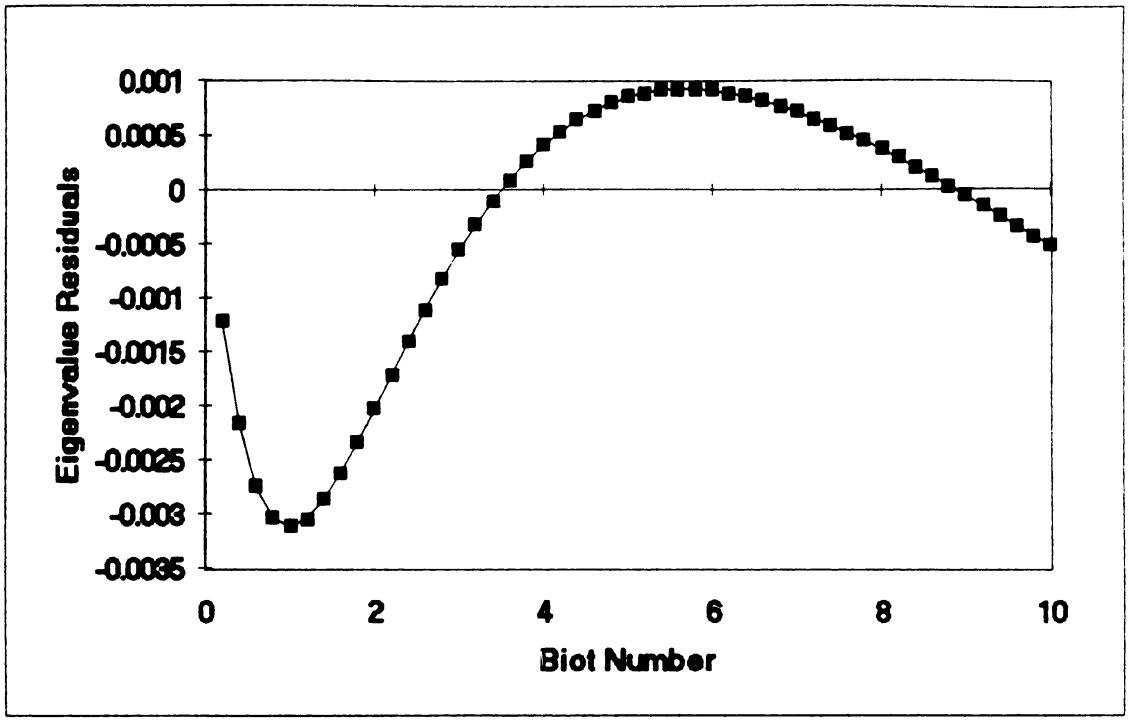

Figure 2-3 Eigenvalue Residuals as a Function of Biot Number for the X33 Case

With the $\Delta\beta_m$ term calculated, a revised value for the β_m can be calculated as follows

$$\beta_m^{i+1}=\Delta\beta_m+\beta_m^i \qquad (2\text{-}19)$$

where the *i* superscript designates the iteration from 1 to convergence. For the work conducted as part of this research, eigenvalues were computed to six significant figures.

Once the first eigenvalue has been computed to a satisfactory degree of accuracy, the initial value for subsequent eigenvalues is normally obtained by adding π to the previously calculated eigenvalue. Newton's method is

applied stat

for a rate p

eigenvalues,

(31) for sma

and for large

$$\beta_n \sim n\pi + \cdots$$

where

$$\beta_n = \left[\cdots \right.$$

and β' is a

The n

convergence

varies depe

thickness a

in the exper

solution wh

exponential

significant

applied again in each case until convergence is obtained. For a more refined initial estimate of subsequent eigenvalues, the following equation is provided in reference [51] for small Biot numbers

$$\beta_m \approx (m-1)\pi + \frac{2Bi}{(m-1)\pi} \tag{2-20}$$

and for large Biot numbers

$$\beta_m \approx (m-1)\pi + \frac{3}{2(3+2Bi)}\left[(m-1)\pi - \frac{Bi^2}{\beta_m'}\right] B_m \tag{2-21}$$

where

$$B_m = \left[1 + \frac{8Bi(3+2Bi)}{3\left((m-1)\pi - \frac{Bi^2}{\beta_m'}\right)}\right]^{1/2} - 1 \tag{2-22}$$

and β_m' is arrived at from Equation (2-20).

The number of eigenvalues necessary in order to achieve convergence of the infinite series temperature solution varies depending on the value of diffusivity, sample thickness and the time associated with the first time step in the experiment. Since the term in the infinite series solution which drives the series to convergence is the exponential, a convenient convergence criterion for six significant figure results is

Taking the

where r_i is

Since a typ
eigenvalue
can be expre

Since r_i is
number of ei

Since the eig
number of req
initial time

$$\frac{e^{-\frac{\beta_1^2 \alpha t}{L^2}}}{e^{-\frac{\beta_n^2 \alpha t}{L^2}}} = 10^6 \qquad (2\text{-}23)$$

Taking the log of both sides we have approximately

$$-\beta_1^2 t^* + \beta_n^2 t^* = 14 \qquad (2\text{-}24)$$

where t^* is the non dimensional time defined as

$$t^* = \frac{\alpha t}{L^2} \qquad (2\text{-}25)$$

Since a typical value for β_n is approximately $n\pi$, the eigenvalue to be calculated in order to achieve convergence can be expressed approximately as

$$\beta_n = \sqrt{\frac{14 + \pi^2 t^*}{t^*}} \qquad (2\text{-}26)$$

Since t^* is typically on the order of 0.01, we have the number of eigenvalues necessary for convergence expressed as

$$n = \frac{1}{\pi}\sqrt{\frac{14}{t^*}} \qquad (2\text{-}27)$$

Since the eigenvalues are very close to $n\pi$ in value, the number of required eigenvalues for convergence for a typical initial time step measurement of .01 unit of non-dimensional

ture is 12.

2.5 [illegible]

Using a

derivative a

derivative,

$$\frac{\partial}{}$$

In this nota

node to whic

are numbered

superscript

temperature

present time

by

$$\frac{\partial}{2}$$

$$+h$$

and the right

time is 12.

2.5 FINITE DIFFERENCE METHOD

Using a backward difference scheme for the time derivative and a central difference scheme for the spacial derivative, the energy equation becomes

$$\rho c_p \frac{T_i^j - T_i^{j-1}}{\Delta t} = k \frac{T_{i+1}^j - 2T_i^j + T_{i-1}^j}{\Delta x^2} \tag{2-28}$$

In this notation, the i subscript represents the spacial node to which the temperature applies. The spacial nodes are numbered from right to left from zero to n. The j superscript represents the time step to which the temperature refers, where time j is considered to be the present time. The left boundary condition is approximated by

$$\frac{\rho c_p \Delta x}{2\Delta t}\left(T_0^j - T_0^{j-1} + T_1^j - T_1^{j-1}\right) + h(T_0 - T_\infty) + k\left(\frac{T_0 - T_1}{\Delta x}\right) = 0 \tag{2-29}$$

and the right boundary condition by

The elas

setting all

the exception

represents th

the entire en

The solu

numerical sol

this particul

series expans

the numerical

the non-linea

chapter. Si

the computati

this work, i

agreement be

adding the n

Combinin

with real inte

ial equations

ion, all real

$$\frac{\rho c_p \Delta x}{2\Delta t}\left(T_n^j - T_n^{j-1} + T_{n-1}^j - T_{n-1}^{j-1}\right)$$
$$+h(T_n - T_\infty) + k\left(\frac{T_n - T_{n-1}}{\Delta x}\right) = 0 \qquad (2\text{-}30)$$

The flash heating is simulated in this problem by setting all initial temperatures at zero, i.e. ambient, with the exception of T_o^0 which is set at $2q_o/\Delta x \rho c_p$. This represents the temperature rise resulting from absorption of the entire energy of the flash at the surface node, T_0.

The solution to these equations, gives the direct numerical solution to the problem. Although the solution to this particular problem can be found exactly by the infinite series expansion mentioned above, it is necessary to build the numerical solution in preparation for the addition of the non-linear radiation terms to be utilized in the next chapter. Since this numerical method serves as a basis for the computation of direct solutions for subsequent models in this work, it is very important to observe accurate agreement between this and the exact solution prior to adding the non-linear terms.

Combining the two boundary condition equations above with n-1 interior equations, such as equation (2-28), leaves n+1 equations and n+1 unknowns. At the initial condition, t=0, all n+1 node temperatures are assumed to be known. The

n+1 unknowns in the first set of simultaneous equations to be solved are the n+1 node temperatures at the first time step. The first of the n+1 equations, the equation generated by the left hand boundary condition, has two unknowns, T_0 and T_1. The second equation has three unknowns, T_0, T_1 and T_2. This overlap continues until the n+1 equation which, like equation 1, has two unknowns. These are T_{n-1} and T_n. In matrix form, this set of equations takes the form of [A][T]=[D] where the [A] matrix is n+1 by n+1, and the [T] and [D] vectors are n+1 by 1. The [A] matrix is completely zero except for the main diagonal and one place either side of the main diagonal. This is known as a tri-diagonal matrix. The [T] vector contains the unknown temperatures for each node and the [D] vector contains the temperatures from the previous time step.

The method of solving the tri-diagonal matrix generated by these equations is very important and can significantly affect the results of the calculations. Although algebraically correct, solving the equations sequentially by substitution can generate roundoff error through successive close subtractions, significantly degrading the accuracy of the solution. In contrast to this method of evaluating the tri-diagonal matrix, the equation transformation method as outlined in reference [24] eliminates this accumulation of

errors. Giv-

form as foll

$$\begin{bmatrix} c_1 & & & & \\ a_2 & & & & \\ & \ddots & & & \\ & & \ddots & & \\ & & & a_n & c_n \end{bmatrix}$$

we define

$$c_r' = \frac{c_r}{b_r - a_r}$$

for r=1,2,3, ..

equivalent to

the following e

for r=0,1,2,...,

in table 2-1 in

solution.

Subsequent ter

errors. Given a tri-diagonal matrix expressed in expanded form as follows

$$\begin{vmatrix} b_0 & c_0 & 0 & 0 & 0 & 0 & \dots & 0 & 0 & 0 \\ a_1 & b_1 & c_1 & 0 & 0 & 0 & \dots & 0 & 0 & 0 \\ 0 & a_2 & b_2 & c_2 & 0 & 0 & \dots & 0 & 0 & 0 \\ \vdots & \vdots & \vdots & \vdots & \vdots & \vdots & \dots & \vdots & \vdots & \vdots \\ 0 & 0 & 0 & 0 & 0 & 0 & \dots & a_{n-1} & b_{n-1} & c_{n-1} \\ 0 & 0 & 0 & 0 & 0 & 0 & \dots & 0 & a_n & b_n \end{vmatrix} \begin{vmatrix} T_0 \\ T_1 \\ T_2 \\ \vdots \\ T_{n-1} \\ T_n \end{vmatrix} = \begin{vmatrix} d_0 \\ d_1 \\ d_2 \\ \vdots \\ d_{n-1} \\ d_n \end{vmatrix} \tag{2-31}$$

we define

$$c_0^* = \frac{c_0}{b_0} \qquad d_0^* = \frac{d_0}{b_0} \tag{2-32}$$

Subsequent terms are defined through the recursion relation

$$c_r^* = \frac{c_r}{b_r - a_r c_{r-1}^*} \qquad d_r^* = \frac{d_r - a_r d_{r-1}^*}{b_r - a_r c_{r-1}^*} \tag{2-33}$$

for r=1,2,3, ... n. When d_n^* is finally calculated, this is equivalent to T_n. The other temperatures are calculated by the following expression

$$T_r = d_r^* - c_r^* T_{r+1} \tag{2-34}$$

for r=0,1,2,...,n-1. The results of this method are shown in Table 2-1 in comparison to the results from the exact solution.

son of
ues Sh

TIME	EXACT SOLUTION
0.06	0.9
0.08	0.9
0.10	0.9
0.12	0.9
0.14	0.9
0.16	0.9
0.18	0.9
0.20	0.9
0.22	0.9
0.24	0.9
0.26	0.9
0.28	0.9
0.30	0.9
0.32	0.9
0.34	0.9
0.36	0.9
0.38	0.9
0.40	0.9
0.42	0.9
0.44	0.9
0.46	0.9
0.48	0.9
0.50	0.9
0.52	0.9
0.54	0.9
0.56	0.9
0.58	0.9
0.60	0.9
0.62	0.9
0.64	0.9
0.66	0.9
0.68	0.9
0.70	0.9
0.72	0.9
0.74	0.9
0.76	0.9
0.78	0.9
0.80	0.9
0.82	0.9
0.84	0.9
0.86	0.9
0.88	0.9
0.90	0.9
0.92	0.9
0.94	0.9
0.96	0.9

* The first
percent of

The ex
difference
to the exa
of the mag
sequential
diagonal m
desired wi
solution s
eliminatio

Table 2-1

Comparison of Finite Difference Method to the Exact Solution
Values Shown are in Percent Error From Exact Solution
α=L=1 Δt=.0005 Bi=0

TIME	EXACT SOLUTION	Δx=1/30	Δx=1/60	SPLIT GRID* Δx=1/30
0.06	0.07142	1.093531	0.449454	1.503115
0.12	0.405587	-0.11292	-0.04635	-0.14088
0.18	0.663191	-0.15863	-0.10148	-0.18787
0.24	0.81295	-0.12215	-0.08525	-0.14183
0.3	0.896468	-0.08511	-0.06169	-0.09785
0.36	0.942727	-0.05696	-0.04211	-0.06519
0.42	0.968321	-0.03738	-0.02799	-0.04256
0.48	0.982477	-0.02392	-0.01812	-0.02718
0.54	0.990308	-0.01515	-0.01151	-0.01717
0.6	0.994639	-0.00945	-0.00724	-0.01067
0.66	0.997035	-0.00582	-0.00451	-0.00659
0.72	0.99836	-0.00351	-0.0027	-0.00402
0.78	0.999093	-0.0022	-0.0017	-0.00244
0.84	0.999498	-0.0013	-0.001	-0.00143
0.9	0.999722	-0.0007	-0.0006	-0.00082
0.96	0.999846	-0.0004	-0.0003	-0.00047

* The first five nodes of the 30 total were in the first two percent of the material.

The example shown in Table 2-1 compares the finite difference solution, using the tri-diagonal matrix method, to the exact solution. These errors are approximately 1/10 of the magnitude of the errors generated when using a simple sequential elimination algebraic scheme in solving the tri-diagonal matrix. More importantly, the time grid can be refined without instability when using the tri-diagonal solution scheme given by reference [24]. The algebraic elimination method becomes completely unstable for very fine

time grids.

As an

greater le

attempted

treat the

might be re

where the

the exampl

actually s

spacing,

that the

uniform g

a uniform

2.6 PARA

With

direct so

problem c

minimum n

the greate

procedure

calculate

obtained

condition

time grids.

As an additional area of investigation, pursuant to a greater level of accuracy, a split spacial grid was attempted in the finite difference solution. In order to treat the flash problem, it was suspected that a finer grid might be required at the left hand edge of the material where the temperature derivatives are extremely large. In the example shown in Table 2-1, the refined grid scheme is actually shown to be somewhat inferior to the uniform grid spacing, using 30 nodes in each case. It was discovered that the 30 node split grid was superior to the 20 node uniform grid, but the best utilization of nodes seemed to be a uniform distribution.

2.6 PARAMETER ESTIMATION

With the appropriate methods in place for computing the direct solution, the parameter estimation aspect of the problem can be undertaken. It is desirable to solve for the minimum number of parameters necessary. This facilitates the greatest degree of stability in the parameter estimation procedure and the greatest degree of confidence in the calculated parameters. The three parameters shown below are obtained by dividing the differential equation and boundary conditions by k. Estimation using two parameters instead of

three is in

parameter e

than the re

The unknown

$$\beta =$$

The third pa

mber simpl

der to fin

sed as outl

squares was

results are

and Gauss-Ma

assumptions

1.

the

2.

dura

3.

over

4.

unre

three is investigated in detail in Chapter 6, however the parameter estimation algorithm was found to be less robust than the method which used the three parameters given below. The unknown parameters are for this model are

$$\beta_1=\alpha=\frac{k}{\rho c_p} \quad \beta_2=\frac{q_0}{k} \quad \beta_3=\frac{h}{k} \tag{2-35}$$

The third parameter can be used as the more familiar Biot number simply by multiplying by the sample thickness, L. In order to find the parameters, the method of least squares is used as outlined in reference [25]. The method of least squares was chosen because it is a simple method and the results are the same as those obtained by maximum likelihood and Gauss-Markov, assuming that the following statistical assumptions are valid:

1. The measurement errors are additive in nature to the true (but unknown) temperatures.
2. The measurement errors, considered over the duration of the experiment, have a zero mean value.
3. The measurement errors have a constant variance over the duration of the experiment.
4. The magnitude of each measurement error is unrelated to it's predecessors or successors. In

othe

5.

dura

Gaus

The method o

expression

In matrix for

In order to m

and error, the

calculated.

derivatives of

to each of the

coefficients a

respective par

sensitivity co

magnitudes of

example, the s

parameter in t

other words, the errors are uncorrelated.

5. The measurement errors, considered over the duration of the experiment, fall in a normal, or Gaussian, distribution pattern.

The method of least squares minimizes of the following expression

$$S=\sum_{i=1}^{n}(Y_i-T_i)^2 \tag{2-36}$$

In matrix form this becomes

$$S=[\boldsymbol{Y}_i-\boldsymbol{T}_i]^T[\boldsymbol{Y}_i-\boldsymbol{T}_i] \tag{2-37}$$

In order to minimize this expression, aside from using trial and error, the sensitivity coefficients must first be calculated. This is accomplished by taking partial derivatives of the direct temperature solution with respect to each of the parameters, one at a time. The sensitivity coefficients are then normalized by dividing by the respective parameter. In this way, the units of the sensitivity coefficients are always in temperature and the magnitudes of the coefficients are directly comparable. For example, the sensitivity coefficient for β_1, the first parameter in the model discussed above, is

$$X_1=\beta_1\frac{\partial T}{\partial \beta_1} \tag{2-38}$$

A graph o
function
for the c
coefficie
laborator
diffusivi
experimen
Shot numb
condition
two sens
sensitiv
shape th
parameter

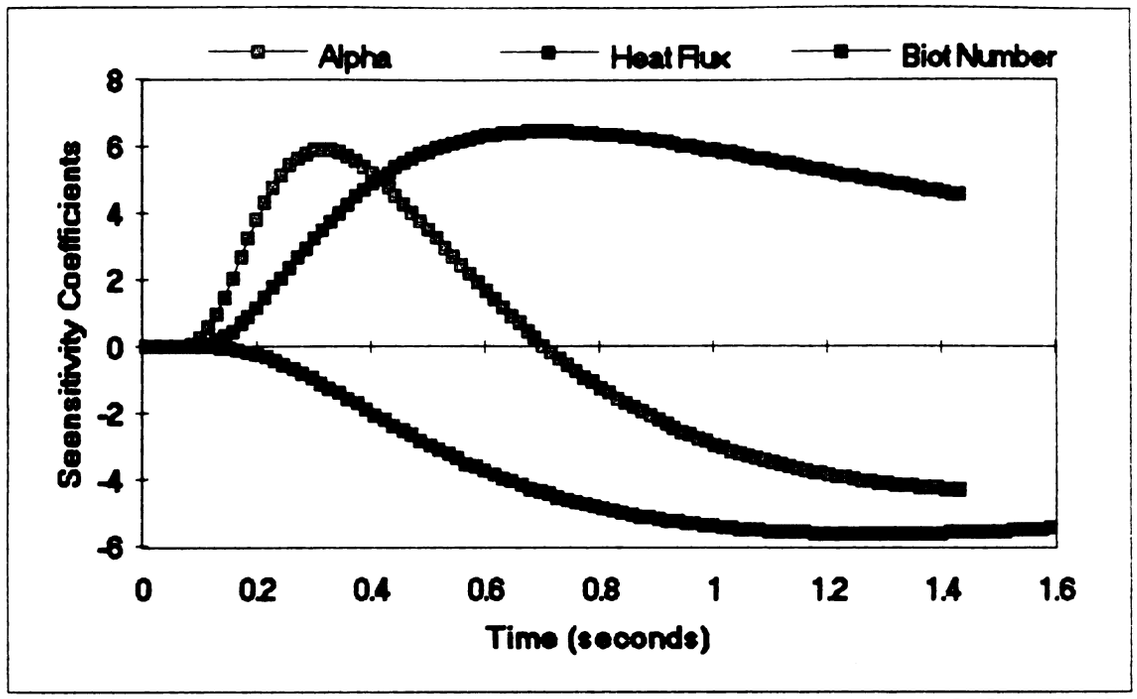

Figure 2-4 Normalized Sensitivity Coefficients for CBCF at 700°C

A graph of the sensitivity coefficients for this model, as a function of time, is shown in Figure 2-4. The parameters for the direct solution from which these sensitivity coefficients were taken correspond to those of an actual laboratory experiment with a Biot number of 0.142 and a diffusivity of 0.33 mm^2/sec. The nature of the flash experiments is such that the heat flux parameter and the Biot number are somewhat correlated, an undesirable condition. This is evidenced by the similar shape of the two sensitivity coefficient curves. The diffusivity sensitivity coefficient curve, however, has a different shape than the others which makes it a more salient parameter. This characteristic suggests a good experiment

esign for e

f interest.

Using t

equations ca

The measured

is assigned

given the sy

repression pr

parameters,

required. As

sensitivity c

each parameter

shown below.

iterations, u

T *

The term Δb co

estimated para

calculated tem

temperature.

T*+1 = T

design for estimating diffusivity, since it is the parameter of interest.

Using these sensitivity coefficients, a set of equations can be developed to be solved by least squares. The measured value of temperature for a given time step, i, is assigned the symbol Y_i and the calculated solution is given the symbol T_i. In order to perform the non-linear regression procedure, an initial estimate for the parameters, designated b_1, b_2, and b_3 in this case, is required. Assuming a locally linear approximation to the sensitivity coefficients, a revised or improved value for each parameter can be found by the partial Taylor Series shown below. A superscript designates the number of iterations, using the letter k.

$$T^{(k+1)} \approx T^{(k)} + \sum_{j=1}^{3} \frac{\partial T}{\partial b_j} \Delta b_j \qquad (2\text{-}39)$$

The term Δb corresponds to the adjustment necessary in the estimated parameter to affect a change from the initial calculated temperature to the refined calculated temperature. This can also be expressed as

$$T^{(k+1)} \approx T^{(k)} + \sum_{j=1}^{3} \frac{\partial T}{\partial b_j} (b_j^{(k+1)} - b_j^{(k)}) \qquad (2\text{-}40)$$

Using this principle, an appropriate change in the estimated parameter can be found by knowing the desired shift in temperature necessary to make the calculated temperature of the model match those of the measurements. Substituting Y as the symbol for the measured temperature, and using the method of ordinary least squares to solve for the revised parameters, we have, in matrix form, as given by reference [25]

$$\boldsymbol{b}^{(k+1)}=\boldsymbol{b}^{(k)}+(\boldsymbol{X}^{(k)T}\boldsymbol{X}^{(k)})^{-1}\boldsymbol{X}^{(k)T}(\boldsymbol{Y}-\boldsymbol{T}^{(k)}) \tag{2-41}$$

This process is repeated until successive iterations result in a change of less than 0.1 percent in any parameter between iterations. At this point, convergence is considered to have been obtained. The residuals, expressed as

$$\sigma_r^2=\sum_{i=1}^{n}(Y_i-\hat{T}_i)^2=\sum_{i=1}^{n}e_i^2 \tag{2-42}$$

are considered minimized where the "hat" designation on the calculated temperature signifies the calculated temperature based on the converged parameter values.

2.7 MODEL INADEQUACIES

The primary means of determining the adequacy of the direct solution is to examine the residuals, e_i. Assuming

an appropri

and the rea

parameters

measurement

noise which

positive to

A like

characteris

signature

positive or

characteris

indication,

specificall

It is

characteris

model, and

problem wit

phenomena r

conducted.

present is

experiments

the curves

signature s

repeatable

an appropriate model is used, the calculated direct solution and the measured data should match identically once the parameters have been found. The unavoidable presence of measurement errors should be limited to small background noise which causes the residuals to oscillate randomly from positive to negative about zero.

A likely indication of an inadequate model is a characteristic signature in the residuals. A characteristic signature is exhibited by long periods of continuous positive or negative residuals. Another problem of which a characteristic signature in the residuals can be an indication, is a problem with the measurements, specifically, correlated errors.

It is important to make a distinction between a characteristic signature, which suggests an ill-applied model, and correlated measurement errors, which suggest a problem with the measuring instrument. Both of these phenomena may look very similar if only one experiment is conducted. One way of discerning which of these problems is present is to plot the residuals from two similar experiments over top of each other. If the basic shape of the curves is the same, this suggests a characteristic signature since correlated errors are not expected to be repeatable from one experiment to another. If correlated

errors are

should lo

Exam

Figures 2

measureme

taking th

maximum

a phenome

the model

Anot

stabilit

estimates

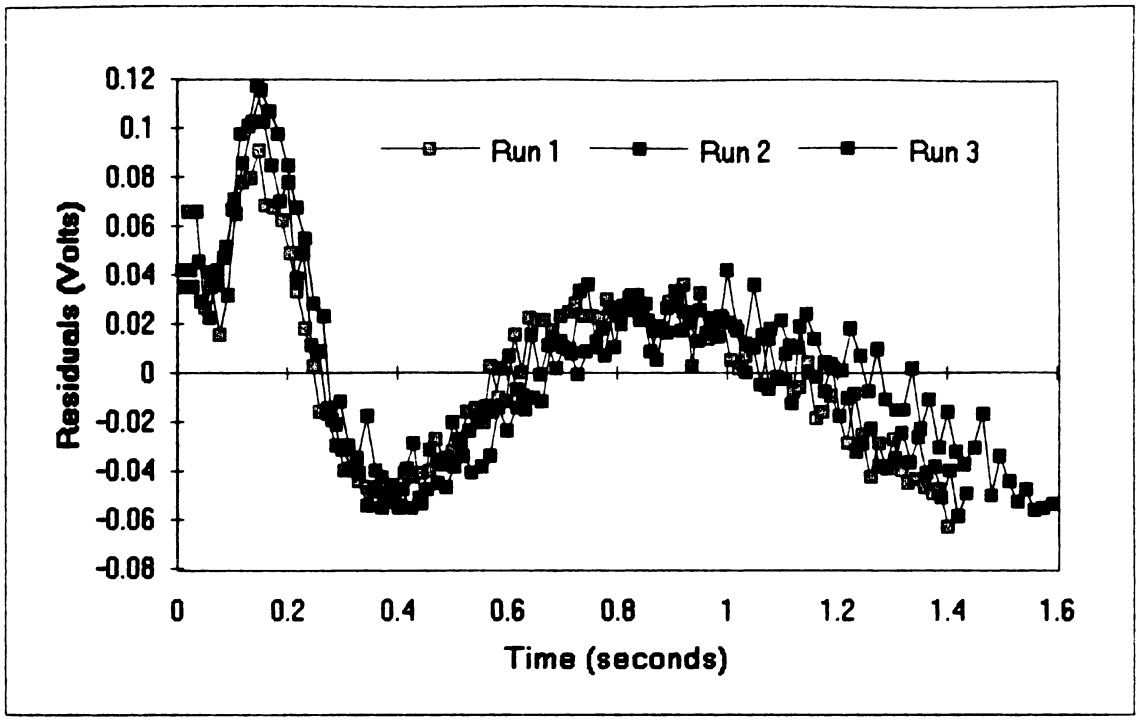

Figure 2-5 Residuals from Model 1 used on CBCF Data at 700°C

errors are observed, the "signature" from each experiment should look different than the others.

Examples of characteristic signatures are shown in Figures 2-5 and 2-6. As a basis of comparison, the maximum measurement value in these experiments was approximately 6.8 making the maximum residual value roughly 5 percent of the maximum measurement. This appears to be a classical case of a phenomenon in the experiment which is not accounted for in the model.

Another key indication of model inadequacy is the stability of the sequential estimates. The sequential estimates are each calculated for their respective times,

each assum

each addit

parameter

estimate

the equati

$$b^{(k+1)} =$$

With three

sequential

measuremen

and the $\mathbf{Y}$-

be 3 x 1 t

point, a n

vector for

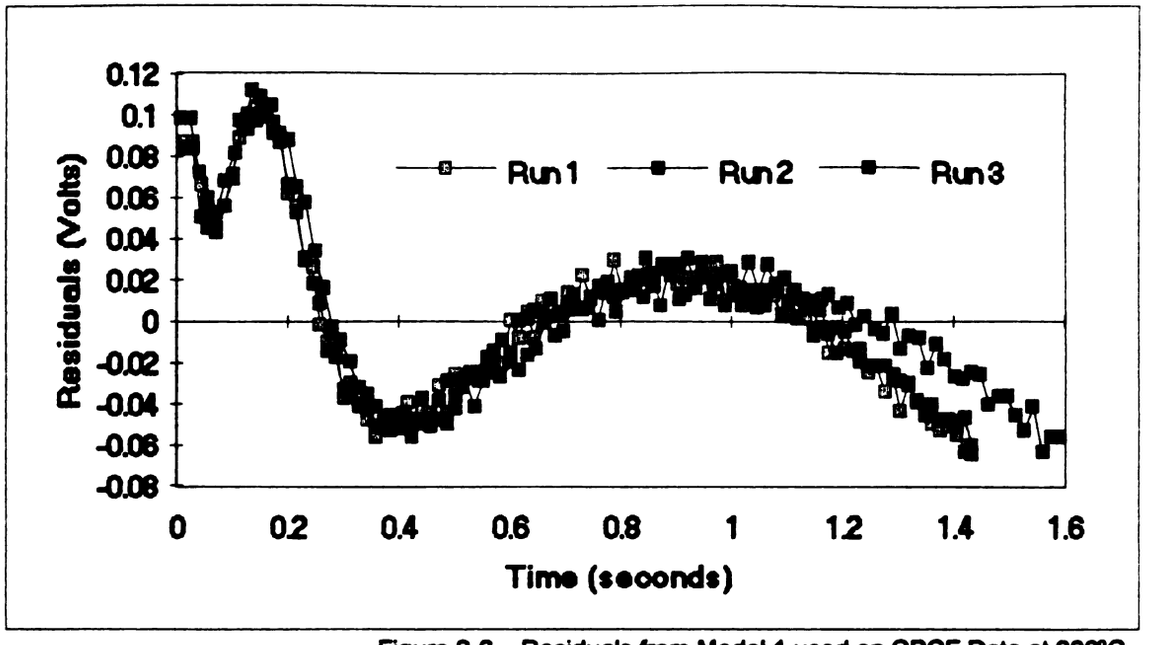

Figure 2-6 Residuals from Model 1 used on CBCF Data at 600°C

each assuming no subsequent information is available. As each additional data point is added, the value of each parameter should ideally be unchanged from the parameter estimate generated at the previous time. For example, in the equation

$$\mathbf{b}^{(k+1)} = \mathbf{b}^{(k)} + (\mathbf{X}^{(k)T}\mathbf{X}^{(k)})^{-1}\mathbf{X}^{(k)T}(\mathbf{Y}-\mathbf{T}^{(k)}) \qquad (2\text{-}43)$$

with three unknown parameters for this model, the first sequential estimate may be calculated after say 10 measurements. In this case, the $\mathbf{X}$ matrix would be 10 x 3 and the $\mathbf{Y}-\mathbf{T}$ vector would be 10 x 1. The final product would be 3 x 1 to match the $\mathbf{b}^{(k)}$ and the $\mathbf{b}^{(k+1)}$ vectors. At this point, a new $\mathbf{b}^{(k+1)}$ vector is calculated and becomes the $\mathbf{b}^{(k)}$ vector for the next iteration. Now another time step is

added to the equations so that the $\mathbf{X}$ matrix becomes 11 x 3 and the $\mathbf{Y-T}$ vector becomes 11 x 1. A new $\mathbf{b}^{(k+1)}$ vector is now calculated and the process continues. The sequential estimates can be plotted as functions of time and observed for stability.

In order to avoid the computational expense of calculating the matrix inverse in the explicit form shown above, the equation can be re-written in implicit form as

$$\mathbf{X}^{(k)T}\mathbf{X}^{(k)}(\mathbf{b}^{(k+1)}-\mathbf{b}^{(k)})=\mathbf{X}^{(k)T}(\mathbf{Y}-\mathbf{T}^{(k)}) \qquad (2\text{-}44)$$

where the vector $\mathbf{b}^{(k+1)}$ is the only unknown. In the present example of the estimation of three parameters, the $\mathbf{X}^T\mathbf{X}$ matrix is 3 x 3, the $\mathbf{b}^{(k+1)}-\mathbf{b}^{(k)}$ vector is 3 x 1 and the $\mathbf{X}^T(\mathbf{Y-T})$ vector is also 3 x 1. Using P-L-U decomposition as set forth in reference [26], the $\mathbf{b}^{(k+1)}$ vector can be found by reducing the $\mathbf{X}^T\mathbf{X}$ matrix to a lower diagonal with zeros in the upper half using Gaussian elimination. After scaling the equations to minimize numerical rounding errors, the $\mathbf{b}^{(k+1)}$ vector can be found by simple substitution. Another alternative to calculating the matrix inverse is to use the matrix inversion lemma as described in reference [25].

Figure 2-7 shows a graph of the sequential estimates for the Oak Ridge National Laboratory experiment from which the residual curve was generated in Figure 2-5. This figure

shows scr

with time

model.

examined

signature

the seque

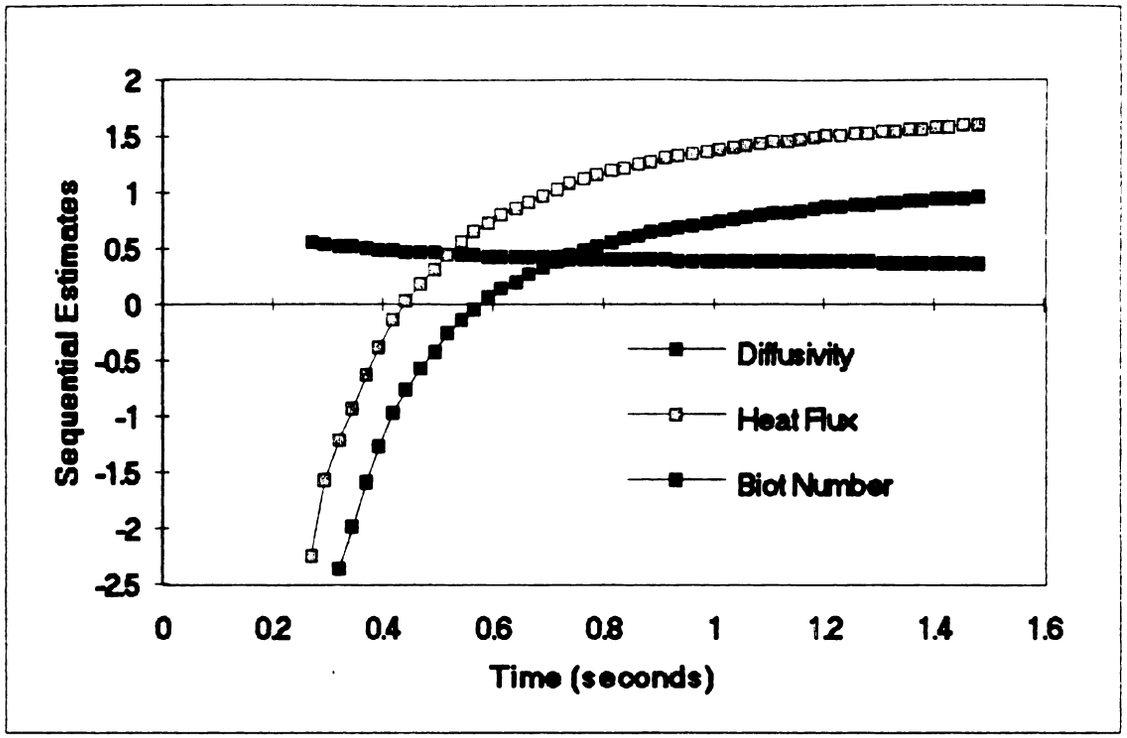

Figure 2-7 Sequential Estimates of CBCF Data at 700°C

shows some incremental change in the parameter estimates with time which is an indication of some inadequacy in the model. In the following chapters, various models will be examined in an effort to account for the characteristic signature in the residuals and the lack of consistency in the sequential parameter estimates.

CHAPTER 3

MODELING INTERNAL RADIATION

3.1 INTRODUCTION

As discussed in Chapter 2, one indication of a disparity between the mathematical model and the physical mechanism in an experiment, is a signature in the residuals. The residual curves of the experiments which were conducted at the Oak Ridge National Laboratory, as exhibited in Chapter 2, serve as examples of characteristic signatures. As discussed in Chapter 2, a characteristic signature is a pattern which repeats itself when comparing residual curves of successive experiments and indicates a disparity between the model and the measured data. Also, it is important to make a distinction between a characteristic signature, which suggests an ill-applied model, and correlated measurement errors, which suggest a problem with the measuring instrument.

Both of these phenomena may look very similar if only one experiment is conducted. As evidenced by the residual graphs from the six experiments plotted in Chapter 2, a characteristic signature is present in the CBCF experimental data. These curves point to a characteristic signature

since corr

from one e

observed, -

different -

shown in Ch

experiments

experiments

using diffe

suggests an

material whi

mathematical

model.

One poss

heat flow is

kinetic condi

dominant heat

the CBCF mate

such a mechan

medium. The p

on a localized

transferring h

of the continu

radiant exchan

by radiation f

since correlated errors are not expected to be repeatable from one experiment to another. If correlated errors are observed, the "signature" from each experiment should look different than the others. The characteristic signature shown in Chapter 2 is not only present in successive experiments on the same material, but is exhibited in experiments from different laboratories around the world using different materials. The shape of this residual curve suggests an initial rate of heat transfer through the material which is more rapid than that which is mathematically predicted using the conventional conduction model.

One possible explanation for the more rapid initial heat flow is that a mechanism other than conventional kinetic conduction may be at work, superimposed on the dominant heat transfer mechanism of conduction. Although the CBCF material is considered opaque, radiation could be such a mechanism, using the material as a participative medium. The principle which drives this mechanism is based on a localized area of heated material in the continuum transferring heat by radiation to a lower temperature part of the continuum which is close enough to allow direct radiant exchange. The process continues, spreading the heat by radiation from the warmer parts of the material to the

co

ac

com

com

fac

sol

cre

che

al.,

diff

comp

heat

param

exper

a para

conduc

overa

through

Was th

remain

In

Presen

simulat

cooler parts in a diffusion-like process. All of this would take place in addition to and simultaneously with conventional kinetic conduction. Modeling the combined conduction and internal radiation mechanisms is more complex mathematically and the differential equation cannot be solved explicitly. The solution must be obtained numerically.

Internal radiation has been shown to be evident in other materials such as alumina powders as shown by Hahn et. al., in reference [36]. In this alumina work, the thermal diffusivity was found in a de-coupled way from the radiative component of heat transfer. The radiation portion of the heat transfer was assumed by extrapolating known radiation parameters at temperatures other than that at which the experiment was conducted. The radiation was then treated as a parallel heat transfer mechanism superimposed on the conduction mechanism. The radiation contribution to the overall heat transfer was assumed as a known quantity throughout the duration of the experiment. The diffusivity was then found using conventional conduction to model the remainder of the heat transfer.

In contrast to this method, the objective of the present research is to compute radiative parameters simultaneously with the kinetic conductivity or diffusivity

parameters. The remainder of this chapter discusses the various aspects of computing parameters related to combined conduction and internal radiation. A model is developed to accomplish this and is referred to as "Model 2". The non-radiative model discussed in Chapter 2 is referred to hereafter as "Model 1". Section 3.2 provides a development of the direct solution and experimental design considerations. Numerical aspects of computing the direct solution are addressed in Section 3.3 and examples are shown of various direct solutions over a wide range of selected parameters. Section 3.4 presents the parameter estimation aspects and sensitivity coefficients for this model. This section includes a test problem in an attempt to correctly extract parameters from an exact solution with known parameters. A reduction in the number of unknown parameters is attempted in an effort to stabilize the parameter estimation procedure. An investigation into the residual signature is shown for a case where an exact solution with internal radiation is analyzed by a parameter estimation model assuming no internal radiation. Analysis of actual laboratory data is performed in Section 3.5 with results shown for a number of different approaches. Finally, an intergo-differential model is discussed in Section 3.6 which is more applicable to materials which are optically thin.

3.2

wher

susp

char

cons

thic

opti

medi

thic

inspe

prop

absc

intera

is co

unlike

T

intern

appropr

behavio

charac

allows

When so

materia

3.2 DIRECT SOLUTION DEVELOPMENT

The type of model applied to a particular experiment where combined conduction and internal radiation are both suspected as operative mechanisms, depends on the optical characteristics of the participative medium. The primary consideration in selecting a model is based on the optical thickness of the material. A material is considered optically thick if the mean free path of a photon in the medium is relatively short in comparison to the sample thickness. These materials appear opaque upon visual inspection. Conversely, in an optically thin material, many photons are able to pass through the medium without being absorbed. Even though a photon may undergo many scattering interactions as it passes through a material, the material is considered optically thin if absorption of the photon is unlikely.

The method of modeling the combined conduction and internal radiation as diffusive processes is most appropriate for materials which exhibit optically thick behavior. This model is best suited to the physical characteristics of the CBCF material being studied and allows a solution to be generated at a relatively rapid rate when solving the equations numerically. Optically thin materials are more appropriately modeled using an integro-

len

mater

T

which

In this

conduc

coeffi

and the

length.

represe

or the

scatter

corresp

zero me

heat tra

differential approach discussed in more detail in Section 3.6. The diffusive model, as given in references [1],[8],[9] and [10], is used in evaluating optically thick materials.

The radiative heat flux vector for this model is

$$q_r = -\frac{16\sigma_b T^3}{3\kappa}\nabla T \qquad (3\text{-}1)$$

which can also be expressed as

$$q_r = -k_r \nabla T \quad where \quad k_r = \frac{16\sigma_b T^3}{3\kappa} \qquad (3\text{-}2)$$

In this context, k_r can be thought of as the "radiative conductivity". The κ term is known as the "extinction coefficient" which is the sum of the absorption coefficient and the scattering coefficient, each having units of inverse length. The reciprocal of the extinction coefficient represents the mean free path of a photon in the material, or the mean distance traveled without an absorption or scattering interaction. When, κ tends toward infinity, this corresponds to negligible radiation transfer due to a near-zero mean free path of the photons. Conversely, radiant heat transfer is maximized when κ is small, corresponding to

a long p

transfer

The

3.729×1

equation

overall

component

where k

thermal

dimension

In order

boundary

$-/k_z$

Additionally

a long photon mean free path and a very rapid rate of heat transfer through the material.

The σ_b term is the Stefan-Boltzmann constant which is 5.729×10^{-8} W/m^2K^4. Additionally, all temperatures in this equation must be expressed as absolute temperatures. The overall heat flux, including conductive and radiative components, then becomes

$$q = q_r + q_c = -(k_r + k)\nabla T \tag{3-3}$$

where k once again corresponds to the conventional kinetic thermal conductivity. The energy equation in the x dimension, with no internal heat generation, becomes

$$\rho c_p \frac{\partial T}{\partial t} = -\nabla \cdot q = \frac{\partial}{\partial x}\left[(k_r + k)\frac{\partial T}{\partial x}\right] \tag{3-4}$$

In order to solve for a temperature solution, the proper boundary conditions must be applied. They are

$$-(k_r + k)\left|\frac{\partial T}{\partial x}\right|_{x=0} = q_0\delta(t) + h(T_\infty - T_{x=0}) \tag{3-5}$$

$$-(k_r + k)\left|\frac{\partial T}{\partial x}\right|_{x=L} = h(T_{x=L} - T_\infty) \tag{3-6}$$

Additionally, the initial temperature throughout the

material i

discussed

are consid

the heat t

left hand

combined b

boundary c

represents

a function

surface to

By now

unknown par

Groups 1, 3

utilized in

Groups are

Chapter 2,

and the bou

Groups cont

fourth Paran

number by m

Parameter, 3

material is assumed to be T_∞. As in the non-radiative model discussed in Chapter 2, the parameters in these equations are considered to be constant throughout each experiment and the heat transfer is assumed to be one dimensional. The left hand side of each boundary condition represents the combined heat flux into or out of the solid side of the boundary due to conduction and radiation. The $q_o\delta(t)$ term represents the heat flux at the boundary due to the flash as a function of time. The heat losses from the material surface to the surroundings is modeled as convection.

By dividing through these equations by k, the number of unknown parameters can be reduced to the four groups

$$\beta_1=\alpha=\frac{k}{\rho c_p} \quad \beta_2=k\kappa \quad \beta_3=\frac{q_0}{k} \quad \beta_4=\frac{h}{k} \tag{3-7}$$

Groups 1, 3 and 4 are the same as the three parameters utilized in the model presented in Chapter 2. Because the groups are obtained the same way as those presented in Chapter 2, which is by dividing the differential equation and the boundary conditions by *k*, each of the parameter groups contains the kinetic thermal conductivity term. The fourth parameter can be expressed as the more familiar Biot number by multiplying by the sample thickness, L. The parameter, β_2, represents the additional degree of freedom

afforded b

This term

temperatu

proportio

temperatu

way of dea

related t

In ar

order of

differenti

performed

parameter

conductivi

than therm

Parameter

the magnit

presented

following

to give ap

Parameters

diffusivit

afforded by the additional mechanism of internal radiation. This term is expressed as shown rather than k_r since k_r is a temperature dependent term. The β_2 parameter is proportional to k/k_r with the known constants and temperature variabilities divided out. This is an easier way of dealing with the second parameter, the only parameter related to the radiative transfer.

In an effort to optimize experiment design factors, an order of magnitude analysis for each term in the differential equation and the boundary conditions can be performed in order to determine optimum magnitudes of parameter groups. It is desirable to have a radiative conductivity on par with the thermal conductivity, or larger than thermal conductivity, in order for the radiative parameter to be adequately estimated. This is evidenced by the magnitudes of the sensitivity coefficient curves presented later in this chapter. Additionally, the following experiment geometry should be established in order to give approximately equal weighting to each of the parameters. This provides the proper combination of diffusivity, sample thickness and experiment time duration.

$$\frac{L^2}{t}=2\alpha \qquad (3\text{-}8)$$

Sinc

dire

appr

all

of t

When

allo

a si

expe

a va

regi

a tea

temp

able

Chapt

Notwi

direc

Notwi

Where

Since the experiment time duration is normally of a non-dimensional time of 0.5, the optimum thickness will be approximately the square root of the diffusivity.

Although it is essential to simultaneously calculate all parameters, the heat loss coefficient and the magnitude of the heat flux are not normally parameters of interest. When this is the case, the optimum experiment design would allow heat loss to be assumed as zero which would result in a simpler model with fewer parameters to estimate. In experiments performed at high temperatures, however, even in a vacuum, surface heat losses are quite high and far from negligible. In cases such as these, it is desirable to use a heat flux that is of large enough magnitude to allow temperature readings to be two orders of magnitude above the ambient noise.

As with the linear differential equation outlined in Chapter 2, the non-linear conduction-radiation model can be non-dimensionalized. With the addition of one non-dimensional group to the three developed in Chapter 2, the non-dimensional form of the equation is

$$\frac{\partial T^*}{\partial t^*} = \frac{\partial}{\partial x^*}\left[\left(1 + k^*_{ro}\frac{T^{*3}}{T^{*3}_\infty}\right)\frac{\partial T^*}{\partial x^*}\right] \qquad (3\text{-}9)$$

where T_∞ is the experiment ambient absolute temperature and

$\Gamma_1 =$

This

Equation

terms lis

condition

$\left\{ 1 \right.$

In Equatio

groups are

$\frac{1'x'}{\alpha}$

with x' and

four groups

defined as to

$$T^+=\frac{T}{q_0/(L\rho c_p)} \qquad T_\infty^+=\frac{T_\infty kL}{q_0\alpha} \qquad x^+=\frac{x}{L} \tag{3-10}$$

$$t^+=\frac{t\alpha}{L^2} \qquad k_{ro}^+=\frac{16\sigma_b T_\infty^3}{3k\kappa} \tag{3-11}$$

This differential equation is obtained by dividing Equation (3-4) by k and substituting the non-dimensional terms listed in equations (3-10) and (3-11). The boundary conditions can be non-dimensionalized in the same way as

$$-\left(1+k_{ro}^+\frac{T^{+3}|_{x^+=0}}{T_\infty^{+3}}\right)\frac{\partial T^+}{\partial x^+}|_{x^+=0}=\frac{L^2\delta(t)}{\alpha}+Bi\,(T_\infty^+-T^+|_{x^+=0}) \tag{3-12}$$

$$\left(1+k_{ro}^+\frac{T^{+3}|_{x^+=1}}{T_\infty^{+3}}\right)\frac{\partial T^+}{\partial x^+}=Bi\,(T_\infty^+-T^+|_{x^+=1}) \tag{3-13}$$

In Equations (3-9) to (3-13), the four dimensionless unknown groups are

$$\frac{L^2\delta(t)}{\alpha},\ Bi,\ T_\infty^+ \text{ and } k_{ro}^+ \text{ where } k_{ro}^+=\frac{k_{ro}}{k}=\frac{16\sigma_b T_\infty^3}{3k\kappa} \tag{3-14}$$

with x^+ and t^+ as independent variables. By varying these four groups in the direct problem, some insight can be gained as to how these factors affect the direct solution.

Several pl

conduction

this chap

3.3 NUMER

In t

for this

conductiv

temperatu

differen

the spac

and the

Substitut

Several plots of these direct solutions under various conditions are shown in Figures 3-1 through 3-6 later in this chapter.

3.3 NUMERICAL ASPECTS OF THE SOLUTION

In the first attempt at computing the direct solution for this model, the temperature dependent radiant conductivity, k_r, was calculated for each node using the temperature at the applicable node. For example, from the differential equation

$$\rho c_p \frac{\partial T}{\partial t} = \frac{\partial}{\partial x}\left[(k_r + k)\frac{\partial T}{\partial x}\right] \qquad (3\text{-}15)$$

the spacial derivative can be approximated as

$$\frac{\partial T}{\partial x} = \frac{T_{i+1}^{j} - T_i^{j}}{\Delta x} \quad or \quad \frac{\partial T}{\partial x} = \frac{T_i^{j} - T_{i-1}^{j}}{\Delta x} \qquad (3\text{-}16)$$

and the time derivative can be approximated as

$$\frac{\partial T}{\partial t} = \frac{T_i^{j} - T_i^{j-1}}{\Delta t} \qquad (3\text{-}17)$$

Substituting this into equation (3-15) we have

This

A typ

scre

wher

As

the

the

ter

whe

eq

ca

$$\rho c_p \frac{T_i^j - T_i^{j-1}}{\Delta t} = \frac{\partial}{\partial x}\left[(k_r + k)\frac{T_{i+1}^j - T_i^j}{\Delta x}\right] \tag{3-18}$$

This can in turn be approximated as

$$\rho c_p \frac{T_i^j - T_i^{j-1}}{\Delta t} = \frac{(k_r + k)\left[\frac{T_{i+1}^j - T_i^j}{\Delta x} - \frac{T_i^j - T_{i-1}^j}{\Delta x}\right]}{\Delta x} \tag{3-19}$$

A typical equation in the tri-diagonal matrix using this scheme then becomes

$$-T_{i-1}^j + (2+B)T_i^j - T_{i+1}^j = BT_i^{j-1} \tag{3-20}$$

where

$$B = \frac{\rho c_p \Delta x^2}{k\Delta t\left(1 + \frac{16\sigma_b T_i^3}{3k\kappa}\right)} \tag{3-21}$$

As defined in Chapter 2, the temperature subscripts refer to the position within the one-dimensional geometric grid and the superscripts refer to the time step to which the temperature applies.

This method was found to be inadequate in its accuracy when used to analyze an insulated case, i.e. Biot number equal to zero. A value of $k_{ro}/k=1$ was used in each test case using this method shown in Table 3-1. In each case,

the temperature rise should be one unit of non-dimensional temperature. This is because the contrived sample is considered insulated and, in order to satisfy the First Law of Thermodynamics, the temperature rise should be the same in each case since the flash magnitudes are the same in each case.

The reason for the inadequacy of this method was that temperature differences at the boundaries of the control volume surrounding each node were not taken into account in computing the radiant heat flux at those boundaries. Instead, the temperature of the node at the center of the control volume was used in computing the radiant conductivity at both of the corresponding control volume boundaries. This resulted in a disparity between radiant conductivity calculated at common boundaries of adjacent control volumes based on differing center node temperatures. The resulting error generated using this method is shown in Table 3-1. The "No Radiation" case differs from the $T_\infty=0$ case in that one simulation accounts for kinetic conductivity only and the other is performed at an ambient temperature of absolute zero with internal radiation present as a heat transfer mechanism. In the latter case, $k_{r_o}=0$ but k_r is non-zero once heat is added to the sample from the flash.

Table 3-1

Comparison of Direct Solutions Using Non-Radiative Model and Center Node Temperature to Define k_r in Radiative Model.

NON-DIM TIME	NO RADIATION	$T_\infty^+=0$	$T_\infty^+=10$	$T_\infty^+=100$
0.06	0.075954	0.075827	10.0757	100.087
0.12	0.402901	0.402222	10.4015	100.417
0.18	0.651622	0.650522	10.6493	100.648
0.24	0.800543	0.799191	10.7977	100.781
0.3	0.886319	0.884822	10.8832	100.855
0.36	0.935278	0.933697	10.9319	100.896
0.42	0.963161	0.961534	10.9597	100.918
0.48	0.979033	0.977379	10.9755	100.93
0.54	0.988067	0.986397	10.9845	100.937
0.6	0.993209	0.99153	10.9896	100.941
0.66	0.996135	0.994451	10.9926	100.943
0.72	0.9978	0.996114	10.9942	100.944
0.78	0.998748	0.99706	10.9952	100.945
0.84	0.999287	0.997599	10.9957	100.945
0.9	0.999594	0.997905	10.996	100.945
0.96	0.999769	0.99808	10.9962	100.945
1.02	0.999869	0.998179	10.9963	100.945
1.08	0.999925	0.998236	10.9963	100.945
1.14	0.999957	0.998268	10.9964	100.945
1.2	0.999976	0.998286	10.9964	100.945

As in the numerical solution outlined in Chapter 2, the initial condition for this problem attempts to simulate the flash by setting all temperatures at T_∞ with the exception of the temperature at the i=0 node, which is set at $2q_o/\Delta x\rho c_p$. This represents the temperature rise resulting from absorption of the entire energy of the flash at the surface node. As the ambient temperature increases, the effect of the radiant conductivity increases due to the

ubic depe

the rate

case. Th

rapid att

In a

average t

conductiv

two. This

adequately

In other

computing

conductiv

the tri-di

radiant co

adjacent e

illustrate

values for

calculate

conductiv

general, a

within eac

Apply

as Equation

side of no

cubic dependence on temperature. This can be observed in the rate at which the final temperature is attained in each case. The higher ambient temperature cases result in a more rapid attainment of the final temperature.

In a second approach to solving the direct problem, an average temperature was used to determine the radiant conductivity between T_{i-1} and T_i as well as between T_i and T_{i+1}. This technique was implemented in order to more adequately balance the radiant heat transfer between nodes. In other words, without averaging the temperatures used in computing the local radiant conductivity, the radiant conductivity assumed at a particular node in one equation in the tri-diagonal matrix is not necessarily the same as the radiant conductivity assumed at that same node in an adjacent equation. This factor led to the inaccuracies illustrated in Table 3-1. With regard to time, no average values for radiant conductivity were required to be calculated between time steps. This is because radiant conductivity changes between time steps at each node in general, and all radiant conductivity values are consistent within each time step, without mis-matched overlap.

Applying this method to the differential equation shown as Equation (3-15), the discretization of the right hand side of node *i* becomes

and the

nce i

where

In this

right or

superscri

and T_i is

temperatur

discretiza

derivative

$$\rho c_p \frac{T_i^j - T_i^{j-1}}{\Delta t} = \frac{\partial}{\partial x}\left[(k_r^R + k) \frac{T_{i+1}^j - T_i^j}{\Delta x} \right] \tag{3-22}$$

and the corresponding equation for the left hand side of node i is

$$\rho c_p \frac{T_i^j - T_i^{j-1}}{\Delta t} = \frac{\partial}{\partial x}\left[(k_r^L + k) \frac{T_i^j - T_{i-1}^j}{\Delta x} \right] \tag{3-23}$$

where

$$k_r^L = \frac{2\sigma_b (T_{i-1}^j + T_i^j)^3}{3\kappa} \tag{3-24}$$

$$k_r^R = \frac{2\sigma_b (T_i^j + T_{i+1}^j)^3}{3\kappa} \tag{3-25}$$

In this notation, the superscript "R" or "L" refer to the right or left temperature used in the T^3 term. The "L" superscript indicates the average temperature between T_{i-1} and T_i is used and the "R" superscript indicates the average temperature between T_i and T_{i+1} is used. Completing the discretization by approximating the second partial derivative of temperature with respect to x we have

$$\rho c_p \frac{T_i^j - T_i^{j-1}}{\Delta t} = \frac{1}{\Delta x}\left[(k_r^R + k)\frac{T_{i+1}^j - T_i^j}{\Delta x} - (k_r^L + k)\frac{T_i^j - T_{i-1}^j}{\Delta x}\right] \qquad (3\text{-}26)$$

Re-arranging this equation so as to be used in the tri-diagonal matrix of the finite difference scheme we have the non-dimensional form

$$-\left(1 + \frac{k_r^L}{k}\right) T_{i-1} + \left(2 + \frac{\Delta x^2}{\alpha \Delta t} + \frac{k_r^L + k_r^R}{k}\right) T_i - \left(1 + \frac{k_r^R}{k}\right) T_{i+1} = \frac{\Delta x^2}{\alpha \Delta t} T_i^{j-1} \qquad (3\text{-}27)$$

In deriving the left hand boundary condition using this scheme, we consider a control volume which encompasses the volume of material bounded by the two left hand nodes, which are numbered 0 and 1. The time rate of change of energy content of this element can be expressed as

$$\frac{\rho c_p \Delta x}{2\Delta t}(T_0^j + T_1^j - T_0^{j-1} - T_1^{j-1}) \qquad (3\text{-}28)$$

The rate of heat transfer from the surface at node 0 is

$$h(T_0^j - T_\infty) \qquad (3\text{-}29)$$

The rate of conduction into the solid material is

in

law of

re-arra

diagona

non-di

In this

This be

Likewis

equatio

$$\frac{T_0^j - T_1^j}{\Delta x}(k+k_r) \tag{3-30}$$

Combining these three factors in accordance with the first law of thermodynamics we have

$$\frac{\rho c_p \Delta x}{2\Delta t}(T_0^j + T_1^j - T_0^{j-1} - T_1^{j-1}) + h(T_0^j - T_\infty) + \frac{T_0^j - T_1^j}{\Delta x}(k+k_r) = 0 \tag{3-31}$$

Re-arranging this equation so as to be used in the tri-diagonal matrix of the finite difference scheme we have the non-dimensional form

$$\left(\frac{\Delta x^2}{2\alpha\Delta t} + 1 + \frac{k_r}{k} + \frac{Bi}{N}\right) T_0^j + \left(\frac{\Delta x^2}{2\alpha\Delta t} - 1 - \frac{k_r}{k}\right) T_1^j = \frac{\Delta x^2}{2\alpha\Delta t}(T_0^{j-1} + T_1^{j-1}) + \frac{Bi}{N} T_\infty \tag{3-32}$$

In this equation, N refers to the number of spacial nodes. This becomes the first equation in the tri-diagonal matrix. Likewise, the right hand boundary condition becomes the last equation in the tri-diagonal matrix as

$$\left(\frac{\Delta x^2}{2\alpha\Delta t} + 1 + \frac{k_r}{k} + \frac{Bi}{N}\right) T_N^j + \left(\frac{\Delta x^2}{2\alpha\Delta t} - 1 - \frac{k_r}{k}\right) T_{N-1}^j = \frac{\Delta x^2}{2\alpha\Delta t}(T_N^{j-1} + T_{N-1}^{j-1}) + \frac{Bi}{N} T_\infty \tag{3-33}$$

In these equations, the radiant conductivity term is

$$k_r = \frac{2\sigma_b (T_0^{j-1} + T_1^{j-1})^3}{3\kappa} \qquad (3\text{-}34)$$

or

$$k_r = \frac{2\sigma_b (T_N^{j-1} + T_{N-1}^{j-1})^3}{3\kappa} \qquad (3\text{-}35)$$

as applicable.

The results of implementing this scheme are shown in Table 3-2, again using an imposed condition of zero surface heat loss in order to compare the radiative model accurately with the non-radiative model. As with the previous attempt at this solution, a value of $k_{r_o}/k=1$ is used in each case. In each solution, the final temperature is very close to one non-dimensional degree above the ambient temperature which is what is expected from the physical parameters of the problem. As in the previous case, the heat transfer takes place much more quickly at the higher ambient temperatures due to the greater effect of radiant conductivity. The non-dimensional time in this table is based on the kinetic conductivity only and is not affected by variations in radiant conductivity. The solutions are all generated by finite difference using 20 spacial nodes and a time step of

Table 3-2

Comparison of Direct Solutions Using Non-Radiative Model and Averaged Node Temperatures to Define k_r in Radiative Model.

NON-DIM TIME	NO RADIATION	T_∞^*=10	T_∞^*=100	T_∞^*=400
0.06	0.075954	10.075979	100.09284	400.88195
0.12	0.402901	10.402959	100.44162	400.99301
0.18	0.651622	10.651674	100.68633	400.99934
0.24	0.800543	10.800582	100.82657	400.99993
0.3	0.886319	10.886346	100.90445	400.99999
0.36	0.935278	10.935296	100.94739	400.99999
0.42	0.963161	10.963173	100.97104	401
0.48	0.979033	10.979041	100.98406	401
0.54	0.988067	10.988072	100.99122	401
0.6	0.993209	10.993212	100.99517	401
0.66	0.996135	10.996137	100.99734	401
0.72	0.9978	10.997801	100.99853	401
0.78	0.998748	10.998749	100.99919	401
0.84	0.999287	10.999288	100.99955	401
0.9	0.999594	10.999595	100.99975	401
0.96	0.999769	10.999769	100.99986	401
1.02	0.999869	10.999869	100.99992	401
1.08	0.999925	10.999925	100.99995	401
1.14	0.999957	10.999957	100.99997	401
1.2	0.999976	10.999976	100.99998	401

0.01 units of non-dimensional time. A comparison of the non-radiative model using finite difference and exact methods is shown in Chapter 2.

Figures 3-1 through 3-3 show examples of the direct solution for various cases. There are four basic parameters that can be varied for this model which have an effect on the direct solution. They are α, T_∞^*, Bi and k_{ro}/k. The three that offer the most insight are T_∞^*, Bi and k_{ro}/k. Varying α simply changes the time scale of the temperature

Non-Dimensional

Plot o

The e

exami

held a

the ou

tempera

Number

the spe

due to

dimensio

reaches

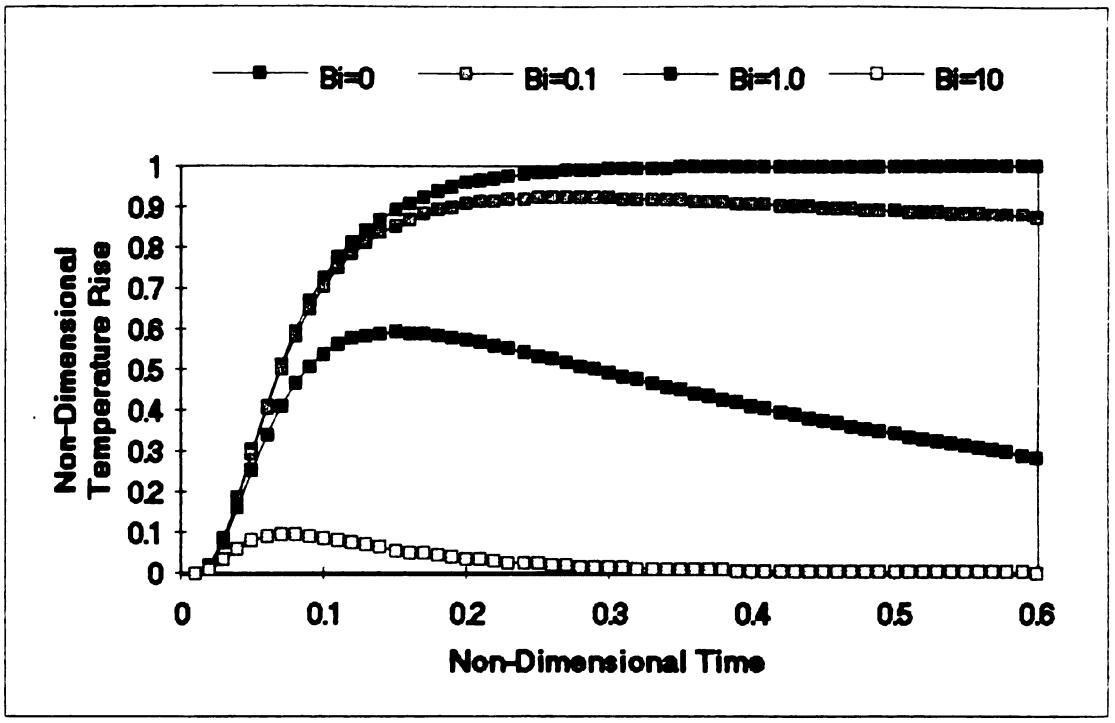

Figure 3-1 Non-Dimensional Temperature as a Function of Time $k_{\infty}/k=1.0$ $T_{\infty}^{*}=100$

plot of the non-heated side of the sample and little else. The effects of variations of the other parameters are examined throughout the remainder of this section with α held at unity.

Figure 3-1 shows the effect of varying Biot Number with the other parameters held constant. The non-dimensional temperature history at $x^{*}=1$ is shown in each case. A Biot Number of zero corresponds to an insulated condition, and the specimen is heated to a non-dimensional temperature of 1 due to the heat addition of the flash, which also has a non-dimensional magnitude of 1. None of the other cases ever reaches a temperature of 1 because of heat loss via

Non-Dimensional
Temperature Rise

correct

number

approxi

insulat

especia

energy

be condu

Fig

conducti

Parabete

conducti

Pure Kine

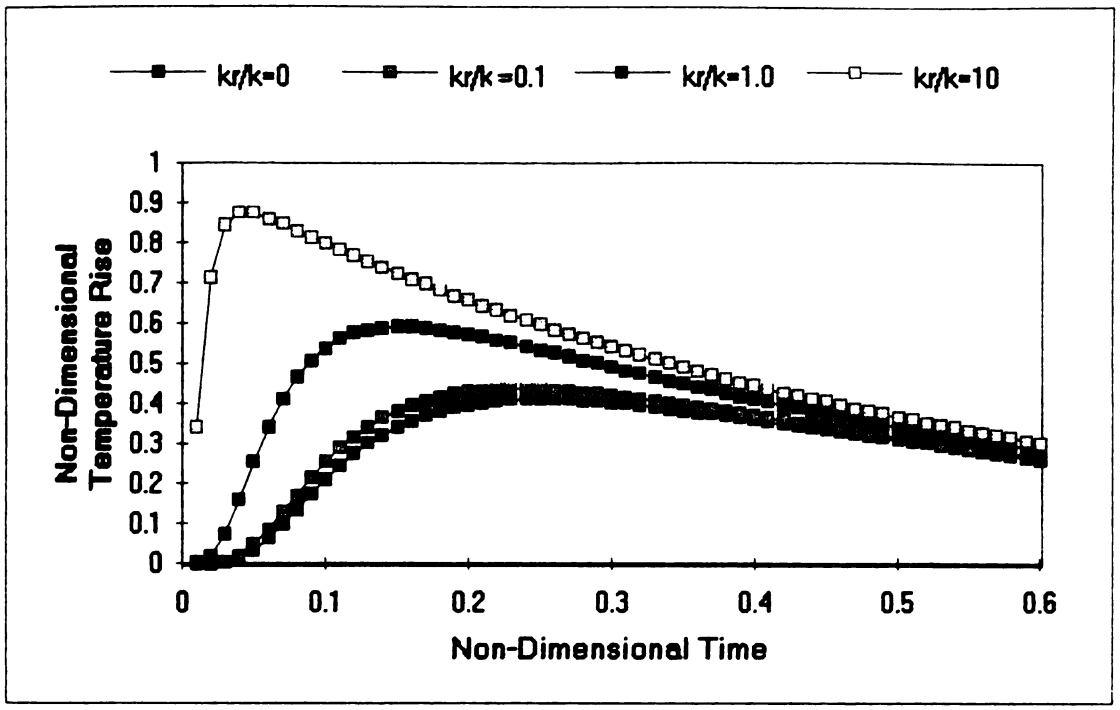

Figure 3-2 Non-Dimensional Temperature as a Function of Time Bi=1.0 T_-^*=100

convection. The most extreme case shown is with a Biot number of 10 where the maximum temperature reached is approximately one order of magnitude smaller than the insulated case. Due to the greater rate of heat loss, especially from the heated side of the specimen, most of the energy is transferred away from the material before it can be conducted to the non-heated side.

Figure 3-2 shows the results of allowing the conductivity ratio, k_{ro}/k, to vary while the other parameters remain constant. The limiting case with a conductivity ratio of zero corresponds to a condition of pure kinetic conduction with no radiant heat transfer. As

the conductivity ratio increases, the peak temperature becomes larger and occurs at an earlier time. The rate of heat transfer through the solid increases with an increasing conductivity ratio because, the addition of radiant heat transfer has the effect of adding a temperature dependent conductivity to the existing kinetic conductivity which is assumed to be independent of temperature. This effective increase in conductivity causes the faster response seen in the curves. The peak temperature becomes higher with increasing conductivity ratio because the dominant mechanism of heat transfer tends to be internal, by means of conduction and radiation, with comparatively less external convection. This causes the non-heated side of the specimen to receive more energy than in a case where convection is dominant and much of the heat is carried away from the heated surface before it can be transferred to the non-heated surface. An additional feature of the model which influences this phenomenon is that the Biot Number is based only on kinetic conductivity and not on the radiant conductivity. The internal heat transfer tends to dominate very quickly then, whenever the conductivity ratio is increased. In the limiting case of an extremely large conductivity ratio, the sample behaves much like a lumped system where the heating at the time of the flash is uniform

Non-Dimensional

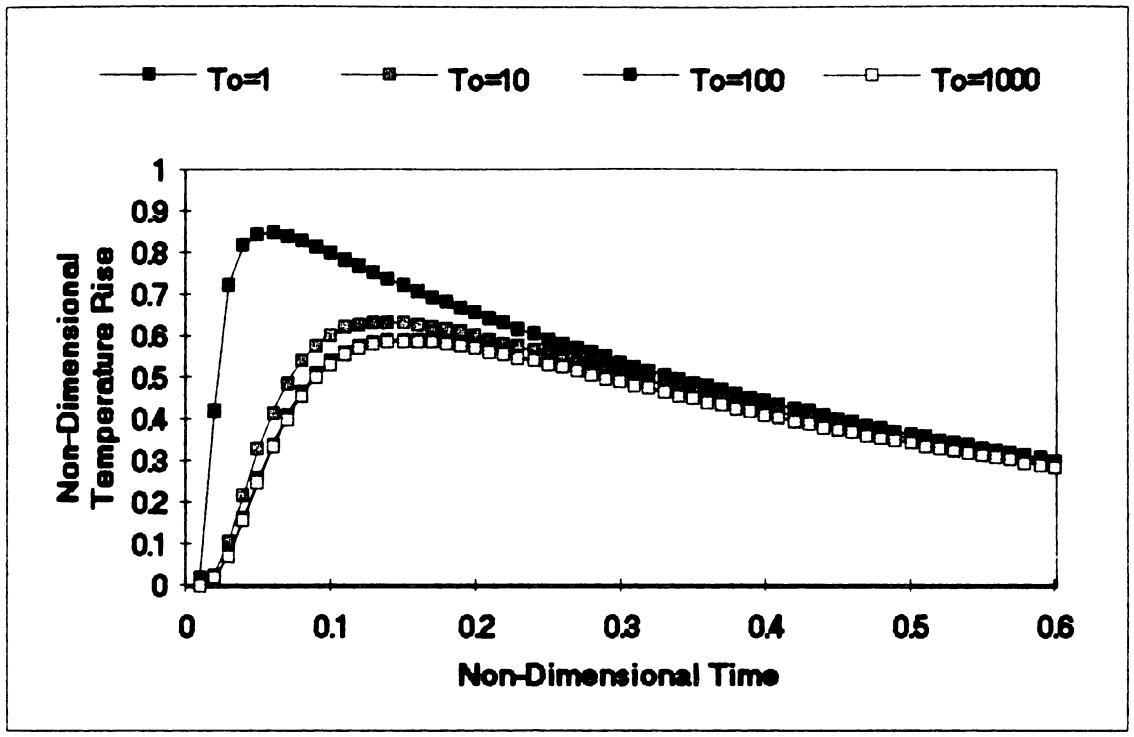

Figure 3-3 Non-Dimensional Temperature as a Function of Time Bi=1 $k_{to}/k=1$

throughout the material, causing the non-heated temperature to go to a non-dimensional value of one at the time of the flash and decaying due to convective losses thereafter. In such a case, it would not be possible to measure the diffusivity or radiative conductivity. In order to accomplish parameter estimation in such a case, it would be necessary to use a much thicker sample.

Figure 3-3 examines the case where T_{∞}^{+} is allowed to vary and the other parameters are held constant. With a value of T_{∞}^{+} at 10 or above, the results are all very similar since the temperature rise in the material is relatively small in these cases compared to the ambient

temperature. With $T_\infty^*=1$ on the other hand, the effects of an increased effective conductivity can be seen, similar to that observed in Figure 3-2. Since the temperature rise in the material is approximately on a par with the ambient temperature, the effect of the T^3 term in the equation for k_r/k causes this ratio to rise locally to extremely large values, even though the ratio based on ambient temperature is held the same in this example, as in the other curves. Although the condition of $T_\infty^*=1$ is not very realistic from an experimental point of view, it is a situation that makes extraction of the radiative conductivity parameter somewhat easier because its temperature dependence is much more pronounced. This fact highlights the necessity of utilizing very large heat pulse magnitudes at the higher temperatures in order to accomplish adequate parameter estimation.

Figures 3-4 through 3-6 are identical in all respects to Figures 3-1 through 3-3 except that the non-dimensional time is based on the sum of the radiant conductivity and the kinetic conductivity. In other words

$$t^* = \frac{t\left(\frac{k+k_r}{\rho C_p}\right)}{L^2} \qquad (3\text{-}36)$$

The most obvious difference that can be detected in Figures

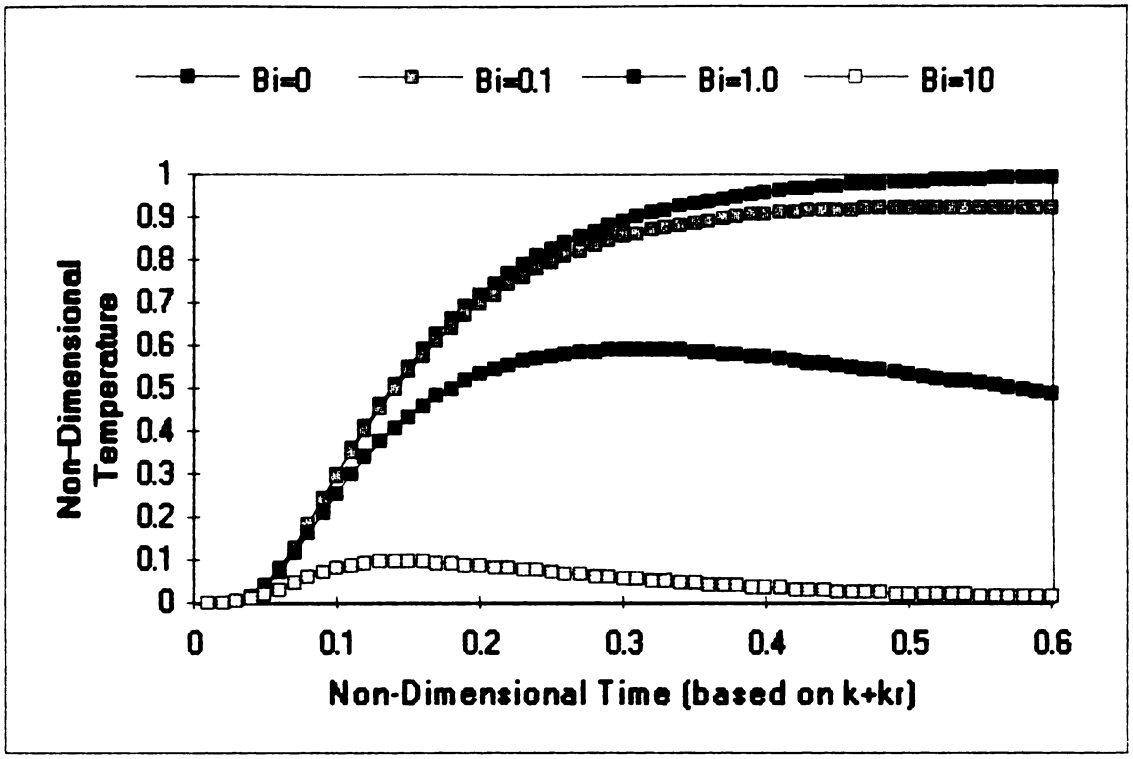

Figure 3-4 Non-Dimensional Temperature as a Function of Time $k_{ro}/k=1.0$ $T_-^*=100$

3-4 through 3-6 is that the time scale is essentially compressed by a factor of 2 because the effective conductivity in determining the non-dimensional time is twice the conductivity used to define non-dimensional time in Figures 3-1 through 3-3. That is, since k_{ro}/k is equal to one throughout both figures, the effective conductivity at ambient temperature is 2k.

Figure 3-4 is nearly identical in all respects to its corresponding Figure 3-1, with the exception of the different time scales noted above. As expected, the limiting case of Bi=0 corresponds to a rising temperature which becomes asymptotic on a non-dimensional value of 1.

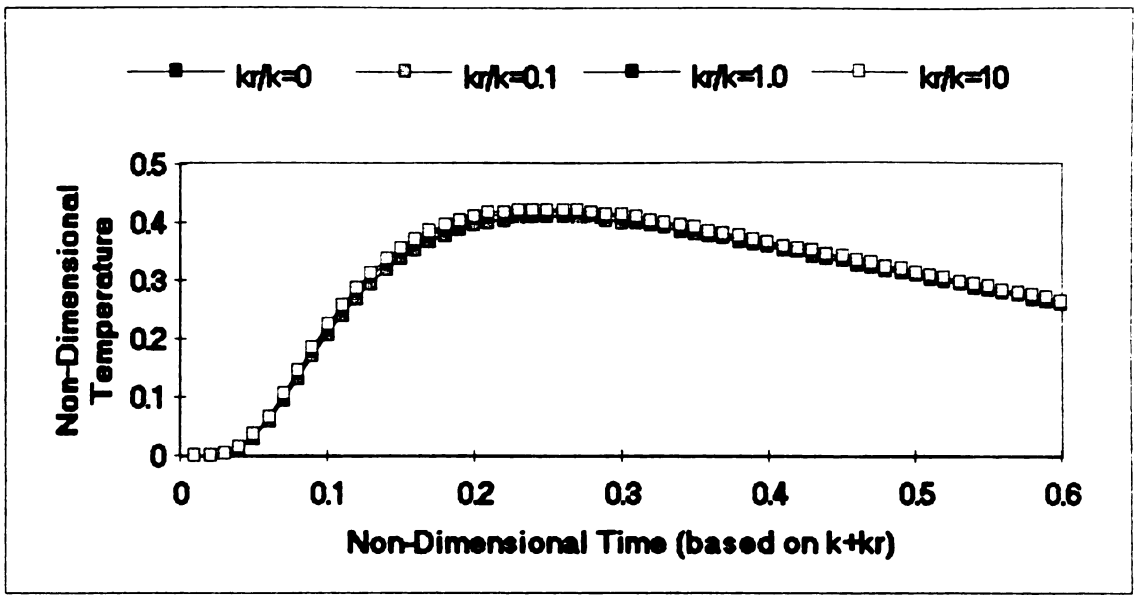

Figure 3-5 Non-dimensional Temperature Bi=1 T_-^*=100

The larger values of Biot number generate temperature curves which reach a peak point followed by a temperature decline due to heat loss.

Figure 3-5 is noticeably different from Figure 3-2 because the curves are virtually on top of one another in Figure 3-5. The only changing parameter between the family of curves in both of these figures is k_{ro}/k. Since the time scale is effectively shifted along with the effective change in conductivity in Figure 3-5, there is almost no difference between the four curves shown on this graph. The only detectable difference between the curves is that the higher k_{ro}/k curves show slightly higher temperatures than the lower k_{ro}/k curves. This is due to the higher rate of heat

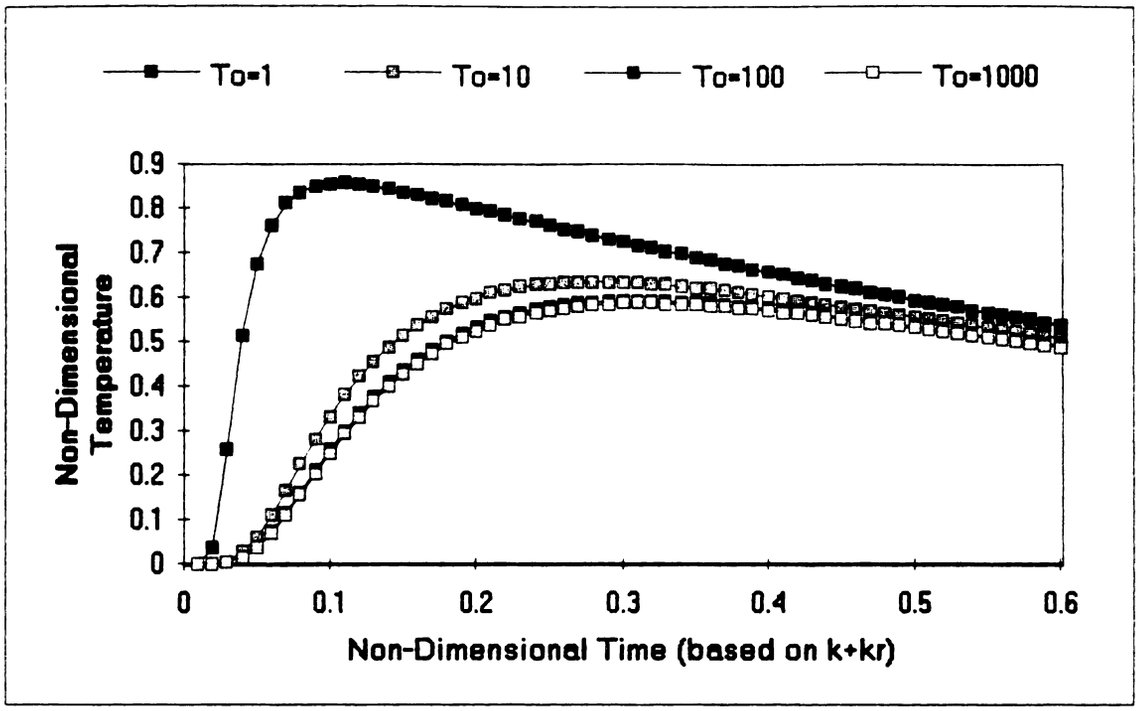

Figure 3-6 Non-Dimensional Temperature as a Function of Time Bi=1.0 k_∞/k=1.0

transfer in the localized areas of elevated temperature near the heated surface brought about by the temperature sensitive nature of the radiant heat transfer.

The curves in this figure would be slightly more varied between each other if a value of T_∞^+=1 were chosen rather than T_∞^+=100. The at the lower non-dimensional temperature, the temperature sensitive radiant conductivity would be more significantly affected by the proportionally larger pulse, thereby causing more of a distinction between curves of varying radiant conductivity.

This concept is illustrated somewhat by Figure 3-6 which again matches very closely its counterpart, Figure 3-3. With a small value of T_∞^+, the magnitude of the pulse

becomes more significant in the radiative transfer mechanism. For example, with $T_\infty^+=1$, the magnitude of the flash effectively doubles the absolute temperature of the material in low heat loss cases, making large temperature gradients inside the material. These large temperature gradients cause a significant impact on local value of the T^3 dependent radiative conductivity. The proportionally larger contribution from radiative conductivity causes heat transfer to be more rapid than in the higher T_∞^+ cases where the pulse heating is less significant.

3.4 PARAMETER ESTIMATION TEST PROBLEM

As with Model 1 discussed in Chapter 2, which did not account for internal radiation, the sensitivity coefficients are plotted below for Model 2. Figure 3-7 shows a plot of the modified sensitivity coefficients for a simulated experiment where the ratio between radiant conductivity and kinetic conductivity (k_{ro}/k) is 1.0, Biot number (Bi) is also 1.0 and non-dimensional ambient temperature (T_∞^+) is 1000. In this plot of sensitivity coefficients, the non-dimensional time is based on the kinetic conductivity only. With a small radiant conductivity, the sensitivity coefficients for this parameter are predictably small. The best experiment design pursuant to extraction of the unknown

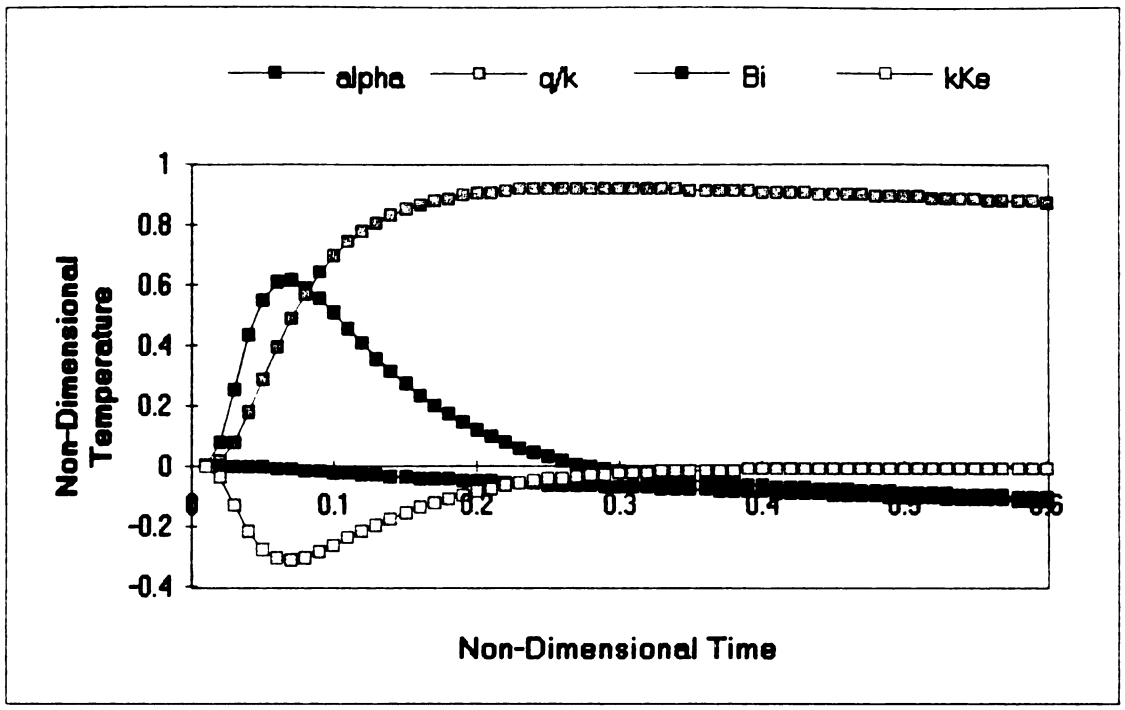

Figure 3-7 Sensitivity Coefficients $k_o/k=1$ $T_-^*=1000$ Bi=0.1

parameters, seems to be with the radiant conductivity approximately on a par with the kinetic conductivity. Of course, this is generally outside the experimentalist's control since it is a material property.

Following the calculation of the sensitivity coefficients, a program was developed to extract parameters from experimental data using the radiative model. The equations used in estimating parameters in the case with internal radiation, Model 2, are not as stable as when attempting to extract the parameters using the non-radiative Model 1. In the non-radiative test case, the parameter estimation method converged with initial parameter estimates

larger than actual parameter values by a factor of up to 3. Initial attempts at extracting parameters using the radiative model would not converge for initial estimates ranging only two percent above the actual values. Part of the reason for this is that solving 4 sets of simultaneous equations for 4 unknowns is inherently more unstable than solving 3 equations for 3 unknowns. More significantly, however, is the fact that the radiative conductivity is essentially a temperature dependent conductivity and is very difficult to separate from the kinetic conductivity when there is no appreciable change in temperature throughout the sample over the course of the experiment. This situation is known as correlation among the parameters. Evidence of this can be clearly seen in Figure 3-7 where the sensitivity coefficient curves for diffusivity and k_{ro}/k appear to be mirror images of each other. This is an undesirable condition in an experiment design because the cause of the unique shape of the measured data curve can be almost equally attributable to either of the two correlated parameters. This phenomenon is manifested in the sensitivity matrix in the final set of parameter estimation equations, making the equations very ill-conditioned.

As a quantitative comparison of the stability of Model 1 and Model 2, with regard to parameter estimation, it is

useful to examine the number of iterations required for convergence. The program developed as part of this research for this application, entitled "flash.exe", requires 9 iterations to reduce the difference between the actual parameter values and the estimated parameter values from 1 percent to 0.1 percent. Comparing this performance to that of the program using Model 1 with no radiation, a 100 percent deviation of initial parameter values may be reduced to 0.1 percent deviation in as few a 6 iterations.

In an effort to accentuate the effect of the radiant conductivity's temperature dependence, another test was performed at a non-dimensional ambient temperature T_∞^* equal to one. Physically, this means that the average rise in the temperature of the material is approximately equal to the absolute ambient temperature. This situation is somewhat unrealistic in an experimental situation, particularly at high ambient temperatures. For example, a test run at room temperature, 273K, would have to be heated to 546K in order to provide a unity value for T_∞^*. The results of this test were that the program was able to reduce a 10 percent initial deviation in all 4 parameters down to 0.1 percent in approximately 6 iterations. The actual values used in this test are shown in Table 3-3.

Table 3-3

Parameter Estimation with $T_\infty^+=1$

	Diffusivity	Heat Flux	Biot Number	k_{ro}/k
Actual Values	1	1	0.1	0.1
Initial Values	1.1	1.1	0.11	0.11
Estimated Values	0.9999977	1.0000008	0.1000018	0.1000016

As a further attempt to refine the process, a reduction was made in the number of parameters estimated in order to minimize the singular nature of the simultaneous equation used in finding the solution. The Model 1 parameter estimation procedure was used to analyze data which was generated using Model 2. It was discovered that the Model 1 parameter estimation procedure interpreted the radiant conductivity as kinetic conductivity, but that the heat flux value was properly estimated. The example shown in Table 3-4 illustrates this result.

Even with the initial parameter values set at 3 times the actual values, the solution converged within 5 or 6 iterations using Model 1 to estimate parameters from the fictitious data generated using the Model 2 direct solution. Since the radiant conductivity is not acknowledged by the Model 1 parameter estimation program, the kinetic and radiative conductivities are simply seen as one conductivity

Table 3-4
Parameter Estimation Using the Model 1 Procedure
on Model 2 Data

	Diffusivity	Heat Flux	Biot Number	k_{ro}/k
Actual Values	1	1	1	1
Initial Values	3.0	3.0	3.0	NA
Estimated Values	1.7265	1.05293	0.58275	NA

which is equal to the sum of k and k_{ro}. For this reason, the value of diffusivity is returned as twice the actual value and the Biot number is ½ of the actual value since diffusivity is directly proportional to conductivity and Biot number is inversely proportional to conductivity. The value of the heat flux, however, is preserved as approximately the correct value due to conservation of energy.

With this fact in mind, an attempt was made to recover 3 parameters using the Model 2 analysis instead of 4 parameters, assuming that the heat flux is known from the Model 1 analysis. The three unknown parameters in this case were

$$\beta_1=\alpha=\frac{k}{\rho c_p} \quad \beta_2=\frac{k_{ro}}{k} \quad \beta_3=Bi \tag{3-37}$$

This method of analysis, however, provided no improvement over the previous method of attempting to simultaneously analyze four parameters. With $T_\infty^*=1$, the method would not converge using exact data unless the initial seed parameter values were within 10 percent of the actual values. At $T_\infty^*=100$, the method would not converge using exact data unless the initial guess for the parameter values was within 1 percent of the actual values. In these test cases, the simulated experiment was errorless. Other combinations of conditions were tried with Biot number and k_{ro}/k equal to 1.0 and 0.1 with similar results. In no case was convergence obtained with an initial parameter guess of more than 10 percent above the actual parameter values. As discussed earlier in this section, the reason for this is the close correlation between the parameters of diffusivity and radiant conductivity, causing the final parameter estimation equations to be ill-conditioned. Without extremely accurate seed values for the parameters, even using errorless data, the parameter estimation problem is unstable.

Extending the investigation of the use of Model 1 to analyze simulated measurements generated using Model 2, several four-parameter direct solutions were generated. This was done in order establish the magnitude of the

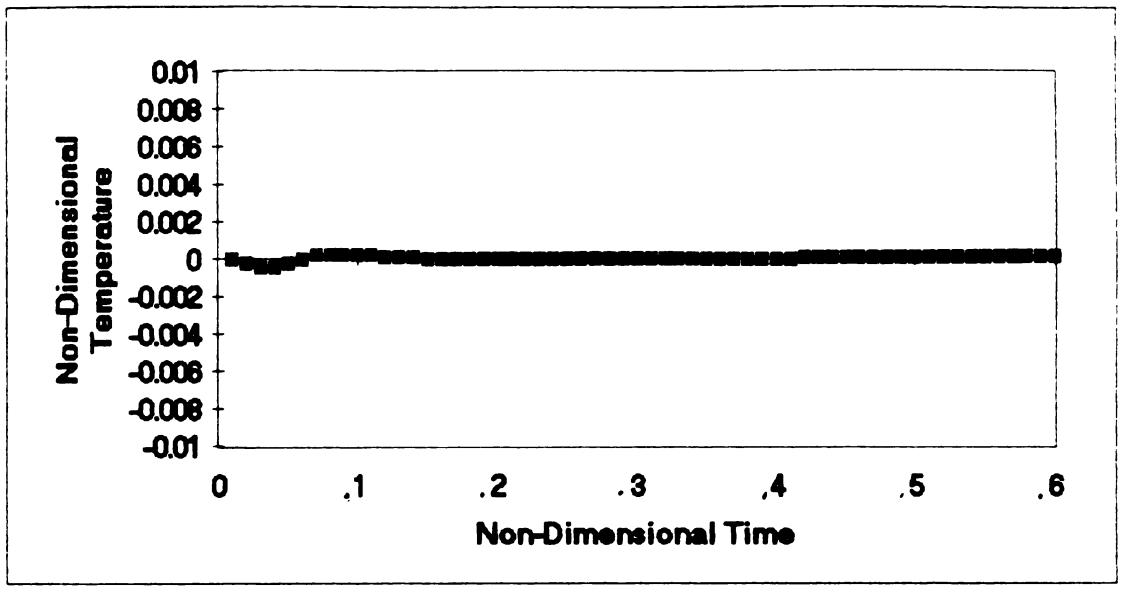

Figure 3-8 Residuals from Analyzing Model 2 Using Model 1 $k_{10}/k=1.0$ $T_\infty^*=100$ Bi=0.1

residual signature using a three-parameter estimating scheme in analyzing a four-parameter problem. Part of this analysis included an examination of how close the estimated parameters came to the known values from the direct solution.

The graph of the residuals, as shown in Figure 3-8, shows the extremely small residual signature resulting from this test problem. A small ripple, which shows up in the first 0.1 unit of time, is the only indication that the chosen model may not be perfectly suited to the experiment. At the maximum value, this ripple reaches a magnitude of 0.000245 with the nominal temperature measurements reaching a magnitude on the order of one. For this problem, the

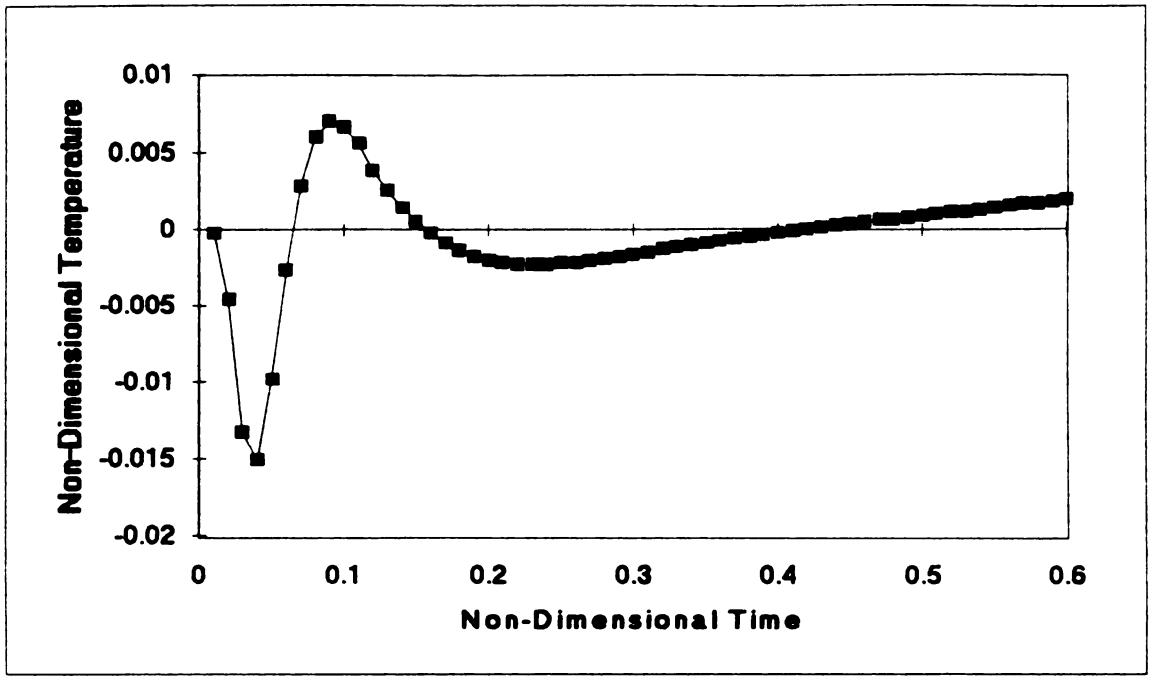

Figure 3-9 Residuals Using Model 1 to Analyze Model 2 k_w/k=0.1 T_-^*=1 Bi=1

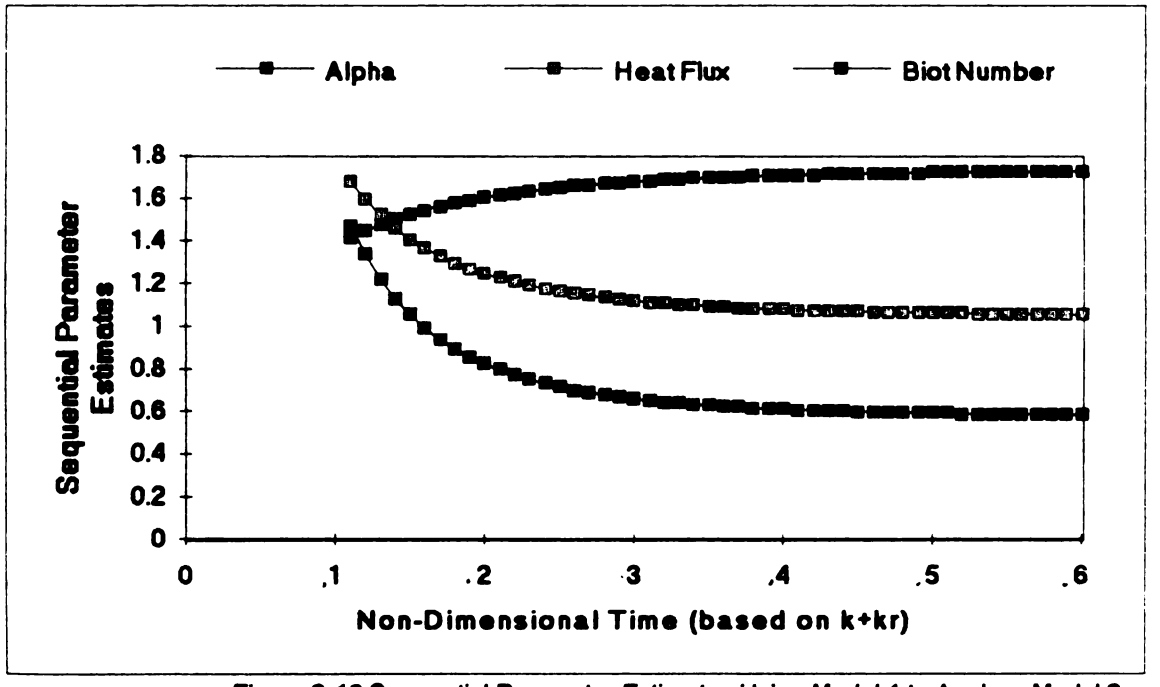

Figure 3-10 Sequential Parameter Estimates Using Model 1 to Analyze Model 2 k_w/k=0.1, T_-^*=1, Bi=1

actual versus estimated parameters were shown in Table 3-4

previously. Had the direct solution been unknown, this set of estimates would have given the impression that the model chosen was perfectly appropriate and that accurate parameters had been obtained.

A drastic change is noted when repeating the above procedure using the same parameters, but with $T_\infty^*=1$ instead of 100. At this level, the magnitude of the temperature rise due to the pulse heating is approximately equivalent to the ambient temperature. This causes the effects of internal radiation to be much more significant, even with the same k_{ro}/k ratio. Figures 3-9 and 3-10 show the residuals and the sequential estimates for this problem, respectively.

Although the residuals are much larger than in the case with $T_\infty^*=100$, they are still only 1.5 percent at the greatest and could still be masked by errors in a real experiment. In this example using exact data, there is an unmistakable signature, however this signature does not match the one shown in the residual curve from the actual data as shown in Chapter 2. In fact, the signature shown in the residual curve in figure 3-9 is nearly a perfect mirror image of the signature from actual data shown in Chapter 2. This seems to imply that internal radiation transport is not responsible for the signature in the residuals from the Oak

Ridge National Laboratory data.

3.5 ANALYSIS OF LABORATORY DATA

As stated in the previous section, the parameter estimation equations were found to be unstable even for errorless data and unrealistically accurate previous knowledge of the parameter values. Using derivative regularization, an attempt was made to analyze actual laboratory data measured at Oak Ridge National Laboratory. The sample measured in this experiment was Carbon Bonded Carbon Fiber (CBCF) as described in Chapter 2. The measurements were taken at an ambient temperature of 700°C. Analysis of this experiment indicated a poor fit of the internal radiation model to the laboratory data. The convergence criteria of 0.1 percent change or less for every parameter between iterations used in the three parameter model was not obtainable for the k_{ro}/k parameter. Although the other three parameters (α, q_0 and Bi) all converged, the k_{ro}/k parameter tended to hover between iterations from -.07 to -.05 without converging in one particular area. Worse yet, the negative value arrived at for k_{ro}/k is physically impossible since there can be no negative radiation. Further confirmation of this model incompatibility was evidenced by the fact that, forcing k_{ro}/k to be positive

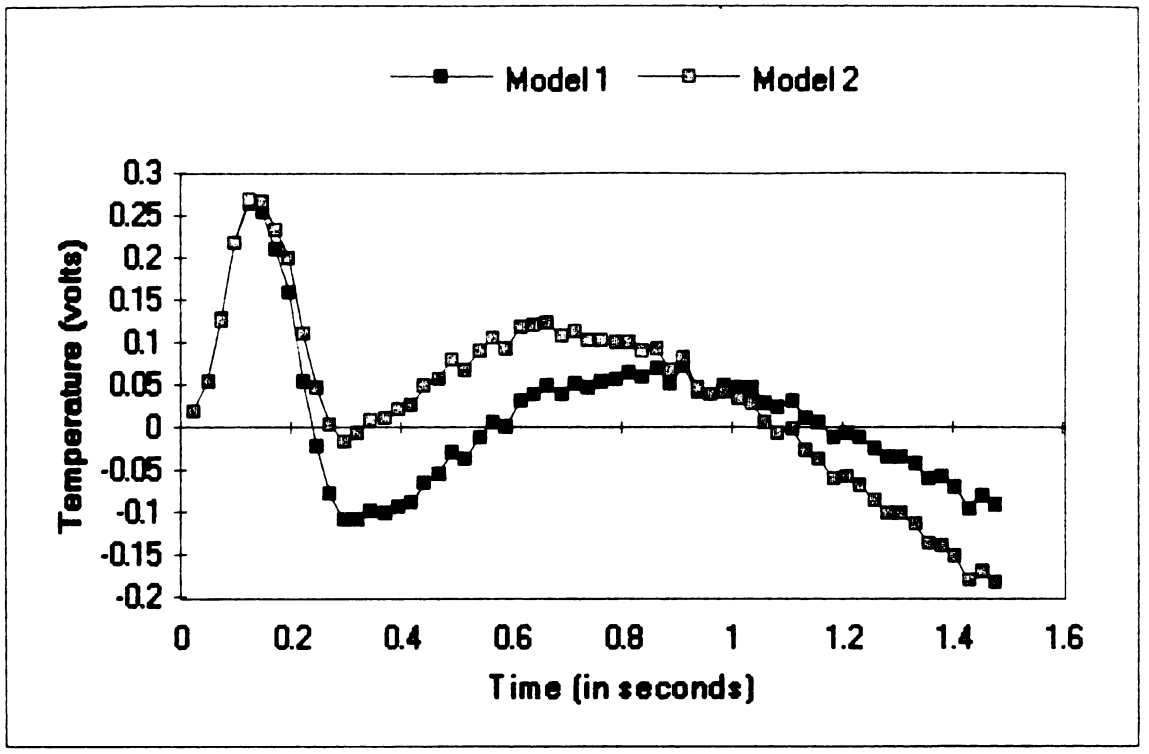

Figure 3-11 Residuals from CBCF Material at 700°C

resulted in non-converging parameters with k_{ro}/k driving to zero. Additionally, model non-comparability is shown by Figure 3-11. This figure compares the residual curves from the Oak Ridge National Laboratory data using Model 1, which assumes no internal radiation, and Model 2, assuming internal radiation. The internal radiation model provides no real improvement in the conformance of the calculated solution to the lab data. Additionally, the fact that the residual curves are mirror images of the known direct solution residual curve, casts serious doubt as to the responsibility of radiation for the residuals in the lab data. Table 3-5 shows the parameters arrived at by each

Table 3-5

Parameter Estimation Comparing Model 1 and Model 2 on actual data taken at 700°C

	Diffusivity	Heat Flux	Biot Number	k_r/k
Model 1	0.3703	16.131	0.9646	NA
Model 2	0.4201	15.206	0.8245	-.06

method. These factors seem to confirm that internal radiation is not evident in the experiment.

3.6 INTEGRO-DIFFERENTIAL APPROACH

A more rigorous model for the combined radiation and conduction problem, accounting for scattering absorption and emission in a gray medium, involves solving an integro-differential equation with appropriate boundary conditions. Considering the one dimensional energy equation,

$$\rho c_p \frac{\partial T}{\partial t} = \frac{\partial}{\partial x}\left(k\frac{\partial T}{\partial x} - q_r\right) \qquad (3\text{-}38)$$

the spacial derivative of the radiant heat flux can be written as given by ref [1] as follows, assuming non-spectrally dependent parameters with isotropic scattering

$$\frac{dq_r}{dx} = -2\pi\kappa\int_0^1 i^+(0,\mu)\exp(-\frac{\kappa x}{\mu})\,d\mu$$
$$-2\pi\kappa\int_0^1 i^-(L,-\mu)\exp(\frac{\kappa(x-L)}{\mu})\,d\mu$$
$$-2\pi\kappa\int_0^x I(x')E_1(x-x')\,dx'$$
$$-2\pi\kappa\int_x^L I(x')E_1(x-x')\,dx' + 4\pi I(x) \qquad (3\text{-}39)$$

The symbols in the above equations are as follows

κ = extinction coefficient $(a+\sigma_s)$

L = thickness of the sample.

x' = Dummy variable of integration.

$i^+(0,\mu)$ = Radiation intensity from the x=0 face into the material.

$i^-(L,-\mu)$ = Radiation intensity from the x=L face into the material.

μ = cos(θ) as measured from the normal to the surface.

$E_n(x)$ is defined in the following equation

$$E_n(x) = \int_0^1 \mu^{n-2}\exp(-\frac{x}{\mu})\,d\mu \qquad (3\text{-}40)$$

Finally, I(x), which is known as the "source equation", can be expressed as follows for isotropic scattering.

$$I(x) = (1-\Omega_0)\,i(x) + \frac{\Omega_0}{4\pi}\int_0^{4\pi} i(x,\omega)\,d\omega \qquad (3\text{-}41)$$

In this expression, Ω_0 is the albedo which is the ratio between the scattering coefficient and the sum of the absorption and scattering coefficients or

$$\Omega_0 = \frac{\sigma_s}{a+\sigma_s} \tag{3-42}$$

The denominator term, $a+\sigma_s$, is sometimes also known as the "extinction coefficient" as noted above. Using ϵ as the emissivity, the intensities shown in the above equations can be expressed as

$$i'(x) = \frac{\epsilon\sigma}{\pi} T^4(x) \tag{3-43}$$

and

$$\int_0^{4\pi} i'(x)\, d\omega = 2\epsilon\sigma T^4(x) \tag{3-44}$$

Using this method of modeling the local intensity, the source function can be simplified as

$$I'(x) = \epsilon\sigma T^4(x)\left(1-\frac{\Omega_0}{2}\right) \tag{3-45}$$

Using this term in the expression for radiant heat flux yields the following expression in T(x,t)

$$\frac{dq_r}{dx} = 4\sigma\kappa\epsilon\left[1-\frac{\Omega_0}{2}\right]T^4(x,t) - 2\sigma\kappa\epsilon\int_0^1(\eta_1-\eta_2)\,\mu d\mu$$
$$-2\sigma\kappa^2\epsilon(1-\frac{\Omega_0}{2})\int_0^L\int_0^1\eta_3 d\mu dx' \qquad (3\text{-}46)$$

where

$$\eta_1 = T^4(0,t)\exp\left(\frac{-\kappa x}{\mu}\right)$$
$$\eta_2 = T^4(L,t)\exp\left(\frac{\kappa}{\mu}(x-L)\right) \qquad (3\text{-}47)$$
$$\eta_3 = T^4(x',t)\mu^{-1}\exp\left(\frac{-\kappa}{\mu}|x-x'|\right)$$

If non-scattering conditions were to be considered, the scattering coefficient, σ_s is zero which causes Ω_0 to be zero. This causes the equation to match the non-scattering forms in references [8],[9] and [10]. With the radiant heat flux gradient now expressed as a function of temperature, the energy equation can now be expressed as a non-linear second order integro-differential equation in T(x,t).

$$\rho c_p\frac{\partial T(x,t)}{\partial t} = \frac{\partial}{\partial x}\left(k\frac{\partial T(x,t)}{\partial x}\right) - \frac{\partial q_r}{\partial x} \qquad (3\text{-}48)$$

This equation requires two boundary conditions and one initial condition in order to be solved. The initial condition is taken as $T(x,0)=T_\infty$ and the boundary conditions for the parameter estimation problem are

$$\left[-k\frac{\partial T}{\partial x}+q_r\right]_{x=0}=q_0\delta(t)+h[T_\infty-T_{x=L}]+\epsilon\sigma[T_\infty^4-T_{x=L}^4] \tag{3-49}$$

$$\left[-k\frac{\partial T}{\partial x}+q_r\right]_{x=L}=h[T_{x=L}-T_\infty]+\epsilon\sigma[T_{x=L}^4-T_\infty^4] \tag{3-50}$$

In a similar manner to the way the spacial derivative of q_r is written, q_r itself can be written as

$$\begin{aligned} q_r =& 2\sigma\epsilon a\int_0^1\{T^4(0,t)\exp(\frac{-ax}{\mu}) \\ & -T^4(L,t)\exp[\frac{a}{\mu}(x-L)]\}\mu d\mu \\ &+2\sigma\epsilon a(1-\frac{\Omega_0}{2})\int_0^x\int_0^1 T^4(x',t)\exp[\frac{a}{\mu}(x-x')]\,d\mu dx' \\ &-2\sigma\epsilon a(1-\frac{\Omega_0}{2})\int_x^L\int_0^1 T^4(x',t)\exp[\frac{a}{\mu}(x-x')]\,d\mu dx' \end{aligned} \tag{3-51}$$

This model requires that 6 parameters be evaluated, which makes it considerably more complex than Model 2 in that regard. The parameters are as follows

$$\beta_1=\alpha=\frac{k}{\rho c_p}\quad \beta_2=\frac{a\epsilon}{k}\quad \beta_3=\Omega_0\quad \beta_4=\frac{q_0}{k}\quad \beta_5=\frac{h}{k}\quad \beta_6=\frac{\epsilon}{k} \tag{3-52}$$

With the difficulty experienced in estimating four parameters in the previous model, it is unlikely that the more complicated model would be practical in estimating additional parameters. Moreover, since the diffusive model

is more appropriate for optically thick materials, the added complexity of the integro-differential solution is not warranted for this experiment.

CHAPTER 4

ALTERNATIVE MODELS WITHOUT INTERNAL RADIATION

4.1 INTRODUCTION

As shown in Chapter 3, the inadequacies of the three parameter model, which includes only diffusivity, heat flux and Biot Number, do not seem to be rectified by the inclusion of internal radiation as a mode of heat transfer in the model. In past research, other phenomena have been studied in order to rectify disparities between measured data and conventional kinetic conduction models.

One of these secondary mechanisms, which has been studied as non-Fourier conduction, is the concept of electron interaction. This mechanism, as put forth by Lin, Hwang and Chang [49], has to do with sub-micron regions of high thermal gradients over very short periods of time, on the order of picoseconds. This model attempts to account for heat transfer by electron interaction within a lattice and is most appropriately applied to thin films of highly conductive material, such as gold.

Since the Carbon Bonded Carbon Fiber (CBCF) material studied here was originally developed as a thermal insulator, other models are investigated as part of this

research in order to find alternatives to the conventional model presented in Chapter 2. The research presented here involves the development of other physical phenomenon which may explain the discrepancy between the calculated direct solution and the measured data from Oak Ridge National Laboratory. None of the models described in Chapters 2 and 3 has been able to adequately explain this disparity.

The remainder of this chapter explores various models in an attempt to more adequately describe the mechanisms of heat transfer taking place in the samples, thereby achieving greater assurance in the parameters estimated. Section 4.2 discusses a linearly temperature dependent conductivity model and a separate model in which the surface heat transfer is purely radiative instead of conductive. Various linear problems which assume constant parameters and some type of flash penetration into the material are discussed in Section 4.3.

In one such model, the assumed time of the flash is considered to have occurred prior to time zero. The time interval between the flash and time zero in this model is treated as a parameter. Also investigated are various forms of internal deposition of the flash which are treated as initial condition temperature distributions. Also discussed is the concept of surface transmissivity which addresses the

disproportionate amounts of heat deposited on the surface of non-homogeneous or coated materials. Section 4.3 also briefly identifies several models used in the development of the more preeminent models ultimately used in describing the observed phenomenon. The exact mechanisms of the flash penetration are dealt with in Section 4.4 wherein the extinction coefficient is shown to be related to the parameters calculated by the salient models. Finally, the models deemed most appropriate are utilized in Section 4.5 to analyze data from several laboratories around the world, comparing the various thermal parameters.

4.2 NON-LINEAR TEMPERATURE DEPENDENT MODELS

Pursuant to the notion that the signature in the residuals may be due to a simple temperature dependent conductivity rather than an internal radiation phenomenon, a direct model was developed which assumed a linear dependence of conductivity on temperature with no internal radiation. The differential equation for this model is

$$\rho c_p \frac{\partial T}{\partial t} = \frac{\partial}{\partial x}\left[\left(k_0 + k_1 (T - T_\infty)\right)\frac{\partial T}{\partial x}\right] \qquad (4\text{-}1)$$

where k_0 and k_1 are coefficients of a linearly temperature-dependent conductivity with units of W/mK and W/mK^2,

respectively. The boundary conditions for this model are as follows

$$-\left(k_0+k_1(T_{x=0}-T_\infty)\right)\left.\frac{\partial T}{\partial x}\right|_{x=0} = q_0\delta(t)+h(T_\infty-T_{x=0}) \qquad (4\text{-}2)$$

$$-\left(k_0+k_1(T_{x=L}-T_\infty)\right)\left.\frac{\partial T}{\partial x}\right|_{x=L} = h(T_{x=L}-T_\infty) \qquad (4\text{-}3)$$

The initial condition for this problem is assumed to be $T=T_\infty$. This problem was solved in a similar manner to the model for internal radiation using a finite difference method.

The direct solution generated by this temperature sensitive conductivity model was analyzed using the three-parameter Model 1 in order to estimate parameters. The direct parameters used and the parameter estimates are shown in Table 4-1. Figures 4-1 and 4-2 show graphs of the sequential parameters and the residuals, respectively, for this parameter estimation problem. Like the internal radiation case discussed in Chapter 3, the sequential parameter graph shows that the parameter estimation model is not well suited for the simulated laboratory data. The sequential parameters are not constant toward the end of the experiment indicating a mismatch between the direct solution and the model used in parameter estimation. Moreover, the graph of the residuals does not at all

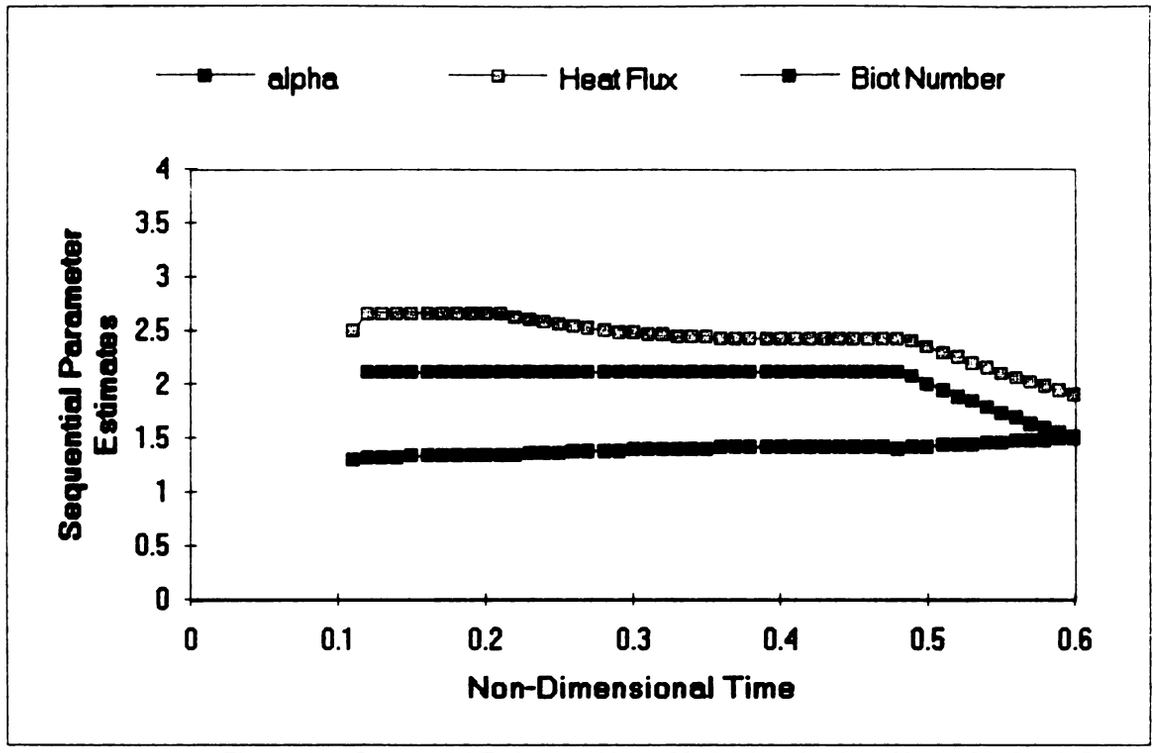

Figure 4-1 Sequential Estimates Using Model 1 to Analyze Model 3 k_1/k_0=1, Bi=1

Table 4-1

Parameter Estimation Using the Model 1 Procedure on Model 3 Data

	Diffusivity	Heat Input	Biot Number	k_1/k_0
Actual Values	1	1	1.0	1.0
Estimated Values	1.4936	1.9006	1.5064	NA

resemble the graph of residuals shown in Chapter 2 for the actual experimental data. This set of results seems to indicate that the linearly temperature dependent conductivity is not a reasonable explanation for the behavior observed in the Oak Ridge National Laboratory experiments.

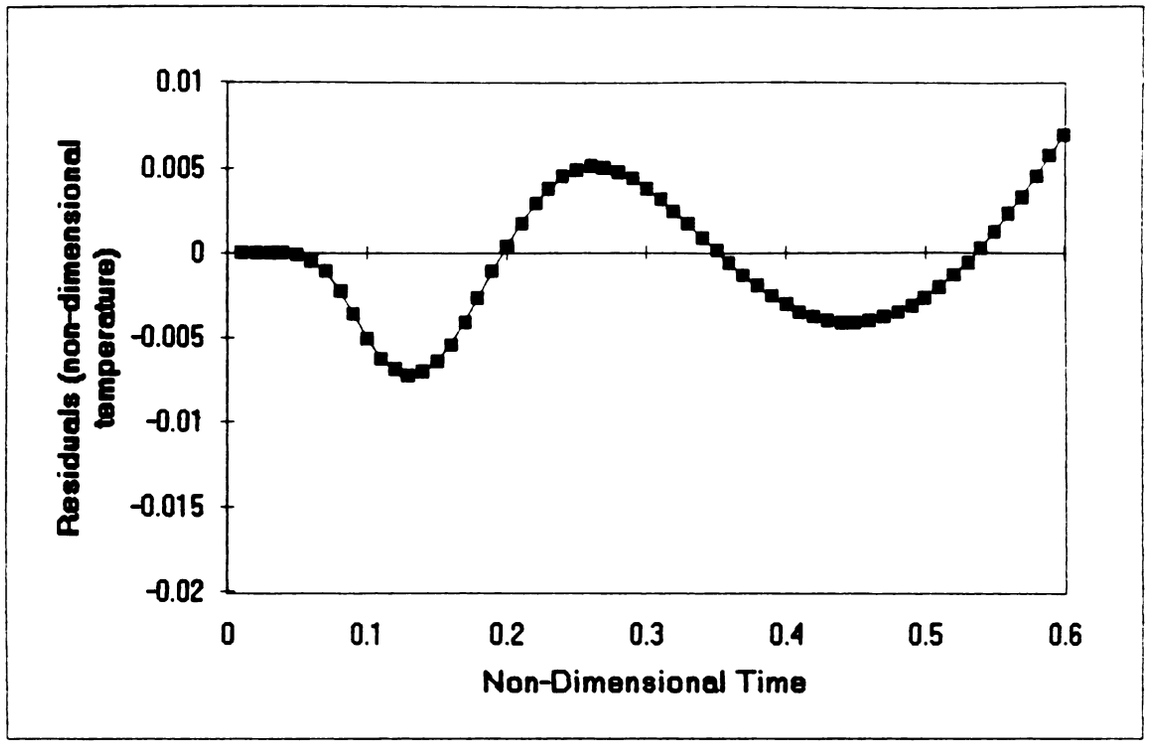

Figure 4-2 Residuals Using Model 1 to Analyze Model 3 k_t/k_o=1, Bi=1

Figure 4-3 shows a comparison of residuals from actual data as measured at Oak Ridge National Laboratory with the CBCF sample at 700°C. The two sets of residuals are generated from Model 1, which assumes conventional kinetic conduction with constant conductivity, and Model 3 which assumes a linearly temperature dependent conductivity. Once again, there is no real improvement in the fit of Model 3 over Model 1. This is to be expected since the residual curve of the exact solution of Model 3, when analyzed with Model 1, does not match the residual curve signature from the laboratory data when analyzed by Model 1.

Another possible explanation for the residual behavior

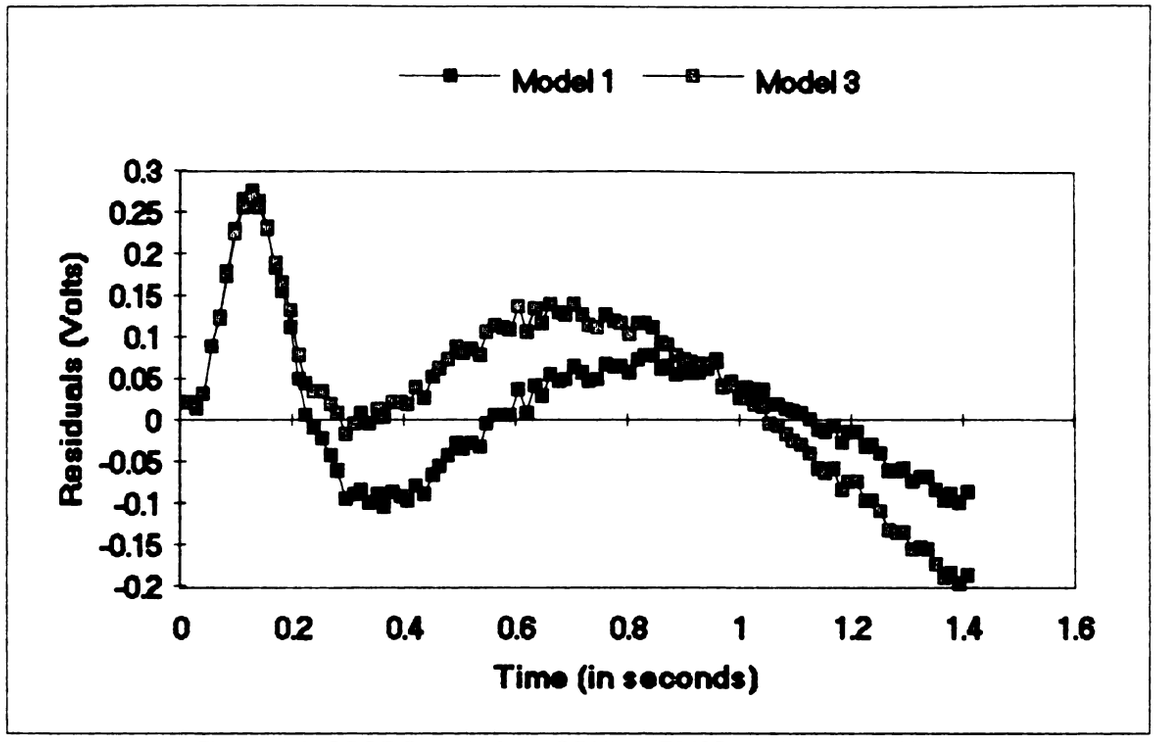

Figure 4-3 CBCF Sample from ORNL at 700°C Analyzed with Model 1 and Model 3

exhibited in the Oak Ridge experiments is that the dominant mode of heat transfer at the surfaces is radiation as opposed to convection. At the higher temperatures of 700°C, it may be likely that the model used in estimating parameters was not properly accounting for this. A direct solution was generated utilizing a constant kinetic conductivity in the material continuum and pure radiation at the surfaces. The differential equation for this problem is

$$\rho c_p \frac{\partial T}{\partial t} = k \frac{\partial^2 T}{\partial x^2} \qquad (4\text{-}4)$$

and the boundary conditions are

Table 4-2

Parameter Estimation Using Model 1 to Analyze Surface Radiation Model Data

	Diffusivity	Heat Input	Biot Number	ϵ
Actual Values	1	1	NA	1.0
Estimated Values	0.938	1.607	10.87	NA

$$-k\left[\frac{\partial T}{\partial x}\right]_{x=0} = q_0\delta(t) + \epsilon\sigma_b(T_\infty^4 - T_{x=0}^4) \qquad (4\text{-}5)$$

$$-k\left[\frac{\partial T}{\partial x}\right]_{x=L} = \epsilon\sigma_b(T_{x=L}^4 - T_\infty^4) \qquad (4\text{-}6)$$

where ϵ represents the surface emissivity of the sample. The initial condition for this problem is assumed to be $T=T_\infty$. A finite difference scheme was used which was similar to the internal radiation model in order to generate the direct solution. As in the cases above, this direct solution was analyzed by the three-parameter model. Table 4-2 shows the direct solution parameters and the estimated parameters for this problem

Figures 4-4 and 4-5 show graphs of the residuals and sequential parameters for this problem, respectively. The sequential parameter estimates give some indication that the model is not completely appropriate for the data, particularly in the Biot number curve where the value drops off with time toward the end. The residual curve, however,

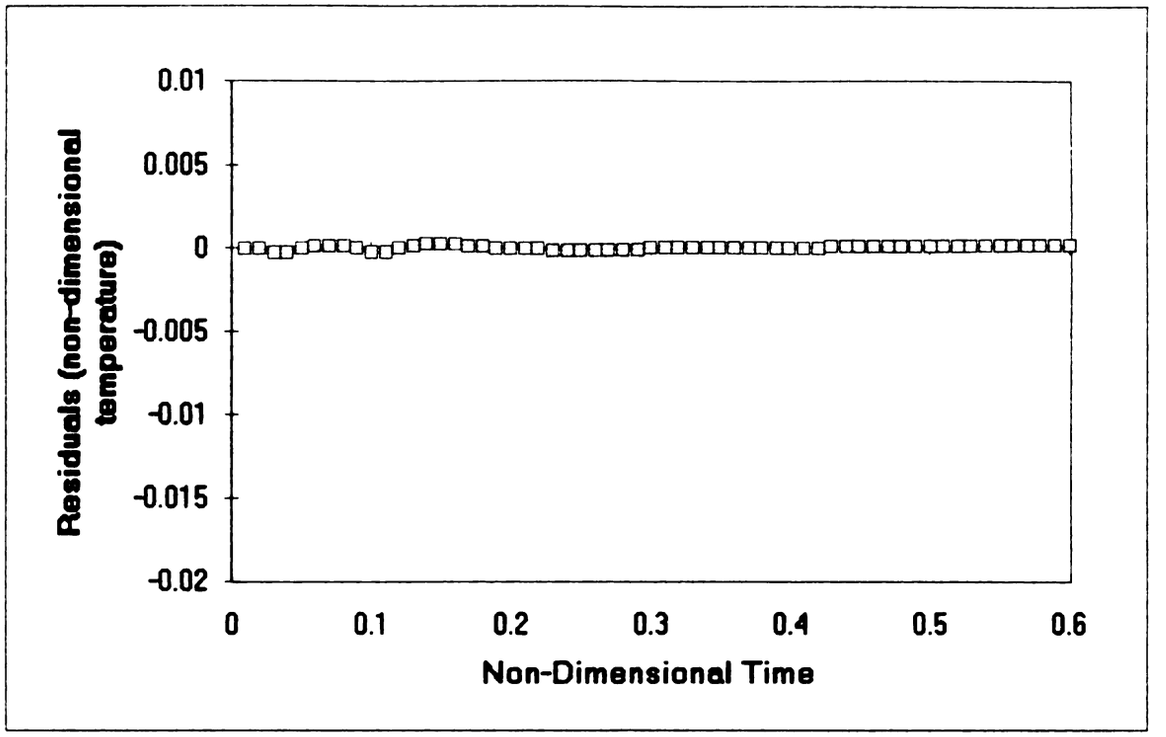

Figure 4-4 Residuals Using Model 1 to Analyze a Surface Radiation Direct Solution (α=1, Bi=1)

gives virtually no indication that there is any deviation between the data and the estimate. The largest individual residual in this case is approximately .02 percent of the maximum temperature measurement. This model does not seem to explain the phenomenon observed in the Oak Ridge National Laboratory measured data.

4.3 VARIOUS INITIAL CONDITION MODELS

In contrast to modeling a temperature-dependent variable as an explanation for the behavior exhibited by the Oak Ridge National Laboratory data, an attempt was made as part of this research to explain the departure from the

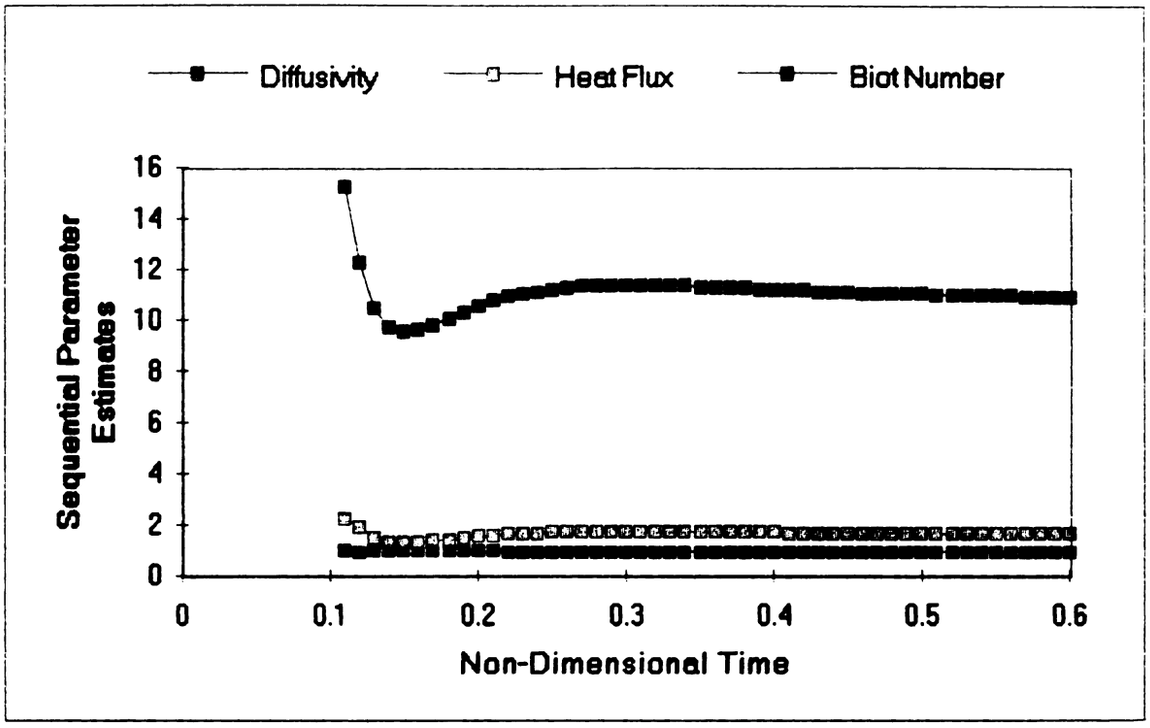

Figure 4-5 Sequential Estimates Using Model 1 to Analyze a Surface Radiation Direct Solution (α=1, Bi=1)

conventional model in terms of the penetration of the flash at the moment of heating. This principle assumes that the flash penetrates the sample and is instantaneously absorbed by the material internally. This distribution of energy at the time of the flash can effectively be modeled as an initial condition.

4.3.1 INITIAL TIME SHIFT, MODEL 4

A simple attempt at duplicating the signature in the Oak Ridge National Laboratory measured data was pursued by shifting the time scale of the measured data by an amount, designated as Δt, from the given "time zero" of the

experiment. In this case, an exact solution was used of the differential equation described in Chapter 2 and was simply offset by a pre-determined Δt. This time shift served to effectively advance the time of the heating pulse prior to time zero. In order to estimate an accurate effective time shift of the heating pulse, the quantity Δt was treated as a parameter.

Another way of considering the time-shift model, designated as Model 4, is to think of it as an initial condition of penetrated heating. This initial temperature distribution happens to have a form which is somewhat similar to an exponential temperature distribution. As in the cases above, this direct solution was analyzed by the three-parameter model. Table 4-3 shows the direct solution parameters and the estimated parameters for this problem. A considerable error of 14 percent arises in the estimated value for diffusivity due to the introduction of the time offset of .01 units of non-dimensional time. The time shift toward early heating seems to be a phenomenon by which the more rapid initial heat transfer could be manifest in the actual laboratory experiment.

The actual laboratory data from Oak Ridge National Laboratory was also analyzed using Model 4. The standard deviation of these residuals is 0.009935 which is extremely

Table 4-3

Parameter Estimation Using the Model 1 Procedure on a Model 4 Direct Solution

	Diffusivity	Heat Flux	Biot Number	Δt
Actual Values	1	1	1	0.01
Estimated Values	1.144	0.9102	0.8314	NA

small in comparison with measurements which are typically on the order of 6. By comparison, the standard deviation of the residuals generated from using Model 1 as the mathematical model are approximately 0.04, over 4 times the magnitude as compared with Model 4.

The most significant aspect of this analysis is that the estimates of the parameters of interest are significantly altered between Model 1 and Model 4. The estimate for diffusivity is 26 percent lower and Biot number is 65 percent higher using model 4 as opposed to Model 1. As can be seen from the residuals, the estimates using Model 4 appear to be the most valid of any of the models applied thus far.

4.3.2 EXPONENTIAL INITIAL DISTRIBUTION, MODEL 5

Assuming that the Oak Ridge National Laboratory data was recorded accurately and that there is no time shift

between the measurement time scale and the true time scale, then a logical physical explanation for the apparent time shift is radiation penetration. More specifically, even though there seems to be no evidence of internal radiation as a heat transfer mechanism subsequent to the flash, it is still possible that the radiation wavelength of the flash itself is such that a non-negligible mean free path exists inside the material for photons of that energy. The manifestation of this phenomenon would be best modeled as an initial condition since the flash takes place over such a short period of time. This model is very similar to Model 4 in terms of a non-uniform initial temperature distribution, but is based on a much more reasonable physical explanation as to its origin.

As a first attempt at modeling this phenomenon, an exponential distribution was chosen since this most closely corresponds to the principle embodied in Bouger's Law, as discussed in reference [1]. The mechanism of this absorption is also modeled in Section 4.4. In order to calculate the direct solution for this model, a Green's function solution was chosen for convective conditions at both boundaries and zero ambient temperature. The Green's function solution equation for this problem reduces to a single integral for the initial condition of

$$T(x,t)=\int_{x'=0}^{L} G_{X33}(x,t|x',0)\,F(x')\,dx' \qquad (4\text{-}7)$$

where F(x') is the initial temperature distribution in the material, or in this case

$$F(x')=\frac{q_0\, e^{-\frac{x'}{a}}}{\rho c_p a\left(1-e^{-\frac{L}{a}}\right)} \qquad (4\text{-}8)$$

where *a* is a measure of the penetration of the flash. The denominator of this term is arrived at by normalizing the exponential temperature distribution to the magnitude of the heating that brought about the temperature rise. In this case

$$q_0=\rho c_p \int_{x=0}^{L} F(x)\,dx \qquad (4\text{-}9)$$

The F(x) defined above satisfies this equation. The Green's function for X33 is given as

$$G_{X33}(x,x'|\,t-\tau)=\frac{2}{L}\sum_{m=1}^{\infty} e^{-\beta_m^2\alpha(t-\tau)/L^2}\,A_m(x)A_m(x') \qquad (4\text{-}10)$$

where

$$A_m(x)=\frac{\beta_m\cos\left(\beta_m\frac{x}{L}\right)+Bi\,\sin\left(\beta_m\frac{x}{L}\right)}{\beta_m^2+Bi^2+2Bi} \qquad (4\text{-}11)$$

and

$$A_m(x') = \beta_m \cos\left(\beta_m \frac{x'}{L}\right) + Bi \sin\left(\beta_m \frac{x'}{L}\right) \tag{4-12}$$

Integrating Equation (4-7) we have

$$T(L,t) = \frac{2q_0\alpha}{kLa(1-e^{-L/a})} \sum_{m=1}^{\infty} e^{-\beta_m^2 \alpha t/L^2} C_1 (C_2 - C_3) \tag{4-13}$$

where

$$C_1 = \frac{\beta_m [\beta_m \cos(\beta_m) + Bi \sin(\beta_m)]}{\left(\beta_m^2 + Bi^2 + 2Bi\right)\left(\frac{1}{a^2} + \frac{\beta_m^2}{L^2}\right)} \tag{4-14}$$

$$C_2 = \left(\frac{\beta_m^2}{L} - \frac{Bi}{a}\right) e^{-\frac{L}{a}} \sin(\beta_m) \tag{4-15}$$

$$C_3 = \left(\frac{\beta_m}{a} + \frac{\beta_m Bi}{L}\right)\left(e^{-\frac{L}{a}} \cos(\beta_m) - 1\right) \tag{4-16}$$

Figure 4-6 displays the sensitivity coefficients for the exponential penetration model, Model 5. The sensitivity coefficient for the penetration parameter, *a*, appears to be somewhat correlated with the diffusivity sensitivity coefficient. Experience has shown, however, that it is different enough to allow independent estimation of the four parameters. In spite of the apparent correlation between

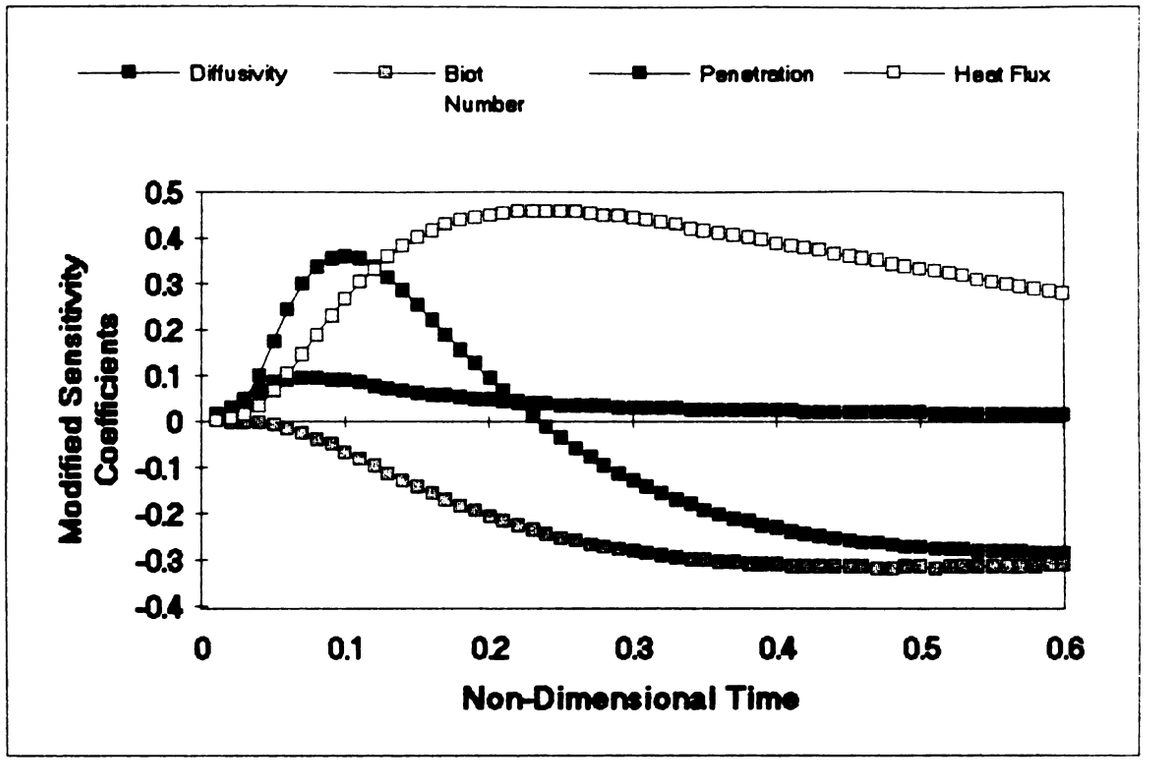

Figure 4-6 Modified Sensitivity Coefficients for Model 5 (alpha=1, Bi=1, a=0.1)

diffusivity and *a*, and between heat flux and Biot Number, the parameter estimates converged without the benefit of using derivative regularization.

Next, Models 1, 4 and 5 were tested on CBCF data measured at 700°C at Oak Ridge National Laboratory. In contrast to the first three models, the standard deviation of the residuals for Model 4, which treats the time-shift of the heating pulse as a parameter, gives significantly improved results over each of the other models. Table 4-4 shows the parameters arrived at by each method. A large reduction in residuals is gained in implementing the time-shift model, Model4, over the simple three-parameter Model.

Table 4-4

Parameter Estimation Comparing Models 1,4 and 5
on actual data taken at 700°C

Model	Diffus-ivity	Heat Flux	Biot Number	At or a	Resid
1	0.3400	19.138	1.2765	NA	0.03202
4	0.3027	22.203	1.5550	0.0121	0.01212
5	0.3066	19.753	1.5178	0.0682	0.01098

Additional gains are realized when utilizing the exponential penetration feature of Model 5. The results using Models 4 and 5 are somewhat similar in that both return lower values for diffusivity than the simpler Model 1. The estimated Biot number is also higher in each of these cases than that calculated by Model 1. These factors suggest that both models are, to some extent, accomplishing the same thing through different means. That is, they both model a more rapid heat transport in the early times than would be predicted by the conventional Model 1 assumptions.

It can be instructive to test the shape of the residuals generated when using Model 1 to analyze a direct solution generated from the time shift or penetration models. Using each of these models as a direct solution and analyzing them using Model 1, the signatures of the residuals are very similar to one another and to the signature generated when analyzing the laboratory data with Model 1. Figure 4-7 shows a comparison of Models 4 and 5 as

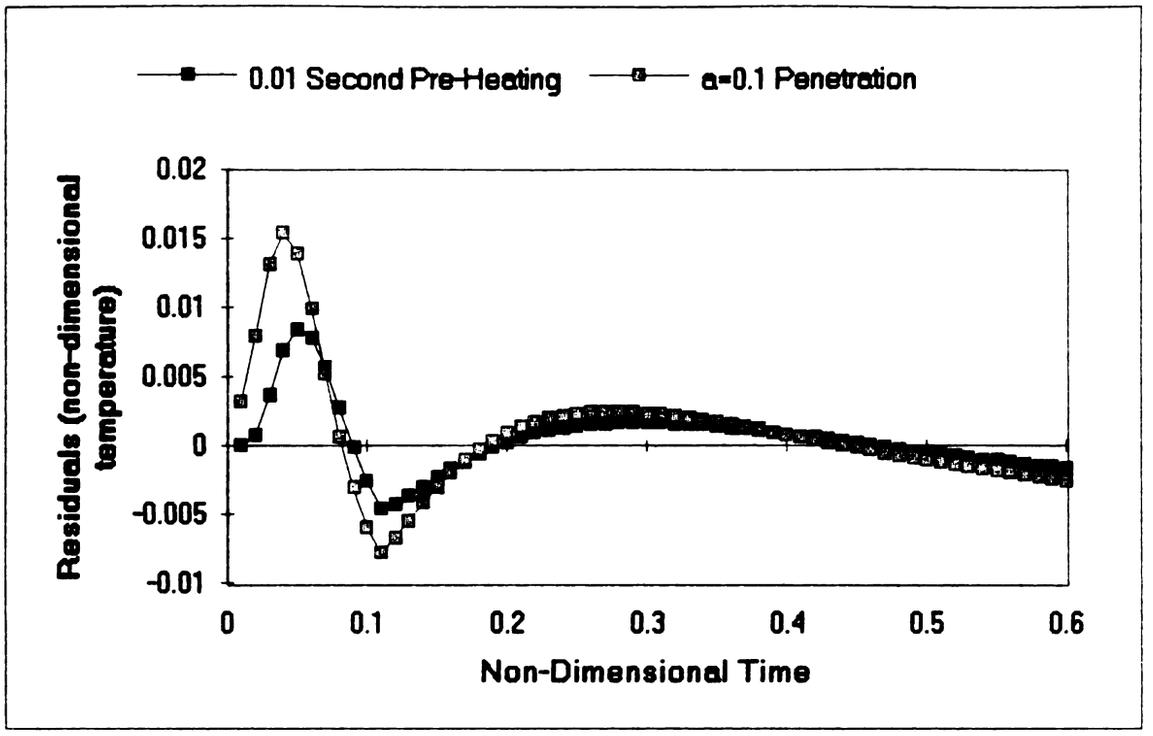

Figure 4-7 Using Model 1 to Analyze Direct Solutions of Models 4 and 5 (α=1, Bi=1)

analyzed by Model 1. In this example, a value of $\Delta t=0.01$ is used in the direct solution generated from Model 4 and a value of $a=0.1$ is used in Model 5.

In using Model 5 on actual laboratory data, Figure 4-8 shows residuals for the Oak Ridge National Laboratory data. This figure shows a near-elimination of the signature resulting from Model 1. The signature, generated from the Model 1 analysis of the laboratory data, is evidently caused by some manner of penetration of the flash into the material at the instant of heating.

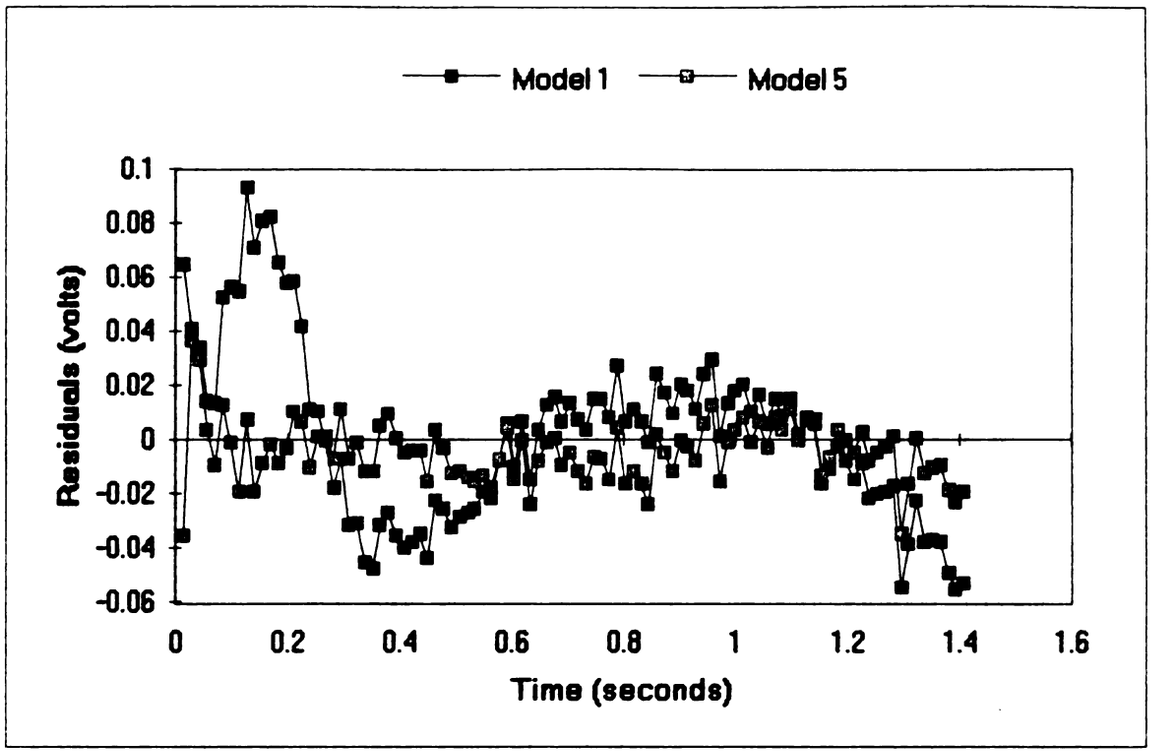

Figure 4-8 CBCF Sample from ORNL at 700°C Analyzed with Model 1 and Model 5

4.3.3 VARIOUS INITIAL CONDITIONS, MODELS 6-16

Following the development of Model 5, a series of models were studied which use various initial conditions based on the premise that the radiation from the flash penetrates the surface of the material. The pursuit of the best approximation for the distribution of this energy becomes the primary objective in the development of these subsequent models. The desired outcome is to minimize the residuals and, in particular, eliminate any characteristic signature.

A summary of Models 1-4 is as follows

Model 1 Conventional conduction using only the

three basic parameters of diffusivity, heat flux and Biot number.

Model 2 — Combined internal radiation and conduction as described in Chapter 3.

Model 3 — Linear temperature variable conductivity with the fourth parameter being the rate of change of thermal conductivity as a function of temperature.

Model 4 — Time shift at the time of the heating pulse with the fourth parameter being the magnitude of the time shift.

The remainder of the models studied as part of this research involve various forms of initial temperature distributions with conventional conduction thereafter. The initial conditions assumed for Models 5 through 16 are graphically presented in Figures 4-9 through 4-20. The corresponding parameters to be estimated are shown. In each case, the initial condition parameters were estimated simultaneously with the three basic parameters from Model 1, namely α (thermal diffusivity), q_o (heat pulse magnitude), and the Biot Number. The additional parameters in each model range in number from 1 to 3, so that the number of simultaneously estimated parameters ranges from 4 to 6. None of these

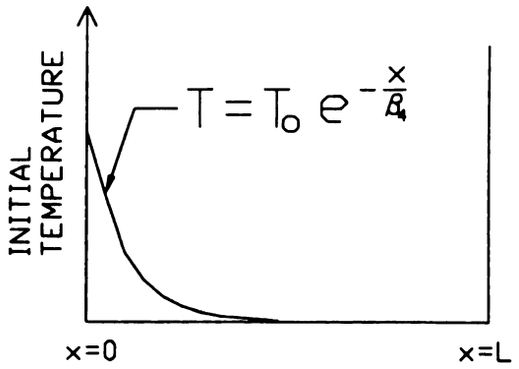

Figure 4-9 (Model 5) Exponential distribution of initial penetration of the flash in the material with the fourth parameter measuring the degree of penetration. In this and subsequent models, the term T_o is not needed since this temperature is indirectly prescribed by the heat flux parameter.

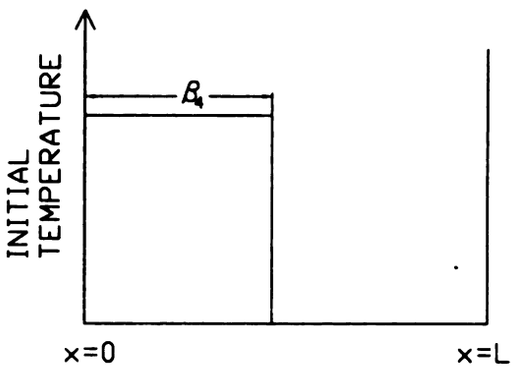

Figure 4-10 (Model 6) Rectangularly distributed initial penetration with the fourth parameter being the distance of penetration.

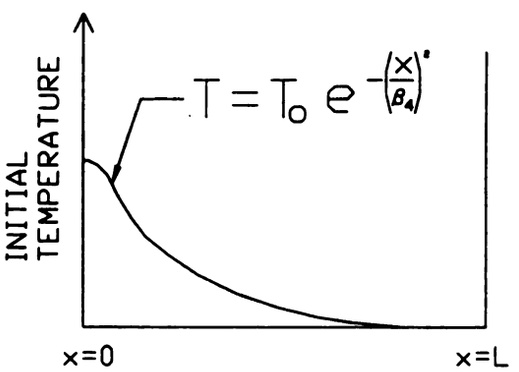

Figure 4-11 (Model 7) Exponential squared distributed initial penetration with the fourth parameter a measurement of the degree of penetration.

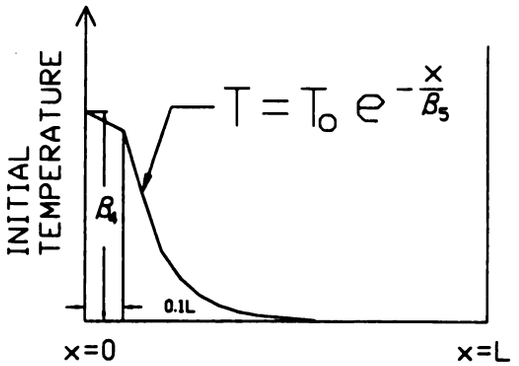

Figure 4-12 (Model 8) Linear temperature distribution over the first 10 percent of the incident side of the material followed by exponentially distributed initial penetration thereafter. The fourth parameter is the magnitude of the initial temperature at the heated surface and the fifth parameter is a measure of the degree of exponential penetration.

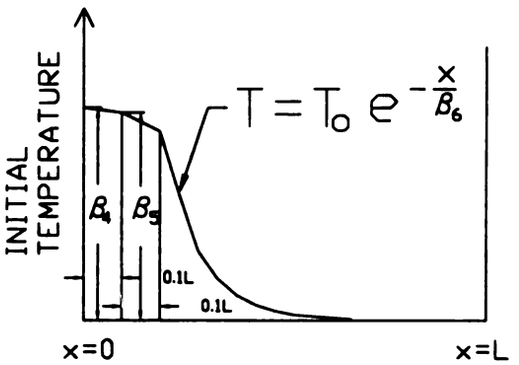

Figure 4-13 (Model 9) Two linear and one exponential penetration zones. The fourth and fifth parameters are the temperatures at L=0 and L=0.1, respectively. The sixth parameter is a measure of the degree of exponential penetration.

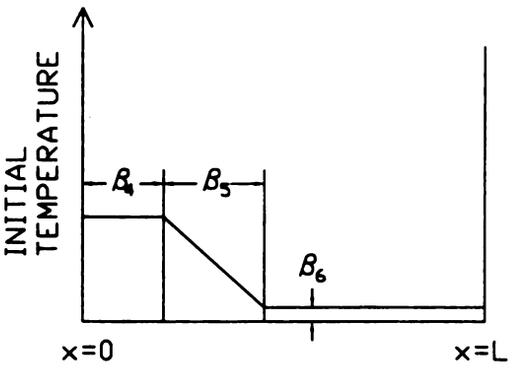

Figure 4-14 (Model 10) Two constant and one linear penetration zone as functions of penetration. The fourth parameter measures the depth of the first constant penetration zone. The fifth parameter measures the depth of the linear penetration zone and the sixth parameter is the initial temperature of the second constant penetration zone.

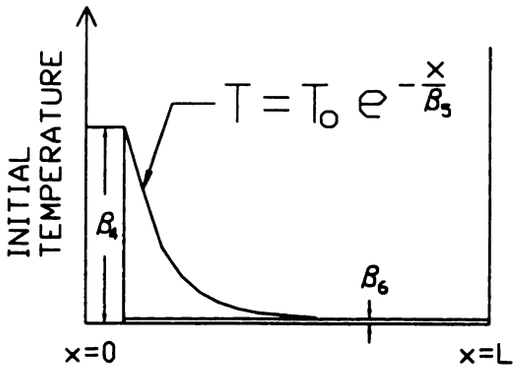

Figure 4-15 (Model 11) One constant penetration zone and one combined exponential plus constant zone. The fourth parameter measures the depth of penetration in the first constant zone. The second parameter measures the depth of the exponential penetration and the sixth parameter measures the magnitude of the second constant zone.

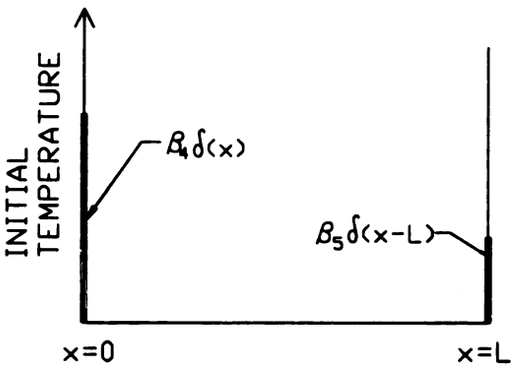

Figure 4-16 (Model 12) One surface flash on each side of the sample. The fourth parameter measures the magnitude of the flash at x=L.

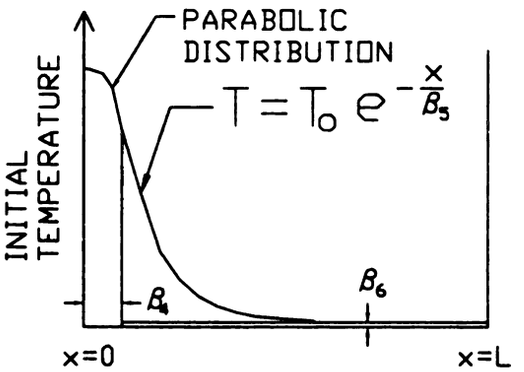

Figure 4-17 (Model 13) Parabolic distribution at the incident side of the sample with a combined exponential and constant zone. The fourth parameter measures the depth of the parabolic penetration. The fifth parameter measures the depth of the exponential penetration and the sixth parameter measures the magnitude of the second constant zone.

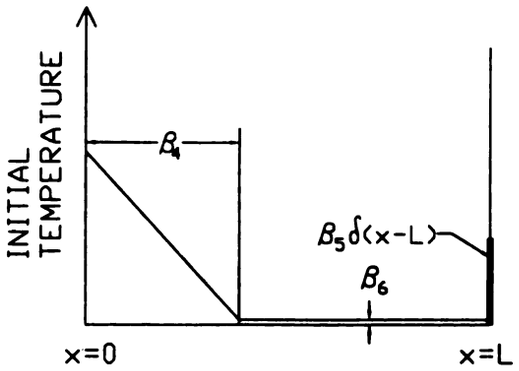

Figure 4-18 (Model 14) One linear and one constant zone with surface heating at the x=L face. The fourth parameter measures the depth of the linear penetration, the fifth parameter measures the magnitude of the constant zone and the sixth parameter measures the magnitude of the flash at x=L.

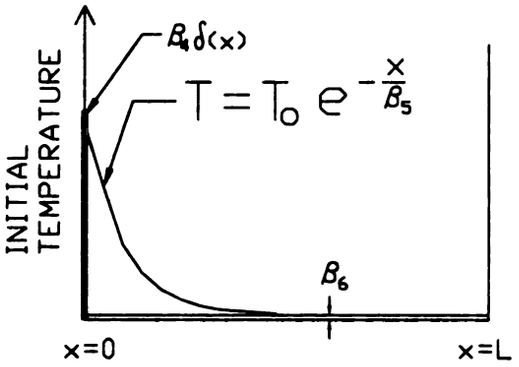

Figure 4-19 (Model 15) Surface heating at x=0 and a penetration zone with combined exponential and constant distribution. The fourth parameter is the maximum temperature associated with the exponential component of the penetration. The fifth parameter measures the depth of the exponential penetration. The sixth parameter measures the magnitude of the constant penetration.

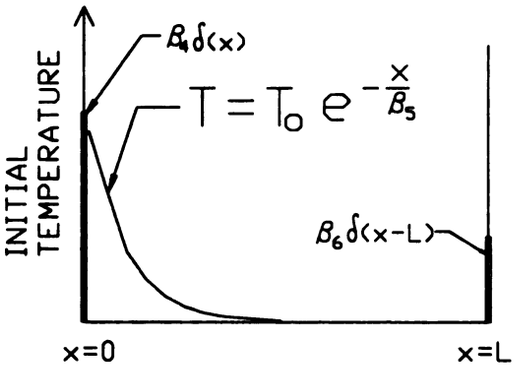

Figure 4-20 (Model 16) Surface heating at x=0 and x=L with exponential penetration. The fourth parameter is the magnitude of the maximum temperature associated with the exponential distribution. The fifth parameter measures the depth of the exponential penetration. The sixth parameter measures the magnitude of the surface heating at x=L.

models was shown to offer significantly improved performance over Model 5 when analyzing laboratory data and, in most cases, convergence was not obtained. These models were essential, however, in the development of Model 17 discussed in the next section.

4.3.4 TWO SIDED FLASH WITH PENETRATION, MODEL 17

In the process of refining models 6-16, it became clear that, in many of the experiments, the sample was heated on both sides (x=0 and x=L) presumably due to reflection of the laser flash inside the furnace or test device. This phenomenon is shown in the graph of the raw data in Figure 4-21 as evidenced by the prompt rise in surface temperature at time zero followed by the rapid decline in surface temperature during the first several time steps. The prompt rise in temperature for the first time step in this figure is quite significant and amounts to approximately 5% of the full scale temperature rise.

Additionally, it became evident in many of the experiments that penetration of the sample surface was not complete. A large percentage of the energy was absorbed at the immediate surface and the remainder seemed to be deposited in an exponential fashion.

As a slight variation of Model 16, Model 17 assumes

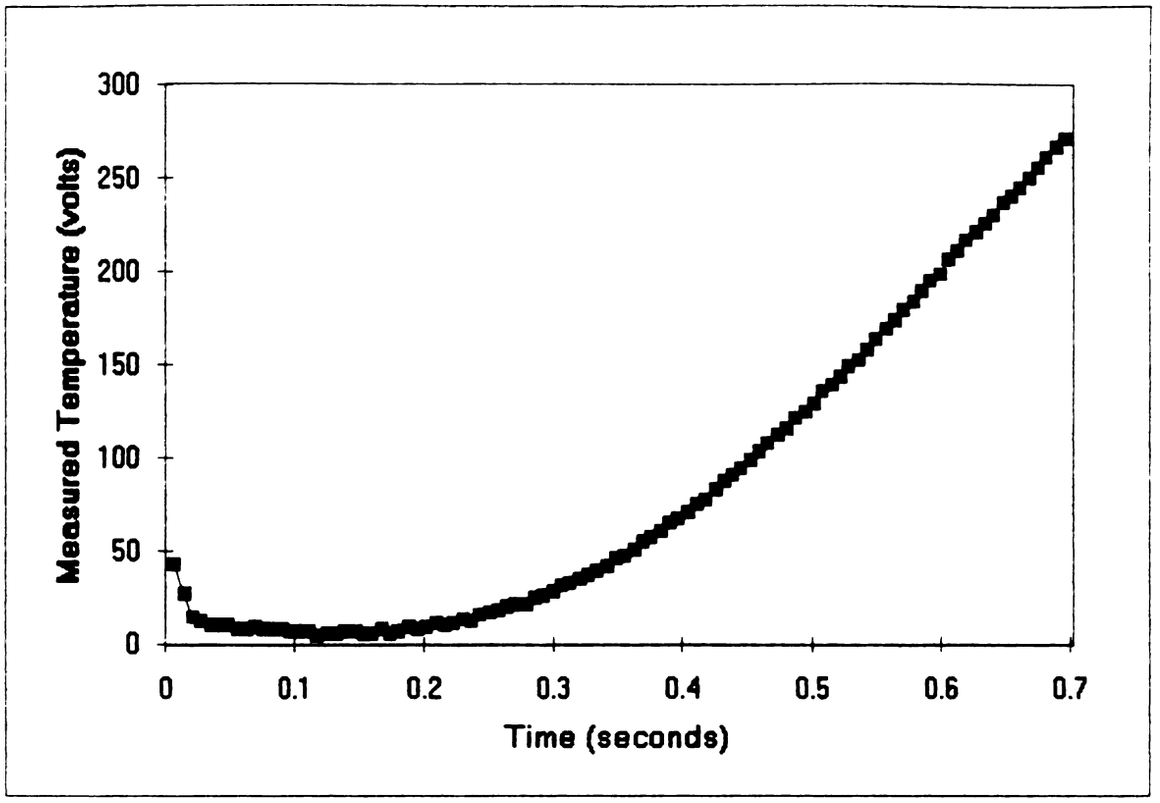

Figure 4-21 The First 100 Points of File A_R1 Showing Initial Temperature Decay

that a there is a deposit of energy on both surfaces of the sample, that is, at x=0 and at x=L. In this model, at the time immediately following the flash, the temperature just inside the sample is substantially less than that at the surface. In other words, $T(x=0)>T(x=0^+)$ and $T(x=L)>T(x=L^-)$. The initial temperature distribution inside the material is assumed to be an exponential, with maximum temperatures at $x=0^+$ and $x=L^-$. Expressed mathematically, the initial temperature distribution for Model 17 is

$$T(x) = T_1 L\delta(x) + T_2 e^{-\frac{x}{a}} + T_3 e^{\frac{L-x}{a}} + T_4 L\delta(x-L) \qquad (4\text{-}17)$$

where T_1, T_2, T_3, and T_4 are each different contributions to the initial temperature distribution. These parameters must be estimated simultaneously with the three basic parameters sought in Model 1.

Model 17 assumes that the sample is actually being heated on both sides, presumably due to a reflection of the flash inside the furnace. If the mechanism of heating is the same on both sides of the sample, then the degree of penetration will also be the same. Using this concept of symmetry, a redundant parameter in this model can be eliminated by assuming that

$$T_4 = T_1 \frac{T_3}{T_2} \tag{4-18}$$

This is reasonable since the mechanism of radiation and penetration and absorption should be the same on both surfaces even though the radiation magnitudes on each side are different. The Green's function solution equation is the same as used in Model 5 above, which is

$$T(x,t) = \int_{x'=0}^{L} G_{x33}(x,x' \mid t-\tau) F(x') dx' \tag{4-19}$$

where F(x') is the initial temperature distribution in the material, or in this case

$$F(x') = \frac{q_0\left(T_1 L\delta(x) + T_2 e^{-\frac{x'}{a}} + T_3 e^{\frac{L-x'}{a}} + T_1 \frac{T_3}{T_2} L\delta(L-x) \right)}{\rho c_p \left(L(T_1 + T_1 \frac{T_3}{T_2}) + (T_2+T_3)a(1-e^{-\frac{L}{a}}) \right)} \qquad (4\text{-}20)$$

The denominator of this term is found by normalizing the exponential temperature distribution to the magnitude of the heating that brought about the temperature rise. In this case

$$q_0 = \rho c_p \int_{x=0}^{L} F(x)\,dx \qquad (4\text{-}21)$$

The F(x') defined above satisfies this equation. The Green's function for X33 is given as

$$G_{X33}(x, x', t-\tau) = \frac{2}{L}\sum_{m=1}^{\infty} e^{-\beta_m^2 \alpha (t-\tau)/L^2} A_m(x) A_m(x') \qquad (4\text{-}22)$$

where

$$A_m(x) = \frac{\beta_m \cos\left(\beta_m \frac{x}{L}\right) + Bi \sin\left(\beta_m \frac{x}{L}\right)}{\beta_m^2 + Bi^2 + 2Bi} \qquad (4\text{-}23)$$

and

$$A_m(x') = \beta_m \cos\left(\beta_m \frac{x'}{L}\right) + Bi \sin\left(\beta_m \frac{x'}{L}\right) \qquad (4\text{-}24)$$

Integrating this with respect to dx' gives

$$T(L,t)=\frac{2q_0\alpha}{kLa(1-e^{-L/a})}\sum_{m=1}^{\infty}e^{(-\beta_m^2\alpha t/L^2)}\left[\frac{\beta_m\cos(\beta_m)+Bi\sin(\beta_m)}{\beta_m^2+Bi^2+2Bi}\right]C_m \quad (4\text{-}25)$$

where

$$C_m=\frac{T_2aL}{L^2+a^2\beta_m^2}\left[(a\beta_m^2-LBi)e^{-\frac{L}{a}}\sin(\beta_m)-(L\beta_m+a\beta_mBi)\left(e^{-\frac{L}{a}}\cos(\beta_m)-1\right)\right]+$$

$$\frac{T_3aL}{L^2+a^2\beta_m^2}\left[(L\beta_m-aBi\beta_m)\left(\cos\beta_m-e^{-\frac{L}{a}}\right)+(a\beta_m^2+LBi)\sin\beta_m\right]+$$

$$\beta_mT_1L+T_1\frac{T_3}{T_2}L\left(\beta_m\cos\beta_m+Bi\sin\beta_m\right) \quad (4\text{-}26)$$

Using Equation 4-25 as the direct solution for analysis of experimental data, the residuals are among the lowest of any model attempted. Model 17 has the additional advantage of being consistent with the physical explanation for the mechanism of the flash penetration on both sides of the sample. In other words, both sides of the sample are treated equally in Model 17. Figure 4-22 shows a comparison of the residuals from analyzing the same data file using Models 1,4,5 and 17. A great reduction is brought about in the signature by models 4 and 5, however Model 17

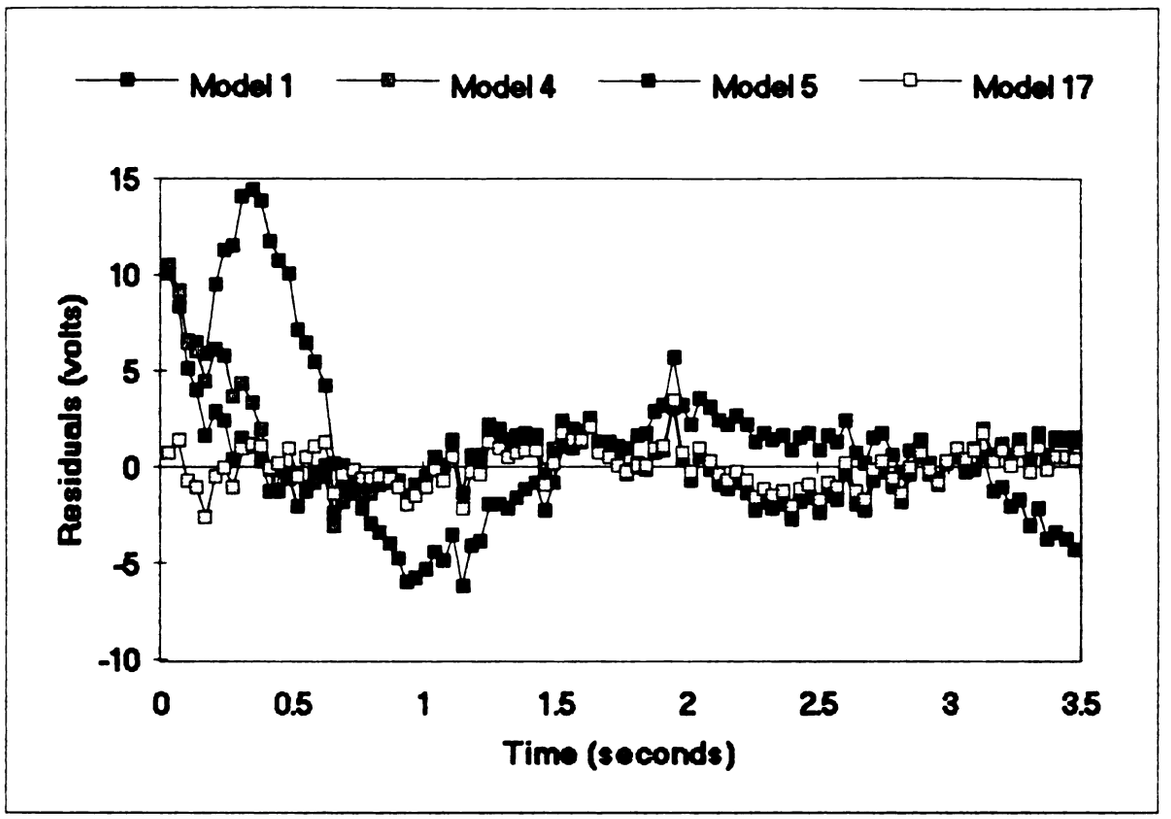

Figure 4-22 Residuals from File A_R1 Comparing Models 1,4,5 and 17

essentially eliminates any signature in the residuals. This is especially so in the early time measurements.

4.3.5 SURFACE TRANSMISSIVITY

A concept which makes Model 17 more manageable in terms of physical relevance is that of "surface transmissivity". Developed as part of this research, this concept is employed as a parameter in Model 17 so as to make the results of the parameter estimation method more physically tangible. This parameter is defined as the energy penetrating the surface per unit energy incident on the surface. This parameter has

a range in value from 0 to 1 and is estimated in Model 17 as parameter 5 in contrast to considering a maximum temperature coefficient of the exponential penetration. Parameter 4 is the same factor "*a*" in the exponential penetration term used in Model 5. Finally, parameter 6 is the magnitude of the incident energy on the "non-heated" surface.

4.3.6 ELIMINATION OF EXCESS MODELS

Tables 4-5 through 4-7 summarize the models used in analyzing the flash problem and the results from three of the experiments using all of the models. The majority of the models developed did not prove to be appropriate tools for the three experiments detailed above. As shown in Tables 4-5 through 4-7, the standard deviation of the residuals for virtually all models is greater than those resulting from the application of Model 17 to the laboratory data. Additionally, for experiments which exhibit a back-side flash, Model 17 is the most physically sound in terms of providing insight into the mechanism of the flash penetration. Many of the models which use multiple stages of penetration have sensitivity coefficients for the penetration parameters which are highly correlated. This is true in many cases to the extent that unstable parameter estimates can be generated yielding nonsensical results.

Table 4-5

Purdue University Experiment C_R1
L=1.9685mm Δt=.0603 σ_{min}= 0.001164

Model Nmbr.	Diff. (α)	Heat Flux	Biot Number	β_4	β_5	β_6	Resid. (s)
1	.33180	6.3889	.12978	NA	NA	NA	.01492
4	.29928	7.0236	.21692	.08822	NA	NA	.01032
5	.29937	6.9157	.21912	.16151	NA	NA	.00910
6	.29958	6.8577	.21470	.39999	NA	NA	.01076
7	.31241	4.3072	.20412	.11995	NA	NA	.01073
8	.31069	6.7626	.18876	.00605	.67694	NA	.01020
9	.29848	3.5096	.22239	10.580	.01411	3.191	.00542
10	.31194	3.3882	.18395	.00252	.33749	.0010	.00298
11	.31228	3.4093	.18325	.05792	.00087	.0899	.00297
12	.32738	6.4632	.14264	.01857	NA	NA	.00831
13	.31231	3.4099	.18319	.08033	.00074	.0940	.00294
14	.31189	3.4085	.18412	.33946	.00102	.0001	.00298
15	.31733	3.3912	.17089	.28895	1.6E-6	.6109	.00315
16	.31545	3.4057	.17573	.89560	.36966	.0031	.00294
17	.31538	3.4061	.17589	.10026	.3633	.00333	.00294

Table 4-6

Oak Ridge National Laboratory CBCF Sample at 700°C
L=.956mm Δt=.01408 σ_{min}= 0.008687

Model Nmbr.	Diff. (α)	Heat Flux	Biot Number	β_4	β_5	β_6	Resid. (s)
1	.31136	17.855	1.2332	NA	NA	NA	.03698
2	.4021	15.20	0.824	-.0648	NA	NA	.10958
3	.3878	14.17	0.793	-.02	NA	NA	.11098
4	.27615	21.289	1.5609	.02106	NA	NA	.01250
5	.28193	18.642	1.5030	.06963	NA	NA	.01245
6	.27274	18.503	1.5956	.20383	NA	NA	.01303
7	.29248	25.190	1.4650	.10474	NA	NA	.01371
8	.27861	18.576	1.5360	.70794	.05905	NA	.01227
9	.27024	19.615	1.6322	316.24	12.383	.1013	.01514
10	.27486	19.034	1.5730	.16514	.15531	.0002	.00971
11	.27493	19.287	1.5725	.19440	.00023	.0008	.01105
12	.30982	17.979	1.2472	.01586	NA	NA	.03227
13	.27668	19.283	1.5548	.19910	.00037	.0012	.00967
14	.27657	19.397	1.5561	.26725	1.0E-6	.0001	.00904
15	.27824	19.094	1.5398	505.36	1.0E-6	.0601	.01224
16	.27525	17.913	1.5692	1317.5	.04530	.0084	.00902
17	.28360	19.422	1.4860	.0669	1.0	.00723	.01074

Table 4-7

A_R1 Palaiseau France

L=3mm Δt=.0348 σ_{min}= 0.4520

Model Nmbr.	Diff. (α)	Heat Flux	Biot Number	β_4	β_5	β_6	Resid. (s)
1*	1.6017	2920	.08633	NA	NA	NA	4.8113
4*	1.119	3325	.20423	.06850	NA	NA	2.4166
5*	1.418	3236	.1943	.26207	NA	NA	1.9452
6*	1.392	3253	.2059	.69647	NA	NA	2.6606
7*	1.457	1286	.1925	.14913	NA	NA	2.5760
8*	1.480	1046	.1572	.03392	.4825	NA	1.3444
9	1.449	1057	.1738	1.7598	.00823	1.326	1.2523
10	1.441	1056	.17868	.00001	.7781	.0011	1.1840
11	1.4561	1057	.17049	.00001	.00052	.2123	1.1242
12*	1.5819	2953	.09828	7.4990	NA	NA	3.3982
13	1.4598	1054	.16807	.03955	.00032	.2197	1.1235
14	1.4241	1070	.18795	.8721	.00025	.0001	1.3551
15*	1.4573	1056	.16985	4453	2.491	.2214	1.1235
16*	1.1673	1057	.16909	2246	.28605	1.176	1.0311
17*	1.1674	1058	.16893	.2782	.63487	1.4244	1.0417

* Parameter estimates for these models reached convergence

For these reasons, four models were retained for further investigation and comparison in the other experiments. These are models 1,4,5 and 17. In experiments where no back-side flash is exhibited and the surfaces of the sample are not coated, Model 5 is the best choice. In these cases, there is no non-uniform absorption of the flash at the surface and no direct flash heating at x=L. As such, the additional two parameters estimated by Model 17 beyond the four estimated by Model 5 become a handicap and serve only to make the parameter estimation problem more unstable. The three experiments illustrated by Tables 4-5 through 4-7

all exhibit back-side heating, making Model 17 a logical choice in each case. Experiments performed at Oak Ridge National Laboratory using the Anter test equipment, however, exhibited no back-side heating, making Model 5 the best choice for analysis. Surface transmissivity is evident in the Purdue and French experiments, but not in the experiments performed at Oak Ridge National Laboratory. Were it not for the back side flash heating evident in the experiments performed on Holometrix equipment, there would have been no reason to use Model 17 in this case.

Model 1 is the most appropriate to use where the sample is either completely opaque or is well coated such that no penetration is made by the flash. This is the case with many of the experiments analyzed from laboratories in other countries shown in the appendix. Model 4 was retained as a type of second-check method to investigate for penetration of the flash. If neither Model 4 nor 5 shows any improvement over Model 1 for a given experiment, it can be reasonably assured that no type of flash penetration is present.

In order to examine the four salient models in more detail, a temperature correction was applied to each of the three experiments analyzed above in order to determine the effect on the estimated parameters and the residuals. The

temperature corrections are found by averaging the temperature readings prior to the time of the flash and subtracting this value from the temperature readings after the flash as a correction to a measurement bias. The use of this technique assumes a bias in the temperature measurement instrument which, if compensated for, should yield better results in the analysis of the experiment. The compensation was applied to the same three experiments analyzed in Tables 4-5 through 4-7 as a basis of comparison. The errors compensated for were very small, approximately 0.1 percent of the peak temperature reading in each experiment. No appreciable improvement was gained in adding these small correction factors. A summary of the parameter estimation results for the three experiments are shown in Table 4-8.

4.4 ESTIMATING EXTINCTION COEFFICIENT

In the general case of incident radiation on an interactive medium, as given by ref [27], the radiation intensity, as it transfers through the medium, is given by the equation of transfer

$$\mu \frac{\partial I(\tau_L, \theta, \phi)}{\partial \tau_L} = I(\tau_L, \theta, \phi) - S(\tau_L, \theta, \phi) \qquad (4\text{-}27)$$

where I represents the local intensity as a function of θ,

Table 4-8

Using Temperature Compensation

Model Nmbr.	Diff. (α)	Heat Flux	Biot Number	β_4	β_5	β_6	Resid. (s)
CBCF (error -.00458)							
1	.31169	17.829	1.2295				.03791
4	.27573	21.338	1.5641	.02153			.01321
5	.28157	18.656	1.5056	.07042			.01283
17	.283535	19.423	1.4857	1.0000	.00853	.06722	.01057
FRENCH DATA A_R1 (error -.962)							
1	1.2841	2916	.08422				5.0793
4	1.1146	3340	.20754	.07168			2.6297
5	1.1306	3248	.19736	.26774			2.1022
17	1.1676	1058	.16862	.60612	1.5783	.2866	1.0356
PURDUE DATA C_R1 (error -.03199)							
1	.33907	6.3139	.10953				.02472
4	.28746	7.3500	.25017	.14289			.01790
5	.28789	7.1967	.25453	.20094			.01473
17	.31582	3.4356	.17325	.08669	.00490	.5117	.00296

the polar angle of the radiation incident to the control volume; ϕ, the incident angle of azimuth and τ_L, the optical thickness defined as follows

$$\tau_L = \int_0^x \kappa dx' \qquad (4\text{-}28)$$

Also, κ, the extinction coefficient, can be expressed as $\kappa = a + \sigma$ where a and σ are the absorption and scattering coefficients, respectively. Finally, S is the source function and is defined as

$$S(\theta,\phi)=\frac{\Omega_0}{4\pi}\int_0^{\pi}\int_0^{2\pi}p(\theta,\phi,\theta',\phi')\,I(\tau_L,\theta',\phi')\sin\theta'd\theta'd\phi' \qquad (4\text{-}29)$$

where p represents the phase function.

In an emitting medium, the source function also depends upon the local absolute temperature and emissivity. As discussed in Chapter 3, however, emission within the media studied in this research has not been observed. For this reason, scattering and absorption are the only two mechanisms dealt with in the treatment of the flash penetration. At this point, the following assumptions are made

1. The materials are considered grey. All scattering and absorption takes place independent of frequency. In the type of experiment being studied, the measurements are not spectrally sensitive since temperature measurements are made using all frequencies simultaneously.
2. The material will be considered isotropic. The radiation transfer, therefore, will be one dimensional. In this type of experiment, there are no photon detectors which are angularly sensitive and the azimuth dependence of the radiation, if any, cannot be measured.

3. The duration of the flash will be assumed to be instantaneous in comparison to the time scale of the experiment. The temperature distribution inside the sample will therefore will be treated as an initial condition.

Using these assumptions, the transfer equation now becomes

$$\mu \frac{dI(\tau,\mu)}{d\tau} = I(\tau,\mu) - \frac{\Omega_0}{2}\int_{-1}^{1} I(\tau,\mu')\,d\mu' \qquad (4\text{-}30)$$

where Ω_0 is the albedo and $\mu=\cos(\theta)$ as discussed in Chapter 3. The solution of this equation is of the form

$$I(\tau_L,\mu) = \frac{C_0 e^{\psi\tau_L}}{1-\psi\mu} \qquad (4\text{-}31)$$

where C_0 is an arbitrary constant and ψ is the root of the following equation

$$\Omega_0 = \frac{2\psi}{\ln\left(\frac{1+\psi}{1-\psi}\right)} \qquad (4\text{-}32)$$

Table 4-9 shows some sample values of ψ for corresponding values of Ω_0. Both positive and negative values of ψ satisfy this condition. Since the solution of Equation 4-31 expands without bound as τ_L increases for values of positive ψ, the negative values of ψ will be used.

TABLE 4-9

Values of ψ

Ω_0	ψ
0.0	1.0
0.2	0.99991
0.4	0.98562
0.6	0.90733
0.8	0.71041
1.0	0.0

For moderate to low values of the albedo, the value of ψ is near negative 1. Only for values of the albedo near unity, where the dominant radiation interaction is scattering, is the value of ψ small. In any case, since the material is homogeneous, the distribution of the radiation inside the material will be of a pure exponential form. For cases of large albedo, and since the local angle of the intensity is not a concern for the purposes of determining the distribution of temperature, the solution for intensity is

$$I(\tau_L) = C_1 e^{-\tau_L} \qquad (4\text{-}33)$$

The extinction coefficient, as described in Chapter 3, has units of inverse length and corresponds to the reciprocal of the mean free path of a photon in the medium. This is expressed mathematically as $\kappa = \sigma + a$ where σ is the

scattering coefficient and a is the absorption coefficient. Assuming that κ is constant throughout the material, the relationship becomes $\tau_L=\kappa x$.

Using the boundary condition of $I(x=0)=I_0$, where I_0 is the incident intensity, we have

$$I(x)=I_0 e^{-\kappa x} \tag{4-34}$$

Considering now a differential element inside the material, dx, the total deposition of energy into this element by the radiation from the flash using the above model is

$$q=\int_0^t \left[I(x,t')-I(x+dx,t')\right]dt' \tag{4-35}$$

where t represents the duration of the flash. This can also be written as

$$q=\int_0^t \left[I(x,t')-\left(I(x,t')+\frac{\partial I(x,t')}{\partial x}dx\right)\right]dt' \tag{4-36}$$

which in turn becomes

$$q=-\int_0^t \frac{\partial I(x,t')}{\partial x}dxdt' \tag{4-37}$$

If the flash is taken as having constant intensity during

its very short duration, we have $q=\kappa t I(x)dx$ and since $I(x)$ has already been defined as

$$I(x)=I_0 e^{-\kappa x} \tag{4-38}$$

the energy deposited in the differential element becomes

$$q(x)=I_0 \kappa t e^{-\kappa x} dx \tag{4-39}$$

The temperature rise resulting from this deposition of energy is as follows

$$T(x)=\frac{q}{\rho c_p dx} \tag{4-40}$$

Substituting the equation for q(x) into this equation we have

$$T(x)=\frac{I_0 \kappa t}{\rho c_p} e^{-\kappa x} \tag{4-41}$$

This equation is a closed form expression of the initial temperature distribution following the instant of the flash. Therefore, the parameter "a" being evaluated in Model 17 is essentially the reciprocal of the extinction coefficient since the initial temperature distributions were assumed to be of the form $e^{-(x/a)}$. In other words, the parameter *a* is the mean free path of a photon in the material. In the case of all of the experiments analyzed as part of this research,

this mean free path is expressed in millimeters.

4.5 UTILIZING THE MODELS TO ANALYZE DATA

Each of the four principal models 1,4,5 and 17, is utilized in the appendix tables for analysis of laboratory data taken in various locations around the world on various materials. Basic physical information is included on each table, including the applied null value, which is the nominal value of the temperature measuring instrument at ambient temperature with no flash heating.

Models 4 and 5, the time shift model and the exponential penetration model, respectively, are similar in performance as shown by the standard deviation of the residuals.

In utilizing the models on 16 experiments performed in various laboratories throughout the world, the results seem to agree with prior analyses performed by the three experiments studied previously. In analyses performed by other laboratories, heat loss was not accounted for in many cases. For laboratories which did not account for heat loss, the values presented here for diffusivity are lower than the values reported by those laboratories. This is to be expected since an analysis which does not account for heat loss would interpret the temperature reaching an "early

peak" as being attributable to a higher diffusivity. The laboratories which accounted for heat loss produced results which were more closely aligned with the results of Model 1 presented here.

As a rule, Models 4 and 5, which account for flash penetration, produced values for diffusivity which were even lower than those produced by Model 1. This is also to be expected since, with flash penetration, the temperature rise on the measured surface comes more quickly than with no penetration. A model which does not account for penetration would interpret this early rise as a higher diffusivity.

Model 17, which accounts for both surface penetration and reflective heating on the measured side from the flash, seems to produce values of diffusivity which are between the values given by Model 1 and Models 4 and 5. This is partially due to the fact that Model 17 allows for partial penetration and Models 4 and 5 can deal with full penetration only. The following experiments exhibited back-side heating and were most appropriately modeled by Model 17

A_R1 Palaiseau, France

C_R1 West Lafayette, Indiana

L_R1 Poitiers, France

M_R1 Hunan, China

Q_R1 Manchester, United Kingdom

Oak Ridge, Tennessee (on Holometrix System)

The following experiments exhibited no significant back-side heating but did involve flash penetration. They are most appropriately modeled by Model 5

I_R1 Buenos Aires, Argentina

Oak Ridge, Tennessee (on Anter System)

The following experiments exhibited no appreciable back-side flash or flash penetration and are best suited to be analyzed using the three-parameter Model 1.

A_R2 Palaiseau, France

E_R1 Vandoeuvre les Nancy, France

E_R2 Vandoeuvre les Nancy, France

G_R1 Bombay, India

H_R1 Trappes, France

J_R1 Talence, France

K_R1 Belgrade, Yugoslavia

N_R1 Stuttgart, Germany

S_R1 Ardmore, Pennsylvania

One experiment exhibited such an extremely low value of heat loss that it is best dealt with using a two-parameter model involving only heat flux and diffusivity. This experiment was O_R1 LeBarp, France.

There is a great deal of variation in the degree of

surface flash penetration from one sample to another. Experiments performed on materials which were opaque to the flash resulted in no appreciable surface transmissivity whereas more transparent materials exhibited surface transmissivities of 1. Some of this variability, particularly the cases of partial surface absorption, came about because some samples were treated with gold foil coatings prior to running the experiments, for the expressed purpose of minimizing flash absorption. The amount of gold foil applied varied considerably between samples. Deposition thicknesses and application methods can be somewhat arbitrary.

For cases where little or no penetration occurred, there was no advantage to utilizing the advanced models since the parameters measuring penetration were estimated as being very small in magnitude and the confidence regions for these parameters were extremely large. Moreover, the values estimated by the advanced models for diffusivity were virtually unchanged from those estimated using Model 1, with no improvement in the residuals. In these cases, the advanced models proved to be more of a liability than an asset.

Although the values estimated for diffusivity using the advanced models for cases exhibiting penetration were not

radically different from those estimated using Model 1, there is a higher degree of confidence in the accuracy of the estimates. More importantly, the differences in estimated diffusivity are large enough to affect design considerations for applications of re-entry heat shields. The basis of the higher degree of confidence is the removal of a characteristic signature in the residuals, the lower standard deviation of the residuals, the narrower confidence regions and the stability of the sequential parameter estimates.

CHAPTER 5

DERIVATIVE REGULARIZATION

5.1 INTRODUCTION

As explained in Chapter 3, the four-parameter internal radiation model for the flash diffusivity problem is a very ill-posed model when used in parameter estimation. This is due to the strong correlation between kinetic conductivity and radiative conductivity, making the two parameters nearly indistinguishable from one another when trying to estimate them individually, even when using errorless data. In many test cases, a converged solution was not obtainable unless the initial seed value of the parameters used was within one percent of the known parameters using errorless data. Even with an unreasonably large heat flux applied, which tends to accentuate the non-linear nature of the radiant conductivity, the most successful test did not exhibit any stability with initial seed parameters differing from the true values by greater than 10 percent.

Utilizing a method called derivative regularization, devised as part of this research, parameter estimates were obtained for the internal radiation cases as readily as for the three parameter case using ordinary least squares. In

tests utilizing four parameter exact solution data files, the method successfully converged on the correct solution with initial parameter seed values of up to 200 percent larger than the true parameter values. The same convergence criteria were used as with ordinary least squares, whereby each parameter was brought to within 0.1 percent of the actual value used in the direct solution. The success in analyzing this type of problem contrasts the un-aided least squares method which would not bring about convergence unless initial parameter estimates were within one percent of the true values using errorless data. This method was also used in analyzing the data measured at Oak Ridge National Laboratory using the internal radiation model.

The ill-conditioned nature of this parameter estimation problem is manifest in the final set of equations being nearly singular in form. This unstable condition results in extremely wild estimated parameters when attempting to solve the equations. Various methods have been used in the past to bring about stability in this calculation. Reference [25] provides a template by which regularization may be applied using prior information about an experiment and the anticipated parameter values. Reference [27] addresses the mollification method, by which instability can be mitigated though a reduction in the measurement errors. Even with no

measurement errors in simulated experiments, however, the estimation of internal radiation parameters has shown to be highly unstable. By contrast, the type of instability which derivative regularization attempts to reduce, is the numerical singularity which comes about in the parameter estimation equations.

As a means of adding stability to the system of equations, derivative regularization is applied in the form of a matrix pre-multiplier. Similar methods, normally referred to as matrix pre-conditioning, have been used for other ill-conditioned systems. Reference [62], a general treatment of matrix computations, describes the application of pre-conditioning. The use of a pre-conditioning method is fairly straightforward, however the difficult and most critical aspect of the this method is the development of the pre-conditioning matrices for the specific type of problem. As the name implies, derivative regularization employs the time derivatives of the measured data and the sensitivity coefficients in reducing the ill-posed nature of the parameter estimating equations. This information is used in developing the pre-conditioning matrices.

Section 5.2 of this chapter discusses the underlying assumptions for the modifications made to ordinary least squares in order to improve stability using this method.

Section 5.3 discusses a step in the development of derivative regularization which was later refined and improved. This method involved using single cubic splines to approximate whole domain curves. Section 5.4 presents the refined version of the spline approximation method using piece-wise parabolic splines. Aspects of the bias and covariance associated with this method are discussed in Section 5.5. The results of the method are presented in Section 5.6, including the magnitude of reduction achieved in the condition number of the parameter estimation equations.

5.2 DERIVATIVE REGULARIZATION UNDERLYING ASSUMPTIONS

One principle of the method of ordinary least squares which is also employed in the derivative regularization method is the assumption of locally linear sensitivity coefficients. This means that the sensitivity coefficients are assumed to vary linearly with respect to the parameters within the narrow range of interest between the initial guess for the parameter values and the actual values of the parameters. For the flash diffusivity problem, studied in this research, the sensitivity coefficients are non-linear. For this reason, the parameter estimation process is conducted in iterations, re-calculating the sensitivity

coefficients between each iteration. Within a single iteration, however, the sensitivity coefficients can be thought of as being linear.

This concept is employed in the following expression presented in Chapter 2

$$T^{(k+1)} \approx T^{(k)} + \sum_{j=1}^{3} \frac{\partial T}{\partial b_j}\left(b_j^{(k+1)} - b_j^{(k)}\right) \qquad (5\text{-}1)$$

Expressed in words, the k+1 iteration temperature is the new calculated temperature which will minimize the sum of squares of the difference between the calculated and measured temperatures. In graphical terms, if the difference between $T^{(k+1)}$ and $T^{(k)}$ were plotted as a function of time, it would be very much like a plot of the residuals for the applicable iteration. This assumes that the $T^{(k+1)}$ curve is very close to the measured temperature curve. As the equation above states, this curve must be equal to the sum of the sensitivity coefficient curves, each multiplied by the respective change in its estimated parameter from the previous iteration to the present. The approximation sign is shown because the sensitivity coefficients are not truly linear.

The method of derivative regularization takes this concept one step further and requires that the time

derivatives of these curves be matched as well as the simple magnitude of the temperature values themselves. In the case of the first time derivative, we have

$$T^{(k+1)\prime} \approx T^{(k)\prime} + \sum_{j=1}^{3} \frac{\partial T'}{\partial b_j}\left(b_j^{(k+1)} - b_j^{(k)}\right) \qquad (5\text{-}2)$$

where the "prime" symbol designates the first derivative with respect to time. Likewise we have

$$T^{(k+1)\prime\prime} \approx T^{(k)\prime\prime} + \sum_{j=1}^{3} \frac{\partial T''}{\partial b_j}\left(b_j^{(k+1)} - b_j^{(k)}\right) \qquad (5\text{-}3)$$

where the "double prime" symbol designates the second derivative with respect to time. Using derivative regularization, a set of $b_j^{(k+1)}$ parameters is estimated which minimizes the difference between not only the measured and calculated temperatures, but their time derivatives as well, in least squares fashion. In this way, additional information regarding the shape of these curves is employed in bringing about stability.

5.3 CUBIC SPLINE APPROXIMATION

Several methods were attempted, as part of this research, in an effort to minimize the effects of the measurement errors and estimate the derivatives of the

measured data and the direct solution. At first, multiple cubic splines were used to approximate the curves of the sensitivity coefficients, the calculated temperature and the measured temperature. These splines, spanning approximately 10 data points each, were defined as being piecewise continuous with continuity in the first derivative at each end of each spline. These spline junctions are also known as "knots". At first, the splines were calculated sequentially. At the right hand side of the first spline, i.e. the first "knot", the position and slope of the spline end were used as boundary conditions for the position and slope of the left end of the second spline. This method proved to be unworkable when used sequentially because the slopes at the end of each spline tended to become too wild, causing extremely large deviations of the spline from the data being approximated.

As a second attempt at approximating first and second derivatives of the residual curve and the sensitivity coefficient curves, one cubic spline was used for each curve over the entire time domain of the experiment. Each of these curves was expressed as a polynomial with four constants. The constants were determined via least squares analysis of the applicable data points. In the particular case of four unknown parameters, five equations can be

written as follows:

$$\epsilon(t)=a_o t^3+b_o t^2+c_o t+d_o$$

$$X_1(t)=a_1 t^3+b_1 t^2+c_1 t+d_1$$

$$X_2(t)=a_2 t^3+b_2 t^2+c_2 t+d_2 \qquad (5\text{-}4)$$

$$X_3(t)=a_3 t^3+b_3 t^2+c_3 t+d_3$$

$$X_4(t)=a_4 t^3+b_4 t^2+c_4 t+d_4$$

where $X_i(t)$ refers to the four sensitivity coefficient curves and $\epsilon(t)$ designates the measured minus the calculated temperature. Examples of these approximations are shown in Figures 5-1 through 5-3. Figure 5-1 is a plot of the residual curve when comparing the direct solution from the previous iteration to the measured data, along with its cubic spline approximation. Figures 5-2 and 5-3 each show two of the four sensitivity coefficient curves along with their respective spline approximations.

In order to find the parameters from these curves, the principle used is that the four sensitivity coefficient curves should all sum to the residual curve when multiplied by their respective values of $b_i^{(k+1)}-b_i^{(k)}$. As a shorthand notation, we may define $\Delta b_i=b_i^{(k+1)}-b_i^{(k)}$. In equation form, we have

$$\epsilon(t)=\Delta b_1 X_1(t)+\Delta b_2 X_2(t)+\Delta b_3 X_3(t)+\Delta b_4 X_4(t) \qquad (5\text{-}5)$$

Since this is only one equation with four unknowns, $(\Delta b_1, \Delta b_2, \Delta b_3, \Delta b_4)$ the equations of the cubic splines are used

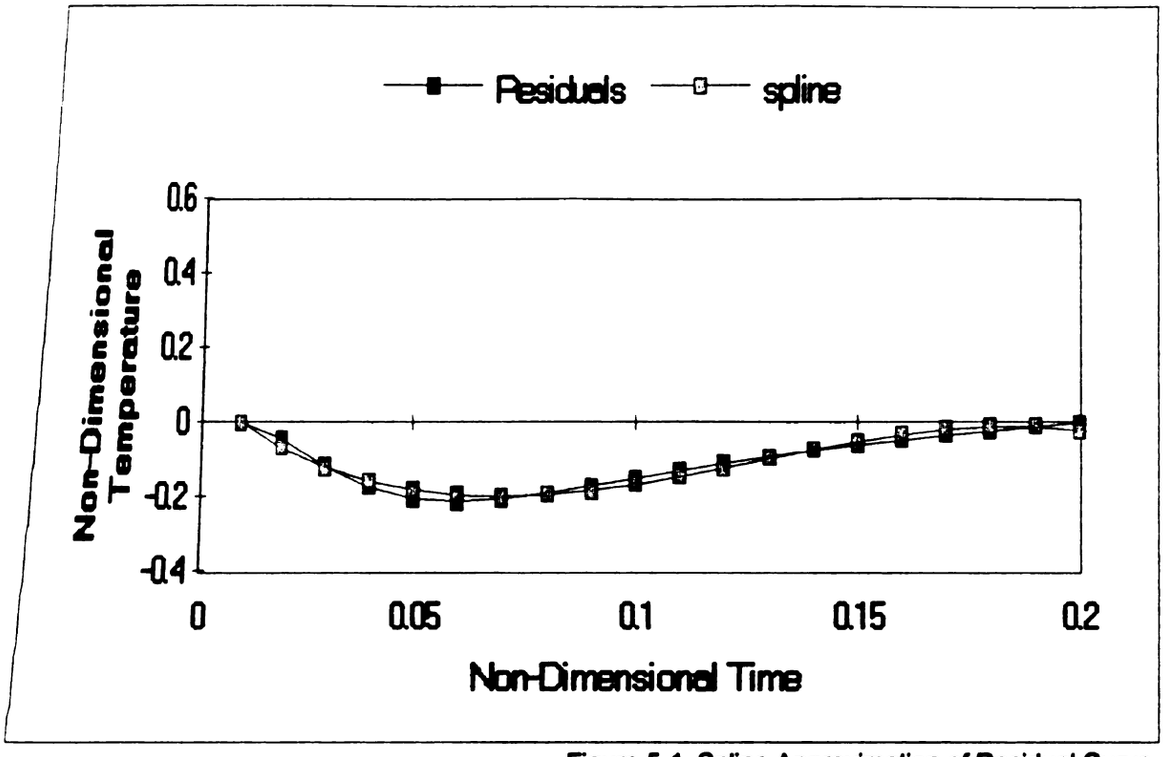

Figure 5-1 Spline Approximation of Residual Curve

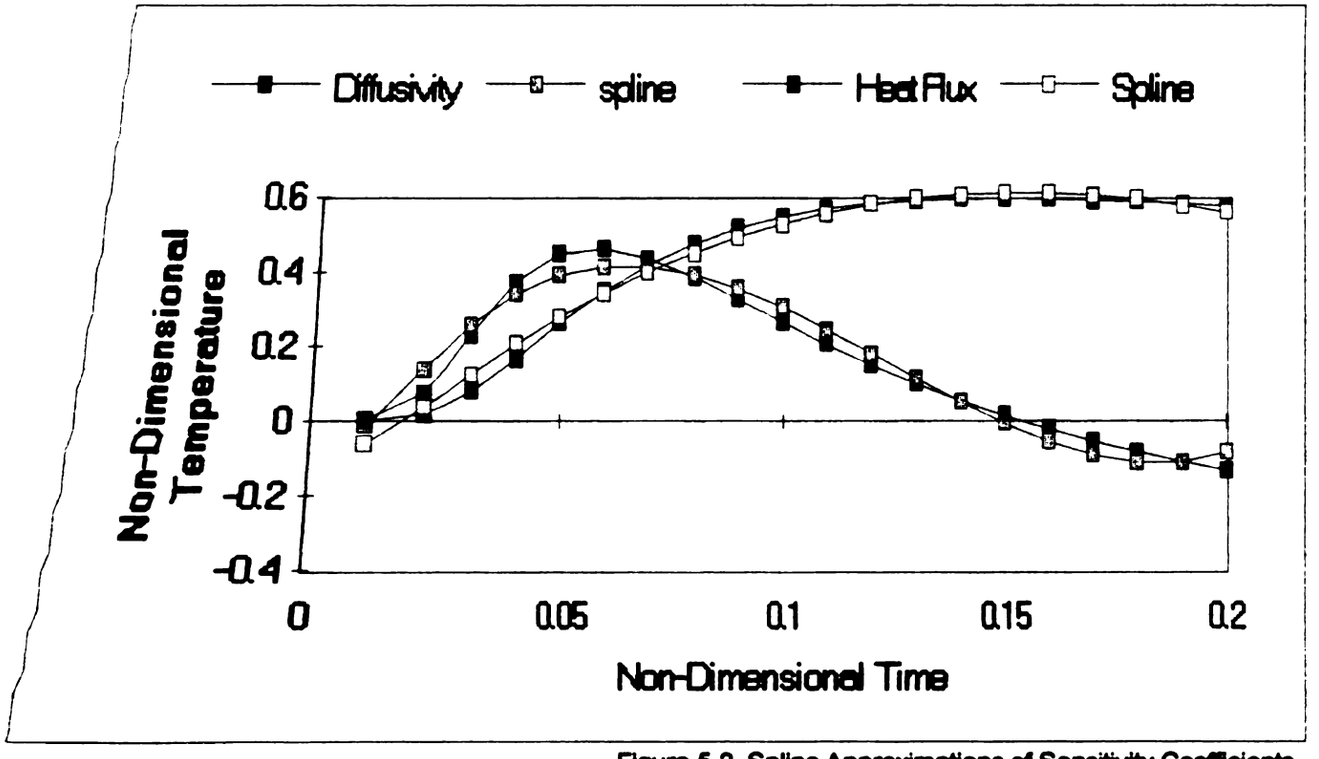

Figure 5-2 Spline Approximations of Sensitivity Coefficients

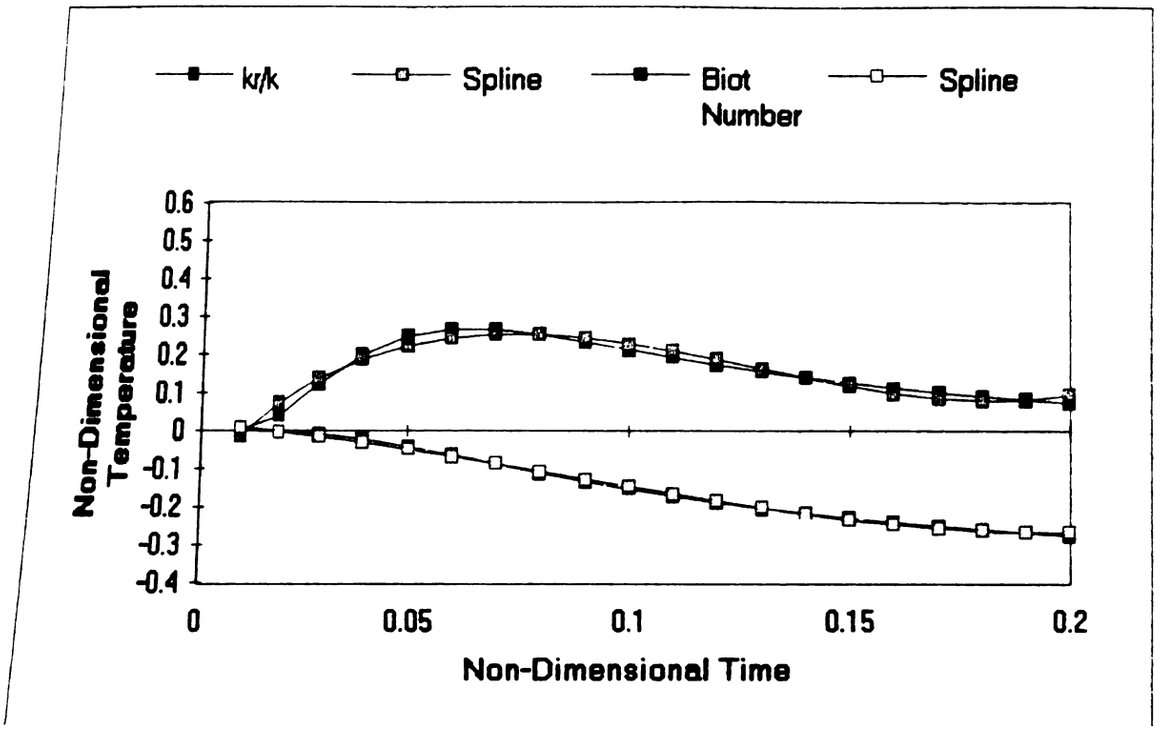

Figure 5-3 Spline Approximations of Sensitivity Coefficients

to generate four equations, namely

$$a_o=\Delta b_1 a_1+\Delta b_2 a_2+\Delta b_3 a_3+\Delta b_4 a_4$$

$$b_o=\Delta b_1 b_1+\Delta b_2 b_2+\Delta b_3 b_3+\Delta b_4 b_4$$

$$c_o=\Delta b_1 c_1+\Delta b_2 c_2+\Delta b_3 c_3+\Delta b_4 c_4 \qquad (5\text{-}6)$$

$$d_o=\Delta b_1 d_1+\Delta b_2 d_2+\Delta b_3 d_3+\Delta b_4 d_4$$

The only unknowns in these equations are a_o, b_o, c_o, and d_o. In practice, this method was found to be ineffectual due to the poor approximation of the sensitivity coefficients made by the splines. Moreover, there was no observed improvement in the stability of the parameter estimation problem brought about by the use of the spline approximations. An improved approximation of the curves was achieved by using one piecewise spline for each measurement point. The whole

domain cubic spline method has been presented here strictly in order to chronicle the development of the derivative regularization method, since the final derivative regularization method is built on the same principles.

5.4 PARABOLIC SPLINE APPROXIMATION

A more successful approximation of the curves of the measurements, the sensitivity coefficients and their derivatives, is a set of parabolic splines, with one spline defined for each time step. Each spline in this method is centered at an individual data point in the curve. Normally seven points are used to define each spline, in which case, the first three and last three data points from the measured data are not used, except in obtaining the splines for the neighboring points. For a typical temperature measurement Y_i, the spline approximation for the measurement, designated $\underline{Y}_i$, is of the form

$$\underline{Y}_i(t) = A_i t^2 + B_i t + C_i \qquad (5\text{-}7)$$

with the first derivative expressed as

$$\underline{Y}_i'(t) = 2A_i t + B_i \qquad (5\text{-}8)$$

and the second derivative as

$$\underline{Y}_i''(t) = 2A_i \qquad (5\text{-}9)$$

For the sake of clean calculations, the center point of each spline, the point of interest, is assigned the arbitrary

time value of t=0 and the domain of the spline is then $-3 \geq t \geq 3$. Considering the above equations at t=0, the values of the functions and their derivatives become

$$\begin{aligned} Y_i(0) &= C_i \\ Y_i'(0) &= B_i \\ Y_i''(0) &= 2A_i \end{aligned} \tag{5-10}$$

In order to find the coefficients A_i, B_i, and C_i, the method of ordinary least squares is utilized. Using seven points as described above, the over-defined set of equations for the spline centered at I=4, for example, is

$$\begin{vmatrix} t_1^2 & t_1 & 1 \\ t_2^2 & t_2 & 1 \\ t_3^2 & t_3 & 1 \\ t_4^2 & t_4 & 1 \\ t_5^2 & t_5 & 1 \\ t_6^2 & t_6 & 1 \\ t_7^2 & t_7 & 1 \end{vmatrix} \begin{vmatrix} A_4 \\ B_4 \\ C_4 \end{vmatrix} = \begin{vmatrix} Y_1 \\ Y_2 \\ Y_3 \\ Y_4 \\ Y_5 \\ Y_6 \\ Y_7 \end{vmatrix} \tag{5-11}$$

This can be expressed in compact form as $[\mathbf{t}][\mathbf{s}]=[\mathbf{y}]$ and the least squares values of $[\mathbf{s}]$ can be found by pre-multiplying both sides by $[\mathbf{t}]^T$. We then have

$$[\mathbf{t}]^T[\mathbf{t}][\mathbf{s}]=[\mathbf{t}]^T[\mathbf{y}] \tag{5-12}$$

From this equation, the values of A_4, B_4, and C_4, are

calculated, expressed in terms of the components of [**t**] and [**y**] only. The value of $\underline{Y}_4$, the point of interest, is equal to C_4. Since the time steps are evenly spaced, they can be expressed as multiples of each other and divided out. This leaves $\underline{Y}_4$ to be expressed in terms of the seven Y_i values alone. Constants designated with the letter m can be found such that

$$\underline{Y}_4 = m_1Y_1+m_2Y_2+m_3Y_3+m_4Y_4+m_5Y_5+m_6Y_6+m_7Y_7 \qquad (5\text{-}13)$$

which can also be put in matrix form as

$$\begin{vmatrix} \underline{Y}_4 \\ \underline{Y}_5 \\ \underline{Y}_6 \\ \vdots \\ \underline{Y}_{n-3} \end{vmatrix} = \begin{vmatrix} m_1 & m_2 & m_3 & m_4 & m_5 & m_6 & m_7 & 0 & 0 & \dots & 0 \\ 0 & m_1 & m_2 & m_3 & m_4 & m_5 & m_6 & m_7 & 0 & \dots & 0 \\ 0 & 0 & m_1 & m_2 & m_3 & m_4 & m_5 & m_6 & m_7 & \dots & 0 \\ \vdots & \vdots & \vdots & \vdots & \vdots & \vdots & \vdots & \vdots & \vdots & \dots & \vdots \\ 0 & \dots & 0 & 0 & m_1 & m_2 & m_3 & m_4 & m_5 & m_6 & m_7 \end{vmatrix} \begin{vmatrix} Y_1 \\ Y_2 \\ Y_3 \\ Y_4 \\ Y_5 \\ \vdots \\ Y_n \end{vmatrix} \qquad (5\text{-}14)$$

Equation 5-14 can be written this way since the m_i arguments are not functions of Y_i and are the same for each spline. Note again that the first 3 and last 3 data points are lost because they are needed to form the first and last splines; hence the points are only approximated by splines from points 4 to n-3. Equation 5-14 can also be written in compact form as

$$[\mathbf{y}] = [\mathbf{M}_0]\,[\mathbf{y}] \qquad (5\text{-}15)$$

Similarly, approximations for the derivative values are

$$[\mathbf{y}'] = [\mathbf{M}_1]\,[\mathbf{y}]$$

$$[\mathbf{y}''] = [\mathbf{M}_2]\,[\mathbf{y}] \qquad (5\text{-}16)$$

Likewise, for the curves of the calculated values of temperature we have

$$[\mathbf{T}] = [\mathbf{M}_0]\,[\mathbf{T}]$$

$$[\mathbf{T}'] = [\mathbf{M}_1]\,[\mathbf{T}] \qquad (5\text{-}17)$$

$$[\mathbf{T}''] = [\mathbf{M}_2]\,[\mathbf{T}]$$

and for the curves of the sensitivity coefficients we have

$$[\mathbf{X}] = [\mathbf{M}_0]\,[\mathbf{X}]$$

$$[\mathbf{X}'] = [\mathbf{M}_1]\,[\mathbf{X}] \qquad (5\text{-}18)$$

$$[\mathbf{X}''] = [\mathbf{M}_2]\,[\mathbf{X}]$$

Exact values for the individual terms of the $\mathbf{M}_0$, $\mathbf{M}_1$, and $\mathbf{M}_2$ matrices for parabolic splines over seven points are shown in Table 5-1

As a note of interpretation, the first and last coefficients of the M_o matrix are negative due to the parabolic shape of the spline. Since the coefficients shown affect only the center point, low measurement values at the end points would tend to make a higher center point of the spline approximation and vise-versa. This allows the parabolic spline to address the end points by affecting the curvature of the spline in order to cause the spline ends to

Table 5-1

Parabolic Spline Matrix Terms

Individual Terms	For $\mathbf{M}_0$ Matrix	For $\mathbf{M}_1$ Matrix	For $\mathbf{M}_2$ Matrix
m_1	-2/21	-3/28	5/84
m_2	1/7	-1/14	0
m_3	2/7	-1/28	-1/28
m_4	1/3	0	-1/21
m_5	2/7	1/28	-1/28
m_6	1/7	1/14	0
m_7	-2/21	3/28	5/84

pass closer to the end measurements. In this same vein, note that the end points provide the largest contribution to the second derivative of the spline.

We now define new vectors, $[\tilde{\mathbf{Y}}]$, $[\tilde{\mathbf{T}}]$ and $[\tilde{\mathbf{X}}]$ where w_1 and w_2 are weighting coefficients in Equation 5-19. Another means of defining these vectors is to use a composite matrix, which incorporates all three of the spline matrices $[\mathbf{M}_0]$, $[\mathbf{M}_1]$ and $[\mathbf{M}_2]$. This matrix is designated as $[\mathbf{M}_c]$ and can be used as a direct conversion from the $[\mathbf{Y}]$ and $[\mathbf{T}]$ vectors to the $[\tilde{\mathbf{Y}}]$ and $[\tilde{\mathbf{T}}]$ and vectors, respectively. The M_c matrix is defined in Equation 5-20.

$$\left|\tilde{\mathbf{Y}}\right| = \begin{vmatrix} \underline{Y_4} \\ \underline{Y_5} \\ \underline{Y_6} \\ \vdots \\ \underline{Y_{n-3}} \\ w_1\underline{Y_4'} \\ w_1\underline{Y_5'} \\ w_1\underline{Y_6'} \\ \vdots \\ w_1\underline{Y_{n-3}'} \\ w_2\underline{Y_4''} \\ w_2\underline{Y_5''} \\ w_2\underline{Y_6''} \\ \vdots \\ w_2\underline{Y_{n-3}''} \end{vmatrix} \quad \left|\tilde{\mathbf{T}}\right| = \begin{vmatrix} \underline{T_4} \\ \underline{T_5} \\ \underline{T_6} \\ \vdots \\ \underline{T_{n-3}} \\ w_1\underline{T_4'} \\ w_1\underline{T_5'} \\ w_1\underline{T_6'} \\ \vdots \\ w_1\underline{T_{n-3}'} \\ w_2\underline{T_4''} \\ w_2\underline{T_5''} \\ w_2\underline{T_6''} \\ \vdots \\ w_2\underline{T_{n-3}''} \end{vmatrix} \quad \left|\tilde{\mathbf{X}}\right| = \begin{vmatrix} \underline{X_4} \\ \underline{X_5} \\ \underline{X_6} \\ \vdots \\ \underline{X_{n-3}} \\ w_1\underline{X_4'} \\ w_1\underline{X_5'} \\ w_1\underline{X_6'} \\ \vdots \\ w_1\underline{X_{n-3}'} \\ w_2\underline{X_4''} \\ w_2\underline{X_5''} \\ w_2\underline{X_6''} \\ \vdots \\ w_2\underline{X_{n-3}''} \end{vmatrix} \tag{5-19}$$

$$\mathbf{M}_c = \begin{vmatrix} \mathbf{M}_0 \\ w_1\mathbf{M}_1 \\ w_2\mathbf{M}_2 \end{vmatrix} \tag{5-20}$$

The conversion using $[\mathbf{M}_c]$ is accomplished using

$$[\tilde{\mathbf{Y}}] = [\mathbf{M}_c]\,[\mathbf{Y}]$$

$$[\tilde{\mathbf{T}}] = [\mathbf{M}_c]\,[\mathbf{T}] \tag{5-21}$$

Similarly, the $[\mathbf{X}]$ matrix can be converted to the $[\tilde{\mathbf{X}}]$ matrix by the conversion

$$[\mathbf{X}^{-}] = [\mathbf{M}_0][\mathbf{X}] \qquad (5\text{-}22)$$

It should be noted that the dimensions of the [Y] and [T] vectors are dimensionally n x 1 where n is the number of measurements. The [$\mathbf{Y}^{-}$] and [$\mathbf{T}^{-}$] vectors are dimensionally 3m x 1 where m=n-6. The reason for the difference of the 6 points between m and n is that the first and last three points are lost because they are ends of a 7 point spline. These vectors contain 3m terms because there is a filtered point, a first derivative approximation and a second derivative approximation for each point.

The [X] matrix, the sensitivity coefficient matrix, undergoes a similar dimensional transformation to that experienced by the [Y] and [T] vectors in the derivative regularization process. The [X] matrix is dimensionally n x p, where p is the number of parameters, and the [$\mathbf{X}^{-}$] matrix is 3m x p. The [$\mathbf{M}_0$], [$\mathbf{M}_1$], and [$\mathbf{M}_2$] matrices are each of dimension m x n. If the individual terms of the [$\mathbf{M}_0$] matrix are denoted as $m_{0,n}$, the [$\mathbf{M}_1$] matrix terms are denoted as $m_{1,n}$ and the [$\mathbf{M}_2$] matrix terms are denoted as $m_{2,n}$, then the [$\mathbf{M}_0$] matrix in expanded form is written as

$$
\begin{bmatrix}
m_{0,1} & m_{0,2} & m_{0,3} & m_{0,4} & m_{0,5} & m_{0,6} & m_{0,7} & 0 & \cdots & 0 & 0 & 0 \\
0 & m_{0,1} & m_{0,2} & m_{0,3} & m_{0,4} & m_{0,5} & m_{0,6} & m_{0,7} & \cdots & 0 & 0 & 0 \\
0 & 0 & m_{0,1} & m_{0,2} & m_{0,3} & m_{0,4} & m_{0,5} & m_{0,6} & \cdots & 0 & 0 & 0 \\
0 & 0 & 0 & m_{0,1} & m_{0,2} & m_{0,3} & m_{0,4} & m_{0,5} & \cdots & 0 & 0 & 0 \\
0 & 0 & 0 & 0 & m_{0,1} & m_{0,2} & m_{0,3} & m_{0,4} & \cdots & 0 & 0 & 0 \\
0 & 0 & 0 & 0 & 0 & m_{0,1} & m_{0,2} & m_{0,3} & \cdots & 0 & 0 & 0 \\
\vdots & \vdots & \vdots & \vdots & \vdots & \vdots & \vdots & \vdots & \cdots & \vdots & \vdots & \vdots \\
0 & 0 & 0 & 0 & 0 & 0 & 0 & 0 & \cdots & m_{0,7} & 0 & 0 \\
0 & 0 & 0 & 0 & 0 & 0 & 0 & 0 & \cdots & m_{0,6} & m_{0,7} & 0 \\
0 & 0 & 0 & 0 & 0 & 0 & 0 & 0 & \cdots & m_{0,5} & m_{0,6} & m_{0,7} \\
w_1 m_{1,1} & w_1 m_{1,2} & w_1 m_{1,3} & w_1 m_{1,4} & w_1 m_{1,5} & w_1 m_{1,6} & w_1 m_{1,7} & 0 & \cdots & 0 & 0 & 0 \\
0 & w_1 m_{1,1} & w_1 m_{1,2} & w_1 m_{1,3} & w_1 m_{1,4} & w_1 m_{1,5} & w_1 m_{1,6} & w_1 m_{1,7} & \cdots & 0 & 0 & 0 \\
0 & 0 & w_1 m_{1,1} & w_1 m_{1,2} & w_1 m_{1,3} & w_1 m_{1,4} & w_1 m_{1,5} & w_1 m_{1,6} & \cdots & 0 & 0 & 0 \\
0 & 0 & 0 & w_1 m_{1,1} & w_1 m_{1,2} & w_1 m_{1,3} & w_1 m_{1,4} & w_1 m_{1,5} & \cdots & 0 & 0 & 0 \\
0 & 0 & 0 & 0 & w_1 m_{1,1} & w_1 m_{1,2} & w_1 m_{1,3} & w_1 m_{1,4} & \cdots & 0 & 0 & 0 \\
0 & 0 & 0 & 0 & 0 & w_1 m_{1,1} & w_1 m_{1,2} & w_1 m_{1,3} & \cdots & 0 & 0 & 0 \\
\vdots & \vdots & \vdots & \vdots & \vdots & \vdots & \vdots & \vdots & \cdots & \vdots & \vdots & \vdots \\
0 & 0 & 0 & 0 & 0 & 0 & 0 & 0 & \cdots & w_1 m_{1,7} & 0 & 0 \\
0 & 0 & 0 & 0 & 0 & 0 & 0 & 0 & \cdots & w_1 m_{1,6} & w_1 m_{1,7} & 0 \\
0 & 0 & 0 & 0 & 0 & 0 & 0 & 0 & \cdots & w_1 m_{1,5} & w_1 m_{1,6} & w_1 m_{1,7} \\
w_2 m_{2,1} & w_2 m_{2,2} & w_2 m_{2,3} & w_2 m_{2,4} & w_2 m_{2,5} & w_2 m_{2,6} & w_2 m_{2,7} & 0 & \cdots & 0 & 0 & 0 \\
0 & w_2 m_{2,1} & w_2 m_{2,2} & w_2 m_{2,3} & w_2 m_{2,4} & w_2 m_{2,5} & w_2 m_{2,6} & w_2 m_{2,7} & \cdots & 0 & 0 & 0 \\
0 & 0 & w_2 m_{2,1} & w_2 m_{2,2} & w_2 m_{2,3} & w_2 m_{2,4} & w_2 m_{2,5} & w_2 m_{2,6} & \cdots & 0 & 0 & 0 \\
0 & 0 & 0 & w_2 m_{2,1} & w_2 m_{2,2} & w_2 m_{2,3} & w_2 m_{2,4} & w_2 m_{2,5} & \cdots & 0 & 0 & 0 \\
0 & 0 & 0 & 0 & w_2 m_{2,1} & w_2 m_{2,2} & w_2 m_{2,3} & w_2 m_{2,4} & \cdots & 0 & 0 & 0 \\
0 & 0 & 0 & 0 & 0 & w_2 m_{2,1} & w_2 m_{2,2} & w_2 m_{2,3} & \cdots & 0 & 0 & 0 \\
\vdots & \vdots & \vdots & \vdots & \vdots & \vdots & \vdots & \vdots & \cdots & \vdots & \vdots & \vdots \\
0 & 0 & 0 & 0 & 0 & 0 & 0 & 0 & \cdots & w_2 m_{2,7} & 0 & 0 \\
0 & 0 & 0 & 0 & 0 & 0 & 0 & 0 & \cdots & w_2 m_{2,6} & w_2 m_{2,7} & 0 \\
0 & 0 & 0 & 0 & 0 & 0 & 0 & 0 & \cdots & w_2 m_{2,5} & w_2 m_{2,6} & w_2 m_{2,7}
\end{bmatrix}
\tag{5-23}
$$

Now that the [$\tilde{\mathbf{Y}}$] and [$\tilde{\mathbf{T}}$] vectors have been defined, with respect to the parameters, the modified sum of squares function

$$S=\sum_{i=4}^{n-3} (\tilde{Y_i}-\tilde{T_i})^2 \qquad (5\text{-}24)$$

can be written in matrix form as

$$S=[\tilde{\boldsymbol{Y}}-\tilde{\boldsymbol{T}}]^T\,[\tilde{\boldsymbol{Y}}-\tilde{\boldsymbol{T}}] \qquad (5\text{-}25)$$

By the same means as shown in Chapter 2, the parameters can be found under this method as follows

$$\boldsymbol{b}^{(k+1)}=\boldsymbol{b}^{(k)}+(\tilde{\boldsymbol{X}}^{(k)T}\tilde{\boldsymbol{X}}^{(k)})^{-1}\tilde{\boldsymbol{X}}^{(k)T}(\tilde{\boldsymbol{Y}}-\tilde{\boldsymbol{T}}^{(k)}) \qquad (2\text{-}26)$$

This equation has the same form as the conventional least squares method outlined in Chapter 2 except that the matrices involved have been treated with the pre-conditioning matrix.

At this point it should be noted that the term $\tilde{\boldsymbol{X}}^T\tilde{\boldsymbol{X}}$ can be rewritten as

$$\tilde{\boldsymbol{X}}^T\tilde{\boldsymbol{X}} = (\boldsymbol{M}_0\boldsymbol{X})^T(\boldsymbol{M}_0\boldsymbol{X})+w_1^2(\boldsymbol{M}_1\boldsymbol{X})^T(\boldsymbol{M}_1\boldsymbol{X})+w_2^2(\boldsymbol{M}_2\boldsymbol{X})^T(\boldsymbol{M}_2\boldsymbol{X}) \qquad (5\text{-}27)$$

which in turn can be rewritten as

$$\tilde{\boldsymbol{X}}^T\tilde{\boldsymbol{X}} = \boldsymbol{X}^T\boldsymbol{M}_0^T\boldsymbol{M}_0\boldsymbol{X} + w_1^2\boldsymbol{X}^T\boldsymbol{M}_1^T\boldsymbol{M}_1\boldsymbol{X} + w_2^2\boldsymbol{X}^T\boldsymbol{M}_1^T\boldsymbol{M}_1\boldsymbol{X} \qquad (5\text{-}28)$$

Factoring out the $\boldsymbol{X}$ matrices we have

$$\tilde{\boldsymbol{X}}^T\tilde{\boldsymbol{X}} = \boldsymbol{X}^T(\boldsymbol{M}_0^T\boldsymbol{M}_0 + w_1^2\boldsymbol{M}_1^T\boldsymbol{M}_1 + w_2^2\boldsymbol{M}_1^T\boldsymbol{M}_1)\boldsymbol{X} \qquad (5\text{-}29)$$

For the sake of compact notation, if we define

$$\boldsymbol{R} = \boldsymbol{M}_0^T\boldsymbol{M}_0 + w_1^2\boldsymbol{M}_1^T\boldsymbol{M}_1 + w_2^2\boldsymbol{M}_1^T\boldsymbol{M}_1 \tag{5-30}$$

Then we can use the shorthand notation of

$$\tilde{\boldsymbol{X}}^T\tilde{\boldsymbol{X}} = \boldsymbol{X}^T\boldsymbol{R}\,\boldsymbol{X} \tag{5-31}$$

This notation can also be used in the definition of the S term being minimized as described above

$$S=[\tilde{\boldsymbol{Y}}-\tilde{\boldsymbol{T}}]^T[\tilde{\boldsymbol{Y}}-\tilde{\boldsymbol{T}}] = [\boldsymbol{Y}-\boldsymbol{T}]^T\boldsymbol{R}[\boldsymbol{Y}-\boldsymbol{T}] \tag{5-32}$$

Finally, the equation for the estimated parameters can be rewritten as follows

$$\begin{aligned}\boldsymbol{b}^{(k+1)} &= \boldsymbol{b}^{(k)} + (\tilde{\boldsymbol{X}}^{(k)T}\tilde{\boldsymbol{X}}^{(k)})^{-1}\tilde{\boldsymbol{X}}^{(k)T}(\tilde{\boldsymbol{Y}}-\tilde{\boldsymbol{T}}^{(k)}) \\ &= \boldsymbol{b}^{(k)} + (\boldsymbol{X}^{(k)T}\boldsymbol{R}\,\boldsymbol{X}^{(k)})^{-1}\,\boldsymbol{X}^{(k)T}\boldsymbol{R}(\boldsymbol{Y}-\boldsymbol{T}^{(k)})\end{aligned} \tag{5-33}$$

In order to examine the nature of the "R" matrix, it is useful to generate a sample of the $\boldsymbol{M}_0^T\boldsymbol{M}_0$, $\boldsymbol{M}_1^T\boldsymbol{M}_1$, and $\boldsymbol{M}_2^T\boldsymbol{M}_2$ matrices that make up the "R" matrix. These are each n x n matrices, as is "R", where n is the number of measurements. In Tables 5-2 through 5-4, three 16 x 16 examples are shown, one for each of the three matrices noted above. As can be seen from these examples, each matrix is diagonally dominant, is repetitive along the diagonal and symmetrical about the diagonal. The repeating portion along the diagonal will be the same for any matrix 13 x 13 or larger.

9.07E-03	-1.36E-02	-2.72E-02	-3.17E-02	-2.72E-02	-1.36E-02	9.07E-03	0	0	0	0	0	0	0	0	0
-1.36E-02	2.95E-02	2.72E-02	2.04E-02	9.07E-03	-6.80E-03	-2.72E-02	9.07E-03	0	0	0	0	0	0	0	0
-2.72E-02	2.72E-02	0.111111	0.122449	0.102041	4.99E-02	-3.40E-02	-2.72E-02	9.07E-03	0	0	0	0	0	0	0
-3.17E-02	2.04E-02	0.122449	0.222222	0.217687	0.14966	1.81E-02	-3.40E-02	-2.72E-02	9.07E-03	0	0	0	0	0	0
-2.72E-02	9.07E-03	0.102041	0.217687	0.303855	0.258503	0.122449	1.81E-02	-3.40E-02	-2.72E-02	9.07E-03	0	0	0	0	0
-1.36E-02	-6.80E-03	4.99E-02	0.14966	0.258503	0.324263	0.244898	0.122449	1.81E-02	-3.40E-02	-2.72E-02	9.07E-03	0	0	0	0
9.07E-03	-2.72E-02	-3.40E-02	1.81E-02	0.122449	0.244898	0.333333	0.244898	0.122449	1.81E-02	-3.40E-02	-2.72E-02	9.07E-03	0	0	0
0	9.07E-03	-2.72E-02	-3.40E-02	1.81E-02	0.122449	0.244898	0.333333	0.244898	0.122449	1.81E-02	-3.40E-02	-2.72E-02	9.07E-03	0	0
0	0	9.07E-03	-2.72E-02	-3.40E-02	1.81E-02	0.122449	0.244898	0.333333	0.244898	0.122449	1.81E-02	-3.40E-02	-2.72E-02	9.07E-03	0
0	0	0	9.07E-03	-2.72E-02	-3.40E-02	1.81E-02	0.122449	0.244898	0.333333	0.244898	0.122449	1.81E-02	-3.40E-02	-2.72E-02	9.07E-03
0	0	0	0	9.07E-03	-2.72E-02	-3.40E-02	1.81E-02	0.122449	0.244898	0.324263	0.258503	0.14966	4.99E-02	-6.80E-03	-1.36E-02
0	0	0	0	0	9.07E-03	-2.72E-02	-3.40E-02	1.81E-02	0.122449	0.258503	0.303855	0.217687	0.102041	9.07E-03	-2.72E-02
0	0	0	0	0	0	9.07E-03	-2.72E-02	-3.40E-02	1.81E-02	0.14966	0.217687	0.222222	0.122449	2.04E-02	-3.17E-02
0	0	0	0	0	0	0	9.07E-03	-2.72E-02	-3.40E-02	4.99E-02	0.102041	0.122449	0.111111	2.72E-02	-2.72E-02
0	0	0	0	0	0	0	0	9.07E-03	-2.72E-02	-6.80E-03	9.07E-03	2.04E-02	2.72E-02	2.95E-02	-1.36E-02
0	0	0	0	0	0	0	0	0	9.07E-03	-1.36E-02	-2.72E-02	-3.17E-02	-2.72E-02	-1.36E-02	9.07E-03

Table 5-2 $M_0^T M_0$ Matrix For 16 Point Example

1.15E-02	7.65E-03	3.83E-03	0	-3.83E-03	-7.65E-03	-1.15E-02	0	0	0	0	0	0	0	0	0
7.65E-03	1.66E-02	1.02E-02	3.83E-03	-2.55E-03	-8.93E-03	-1.53E-02	-1.15E-02	0	0	0	0	0	0	0	0
3.83E-03	1.02E-02	1.79E-02	1.02E-02	2.55E-03	-5.10E-03	-0.01276	-1.53E-02	-1.15E-02	0	0	0	0	0	0	0
0	3.83E-03	1.02E-02	1.79E-02	1.02E-02	2.55E-03	-5.10E-03	-0.01276	-1.53E-02	-1.15E-02	0	0	0	0	0	0
-3.83E-03	-2.55E-03	2.55E-03	1.02E-02	1.91E-02	0.012755	6.38E-03	-5.10E-03	-0.01276	-1.53E-02	-1.15E-02	0	0	0	0	0
-7.65E-03	-8.93E-03	-5.10E-03	2.55E-03	0.012755	0.024235	2.04E-02	6.38E-03	-5.10E-03	-0.01276	-1.53E-02	-1.15E-02	0	0	0	0
-1.15E-02	-1.53E-02	-0.01276	-5.10E-03	6.38E-03	2.04E-02	3.57E-02	2.04E-02	6.38E-03	-5.10E-03	-0.01276	-1.53E-02	-1.15E-02	0	0	0
0	-1.15E-02	-1.53E-02	-0.01276	-5.10E-03	6.38E-03	2.04E-02	3.57E-02	2.04E-02	6.38E-03	-5.10E-03	-0.01276	-1.53E-02	-1.15E-02	0	0
0	0	-1.15E-02	-1.53E-02	-0.01276	-5.10E-03	6.38E-03	2.04E-02	3.57E-02	2.04E-02	6.38E-03	-5.10E-03	-0.01276	-1.53E-02	-1.15E-02	0
0	0	0	-1.15E-02	-1.53E-02	-0.01276	-5.10E-03	6.38E-03	2.04E-02	3.57E-02	2.04E-02	6.38E-03	-5.10E-03	-0.01276	-1.53E-02	-1.15E-02
0	0	0	0	-1.15E-02	-1.53E-02	-0.01276	-5.10E-03	6.38E-03	2.04E-02	2.42E-02	0.012755	2.55E-03	-5.10E-03	-8.93E-03	-7.65E-03
0	0	0	0	0	-1.15E-02	-1.53E-02	-0.01276	-5.10E-03	6.38E-03	0.012755	1.91E-02	1.02E-02	2.55E-03	-2.55E-03	-3.83E-03
0	0	0	0	0	0	-1.15E-02	-1.53E-02	-0.01276	-5.10E-03	2.55E-03	1.02E-02	1.79E-02	1.02E-02	3.83E-03	0
0	0	0	0	0	0	0	-1.15E-02	-1.53E-02	-0.01276	-5.10E-03	2.55E-03	1.02E-02	1.79E-02	1.02E-02	3.83E-03
0	0	0	0	0	0	0	0	-1.15E-02	-1.53E-02	-8.93E-03	-2.55E-03	3.83E-03	1.02E-02	1.66E-02	7.65E-03
0	0	0	0	0	0	0	0	0	-1.15E-02	-7.65E-03	-3.83E-03	0	3.83E-03	7.65E-03	1.15E-02

Table 5-3 $M_1^T M_1$ Matrix for 16 Point Example

3.54E-03	0	-2.13E-03	-2.83E-03	-2.13E-03	0	3.54E-03	0	0	0	0	0	0	0	0	0
0	3.54E-03	0	-2.13E-03	-2.83E-03	-2.13E-03	0	3.54E-03	0	0	0	0	0	0	0	0
-2.13E-03	0	4.82E-03	1.70E-03	-8.50E-04	-2.83E-03	-4.25E-03	0	3.54E-03	0	0	0	0	0	0	0
-2.83E-03	-2.13E-03	1.70E-03	7.09E-03	3.40E-03	-8.50E-04	-5.67E-03	-4.25E-03	0	3.54E-03	0	0	0	0	0	0
-2.13E-03	-2.83E-03	-8.50E-04	3.40E-03	8.36E-03	3.40E-03	-2.98E-03	-5.67E-03	-4.25E-03	0	3.54E-03	0	0	0	0	0
0	-2.13E-03	-2.83E-03	-8.50E-04	3.40E-03	8.36E-03	3.40E-03	-2.98E-03	-5.67E-03	-4.25E-03	0	3.54E-03	0	0	0	0
3.54E-03	0	-4.25E-03	-5.67E-03	-2.98E-03	3.40E-03	1.19E-02	3.40E-03	-2.98E-03	-5.67E-03	-4.25E-03	0	3.54E-03	0	0	0
0	3.54E-03	0	-4.25E-03	-5.67E-03	-2.98E-03	3.40E-03	1.19E-02	3.40E-03	-2.98E-03	-5.67E-03	-4.25E-03	0	3.54E-03	0	0
0	0	3.54E-03	0	-4.25E-03	-5.67E-03	-2.98E-03	3.40E-03	1.19E-02	3.40E-03	-2.98E-03	-5.67E-03	-4.25E-03	0	3.54E-03	0
0	0	0	3.54E-03	0	-4.25E-03	-5.67E-03	-2.98E-03	3.40E-03	1.19E-02	3.40E-03	-2.98E-03	-5.67E-03	-4.25E-03	0	3.54E-03
0	0	0	0	3.54E-03	0	-4.25E-03	-5.67E-03	-2.98E-03	3.40E-03	8.36E-03	3.40E-03	-8.50E-04	-2.83E-03	-2.13E-03	0
0	0	0	0	0	3.54E-03	0	-4.25E-03	-5.67E-03	-2.98E-03	3.40E-03	8.36E-03	3.40E-03	-8.50E-04	-2.83E-03	-2.13E-03
0	0	0	0	0	0	3.54E-03	0	-4.25E-03	-5.67E-03	-8.50E-04	3.40E-03	7.09E-03	1.70E-03	-2.13E-03	-2.83E-03
0	0	0	0	0	0	0	3.54E-03	0	-4.25E-03	-2.83E-03	-8.50E-04	1.70E-03	4.82E-03	0	-2.13E-03
0	0	0	0	0	0	0	0	3.54E-03	0	-2.13E-03	-2.83E-03	-2.13E-03	0	3.54E-03	0
0	0	0	0	0	0	0	0	0	3.54E-03	0	-2.13E-03	-2.83E-03	-2.13E-03	0	3.54E-03

Table 5-4 $M_2^T M_2$ Matrix for 16 Point Example

For virtually all experiments in parameter estimation, there are many more than 13 measurements over the time of the experiment.

Several other items of note related to the three matricies exhibited in these figures include the existence of both positive and negative values and the sums of the interior rows. Since the factored component matricies of each of the three product matricies contain both positive and negative values, it is natural that the product matricies also contain numbers of both signs as brought about in the various cross products. Another similarity of the three product matricies to the factored component matricies is that the interior rows of the "0" matrices sum to 1 and the interior rows of the "1" and "2" matrices sum to zero.

5.5 BIAS AND COVARIANCE

In order to determine if bias exists, we find the expected value of $\mathbf{b}^{(k+1)}$ as calculated using Equation (2-26), and determine if it is equal to the expected value of the true parameter vector, β. As the non-linear iteration process nears convergence, the estimated parameter vector becomes very close to the true parameter vector. As such, the estimated parameter vector can be approximated as

$$\boldsymbol{b}^{(k+1)} \approx \beta + (\boldsymbol{X}^T\boldsymbol{R}\boldsymbol{X})^{-1}\,\boldsymbol{X}^T\boldsymbol{R}(\boldsymbol{Y}-\boldsymbol{T}) \qquad (5\text{-}34)$$

where all non-superscripted matrices are assumed to be of the k iteration. As such, the expected value of **b** is

$$E(\boldsymbol{b}) \approx \beta + (\boldsymbol{X}^T\boldsymbol{R}\boldsymbol{X})^{-1}\,\boldsymbol{X}^T\boldsymbol{R}[E(\boldsymbol{Y}-\boldsymbol{T})] \qquad (5\text{-}35)$$

where **Y-T** is equal to **e**. Assuming that the errors are additive and have zero mean, we can say that the expected value of **e** is zero. Substituting this into Equation (5-35), the expected value of **b** becomes equal to β. This shows that there is no bias associated with the method, which is fortunate, since all commonly used regularization methods come at the price of bias.

Next it is desired to calculate the covariance matrix for the estimated parameter vector **b**. This is defined as

$$cov(\boldsymbol{b}) = E\left[(\boldsymbol{b}-\beta)(\boldsymbol{b}-\beta)^T\right] \qquad (5\text{-}36)$$

where β is the true but unknown vector of parameters. Since the measurement errors are additive, we have

$$\boldsymbol{Y}=\boldsymbol{T}+\boldsymbol{e} \qquad (5\text{-}37)$$

where **e** is the error vector. As we approach convergence using the non-linear least squares method, we expect the differences between calculated temperature values from one iteration to the next to be on the order of the measurement

errors. If this is the case, we can approximate the error vector as

$$\mathbf{X}\mathbf{b}^{(k+1)} \approx \mathbf{X}\mathbf{b}^{(k)} + \boldsymbol{\varepsilon} \tag{5-38}$$

We now define

$$\mathbf{A} = (\mathbf{X}^T\mathbf{R}\mathbf{X})^{-1}\,\mathbf{X}^T\mathbf{R} \tag{5-39}$$

then $\mathbf{A}\mathbf{X}=\mathbf{I}$. If we pre-multiply both sides of Equation 5-38 by $\mathbf{A}$ we have

$$\mathbf{b}^{(k+1)} \approx \mathbf{b}^{(k)} + \mathbf{A}\boldsymbol{\varepsilon} \text{ or } \mathbf{b}^{(k+1)} - \mathbf{b}^{(k)} \approx \mathbf{A}\boldsymbol{\varepsilon} \tag{5-40}$$

Substituting this into the definition of covariance given above we have

$$\mathrm{cov}(\mathbf{b}^{(k+1)}) \approx E[(\mathbf{A}\boldsymbol{\varepsilon})(\mathbf{A}\boldsymbol{\varepsilon})^T] \tag{5-41}$$

Using the covariance matrix definition of

$$\psi = E[\boldsymbol{\varepsilon}\boldsymbol{\varepsilon}^T] \tag{5-42}$$

we now have

$$\mathrm{cov}(\mathbf{b}^{(k+1)}) \approx \mathbf{A}\psi\mathbf{A}^T \tag{5-43}$$

Writing this in expanded form and understanding the $\mathbf{b}$ vector to be of the final iteration we have

$$\mathrm{cov}(\mathbf{b}) \approx (\mathbf{X}^T\mathbf{R}\mathbf{X})^{-1}\,\mathbf{X}^T\mathbf{R}\psi\mathbf{R}\mathbf{X}\,(\mathbf{X}^T\mathbf{R}\mathbf{X})^{-1} \tag{5-44}$$

This is a p x p matrix where p is the number of parameters. The ψ matrix is an n x n matrix where n is the number of measurements. For simplicity, the ψ matrix can be modeled as

$$\psi = \sigma^2[\mathbf{I}] \tag{5-45}$$

where σ^2 is the variance of the measurement errors.

Using this assumption to compare the covariance of the regularized parameters with that of the non-regularized parameters, two models of the sensitivity coefficients were used as a means of comparison. The cubic model utilized a simple cubic curve of

$$T(t) = \beta_1 t^3 + \beta_2 t^2 + \beta_3 t + \beta_4 \qquad (5\text{-}46)$$

as the assumed temperature measurement curve with β_1, β_2, β_3 and β_4 being the four unknown parameters. Using a sample case of 16 equally spaced measurements from t=0.1 to t=1.6, the covariance matrix of **b** for this example is

1.662088	-7.49542	9.065934	-3.20513
-7.49542	40.5623	-53.218	19.70266
9.065934	-53.218	73.44436	-28.1152
-3.20513	19.70266	-28.1152	11.02555

For the regularized case, the covariance matrix is

3.073613	-13.1621	15.62973	-5.47699
-13.1621	64.92957	-83.1152	30.63121
15.62973	-83.1152	111.7891	-42.6842
-5.47699	30.63121	-42.6842	16.73889

As can be seen from comparing these two covariance matrices, the regularized case has higher values by 50 to 80 percent when compared to the non-regularized case. This indicates that the regularization method will give larger errors in the parameters than will the ordinary least squares method.

This is to be expected since the Gauss-Markov Theorem, as given in reference [25], states that the ordinary least squares method will provide the minimum covariance matrix for parameter estimation, assuming the standard statistical assumptions, as given by that reference, are valid for the measurement errors.

Another set of covariance matrices is compared, using 100 points from the internal radiation model presented in Chapter 3. The covariance matrix for the ordinary least squares case for this model, using the thermal parameters α=1, q_0=1, Bi=1 and k_{ro}/k=0.1, is

7648816	125557.5	-7655539	-8.2E+07
125557.5	2117.377	-125607	-1344766
-7655539	-125607	7662336	81976237
-8.2E+07	-1344766	81976237	8.77E+08

Comparing this once again to the case where derivative regularization is used, the covariance matrix is as follows:

13654443	223716.7	-1.37E+07	-1.46E+08
223716.7	3748.345	-223818	-2395863
-1.37E+07	-223818	13678306	1.46E+08
-1.46E+08	-2395863	1.46E+08	1.57E+09

Once again, these values fall somewhere between 50 and 80 percent larger than the covariance for the non-regularized case, indicating that the errors generated using the

derivative regularization method are expected to be larger than those generated from using ordinary least squares. Both of these covariance matrices are significantly larger than in the previous sample problem, indicating that the errors expected in estimating the parameters from the internal radiation test case are significantly larger than those generated from the cubic model.

As a Monte Carlo test of this tendency, 100 simulated experiments were conducted by imposing errors of zero mean and gaussian distribution on a file of an exact direct solution. The true parameter values of the exact solution were unity for diffusivity, Biot Number and heat flux. The standard deviation of the imposed errors was approximately 0.01 and the peak temperature reached was approximately 0.4 non-dimensional temperature units. The exact solution was generated for a simple flash experiment assuming no penetration of the flash. Figure 5-4 shows three distribution curves of the results for the 100 test cases. This graph illustrates the unbiased nature of ordinary least squares and the sharp resolution rendered for each of the parameters. With errors larger than two percent of peak measured temperature, there were essentially no cases with errors in the estimated parameters larger than 5 percent.

Figure 5-5 is a representation of the same test

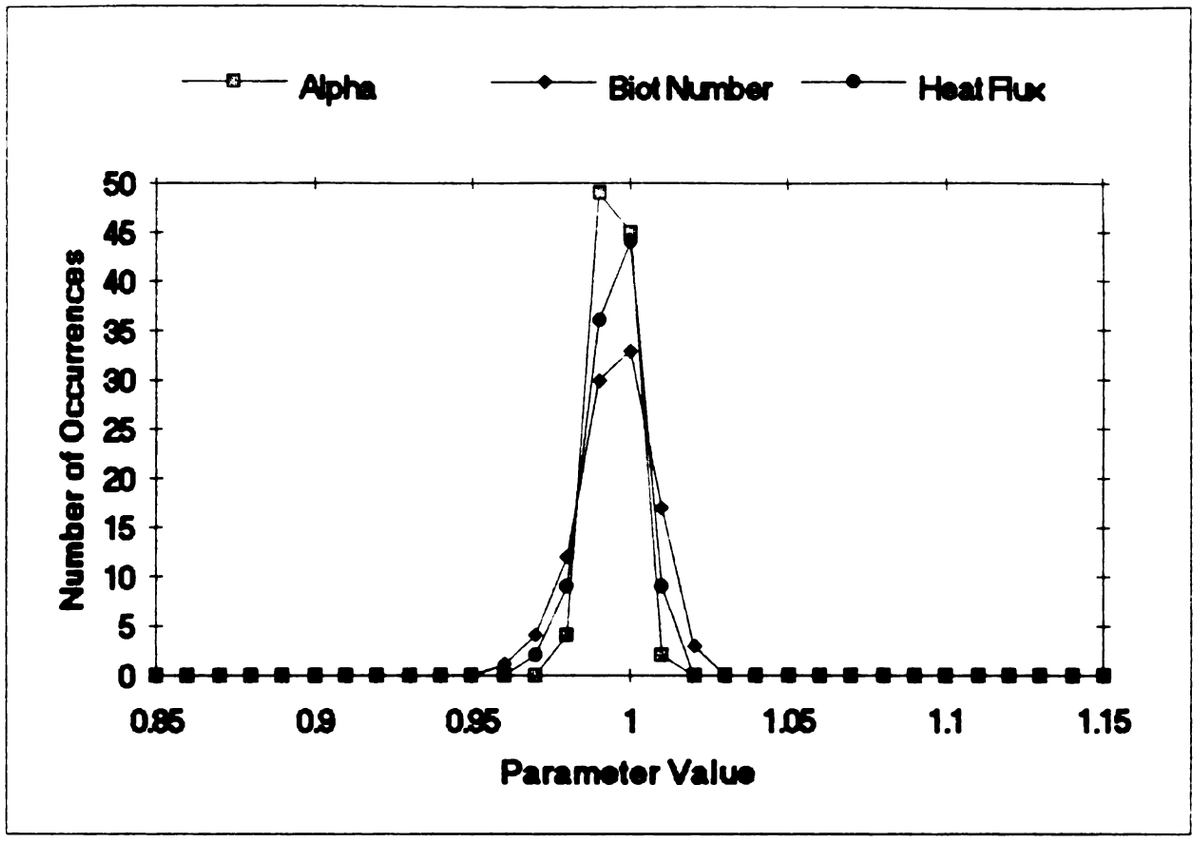

Figure 5-4 Monte Carlo Results Using Ordinary Least Squares

TABLE 5-5

Monte Carlo Results Comparing Derivative Regularization to Ordinary Least Squares

	Non-Regularized	Regularized
Mean Diffusivity	0.999775	1.00027
Mean Biot Number	1.00091	0.99853
Mean Heat Flux	1.000885	0.999075
Diffusivity Std Dev	0.005521	0.013181
Biot Number Std Dev	0.01127	0.037045
Heat Flux Std Dev	0.007924	0.025711

performed using derivative regularization. The same unbiased feature of this method is apparent as evidenced by the symmetrical appearance of the curves about unity. The

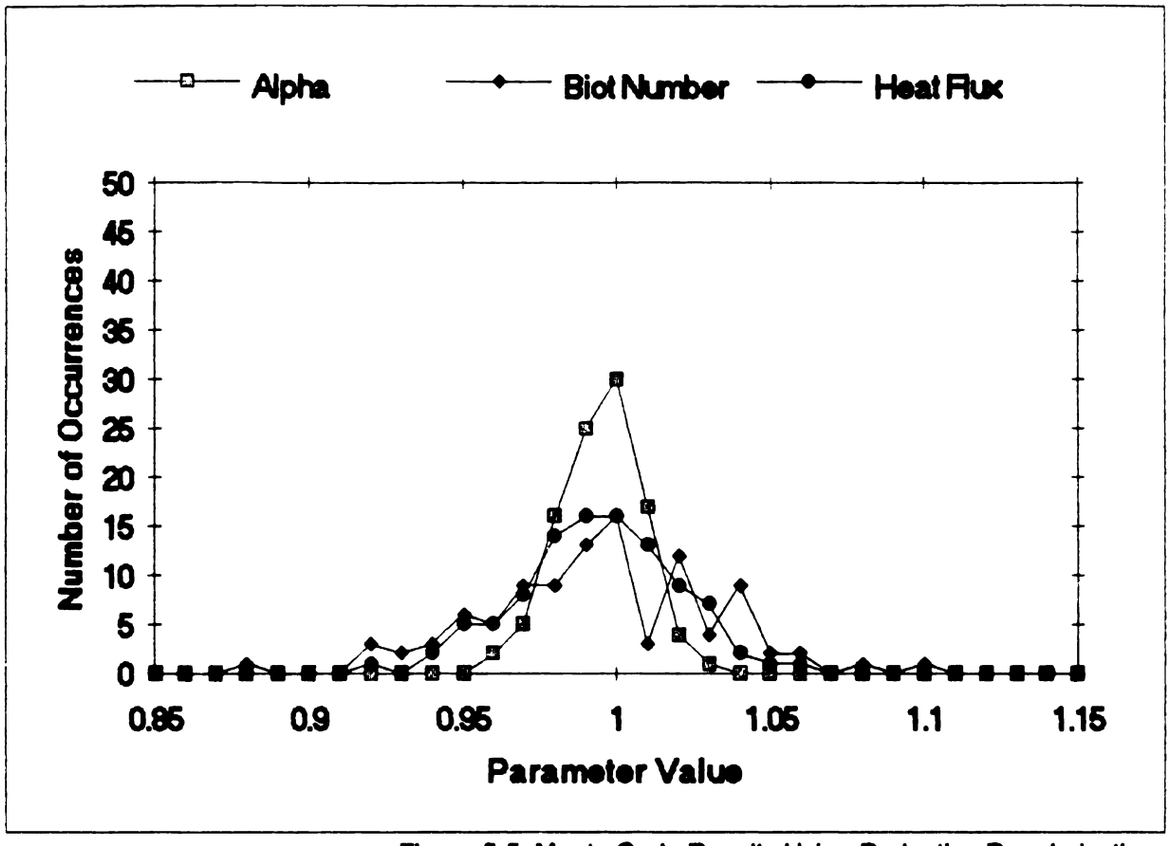

Figure 5-5 Monte Carlo Results Using Derivative Regularization

resolution provided by this method, however, is clearly inferior to ordinary least squares as evidenced by the wider distribution of estimated parameters. Table 5-5 further contrasts the difference between the two methods by comparing the standard deviations of the estimated parameters. The larger standard deviations associated with the derivative regularization method, reaffirm the cost of reduced accuracy in using the method. The unbiased nature of the method is illustrated by noting the average estimated parameters and their close proximity to the true parameter values of unity.

Interestingly, a comparison of the residuals using both methods suggests almost identical performance. The average value of the standard deviation of the residuals is 0.00402 for both methods. This fact might give the impression to the user of the method that the results from one method are just as accurate as the other. As can be seen in the figures and tables associated with this test, however, this is not so.

5.6 MATRIX CONDITION NUMBER

Although the errors associated with the parameter estimates using derivative regularization are expected to be larger than those generated using the method of ordinary least squares, the advantage of the derivative regularization method lies in the reduction of the condition number of the $\mathbf{X}^T\mathbf{X}$ matrix. In many cases in parameter estimation problems, the $\mathbf{X}^T\mathbf{X}$ matrix is so ill-conditioned that no parameters can be calculated; the numerical results become nonsense. It is under these conditions that derivative regularization becomes profitable.

The condition number is a measure of the stability of a set of linear equations. As stated in reference [26], the condition number provides a measure of how reliably the relative residual of an approximate solution reflects the

relative error of the approximate solution. The lowest possible condition number is 1, which is the condition number for the identity matrix. The means of calculation of the condition number is somewhat subjective, hinging on the method used in calculating the matrix norm. The definition of condition number given in reference [26] is the product of the norm of the matrix multiplied by the norm of the inverse of the matrix. The condition number of a general square matrix $\mathbf{A}$ would therefore be

$$\text{Condition Number} = ||\mathbf{A}||\ ||\mathbf{A}^{-1}|| \tag{5-47}$$

where the norm of the matrix $\mathbf{A}$ is defined as

$$||\mathbf{A}|| = \max \frac{||\mathbf{a}_i \mathbf{x}||}{||\mathbf{x}||} \tag{5-48}$$

In this definition, the i subscripts designate any row of the matrix $\mathbf{A}$. The norm of one vector $\mathbf{x}$ as a function of the individual elements of the vector is

$$||\mathbf{x}|| = (|x_1|^n + |x_2|^n + |x_3|^n + \ldots + |x_m|^n)^{1/n} \tag{5-49}$$

Since n can be any whole number $(1,2,3,\ldots,\infty)$, the most commonly utilized norms are the 1,2 and infinity norms. For the sake of convenience, the actual routine used to calculate condition number in the subsequent graphs is found in the commercial mathematical product MATLAB. The results using this method are comparable to the other methods of calculating condition number, particularly when comparing

regularized to non-regularized cases.

The condition numbers for the test cases noted above were found to be sharply reduced by the use of derivative regularization over a wide range of weighing factors. Reductions on the order of approximately 50 are attainable. This allows calculations to be performed to solve the equation

$$\mathbf{b}^{(k+1)}=\mathbf{b}^{(k)}+(\mathbf{X}^{(k)T}\mathbf{R}\,\mathbf{X}^{(k)})^{-1}\mathbf{X}^{(k)T}\mathbf{R}(\mathbf{Y}-\mathbf{T}^{(k)}) \qquad (5\text{-}50)$$

for the parameter vector $\mathbf{b}$ when otherwise no solution is obtainable from the non-regularized equation

$$\mathbf{b}^{(k+1)}=\mathbf{b}^{(k)}+(\mathbf{X}^{(k)T}\mathbf{X}^{(k)})^{-1}\mathbf{X}^{(k)T}(\mathbf{Y}-\mathbf{T}^{(k)}) \qquad (5\text{-}51)$$

Figures 5-6 through 5-9 are plots of the condition numbers for various sample problems. These graphs show the effect of the weighting factors, w_1 and w_2 on the "condition number ratio" which is defined in these examples as the ratio of the condition number of the $\mathbf{X}^T\mathbf{R}\mathbf{X}$ matrix to the condition number of the $\mathbf{X}^T\mathbf{X}$ matrix. Figure 5-6 is an example using 16 simulated data points from a cubic model from the equation

$$Y=b_1t^3+b_2t^2+b_3t+b_4 \qquad (5\text{-}52)$$

with $b_1=b_2=b_3=b_4=1$ as the parameters. The time scale used is from 0 to 1.6 seconds. Figure 5-7 is an example of the same

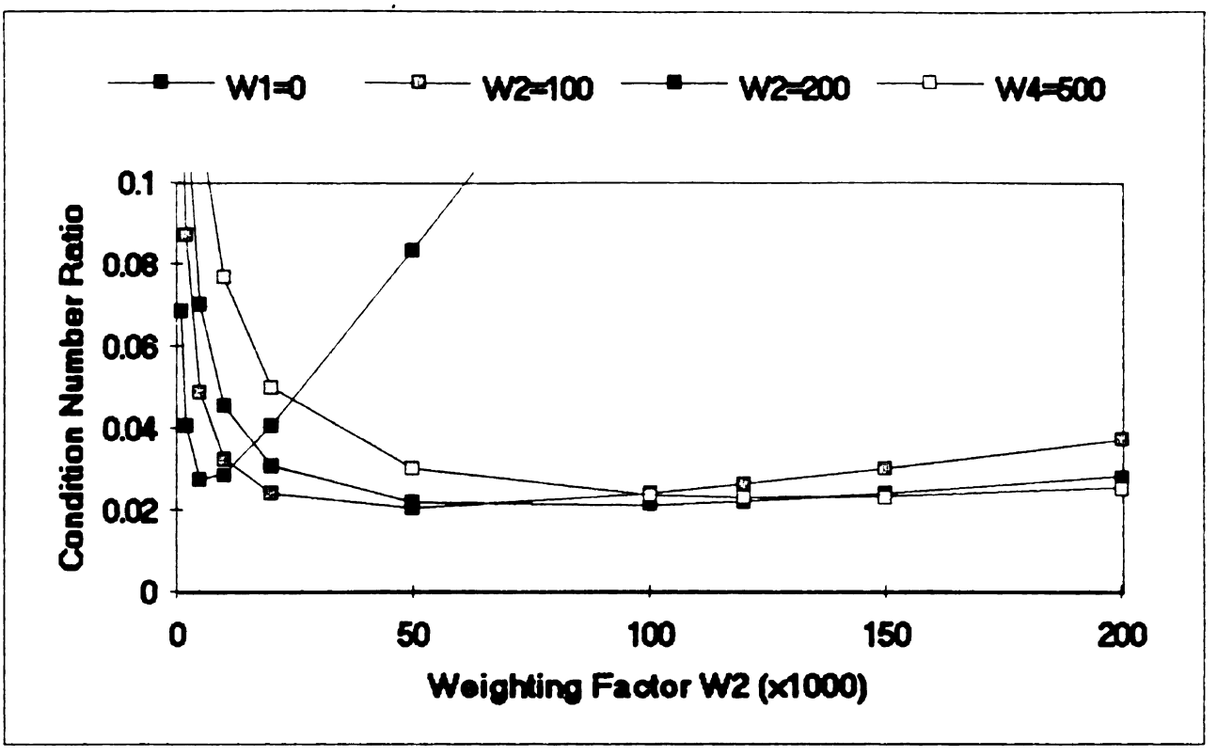

Figure 5-6 Condition Number Ratio for Cubic Case Using 16 Points

model using 100 points over the same time domain as the 16 point example. Larger weighting factors must be used in order to bring about the same reduction in condition number for this case, but approximately the same magnitude of reduction in condition number is obtained. Figure 5-8 plots the same factors for the internal radiation model described in Chapter 3. This figure also is taken from a sample direct solution utilizing 16 time step points. Finally, Figure 5-9 is the same as Figure 5-8 except that 100 points are used instead of 16. The basic shape of these curves is the same as that of Figures 5-8 and 5-9 with the same approximate reduction in condition number. Once again, the examples which utilized more time steps required larger

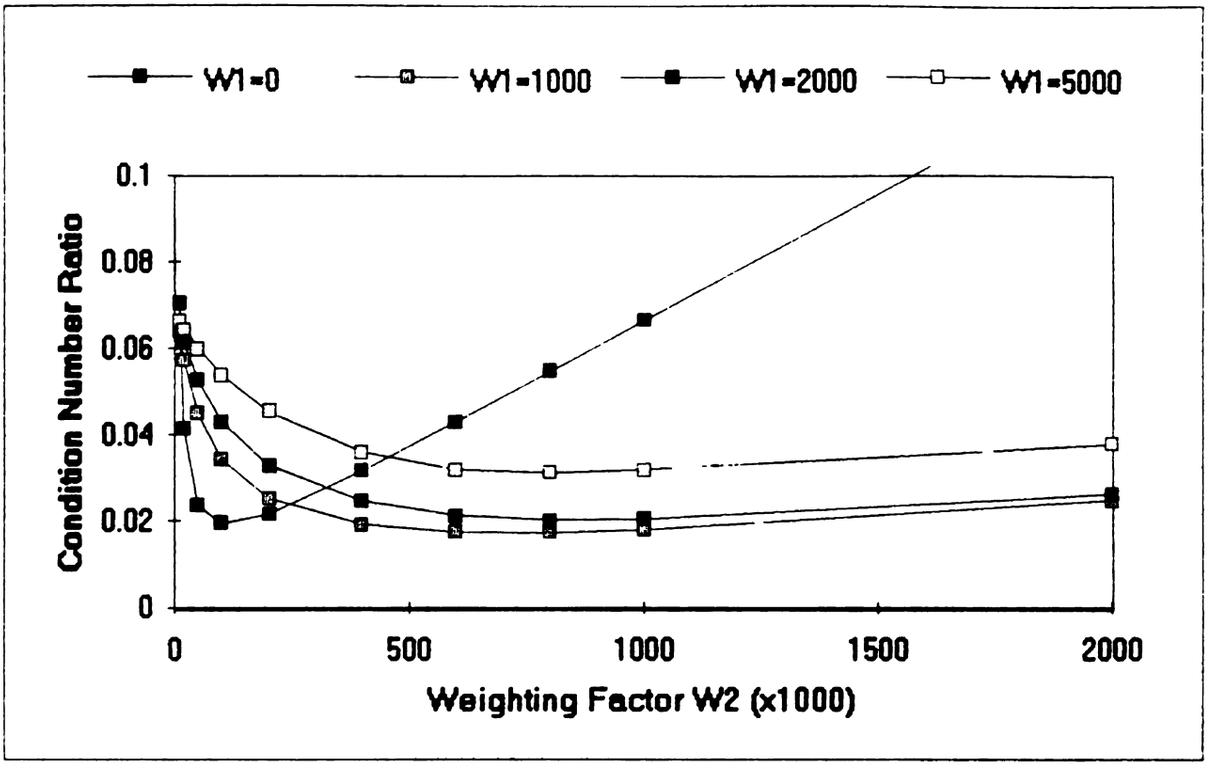

Figure 5-7 Condition Number for Cubic Case Using 100 Points

weighting factors in order to bring about the same reduction in condition number.

The results of the derivative regularization method have also shown to be successful in obtaining convergence in comparison to the ordinary least squares estimation schemes used previously. The decrease in the ill-conditioned nature of the matrices has facilitated the calculation of answers which were previously unavailable. As a first attempt at using the method, the results shown in Table 5-6 were achieved in seven iterations.

Following this test of initial values 20 percent above the actual values, a similar test was run with initial

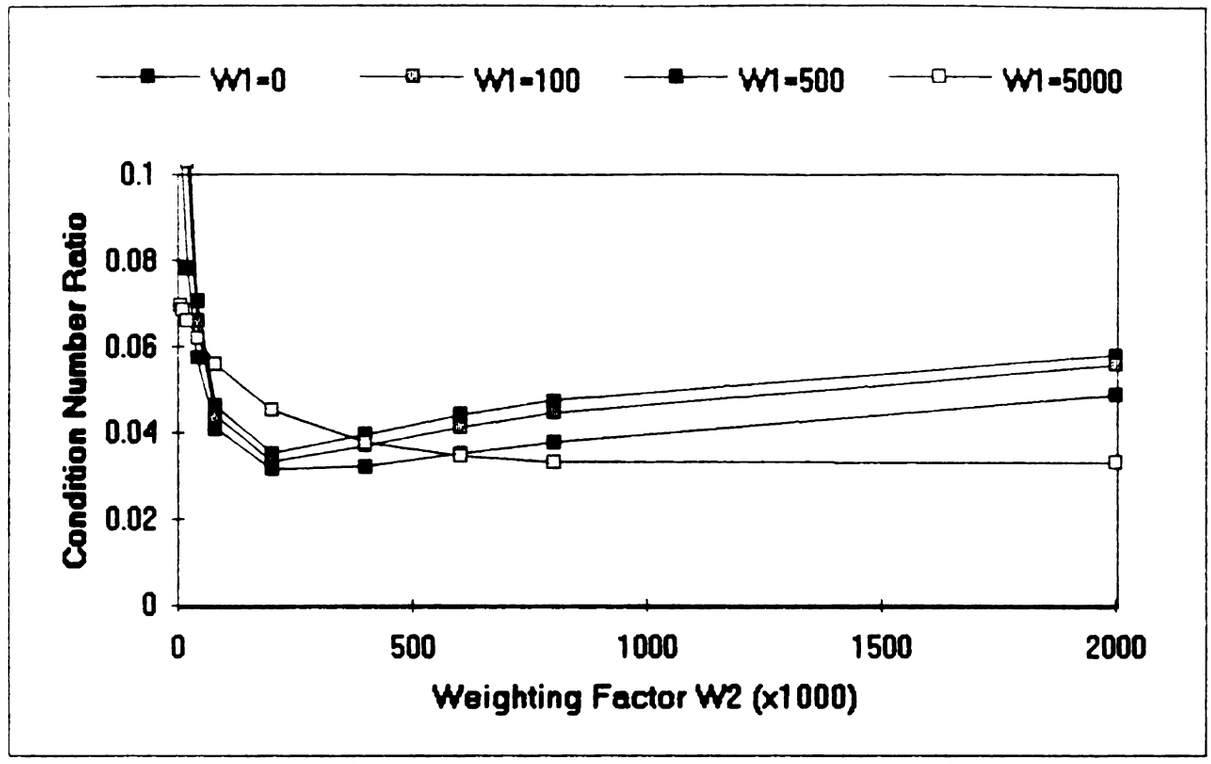

Figure 5-8 Condition Number Ratio for Internal Radiation Case using 16 Points

values 50 percent above parameter actual values. This test did not converge. As an additional attempt at stabilizing the spline parameter estimation procedure, a limit was placed on the maximum allowed change in parameters per iteration of 10 percent. The test run with initial values 50 percent above actual parameter values was re-executed with this restriction in place and convergence was obtained in the same 7 iterations with the same final parameter estimates as shown in Table 5-6. Using this additional restriction, parameter estimates were obtainable with errors for the initial values as high as 200 percent. A marked improvement over ordinary least squares where convergence

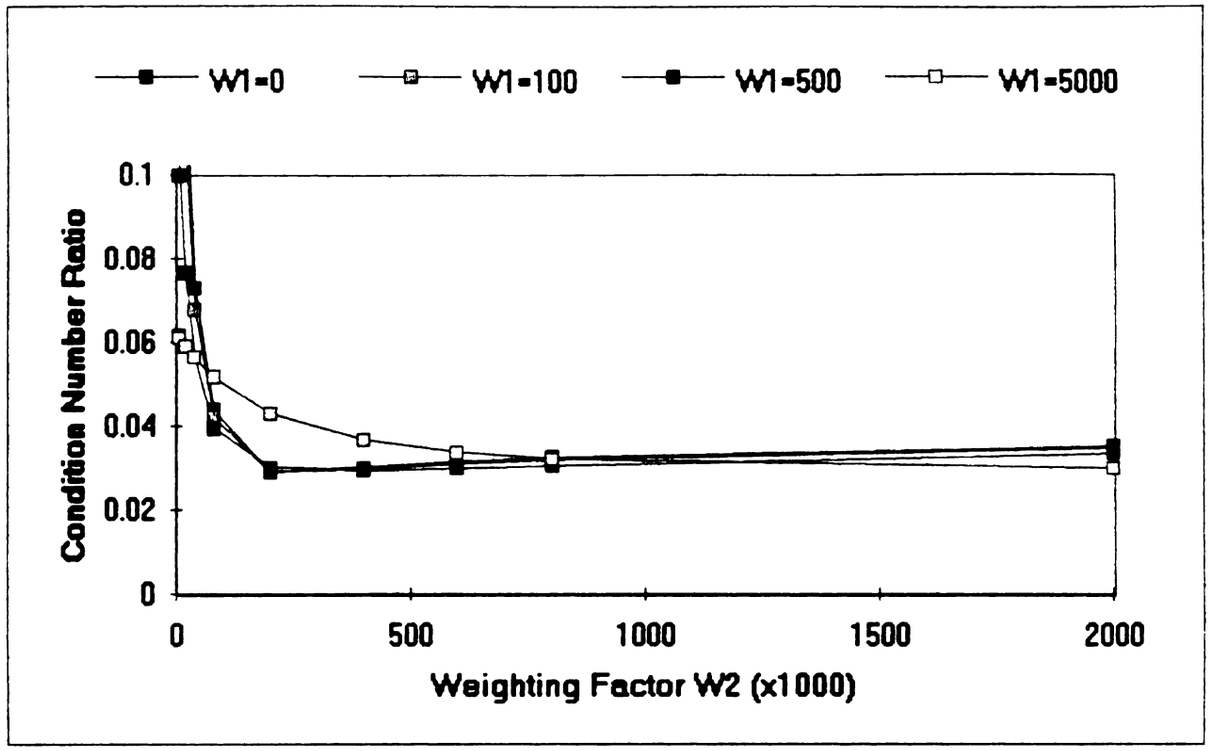

Figure 5-9 Condition Number for Internal Radiation Case Using 100 Points

Table 5-6

Parameter Estimation Using Derivative Regularization

	Diffusivity	Heat Flux	Biot Number	k_{ro}/k
Actual Values	1	1	1	0.1
Initial Values	2.0	2.0	2.0	0.20
Estimated Values	1.00000	1.00000	1.00000	0.10000

was not obtainable beyond a one percent deviation from the initial parameter seed values to the true parameter values.

CHAPTER 6

OPTIMIZING THE ANALYSIS METHOD

6.1 INTRODUCTION

The identification of the most appropriate model for a particular experiment can be a difficult problem since factors which determine model appropriateness are often contradictory between competing models. The length of the measured time scale to be used in the analysis is an example of a difficult experiment design aspect as well. Clearly, temperature readings taken at excessively late times in the experiment contribute virtually no useful information to the analysis and may serve only to degrade the accuracy of the estimates for the parameters of interest. Finding the time window which provides the best information for estimating the parameters can be difficult to identify. The elimination of the heat flux parameter is a popular method used in analysis of flash diffusivity problems, but the effectiveness of this technique is somewhat debatable. This chapter deals with miscellaneous issues affecting the accuracy of various flash diffusivity analysis methods.

Section 6.2 of this chapter deals with the mollification method as a means of smoothing measurement

errors and as a means of estimating the standard deviation of the errors. A method which eliminates the heat flux parameter is discussed in Section 6.3 in the interest of eliminating unnecessary parameters to simplify the parameter estimation process. Section 6.4 deals with the effects of changing the time duration of the experiment in order to optimize experiment design. This section also examines new and existing methods of determining model appropriateness. Various models are compared using these methods. The technique of parameter estimation by sequential experiments is applied in Section 6.5. This method analyzes parameters utilizing data from multiple experiments simultaneously. Section 6.6 discusses the application of frequency distribution routines using fast Fourier transforms on the residual curves generated from various experiments performed in Europe, Asia and the United States. Finally, Section 6.7 provides a summary of analyses performed on samples of various thickness of the same material from Oak Ridge National Laboratory.

6.2 USING MOLLIFICATION

The method of mollification, as described in [26], is a weighted method of smoothing data in order to minimize the effect of measurement errors. In utilizing this method, a

"blurring radius", δ, is selected based on the nature of the measurement errors. This blurring radius is normally expressed in terms of a number of measurements either side of the measurement being mollified. The mollified value of each point in the measured data is determined as follows

$$f(n) = \sum_{i=-3\delta}^{i=3\delta} p(i)\, Y(n+i) \qquad (6\text{-}1)$$

where Y(n) is the value of the measured temperature at measurement point n and p(i) is the weighting function for the measurement point n, a distance *i* measurements away from the point n. The weighting functions are determined as follows

$$p(i) = \frac{1}{\delta\sqrt{\pi}} e^{-\frac{i^2}{\delta^2}} \qquad (6\text{-}2)$$

Using this method,

$$\sum_{i=-3\delta}^{i=3\delta} p(i) \approx 1 \qquad (6\text{-}3)$$

Selecting the blurring radius can be somewhat of an imprecise process. One way of doing this is to gradually increase the blurring radius from 1 to 2 to 3 measurements and graph the mollified points on the same axes as the non-mollified points. In some cases, correlated data will require a larger blurring radius in order to compensate for

the correlation in the errors. If the blurring radius is too small, the mollified data will tend to follow the correlations in the errors. If the blurring radius is too large, however, the mollified data curve may not follow the true data path.

In flash diffusivity experiments the area of the measurement curve most susceptible to a misrepresentation of the data by a large blurring radius is at the peak temperature measurement point. Figures 6-1 through 6-3 show this area of the curve for three blurring radius selections. Figure 6-1 depicts a blurring radius of two measurements. Figure 6-2 depicts a blurring radius of three measurements. Figure 6-3 depicts a blurring radius of five measurements. If a an overly large blurring radius is chosen, this area of the curve will reveal the mollified points continually lower than the measured data. In this case, a blurring radius of 5 measurements seems to be appropriate. The mollified curve appears smooth but still appears representative of the overall measurement magnitudes, even at the peak of the curve.

Figure 6-4 shows a comparison of two residual curves, comparing a mollified case to a non-mollified case using the same mathematical model in analyzing the data. The calculated standard deviation of the residuals using

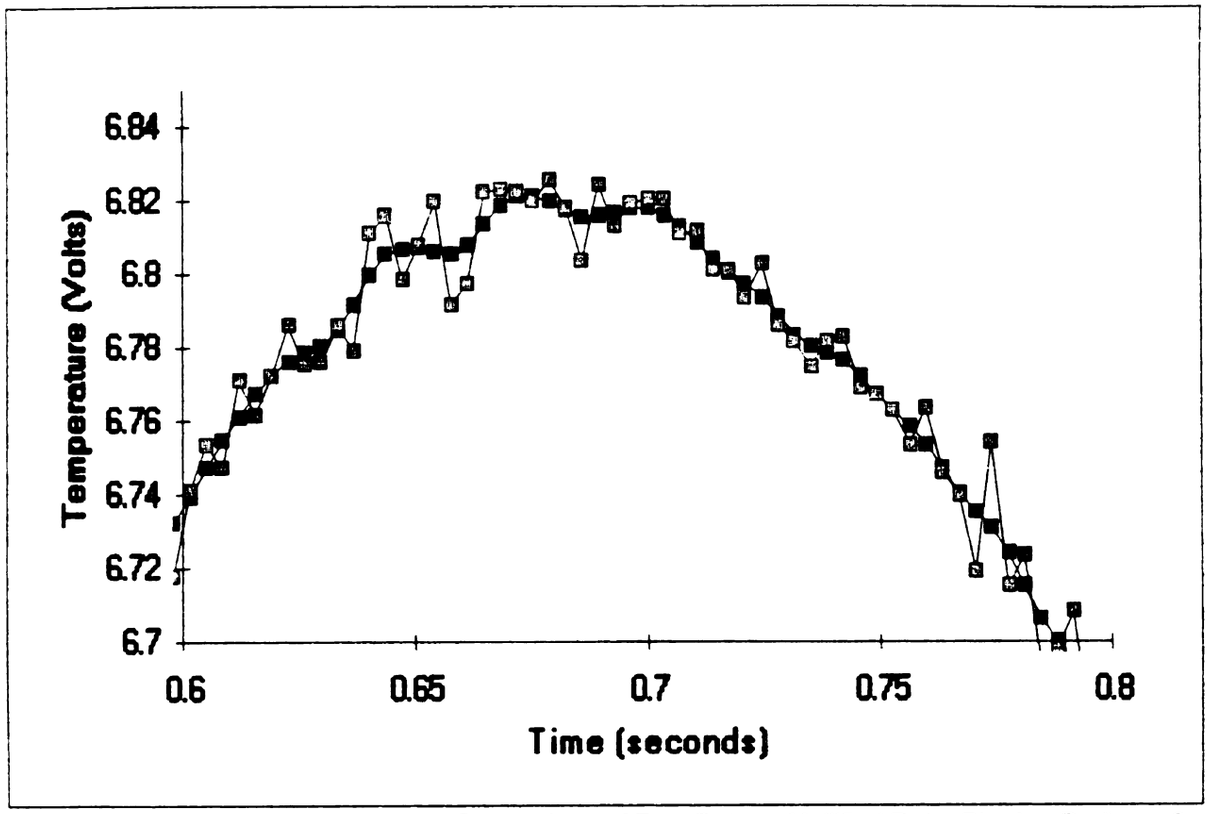

Figure 6-1 A Comparison of Raw Data to Mollified Data, Blurring Radius = 2

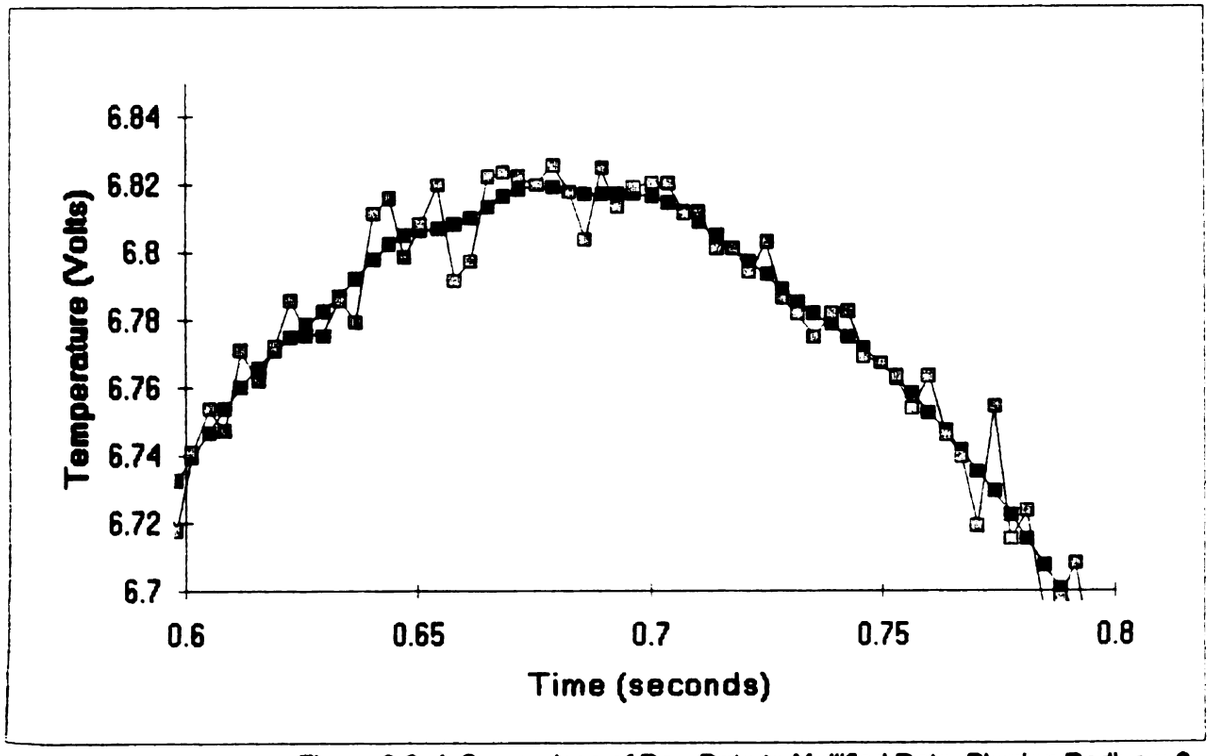

Figure 6-2 A Comparison of Raw Data to Mollified Data, Blurring Radius = 3

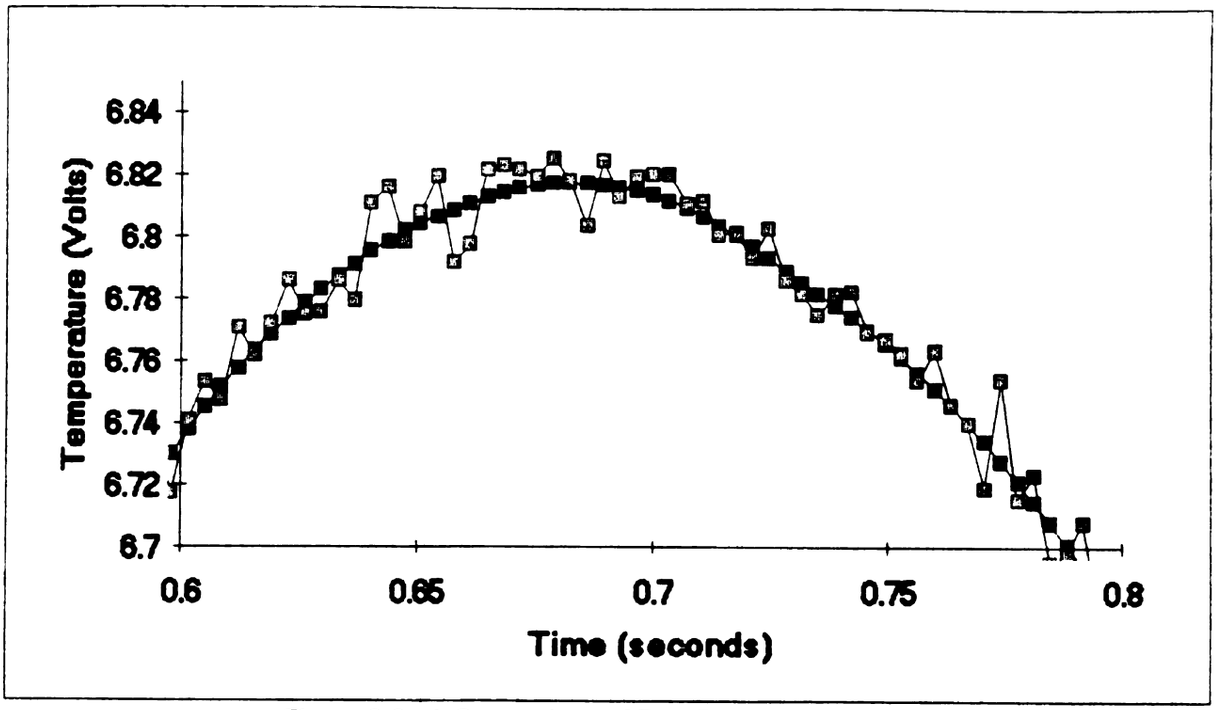

Figure 6-3 A Comparison of Raw Data to Mollified Data, Blurring Radius = 5

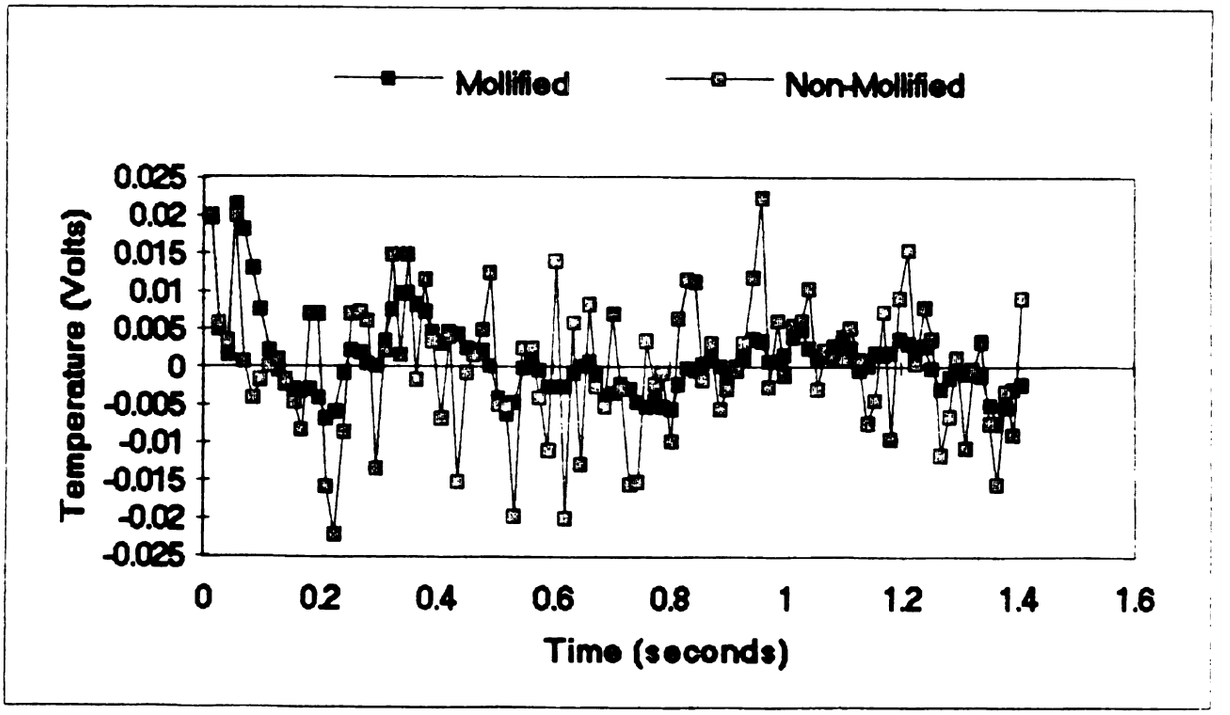

Figure 6-4 A Comparison of Residuals from Mollified and Non-Mollified Data

TABLE 6-1

Comparing Mollified to Non-Mollified Experiment Results

Model Nmbr.	Diff. (α)	Heat Flux	Biot Number	β_4	β_5	β_6	Resid. (s)
ORNL 700°C MOLLIFIED DATA							
1	.31205	17.760	1.22475				.04068
4	.27217	21.727	1.60236	.02408			.00996
5	.27897	18.772	1.53200	.07366			.00857
17	.28077	19.545	1.51312	.07088	1.0000	.00773	.00568
ORNL 700°C NON-MOLLIFIED DATA							
1	.31136	17.855	1.23326				.03697
4	.27615	21.290	1.56101	.02107			.01250
5	.28193	18.643	1.50312	.06964			.01244
17	.28364	19.422	1.48574	.06681	1.0000	.00751	.01074
FRENCH DATA A_R1 MOLLIFIED DATA							
1	1.2816	2917	.08583				4.9883
4	1.1121	3345	.21013	.07187			2.4465
5	1.1288	3250	.19919	.26716			1.8968
17	1.1645	1060	.17134	.29105	.59666	1.4077	0.8719
FRENCH DATA A_R1 NON-MOLLIFIED DATA							
1	1.2813	2920	.08633				4.8113
4	1.1190	3325	.20423	.06850			2.4166
5	1.1344	3236	.19432	.26207			1.9452
17	1.1673	1057	.16894	.27820	.63479	1.4243	1.0417

mollification is shown in Table 6-1. Although the parameters calculated do not differ significantly from the non-mollified cases, the residuals are substantially lower than in the non-mollified cases. Moreover, the differences in the standard deviation of the residuals between models is much more significant in the mollified cases.

The mollification of the data allows the contribution of the measurement errors to be effectively separated from the contribution from model non-compatibility. This allows the differences in accuracy between models to be contrasted more effectively.

For some forms of regularization in the field of inverse problems, it is important to know an "expected" magnitude of the errors in the experiment. Additionally, this information is useful in evaluating the adequacy of a model for a particular set of measured data. If the standard deviation of the residuals is on the same order as the anticipated standard deviation of the errors, a measure of assurance is gained in the validity of the model.

One means of estimating the standard deviation of the errors is to use the mollified curve as the "true values" in the experiment. In this way, the standard deviation is found by computing the sum of the squares of the differences between the mollified data and the raw data or

$$\sigma \approx \sqrt{\sum_{n=1}^{N} \frac{(Y(n)-f(n))^2}{N-1}} \qquad (6\text{-}4)$$

Table 6-2 below shows the results of this method used on a file of simulated data typical of that measured from a CBCF sample at 700°C measured at Oak Ridge National Lab.

TABLE 6-2

Estimated Measurement Errors Using Mollification

Known σ of Errors	Percent of Max. Measurement	Estimated (s) Using Mollification
0.05123	0.753	0.04778
0.02049	0.301	0.01953
0.01028	0.151	0.01057
0.00512	0.075	0.00652
0.00204	0.030	0.00484
0.00020	0.003	0.00445
0.00002	0.0003	0.00445

The diffusivity used was .31, heat flux 19, and Biot Number 1.4, calculated as a direct problem with 400 points. The peak measurement in such a case is approximately 6.8 volts. Errors with a Gaussian distribution and a known standard deviation were superimposed on this exact data. The mollification method was then used as stated above in an effort to approximate the standard deviation of the errors.

When the errors are large, the mollification method performs quite well in estimating the standard deviation of the errors. When the standard deviation of the errors drops below 0.1 percent of the maximum measurement, however, the mollification method is unable to accurately estimate the standard deviation of the errors.

6.3 ELIMINATING THE HEAT FLUX PARAMETER

A distinct handicap of the more advanced models is that

estimating a larger number of parameters simultaneously is an inherently less stable process because a larger number of simultaneous equations must be solved. Whenever possible, parameters which are of no interest should be eliminated from the model, provided model accuracy is not degraded in doing so.

Researchers from the "Institut National Polytechnique de Lorraine et Universite de Nancy" in France have set forth a method by which the heat flux magnitude need not be calculated simultaneously with the other parameters. Since this work was shown to be successful for a three parameter model, reducing the effective number of parameters simultaneously estimated to two, an attempt was made as part of this research to expand this concept to the higher order models.

Using Model 1 as an example, the direct solution as given in Chapter 2 is

$$T(L,t)=\frac{2q_0}{L\rho c_p}\sum_{m=1}^{\infty} e^{-\beta_m^2\alpha t/L^2}\frac{\beta_m[\beta_m\cos(\beta_m)+Bi\sin(\beta_m)]}{(\beta_m^2+Bi^2)\left[1+\frac{Bi}{\beta_m^2+Bi^2}\right]+Bi} \qquad (6\text{-}5)$$

If the maximum point of this curve is found, and referred to as T_{max}, and the corresponding time is referred to as t_{max}, then a scaled solution can be obtained by dividing the above solution by T_{max}, specifically

$$\Theta(L,t)=\frac{T(L,t)}{T_{max}} \tag{6-6}$$

This ratio then becomes

$$\Theta(L,t)=\frac{\sum_{m=1}^{\infty} e^{-\beta_m^2\alpha t/L^2}\dfrac{\beta_m[\beta_m\cos(\beta_m)+Bi\sin(\beta_m)]}{(\beta_m^2+Bi^2)\left[1+\dfrac{Bi}{\beta_m^2+Bi^2}\right]+Bi}}{\sum_{m=1}^{\infty} e^{-\beta_m^2\alpha t_{max}/L^2}\dfrac{\beta_m[\beta_m\cos(\beta_m)+Bi\sin(\beta_m)]}{(\beta_m^2+Bi^2)\left[1+\dfrac{Bi}{\beta_m^2+Bi^2}\right]+Bi}} \tag{6-7}$$

This function has exactly the same shape as the original temperature solution, is dimensionless, is no longer a function of heat flux and has a maximum value of 1.

The sensitivity coefficients are shown for this model in Figure 6-5 and contrasted to those of Model 1. As shown in this figure, both of the sensitivity coefficient curves for the two parameter model cross the zero temperature line at the same point. This is because the maximum temperature measurement is reached at this point and the derivatives with respect to all parameters are zero there. This tends to make the parameters correlated, but is not a severe problem in the two parameter case. When moving to higher order models, however, this correlation becomes more of a handicap and the performance of the parameter estimation procedure becomes very poor.

In Table 6-3, a test case is considered using a

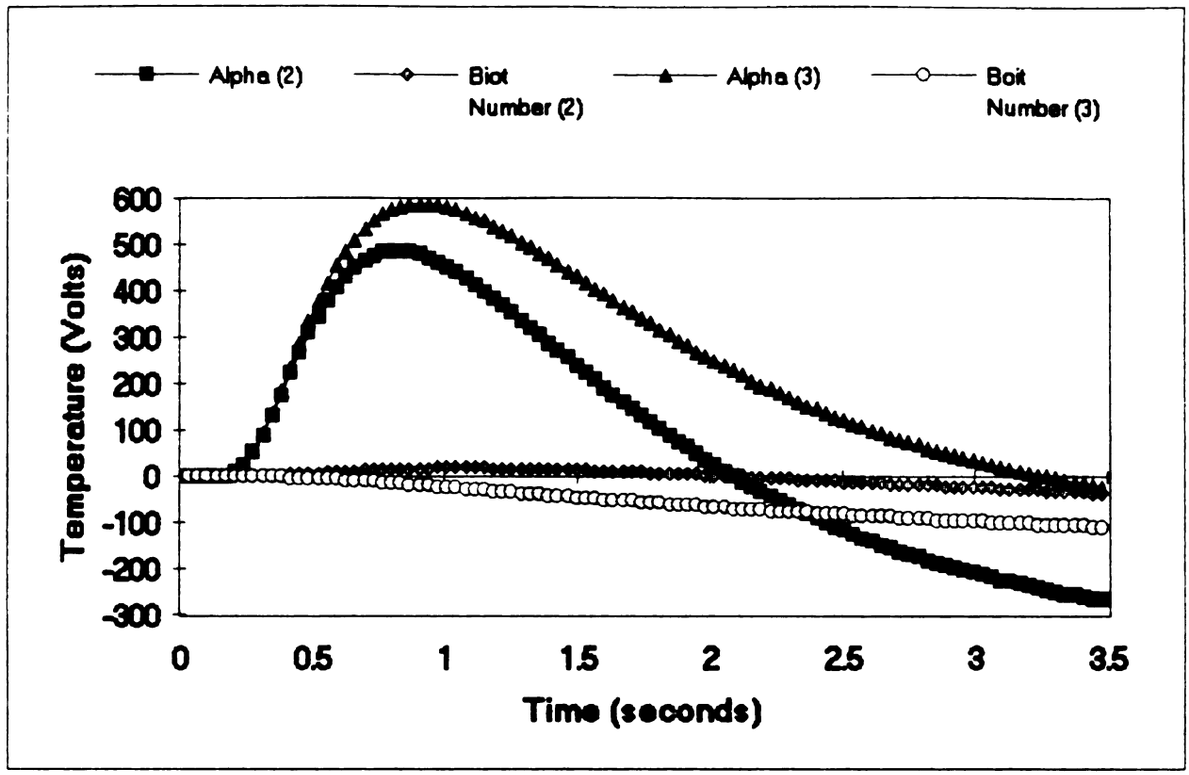

Figure 6-5 Sensitivity Coefficients Comparing 3-Parameter to 2-Parameter Methods

calculated direct solution with imposed errors of standard deviation σ=0.00854 and a maximum temperature "measurement" of 0.7577. A comparison of the two versus three parameter method is shown. As indicated in the table, the 3-parameter model estimated the parameters more accurately than the two parameter model. In regard to diffusivity, the primary parameter of interest, a 2.1 percent error from the true value was reported using the three parameter model. By comparison, the 2-parameter method reported a diffusivity value which was in error by 5.4 percent.

As an additional measure of investigation, a sample

TABLE 6-3

Contrived Test Case Comparing 3-Parameter to 2-Parameter Method

Sample Thickness: L=1.0mm
Maximum Measured Reading: 0.7577
Anticipated Residual Std Dev: σ=0.008854

Model Nmbr.	Diff. (α)	Biot Number	Resid. (s)
Actual	0.3000	2.000	0.00000
2-Parameter	0.2838	2.458	0.01340
3-Parameter	0.2937	2.170	0.00827

problem was studied where heat losses from the sample surface were known to be zero. This problem provided an opportunity to compare a two-parameter model, which estimated diffusivity and heat flux, with a one-parameter model estimating diffusivity only. In a contrived trial problem with diffusivity equal to 0.3 and heat flux equal to 1.0, the sensitivity coefficient curves are virtually identical when comparing the one and two parameter models. The performance in the estimating routines is shown in Table 6-4. In this case, the performance of the two methods is comparable, with the two parameter model having a slightly more accurate estimate of diffusivity than the one parameter model.

In a test comparing the two methods against one another using actual laboratory data, The Oak Ridge National

TABLE 6-4

Contrived Test Case Comparing 2-Parameter to 1-Parameter Method

Sample Thickness: L=1.0mm
Maximum Measured Reading: 1.0
Anticipated Residual Std Dev: σ=0.008854

Model Nmbr.	Diff. (α)	Resid. (s)
Actual	0.3000	0.00000
1-Parameter	0.2954	0.00994
2-Parameter	0.2989	0.00848

TABLE 6-5

ORNL Data at 700°C Using 2-Parameter Method

Model Nmbr.	Diff. (α)	Biot Number	β_3	β_4	β_5	Resid. (s)
RESULTS FROM DIVIDING OUT THE HEAT FLUX PARAMETER						
1	.30995	1.24841				.038129
4	.28226	1.49013	.01789			.015763
17	.29243	1.39531	.05582	1.00000	.00049	.015342
95% Confidence Intervals						
1	.025643					
4	.038407					
17	.063664					
RESULTS FROM COMPUTING THE HEAT FLUX PARAMETER						
1	.31136	1.2332				.036976
4	.27615	1.56101	.02107			.012506
17	.28364	1.48574	.06681	1.0000	.00751	.010741
95% Confidence Intervals						
1	.004431					
4	.005980					
17	.004025					

Laboratory data was used for a CBCF sample at 700°C. The means by which the two methods can be compared are by the standard deviation of the residuals and by the width of the confidence intervals for the parameter of interest. As shown in Table 6-5, the standard deviation of the residuals and the width of the confidence regions for all three models tested are smaller when the heat flux is computed as an independent parameter rather than being divided out in the reduced parameter method.

A concern related to sensitivity coefficients is the way in which they are calculated. The method used in calculating sensitivity coefficients, for all of the experiments studied as part of this research, has been a numerical approximation method. Using this method, the derivatives are approximated by the following expression

$$\beta_i \frac{\partial T}{\partial \beta_i} \approx \frac{T(1.001\beta_i, L, t) - T(\beta_i, L, t)}{.001} \qquad (6\text{-}8)$$

where β_i is the parameter corresponding to the applicable sensitivity coefficient. In order to test the validity of this approximation, several other values were chosen for the magnitude of the perturbation used. The value used in the above equation of 0.1 percent perturbation was tested in

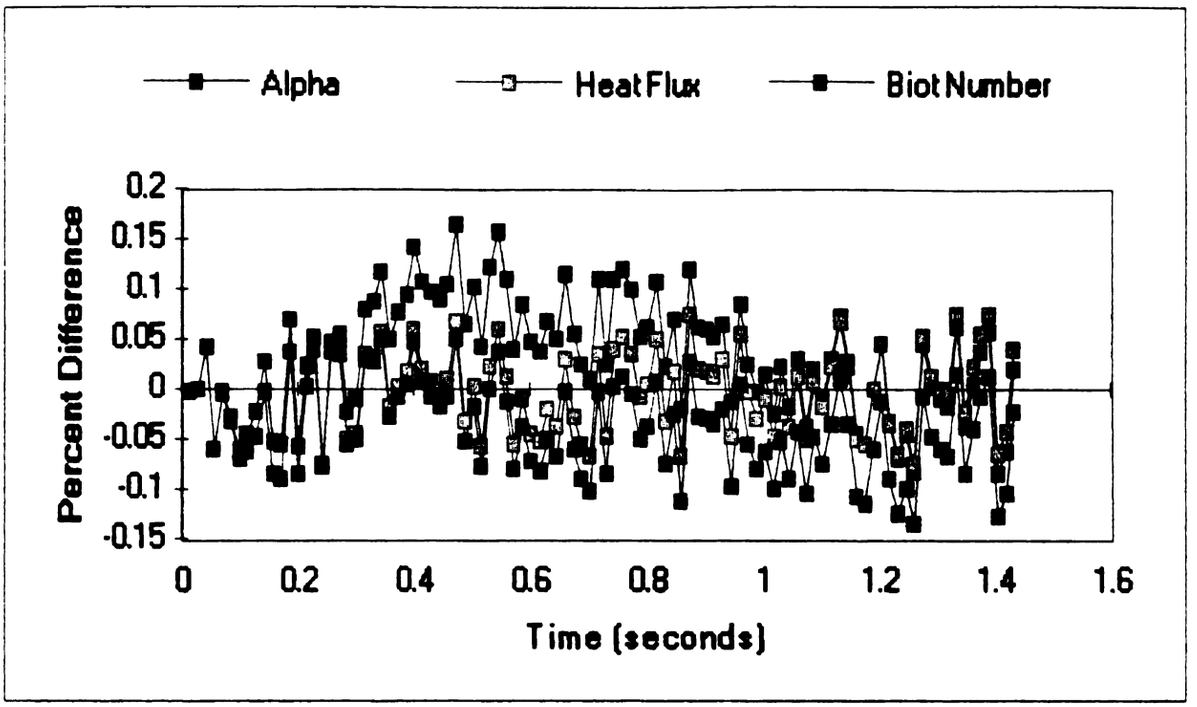

Figure 6-6 Percent Difference of Sensitivity Coefficients Between Perturbations of .001 and .0001

comparison to other values. The percent difference in sensitivity coefficients between using 0.1 percent and 0.01 percent perturbation of the parameters is shown in Figure 6-6. This percent difference seems to be fairly uniform over the length of the experiment. The standard deviation of these differences for each of the parameters is as shown in Table 6-6. The differences at the smaller perturbation values are clearly negligible. At a 10 percent perturbation value however, two of the sensitivity coefficients are different enough from those calculated at the finer perturbations, that convergence time could be affected due to inaccurate estimates at the intermittent iterations.

Examining the use of these sensitivity coefficients in

Percent
Perturbat

0.001
0.01
1.00
10.00

Percen
Pertur

0.001
0.01
0.1
1.0
10.0

estim

resu

Nati

conv

of

con

in

6.4

TABLE 6-6

Various Sensitivity Coefficient Calculations

Percent Perturbation	Standard Deviations of Pct Difference Alpha	Heat Flux	Biot Number
0.001	0.06099	0.041907	0.046979
0.01	0.06099	0.038379	0.049313
1.00	0.42086	0.003837	0.237397
10.00	4.40292	0.004222	2.486596

TABLE 6-7

Results of Calculation Method on ORNL Data

Percent Perturb.	Number of Iterations	Diff.	Heat Flux	Biot Number
0.001	4	.33628	18.9632	.85425
0.01	4	.33628	18.9628	.85422
0.1	4	.33628	18.9629	.85423
1.0	4	.33634	18.9563	.85374
10.0	5	.33687	18.8957	.84923

estimating parameters from actual laboratory data, the results from the CBCF samples measured at 600°C at Oak Ridge National Laboratory are shown in Table 6-7.

As with the sensitivity coefficients, the difference in converged parameter values is negligible until large values of perturbation are used, such as 10 percent. This gives confidence that the perturbation value of 0.1 percent used in the preceding calculations produces satisfactory results.

6.4 DETERMINATION OF APPROPRIATENESS OF COMPETING MODELS

In the interest of avoiding the use of excessive

measurem

scales c

The obje

window c

was the

at 700°C,

contains

the firs

results

primary

The nume

6-8 thro

these re

measurem

another

example,

the 200

the resi

with a n

measurements, analyses were performed over varying time scales on the same experiment and the results were compared. The objective of this comparison was to determine which window of time is most appropriate. The data file studied was the Oak Ridge National Laboratory CBCF sample measured at 700°C, as studied extensively in Chapter 4. The file contains 463 measurements, and was studied in five windows: the first 100, 200, 300, 400 then all 463 points. The results were compared for appropriateness using three primary measurement methods:

1. The standard deviation of the residuals.
2. The width of the confidence region for the parameter of interest, diffusivity.
3. The stability of the sequential parameter estimates for diffusivity.

The numerical results of these analyses are shown in Tables 6-8 through 6-12. Finding the most appropriate model among these results is not immediately obvious, since some measurement criteria are superior using one model and another criterion is superior using another model. For example, comparing Model 1 between Table 6-8 and Table 6-9, the 200 point sample produced a lower standard deviation in the residuals but the 300 point sample resulted in estimates with a narrower confidence interval.

Ambient T
Sample T
Maximum
Anticipa
Applied

Model Di
Nmbr.

1 .3
4 .2
5 .2
17 .3

95% Conf

1 .0
4 .1
5 .0
17 .0

Sample T
Maximum
Anticipa

Model D
Nmbr.
1
4 .3
5 .2
17 .2
.2

95% Co

1
4 .0
5 .0
17 .0
.0

TABLE 6-8

ORNL Data at 700°C Using First 100 points

Ambient Temperature: 700°C
Sample Thickness: L=.956mm
Maximum measured Reading: 6.8258
Anticipated Residual Std Dev: 0.0091074
Applied Null Value: 0

Model Nmbr.	Diff. (α)	Heat Flux	Biot Number	β_4	β_5	β_6	Resid. (s)
1	.36543	8.98728	.01922				.02574
4	.23113	42.0567	3.42080	.03659			.02268
5	.27622	20.6111	1.81798	.07007			.02178
17	.34643	11.3035	.31135	.0506	.2713	.0092	.01130

95% Confidence Interval

1	.011550
4	.127430
5	.041888
17	.026662

TABLE 6-9

ORNL Data at 700°C Using First 200 points

Sample Thickness: L=.956mm
Maximum measured Reading: 6.8258
Anticipated Residual Std Dev: 0.0091074

Model Nmbr.	Diff. (α)	Heat Flux	Biot Number	β_4	β_5		Resid. (s)
1	.32889	14.8203	.91080				.02857
4	.27394	21.7314	1.60360	.02219			.01660
5	.28632	18.0951	1.43088	.06739			.01589
17	.29242	18.3297	1.34449	.0611	1.000	.0090	.01035

95% Confidence Interval

1	.005501
4	.018057
5	.010263
17	.007461

Sample Th
Maximum r
Anticipat

Model Nmbr.	D
1	.3
4	.2
5	.2
17	.2

95% Conf

1	.0
4	.0
5	.0
17	.0

Ambient
Sample
Maximum
Anticip
Applied

Model Nmbr.	
1	
4	.
5	.
17	.
	.

95% Cor

1	
4	.
5	.
17	.

TABLE 6-10

ORNL Data at 700°C Using First 300 points

Sample Thickness: L=.956mm
Maximum measured Reading: 6.8258
Anticipated Residual Std Dev: 0.0091074

Model Nmbr.	Diff. (α)	Heat Flux	Biot Number	β_4	β_5		Resid. (s)
1	.31837	16.7081	1.1200				.03412
4	.27727	21.0698	1.5409	.02102			.01538
5	.28432	18.3207	1.46340	.06901			.01437
17	.28761	18.9482	1.42614	.0645	1.000	.0097	.01023

95% Confidence Interval

1	.004716
4	.009646
5	.006141
17	.004790

TABLE 6-11

ORNL Data at 700°C Using First 400 points

Ambient Temperature: 700°C
Sample Thickness: L=.956mm
Maximum measured Reading: 6.8258
Anticipated Residual Std Dev: 0.0091074
Applied Null Value: 0

Model Nmbr.	Diff. (α)	Heat Flux	Biot Number	β_4	β_5	β_6	Resid. (s)
1	.31136	17.8554	1.2333				.03698
4	.27615	21.2900	1.56101	.02107			.01251
5	.28193	18.6432	1.50312	.06964			.01245
17	.28364	19.4220	1.48574	.0668	1.000	.0075	.01074

95% Confidence Interval

1	.004431
4	.005980
5	.004338
17	.004025

TABLE 6-12

ORNL Data at 700°C Using All 463 points

Sample Thickness: L=.956mm
Maximum measured Reading: 6.8258
Anticipated Residual Std Dev: 0.0091074

Model Nmbr.	Diff. (α)	Heat Flux	Biot Number	β_4	β_5	β_6	Resid. (s)
1	.30897	18.2850	1.2736				.04132
4	.27337	21.6633	1.59526	.02290			.01349
5	.27936	18.8599	1.53652	.07224			.01398
17	.28097	19.6629	1.52054	.0694	1.000	.0081	.01192

95% Confidence Interval

1	.002205
4	.002732
5	.002088
17	.001878

One thing that is clear from Tables 6-8 through 6-12 is that using only the first 100 or 200 points of the data file results in a much wider confidence interval than the tests using more points. Although the standard deviation of the residuals is lower in the 100 and 200 point cases when comparing the Model 1 tests, there is no advantage in the residuals when comparing the Model 17 tests. The wider confidence region therefore makes the 100 and 200 point cases undesirable, as depicted in Tables 6-8 and 6-9, respectively. This trend seems to continue through the rest of the tests involving 300, 400 and 463 points in Tables 6-10 through 6-12, respectively. These three higher

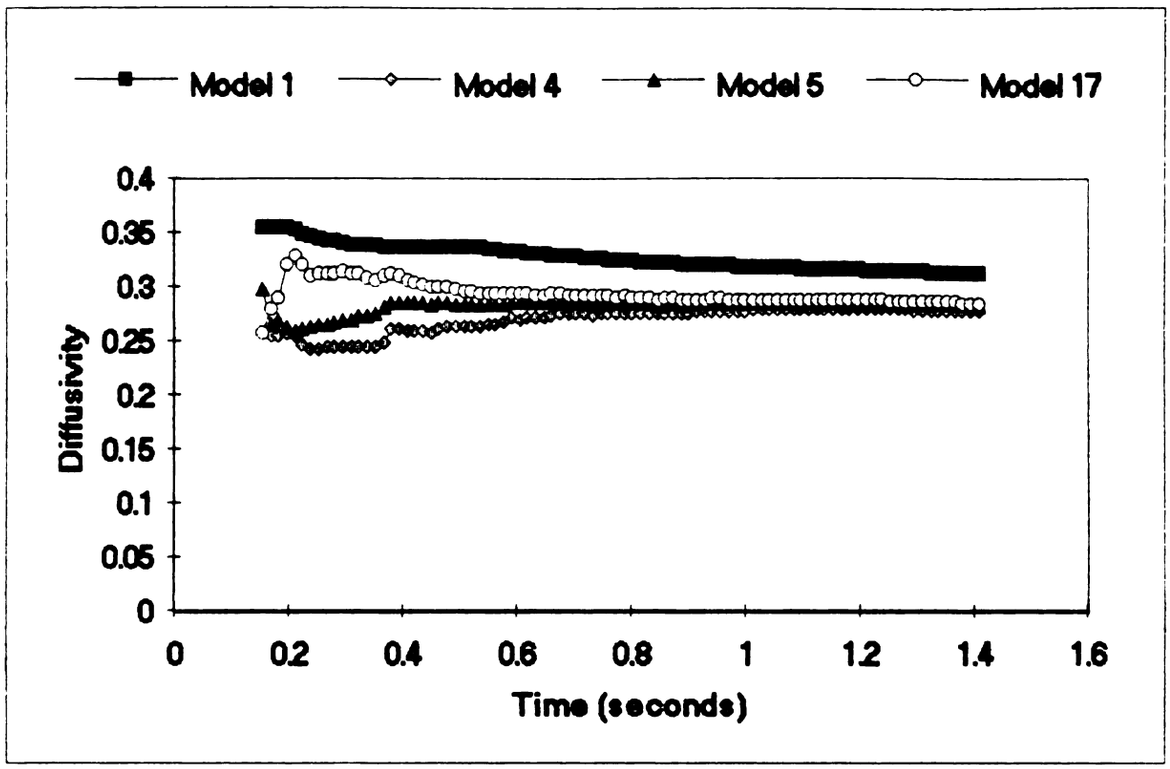

Figure 6-7 Sequential Estimates of Diffusivity (CBCF 700°C)

measurement data files, however, are more difficult to discern between. It is helpful to bring information from the sequential estimates into consideration at this point.

As a means of quantifying the degree to which the sequential estimates vary in the later times of the experiment, the last 50 sequential estimates from each model are averaged by model and the standard deviation of the last 50 points is compared from model to model. For the sequential estimates shown in Figure 6-7, the standard deviations from the last 50 average of the sequential estimates is 0.003642, 0.001493, 0.000909 and 0.001672 for models 1,4,5 and 17, respectively. In this particular

situatio

associat

signific

reason t

sequenti

loss of

simultan

of the

the lab

estimat

informa

simult

one an

resul

ident

elusi

appro

desc

nume

its

para

wher

situation, the most stable sequential estimates were associated with Model 5, however Models 4 and 17 also showed significant improvement over Model 1. The most likely reason that Model 17 exhibits slightly less stable sequential estimates than does Model 5 is in the inherent loss of stability brought about by a greater number of simultaneous parameters to compute. The standard deviation of the residuals from Model 17 indicates a superior fit for the laboratory data used to generate these sequential estimates. Once again, it is difficult to consider information from all three of the evaluation criteria simultaneously in order to evaluate the appropriateness of one analysis over another.

Since many factors come into play when comparing results from competing models in parameter estimation, the identification of a model which is "most appropriate" can be elusive. One highly respected method of determining model appropriateness is the Akaike Information Criterion as described in Reference [34]. This method assigns a numerical value to the performance of a model in terms of its fit to the measured data using a reasonable number of parameters. Specifically, the criterion is

$$\text{AIC} = -2(\text{maximum log likelihood}) + 2k \qquad (6\text{-}9)$$

where k is the number of independent parameters. This

expres

where

the num

conside

the low

is typi

Using t

7.39/*n*

another

On

method

varying

estimat

depende

well su

measure

primari

specific

Bec

One meas

residua

three cr

deviatic

expression can also be written as

$$AIC = n \cdot ln(2\pi) + n \cdot ln(v) + n + 2k \qquad (6\text{-}10)$$

where v represents the variance of the residuals and n is the number of measurements in the experiment. The model considered to be most appropriate is the one which generates the lowest AIC value. Since the variance of the residuals is typically a small number, the AIC is usually negative. Using this method, the variance must decrease by a factor of $7.39/n$ in order to offset the penalty incurred by adding another parameter to a model.

One of the primary comparisons which make a criterion method desirable is the ability to compare the effects of varying the number of measurements on the parameter estimation adequacy. The AIC discussed above is highly dependent on the number of measurements and, as such, is not well suited to comparing models used on varying numbers of measurements for the same experiment. It is used here primarily to test the adequacy of one model against another, specifically, Models 1,4,5 and 17.

Because of this and the fact that the AIC involves only one measured performance criterion, the variance of the residuals, a new method was considered which makes use of three criteria simultaneously. These are the standard deviation of the residuals, the width of the confidence

region,
estima
Si
factors
the thr
respect
scaled
categor
togethe
lowest
the low
form,

where s
deviati
estimat
respect
factors
analysi

6.5 AN

As

region, and the standard deviation of the sequential estimates over the last half of the experiment.

Since the lowest magnitudes of each of these three factors is the most desirable, the lowest number of each of the three categories is used as a scaling factor for its respective category. Each of the three categories is then scaled to this number, so that the lowest number in each category is 1. The scaled factors are then multiplied together to give the total "grade". The model with the lowest grade is then considered the most appropriate model, the lowest possible score being 1. Expressed in equation form,

$$Grade=\left(\frac{s_i}{s_{min}}\right)\left(\frac{cr_i}{cr_{min}}\right)\left(\frac{se_i}{se_{min}}\right) \qquad (6\text{-}11)$$

where s_{min}, cr_{min}, and se_{min} represent the lowest standard deviation of the residuals, confidence region and sequential estimate standard deviation of any of the models considered, respectively. The terms s_i, cr_i, and se_i represent the same factors for the model being graded. The results of this analysis are shown in comparison to AIC in Table 6-13.

6.5 ANALYZING SEQUENTIAL EXPERIMENTS

As experiments are performed over a range of

Number of Msrmnt	
Model 1	
100	
200	
300	
400	
463	
Model 4	
100	
200	
300	
400	
463	
Model 5	
100	
200	
300	
400	
463	
Model	
100	
200	
300	
400	
463	

temper

normal

can be

the va

An alt

TABLE 6-13

Comparison of Model Selection Schemes

Number of Msrmnt	Std Dev Residuals	Conf Region	Std Dev of Seq. Param.	McMasters' Grade	Akaike Infrmtn Criteria
Model 1					
100	0.025739	0.01155	0.003715	68.5788	-442.16
200	0.028565	0.005501	0.00584	56.9831	-848.649
300	0.034117	0.004716	0.004769	47.6463	-1169.41
400	0.036976	0.004431	0.003642	37.0526	-1496.83
463	0.041321	0.002205	0.004069	23.0210	-1630.64
Model 4					
100	0.022682	0.12743	0.011064	1985.741	-465.447
200	0.016596	0.018057	0.005039	93.76717	-1063.86
300	0.015377	0.009646	0.003666	33.76516	-1645.56
400	0.012506	0.00598	0.001493	6.93325	-2362.08
463	0.013493	0.002732	0.000954	2.18371	-2665.02
Model 5					
100	0.021779	0.041888	0.006062	343.4005	-473.572
200	0.015892	0.010263	0.000974	9.864368	-1081.2
300	0.014371	0.006141	0.000838	4.592271	-1686.16
400	0.012448	0.004338	0.000909	3.047968	-2365.8
463	0.013986	0.002088	0.001603	2.906799	-2631.79
Model 17					
100	0.011297	0.026662	0.002264	23.02667	-600.854
200	0.010352	0.007461	0.006274	16.36306	-1248.65
300	0.010233	0.00479	0.001541	2.550586	-1885.91
400	0.010741	0.004025	0.001672	2.440876	-2479.79
463	0.011924	0.001878	0.002513	1.900242	-2775.49

temperatures, individual values of the parameters are normally reported at each temperature. Polynomial curves can be approximated using these points, in order to express the value of these parameters as functions of temperature. An alternative to using the individual experimental results

to construct the polynomial relationships is to analyze individual experiments sequentially in a collaborative fashion to obtain the temperature dependence as discussed in [35]. One advantage of this method is that individual experiments are automatically weighted in comparison with one another based on the number of data points collected in each experiment. Moreover, the experiments can each be assigned weighting factors in proportion to the degree of reliability of each experiment.

In the flash diffusivity experiments, a non-dimensional temperature can be defined as

$$T^* = \frac{T - T_1}{T_3 - T_1} \tag{6-12}$$

In the particular case of a set of experiments measured at Oak Ridge National Laboratory with the Holometrix equipment, the temperatures at which measurements were made were 100, 400, 500, 600, and 700°C. For this example, it is desirable to set T_1=100, T_2=400 and T_3=700°C. The non-dimensional temperature then becomes

$$T^* = \frac{T - 100°C}{600°C} \tag{6-13}$$

so that T*=0 at T=100°C and T*=1 at T=700°C which correspond to the temperature limits of the experiments performed. Due

to the nature of the temperature dependence of diffusivity and Biot number for these experiments, it is desirable to fit the parameters each to respective parabolic curves as functions of temperature. In order to simplify the parabolic equations, we can define parameter coefficients as

$$\alpha_1 = \alpha(100), \quad \alpha_2 = \alpha(400) \quad \text{and} \quad \alpha_3 = \alpha(700)$$

$$Bi_1 = Bi(100), \quad Bi_2 = Bi(400) \quad \text{and} \quad Bi_3 = Bi(700) \qquad (6\text{-}14)$$

Expressions used for the parameters as a function of temperature for Model 1 then become

$$\begin{aligned} \alpha(T^*) &= \alpha_1 + (-\alpha_3 + 4\alpha_2 - 3\alpha_1)\,T^* + 2(\alpha_3 - 2\alpha_2 + \alpha_1)\,T^{*2} \\ Bi(T^*) &= Bi_1 + (-Bi_3 + 4Bi_2 - 3Bi_1)\,T^* + 2(Bi_3 - 2Bi_2 + Bi_1)\,T^{*2} \end{aligned} \qquad (6\text{-}15)$$

There are a total of 7 parameters to be estimated in this case: the six noted above and the magnitude of the heat flux, q_0. The heat pulse term has no dependence on temperature, however, and the information regarding this parameter must be discarded from one experiment to the other so as not to "contaminate" successive calculations from other experiments.

In the analysis of the first experiment, only three parameters can be estimated, namely α_1, Bi_1 and Heat Flux. This is because only one temperature is used per experiment. Estimation of the first three parameters, as in previous cases, is accomplished by approximately minimizing the

following expression

$$S_1=\sum_{j=1}^{M}\sum_{i=1}^{N}(Y_i-T_i)_j^2 \tag{6-16}$$

where the index j refers to the individual experiment and the index i refers to each individual measurement within the applicable experiment. In vector form, this becomes

$$S=\sum_{j=1}^{M}(\mathbf{Y}_j-\mathbf{T}_j)^T(\mathbf{Y}_j-\mathbf{T}_j) \tag{6-17}$$

where $\mathbf{Y}_j$ and $\mathbf{T}_j$ denote the vectors of measurements and calculated values, respectively, for the experiment denoted by the index j.

Taking the derivative of the above equation and setting it equal to zero we have

$$\nabla_{\beta M}S=\sum_{j=1}^{M}2\left[\nabla_{\beta j}(\mathbf{Y}_j-\mathbf{T}_j)^T\right](\mathbf{Y}_j-\mathbf{T}_j) \tag{6-18}$$

since the equations are non-linear, the problem must be solved in an iterative fashion where the iteration is denoted by the superscript (k). The calculated solution $\mathbf{T}(\beta)$ can be approximated by the first 2 terms of the Taylor series as follows

$$\mathbf{T}_j^{(k+1)}=\mathbf{T}_j^{(k)}+\mathbf{X}_j^{(k)}\left(\mathbf{b}_j^{(k+1)}-\mathbf{b}_j^{(k)}\right) \tag{6-19}$$

where $\mathbf{X}_j$ is the sensitivity matrix and $\mathbf{b}_j$ is the calculated parameter vector as opposed to β which refers to the true

but unknown parameter vector. Substituting this expression into the above equation gives

$$\left[\sum_{j=1}^{M} \mathbf{X}_j^{(k)T}\,\mathbf{X}_j^{(k)}\right]\left(\mathbf{b}_M^{(k+1)}-\mathbf{b}_M^{(k)}\right)=\sum_{j=1}^{M}\mathbf{X}_j^{(k)T}\left(\mathbf{Y}_j-\mathbf{T}_j^{(k)}\right) \tag{6-20}$$

where the vector $\mathbf{b}_M^{(k+1)}$ is the unknown.

The approximation of the minimum for S is found using this procedure, rather than the true minimum, because the non-linear sensitivity coefficients for each previously analyzed experiment are not updated to reflect the value of the parameters for subsequent estimates. The parameters cannot be calculated simultaneously because of the random nature of the q_o parameter from one experiment to the other. The **b** vector, the parameter vector, is calculated for each experiment until convergence.

Since, three experiments performed at different temperatures are required in order to estimate three temperature sensitive parameters for diffusivity and Biot number, the values for α_2, α_3, Bi_2 and Bi_3 cannot be calculated at this stage. Some regularization will be required in order to facilitate the calculation. This could be in the form of

$$S=\sum_{i=1}^{N}(Y-T)^2+\omega_1(\alpha_1-\alpha_3)^2+\omega_2(Bi_1-Bi_3)^2 \tag{6-21}$$

The additional constraint of setting α_3 and Bi_3 equal to α_2 and Bi_2, respectively makes the problem stable enough to calculate the first set of parameters. Finally, in the calculation using the third experiment, the regularization terms can be dropped and all parameters will be calculated. Thereafter, the entire set of 7 parameters will be re-calculated with information from the previous experiments being added as prior information to the X^TX and the X^TY matrices. Column and row 7 in each case will be set to zero prior to being added to the next experiment.

Table 6-14 compares the estimates arrived at for diffusivity and Biot Number using three methods. These are

1. Individual experiment results averaged for each temperature at which more than one experiment was performed.

2. Fitting a least-squares parabola through the individual experimental results.

3. Using all of the experiments in a sequential estimation Scheme as described above.

As shown in the table, the results are very close between all of the methods. In the case of these particular experiments from Oak Ridge National Laboratory, the number of measurements for each experiment was approximately the same. Had this not been the case, or if one experiment had

TABLE 6-14

Sequential vs. Individual Estimation

Ambient Temp.	Average Individual	Least Sqrs Curve Fit	Sequential Method
Diffusivity			
100	.32461	.32447	.32748
400	.31351	.31154	.31288
500	.31184	.31517	.31785
600	.32691	.32277	.32775
700	.33277	.33434	.34257
Biot Number			
100	.15379	.15874	.14343
400	.53483	.52030	.50472
500	.74180	.70679	.69697
600	.86154	.92627	.92513
700	1.20691	1.17873	1.18921

been weighted more heavily than another, the results may not have been this close.

Figure 6-8 shows the results from this table in graphical form. Superimposed on the sequential results are the results from analyzing experiments individually. The results from the sequential experiment method basically conform to the parameter values obtained by analyzing the experiments individually. One area of exception is in the region of the three highest temperatures at which the experiments were conducted. Particularly, the results for Biot Number taken at 600°C are not in conformance with the assumed parabolic temperature dependency used in the

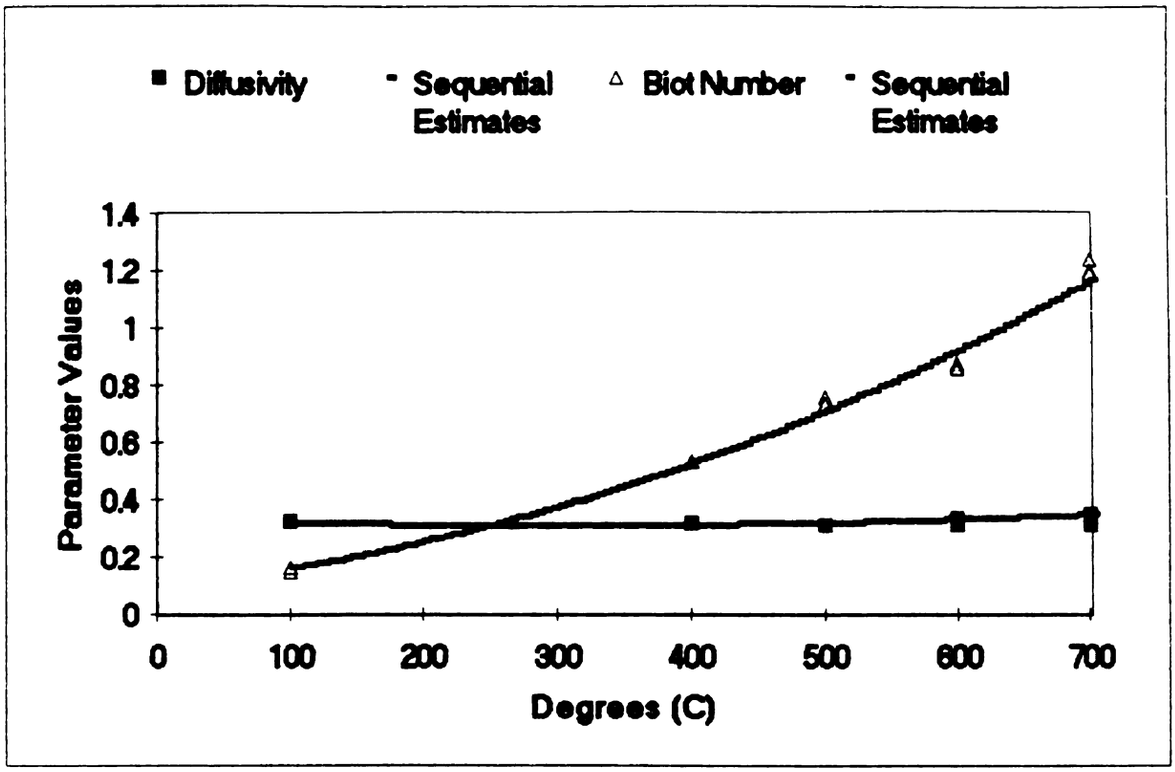

Figure 6-8 Parabolic Fit for Parameters Using Simultaneous Experiment Analysis

sequential experiment method.

In addition to fitting a parabolic curve through the parameters as a function of temperature, these experiments were also analyzed sequentially assuming a cubic dependence of Biot number on temperature. This was investigated due to the radiative nature of the heat transfer from the surfaces at high temperature in a vacuum and the natural tendency toward a cubic relationship in this type of physical phenomenon. The conformance of the data to the cubic shape, however, was less acceptable than that shown in Figure 6-8 which assumed a quadratic dependence. The nature of the heat loss from the surfaces may therefore have a convective

component from partial pressures of gasses present.

Diffusivity, the parameter of interest, is remarkably constant throughout the temperature range in which these experiments were conducted. This has proven true in both the sequential and individual experiment analysis cases. Should sequential estimation be pursued further, a simple and more reasonable model for diffusivity would be as a constant with respect to temperature.

6.6 RESIDUAL FREQUENCY ANALYSIS

Many of the residual curves exhibit characteristic signatures which indicate a disparity between the measured data and the mathematical model. Figure 6-9 shows residuals from three experiments. Each of the three experiments shown in this graph measured different materials. In order to compare the three experiments directly on the same set of axes, the residuals for each experiment were normalized by scaling to a non-dimensional time. Additionally, the vertical axis was scaled to the percent of maximum temperature rise. The three experiments shown in this figure are

A_R1 Palaiseau, France

C_R1 West Lafayette, Indiana

M_R1 Hunan, China

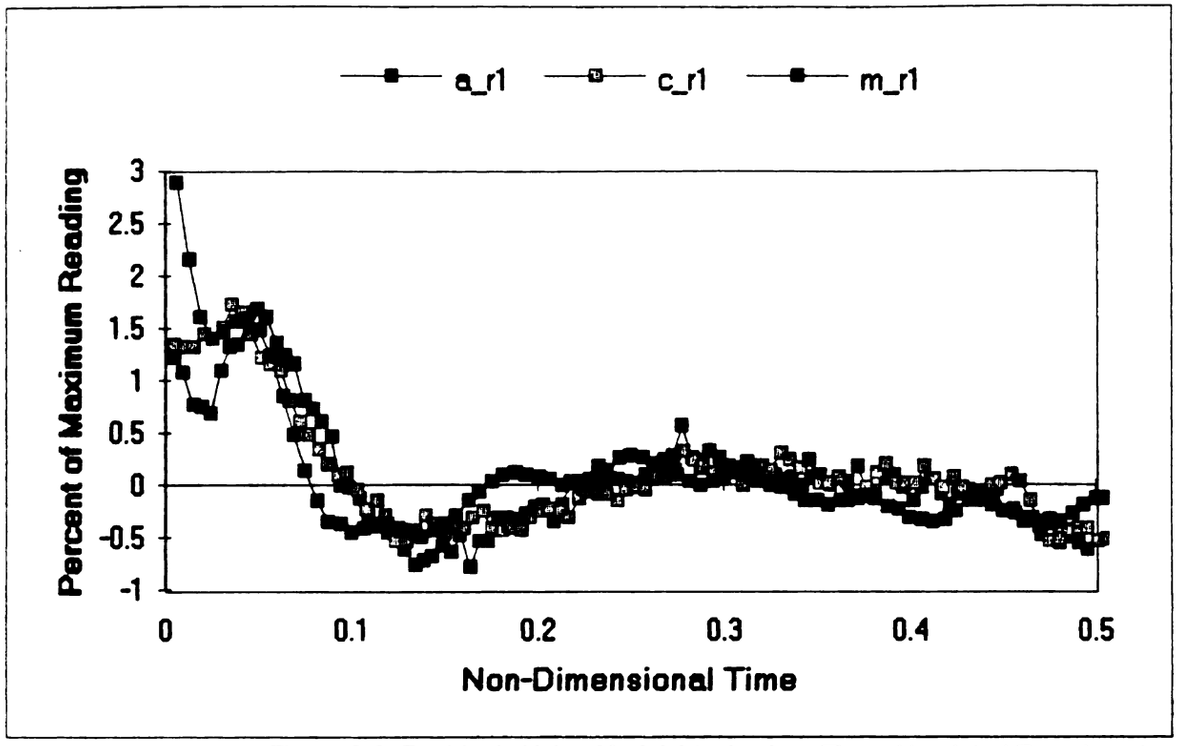

Figure 6-9 Residuals Using Model 1 to Analyze Three Unrelated Experiments

Although the experiments represent different materials at different thicknesses, the characteristic signatures, when compared with one another, are strikingly similar. These curves all exhibit the early temperature rise not predicted by the non-penetrating model, as evidenced by the large rise at approximately 0.05 units of non-dimensional time. Another prominent common feature among these curves is the back-side flash, or flash heating at time zero and x=L. This is evidenced by the non-zero start temperature at the first time step.

Figure 6-10 likewise shows residual curves from three different experiments measured in different laboratories and

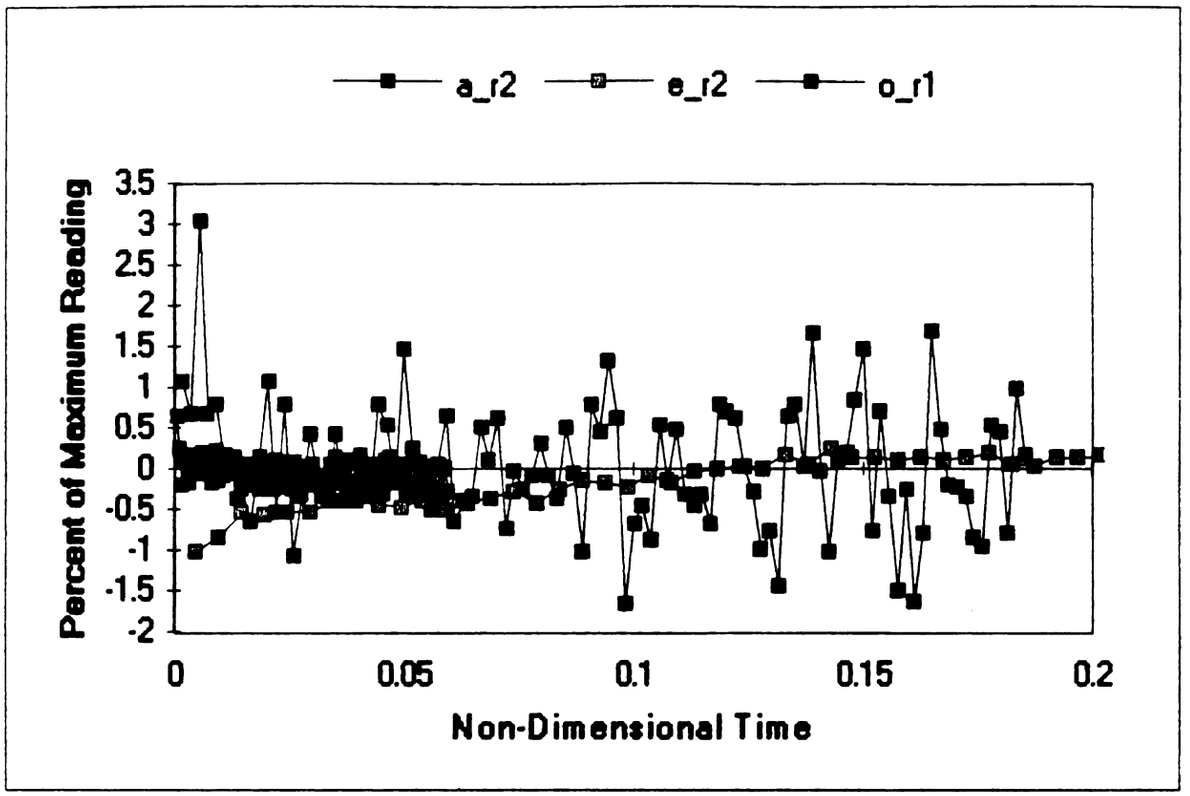

Figure 6-10 Residuals Using Model 1 to Analyze Three Unrelated Experiments

analyzed using Model 1. The experiments featured in this figure are

A_R2 Palaiseau, France

E_R2 Vandoeuvre les Nancy, France

O_R1 LeBarp, France

In contrast to the previous figure, these curves tend to exhibit no distinguishable signature. This suggests that there is no appreciable penetration of the flash nor back-side heating at time zero. For these experiments, Model 1 gives the best overall performance for estimating the parameters. In fact, O_R1 is best suited two a model which assumes Bi=0. This is evidenced by the lack of discernable

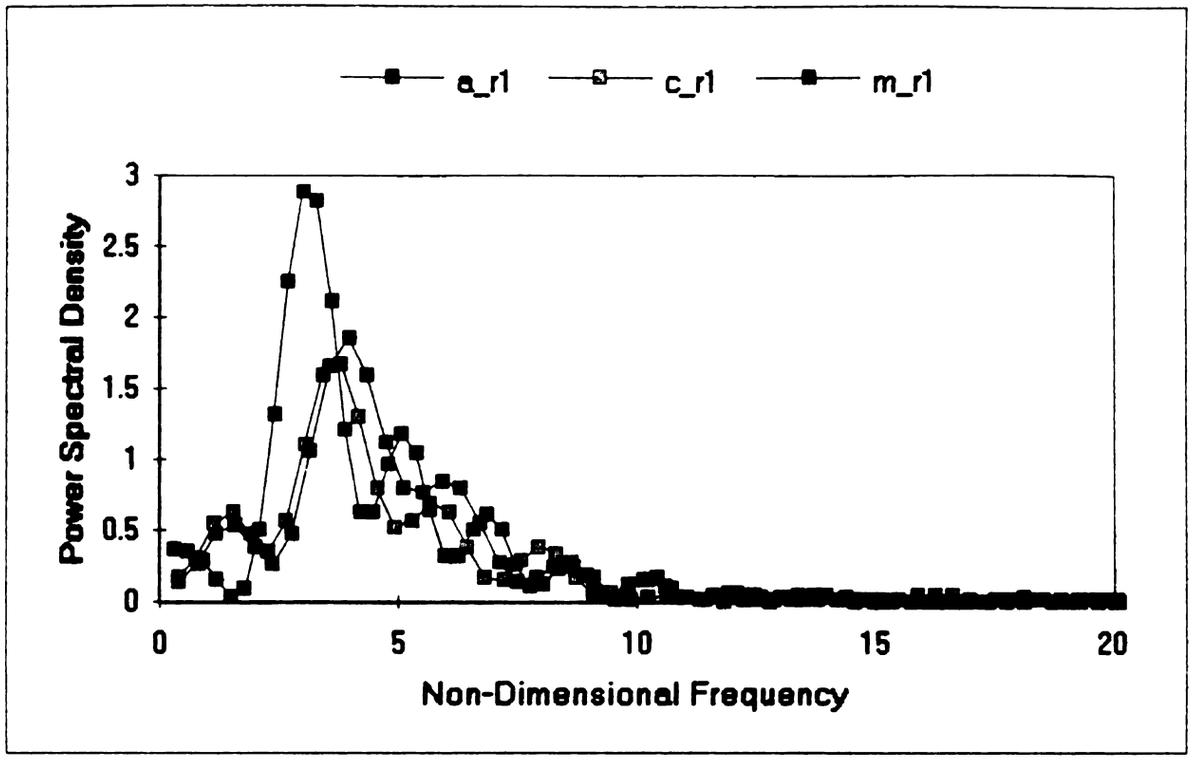

Figure 6-11 Frequency Distribution of Residual Graph Shown in Figure 6-9

improvement in the residuals and wider confidence regions when using the higher order models.

In order to gain more insight into the meaning of the signature, a frequency analysis was performed on these residual curves utilizing the fast Fourier transform provided in the MATLAB software. Figure 6-11 is a plot of the frequency distribution of the residuals shown in Figure 6-9. The predominant frequency is approximately 4 non-dimensional frequency units. This validates the dominant frequency evident in Figure 6-9 which exhibits a period of approximately 0.25 non-dimensional time units in the primary path of the residual graph. The residuals shown in Figure

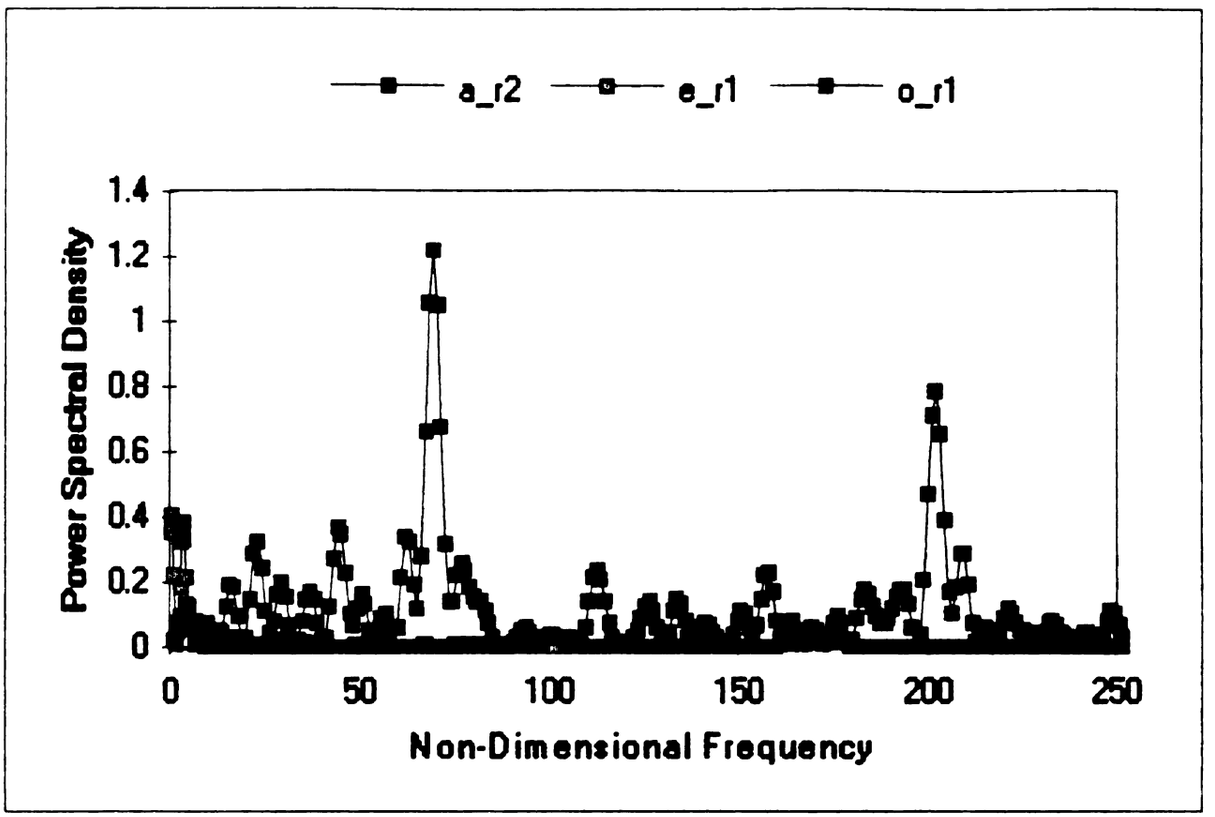

Figure 6-12 Frequency Distribution of Residual Graph Shown in Figure 6-11

6-10 on the other hand, do not have an easily detectable pattern or signature. Therefore, the frequency distribution for this graph, featured in Figure 6-12, does not exhibit the same consensus in terms of dominant frequencies among the experiments. Aside from some very low frequencies evident in experiment e_r2, the only dominant frequencies in this set of experiments seem to be in experiment o_r1. In this case, the frequencies are so high that the most likely source of these signals is measurement noise rather than a mechanism related to heat transfer.

A prominent effect of flash penetration on the estimated parameters, using Model 1 as the analysis model,

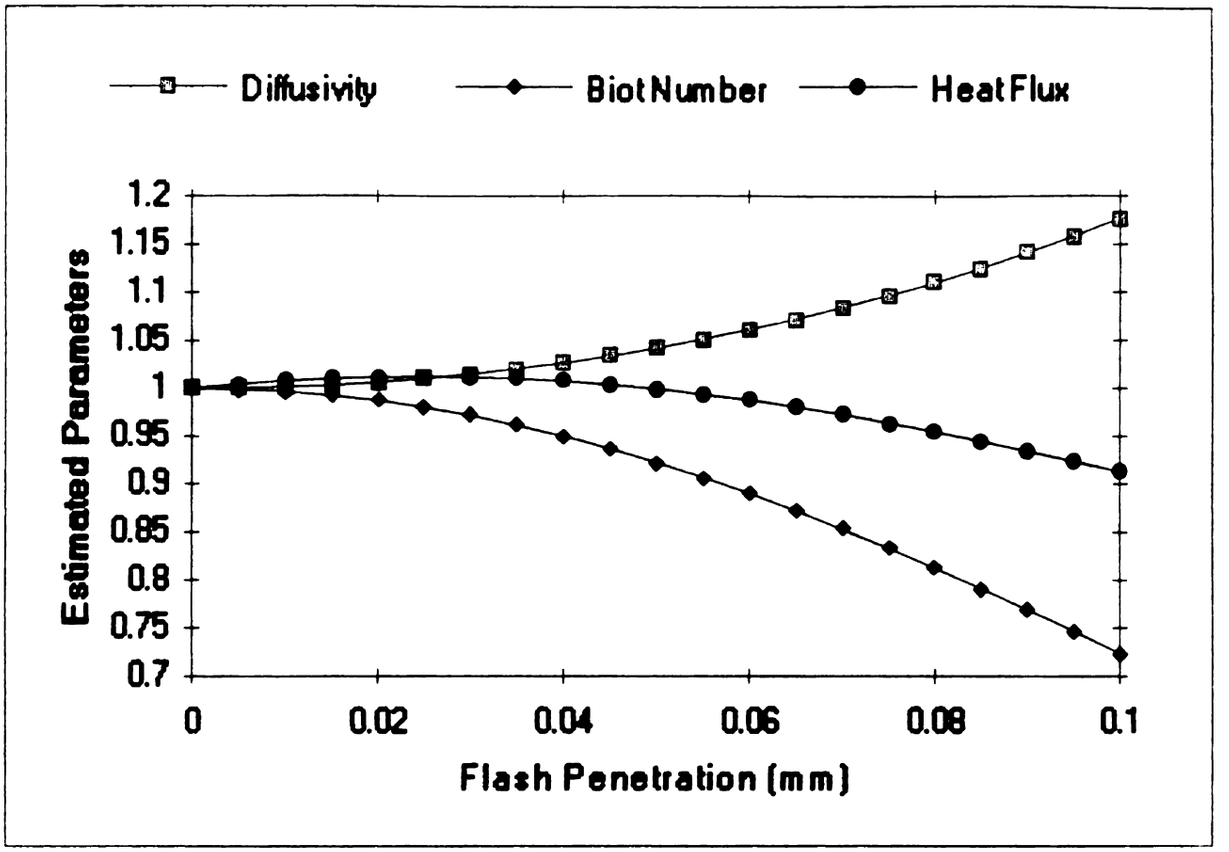

Figure 6-13 Estimated Parameters, Using Model 1, as a Function of Flash Penetration

is that the diffusivity estimates are higher than the true values and Biot number values are lower than the true values. With small exceptions in cases of shallow penetration, the estimated heat flux magnitude is also lower than the true value. In order to determine the extent to which these trends exist, 20 sample experiments were simulated by generating direct solutions which included various depths of penetration using Model 5. The sample thickness (mm), diffusivity (mm^2/sec), Biot number (unitless) and heat flux ($joules/mm^2$) were all set to unity. The depth of exponential penetration was varied from 0 to

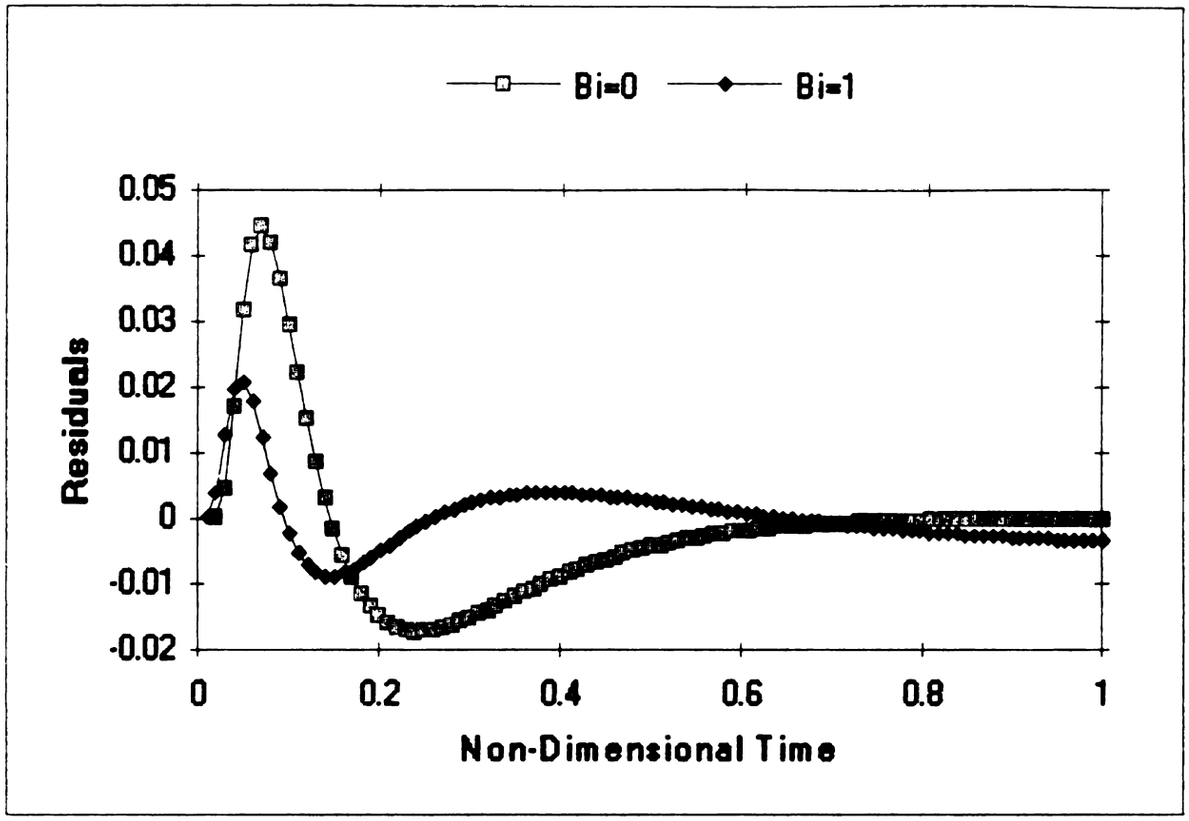

Figure 6-14 Residuals Comparing Direct Solutions With and Without Heat Loss

0.1 mm between experiments. Figure 6-13 shows a plot of the three estimated parameters for each case, using Model 1 to analyze experiments with known penetration. With an exponential penetration depth of 0.1 mm, the error in estimated diffusivity, the parameter of interest, is 17 percent. The error in the Biot number parameter is even larger at 27 percent. The error in estimated heat flux is smaller at only 8 percent.

In order to gain more insight into the physical causes of the unique signature in the residuals, it is helpful to break the problem into component parts so that isolated

effects can be studied individually. To accomplish this, a simulated experiment was generated with a penetration of 0.1 and a Biot number of zero. The results from this analysis were compared to those of an identical experiment with a Biot Number of 1. Figure 6-14 shows a plot of the residuals from analyzing both of these experiments using Model 1.

As observed from the plot of these residuals, the case with no heat loss oscillates only once above and once below the neutral axis. The reason for this pattern is that the estimated diffusivity is higher than that of the actual sample because of the tendency of the method of ordinary least squares to achieve balance in the residuals. In the process of minimizing the sum of the squares of the errors, there must typically be a comparable magnitude of residual points above and below the neutral axis. The only way for the least squares method to accomplish this using Model 1 to analyze a penetration case, is for the diffusivity to be estimated higher than the actual diffusivity so as to mimic the early rise in temperature brought about by the penetration in the experiment. The early rise in temperature cannot be adequately modeled by Model 1, of course, and the residuals show the premature rise in temperature of the experiment beyond that predicted by Model 1. Subsequent to this rise, the measured temperature is

lower than that predicted by Model 1 because the actual diffusivity is not as large as that estimated using Model 1. Consequently, the temperature rise does not continue as would have been predicted by the model. At the end of the experiment, the model temperature and the measured data are once again the same since, with no heat loss, the final non-dimensional temperature is 1.0 in both the penetration and non-penetration cases.

Making the same comparison, assuming surface heat loss this time, reveals just one more set of oscillations. In this case, the same initial behavior is exhibited as in the zero heat loss case for the same reasons. The exception is that this pattern is followed by a period in which the measured temperature is higher than that predicted by the model. The reason for this rise is once again the result of the method of least squares bringing balance to the residuals across the neutral axis in order to offset the latter portion of the experiment. In the last portion of the experiment, the dominant phenomenon affecting the residual curve is brought about by the estimated Biot number being less than the actual Biot number. This causes the measured temperature to be lower than that predicted by the model due to the higher heat loss than predicted. As with the zero heat loss case, the residual curve will eventually

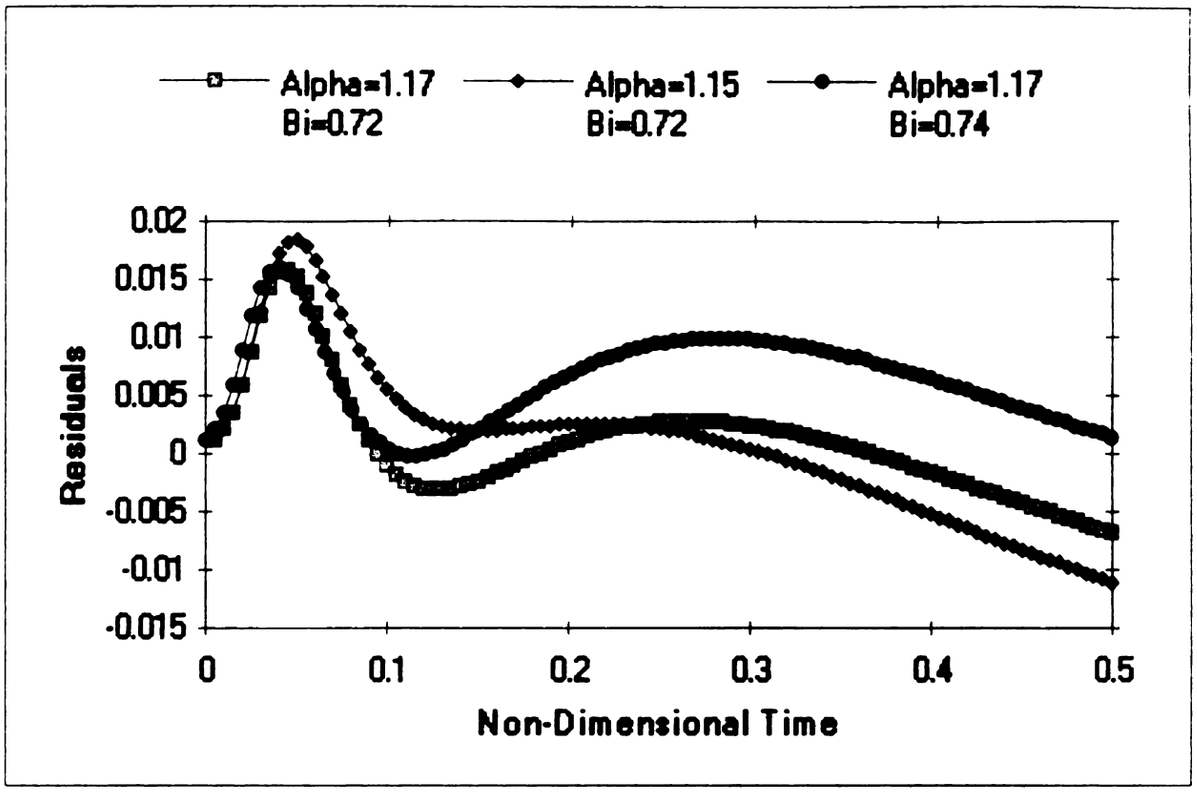

Figure 6-15 Residuals Comparing Various Model 1 Direct Solutions to a Model 5 Case with alpha=1, Bi=1 and Penetration=0.1

go to zero in very late times. This is because both models predict a final temperature of zero as heat is transferred to the surroundings.

In order to investigate the nature of the oscillations further, residual curves were generated comparing direct solutions against each other. The base solution of comparison is the same simulated experiment described above; that is, an exponential penetration of 0.1 mm and a value of unity for diffusivity (mm^2/sec), heat flux ($joules/mm^2$) and Biot Number (unitless). To this baseline experiment, other direct solutions were compared as generated by Model 1 using

various parameters. Figure 6-15 shows a plot of the residuals of three such comparisons. Each curve compares the baseline experiment with a Model 1 solution using the parameters indicated in the legend. These parameters each represent a perturbation of nominally 2 percent on the baseline case. Since these Model 1 solutions were not generated by a minimization of errors, the balance across the neutral axis of the residuals is no longer evident. The second case shown in this figure exhibits only one segment of residuals above the axis and one below, even though it is a case including heat loss. This further confirms that the nature of the oscillations is not brought about by an oscillating heat transfer phenomenon of some kind. Rather, what appears to be a damped sinusoidal oscillation is actually an attempt by the method of least squares to minimize errors when applying a model which does not account for the mechanisms of heat transfer at work in the experiment.

6.7 CBCF ANALYSIS SUMMARY

Experiments were run on Carbon Bonded Carbon Fiber (CBCF) samples at Oak Ridge National Laboratory on samples of four different thicknesses. Two samples were tested for each thickness for a total of 8 samples. Three experiments

Table 6-15

CBCF Samples Measured at ORNL 800°C Using Model 1

Sample	Shot	Diffu-sivity	Biot Number	Residual Std. Dev.	Confidence Interval
1.0mm(a)	1	0.29372	2.16129	0.01743	0.006764
1.0mm(a)	2	0.29521	2.16418	0.01773	0.006605
1.0mm(a)	3	0.29474	2.18856	0.01827	0.006652
1.0mm(b)	1	0.26229	2.44981	0.01483	0.00668
1.0mm(b)	2	0.26362	2.43437	0.01448	0.006375
1.0mm(b)	3	0.26386	2.44566	0.01520	0.006513
		(0.276 ave)			
1.2mm(a)	1	0.35628	2.10463	0.01726	0.004067
1.2mm(a)	2	0.35028	2.39603	0.01865	0.003912
1.2mm(a)	3	0.35182	2.3996	0.01989	0.003951
1.2mm(b)	1	0.31311	2.7485	0.01251	0.003438
1.2mm(b)	2	0.31985	2.64612	0.01323	0.003086
1.2mm(b)	3	0.31887	2.72847	0.01379	0.00311
		(0.332 ave)			
1.4mm(a)	1	0.31651	2.80514	0.01102	0.004696
1.4mm(a)	2	0.32126	2.6718	0.01327	0.005097
1.4mm(a)	3	0.32338	2.6703	0.01422	0.005259
1.4mm(b)	1	0.31935	3.05136	0.01287	0.00528
1.4mm(b)	2	0.31728	3.24799	0.01292	0.004922
1.4mm(b)	3	0.31038	3.65064	0.01314	0.005073
		(0.320 ave)			
1.7mm(a)	1	0.35357	2.2676	0.01328	0.010564
1.7mm(a)	2	0.35779	2.19244	0.01504	0.011163
1.7mm(a)	3	0.36534	2.0309	0.01830	0.013042
1.7mm(b)	1	0.35385	2.92408	0.01316	0.009741
1.7mm(b)	2	0.35418	3.03193	0.01371	0.009742
1.7mm(b)	3	0.36021	2.85595	0.01681	0.011694
		(0.357 ave)			

were run on each sample at each of three temperatures: 800°C, 1000°C and 1200°C. The experimental measurements were analyzed using Models 1 and 5. Model 17 was not used since the Anter flash diffusivity system used in these experiments

Table 6-16

CBCF Samples Measured at ORNL at 800°C Using Model 5

Sample	Shot	Diffu-sivity	Biot Number	Pene-tration	Residual Std. Dev.	Confidence Interval
1.0mm(a)	1	0.25193	2.99722	0.08086	0.00955	0.010766
1.0mm(a)	2	0.25389	2.98195	0.08028	0.009624	0.010459
1.0mm(a)	3	0.25335	3.0202	0.0803	0.009908	0.010531
1.0mm(b)	1	0.22765	3.3298	0.0773	0.013172	0.017718
1.0mm(b)	2	0.22959	3.28179	0.07658	0.01307	0.017288
1.0mm(b)	3	0.22935	3.31184	0.07701	0.013565	0.01743
		(0.240 ave)				
1.2mm(a)	1	0.31202	2.82292	0.08832	0.006764	0.006343
1.2mm(a)	2	0.31327	3.02372	0.08372	0.006259	0.004061
1.2mm(a)	3	0.31443	3.03208	0.08401	0.006966	0.004264
1.2mm(b)	1	0.284	3.39654	0.07632	0.009332	0.008463
1.2mm(b)	2	0.29128	3.23404	0.07545	0.008824	0.006777
1.2mm(b)	3	0.28988	3.35047	0.07584	0.009762	0.007247
		(0.300 ave)				
1.4mm(a)	1	0.27583	3.94772	0.09577	0.006668	0.009531
1.4mm(a)	2	0.27723	3.84954	0.0992	0.007426	0.009327
1.4mm(a)	3	0.27628	3.94693	0.10211	0.00698	0.008325
1.4mm(b)	1	0.27685	4.36154	0.09668	0.008534	0.011719
1.4mm(b)	2	0.27527	4.64669	0.09587	0.008069	0.010354
1.4mm(b)	3	0.27184	5.12257	0.09234	0.010204	0.01355
		(0.276 ave)				
1.7mm(a)	1	0.2704	5.05119	0.14102	0.007662	0.017773
1.7mm(a)	2	0.26935	5.12367	0.14462	0.008426	0.01796
1.7mm(a)	3	0.26371	5.42516	0.15304	0.009548	0.019044
1.7mm(b)	1	0.28006	5.80302	0.13282	0.008521	0.018495
1.7mm(b)	2	0.28151	5.93131	0.13201	0.00869	0.018063
1.7mm(b)	3	0.27342	6.4647	0.14184	0.009716	0.018494
		(0.270 ave)				

allows no back-side heating of the samples. Additionally, the surface transmissivity feature offered by Model 17 was unnecessary in analyzing the CBCF samples since the samples were uncoated and tests of this method showed a surface transmissivity of 100 percent. Tables 6-15 through 6-20

Table 6-17

CBCF Samples Measured at ORNL at 1000°C Using Model 1

Sample	Shot	Diffu-sivity	Biot Number	Residual Std. Dev.	Confidence Interval
1.0mm(a)	1	0.34674	2.99464	0.04664	0.005283
1.0mm(a)	2	0.34678	3.07153	0.05063	0.005617
1.0mm(a)	3	0.34721	3.10568	0.04935	0.005448
1.0mm(b)	1	0.30663	3.61463	0.03847	0.005077
1.0mm(b)	2	0.31011	3.53287	0.04210	0.005378
1.0mm(b)	3	0.30763	3.68227	0.04319	0.005513
		(0.325 ave)			
1.2mm(a)	1	0.38973	3.1199	0.03797	0.003838
1.2mm(a)	2	0.39027	3.14304	0.03709	0.00364
1.2mm(a)	3	0.37718	3.65986	0.04396	0.004467
1.2mm(b)	1	0.3455	3.74152	0.02563	0.003068
1.2mm(b)	2	DNC			
1.2mm(b)	3	0.3314	4.61103	0.04394	0.005401
		(0.360 ave)			
1.4mm(a)	1	0.36514	3.06754	0.03511	0.005999
1.4mm(a)	2	0.36172	3.24589	0.03487	0.006011
1.4mm(a)	3	0.36026	3.28718	0.03216	0.005629
1.4mm(b)	1	DNC			
1.4mm(b)	2	0.32796	5.82739	0.06219	0.006308
1.4mm(b)	3	0.32056	6.43341	0.06498	0.006898
		(0.345 ave)			
1.7mm(a)	1	0.41213	2.30298	0.04380	0.013738
1.7mm(a)	2	0.3812	3.33984	0.05220	0.00903
1.7mm(a)	3	0.39151	2.83499	0.03511	0.011728
1.7mm(b)	1	0.36969	5.2497	0.07193	0.013071
1.7mm(b)	2	0.37837	4.50694	0.07327	0.012368
1.7mm(b)	3	0.36135	5.44462	0.05209	0.009433
		(0.370 ave)			

present the results of the experiments using Models 1 and 5 for analysis.

As can be seen in the tables, there is considerable variation between samples of the same thickness in terms of the estimated diffusivity. For example, the two samples of

Table 6-18

CBCF Samples Measured at ORNL at 1000°C Using Model 5

Sample	Shot	Diffu-sivity	Biot Number	Pene-tration	Residual Std. Dev.	Confidence Interval
1.0mm(a)	1	0.30535	3.91577	0.07348	0.024285	0.008341
1.0mm(a)	2	0.30327	4.0861	0.07493	0.025658	0.008584
1.0mm(a)	3	0.30472	4.1017	0.07397	0.025209	0.008446
1.0mm(b)	1	DNC				
1.0mm(b)	2	0.27514	4.59171	0.07076	0.040361	0.016116
1.0mm(b)	3	DNC				
		(0.29 ave)				
1.2mm(a)	1	0.35102	3.89329	0.07982	0.021702	0.006962
1.2mm(a)	2	0.35431	3.85483	0.07695	0.022854	0.007212
1.2mm(a)	3	0.33179	4.89176	0.0844	0.016186	0.005235
1.2mm(b)	1	0.3144	4.62912	0.07322	0.019423	0.007921
1.2mm(b)	2	DNC				
1.2mm(b)	3	0.29551	6.10489	0.07776	0.037764	0.015732
		(0.33 ave)				
1.4mm(a)	1	0.31467	4.38358	0.10115	0.026491	0.014605
1.4mm(a)	2	0.30934	4.75498	0.10237	0.025232	0.014036
1.4mm(a)	3	0.31007	4.74136	0.10032	0.02267	0.012956
1.4mm(b)	1	DNC				
1.4mm(b)	2	DNC				
1.4mm(b)	3	DNC				
		(0.31 ave)				
1.7mm(a)	1	0.29236	6.16938	0.15974	0.024736	0.02256
1.7mm(a)	2	0.30666	6.2305	0.13004	0.038158	0.020664
1.7mm(a)	3	0.29432	6.46643	0.14616	0.021654	0.021235
1.7mm(b)	1	0.30673	9.08284	0.12361	0.057738	0.02321
1.7mm(b)	2	0.3006	9.03639	0.13212	0.051719	0.021929
1.7mm(b)	3	0.31596	7.96359	0.10823	0.047508	0.023421
		(0.30 ave)				

1.2 mm thickness are sometimes more than 10 percent apart. On the other hand, differences between experiments, or shots, on the same sample are very small, typically on the order of 1 percent. There seems to be no correlation between sample thickness and estimated diffusivity. As a

Table 6-19

CBCF Samples Measured at ORNL at 1200°C Using Model 1

Sample	Shot	Diffu-sivity	Biot Number	Residual Std. Dev.	Confidence Interval
1.0mm(a)	1	0.34443	6.75526	0.06703	0.016502
1.0mm(a)	2	0.35614	6.03611	0.05748	0.012614
1.0mm(a)	3	0.37376	4.88173	0.03820	0.00782
1.0mm(b)	1	0.35334	4.88497	0.01326	0.006047
1.0mm(b)	2	0.34626	5.40619	0.01596	0.007485
1.0mm(b)	3	0.35146	5.1119	0.01459	0.006797
1.2mm(a)	2	0.42094	4.7531	0.00786	0.004319
1.2mm(a)	3	0.46574	3.19036	0.01617	0.007882
1.4mm(a)	2	0.41315	3.68544	0.00665	0.005605
1.4mm(a)	3	0.47133	2.12266	0.01514	0.011436
1.7mm(a)	2	0.51714	1.57495	0.01311	0.017269
1.7mm(a)	3	0.56239	1.02209	0.01463	0.018571

general rule, the estimated diffusivity tends to increase with increasing temperature. The only exception to this is in Sample (a) of the 1.0mm thickness. From 1000°C to 1200°C, the average diffusivity of this sample dropped slightly.

The wide variability of diffusivity of the material, due to non-uniformities in the synthesis process, make validation of the effectiveness of Model 5 over Model 1 somewhat more difficult. If all samples were of uniform consistency, samples of different thicknesses could be compared directly in terms of the effect of thickness on estimated diffusivity. The expected condition in this case would be for estimated diffusivity, using Model 1 as a method of analysis, to be lower for the thicker samples.

Table 6-20

CBCF Samples Measured at ORNL 1200°C Using Model 5

Sample	Shot	Diffu-sivity	Biot Number	Pene-tration	Residual Std. Dev.	Confidence Interval
1.0mm(a)	1	0.28165	13.0422	0.0745	0.052076	0.03243
1.0mm(a)	2	0.28562	12.0443	0.07807	0.035693	0.021968
1.0mm(a)	3	0.30796	8.19113	0.07826	0.011215	0.007647
1.0mm(b)	1	0.30035	7.48131	0.07259	0.003057	0.004722
1.0mm(b)	2	0.28436	9.52066	0.07596	0.004114	0.00647
1.0mm(b)	3	0.29242	8.46244	0.07527	0.002463	0.003905
1.2mm(a)	2	0.37543	6.30423	0.07643	0.004664	0.008828
1.2mm(a)	3	DNC				
1.4mm(a)	2	DNC				
1.4mm(a)	3	DNC				
1.7mm(a)	2	0.36277	3.90979	0.18041	0.009311	0.03368
1.7mm(a)	3	0.39764	2.50712	0.18992	0.010711	0.035501

The estimated values would be lower than those estimated for the thin samples but not lower than the values obtained by using Model 5 as the method of analysis. Model 5 produces lower estimated diffusivities because the phenomenon of flash penetration causes the temperature at the x=L surface to rise more quickly than in the non-penetration cases. The Model 1 method interprets this early rise as a higher diffusivity, thereby resulting in an unrealistically high value being reported. Since Model 5 takes flash penetration into account, the reported diffusivity is lower and closer to the true value.

The reason that the thicker samples should theoretically yield lower estimated diffusivity values is that the flash penetration should not penetrate more deeply

into the surface of a thick sample than that of a thin one. As such, the flash penetration in the thick sample represents a smaller fraction of the sample thickness than does the same penetration in the thin sample. The thick sample is therefore less heavily influenced by flash penetration. This should cause a lower diffusivity to be estimated, which is closer to the true value than that rendered by the thin sample experiment. Unfortunately, the high variability of diffusivity from sample to sample precludes the use of this type of validation for the effectiveness of the penetration model.

Without the availability of a direct comparison test between models of varying thicknesses, the primary validation for the effectiveness of Model 5 in these experiments is the reduction in residuals gained by the application of this model. In many of the individual experiments, the standard deviation of the residuals was reduced by a factor of three. In other cases, there was a more modest reduction, but in no case was there a negligible reduction. The 95 percent confidence regions are wider for the Model 5 analysis, but that is due in large part to the fact that there are four parameters to be simultaneously estimated using Model 5 and only three to be estimated using Model 1. The higher number of simultaneous variables makes

Model 5 inherently less stable to some degree. Nevertheless, in terms of modeling, it is a more accurate portrayal of the physical phenomena taking place in the experiment. Another key indication of the success of Model 5 over Model 1 is the consensus of the uniformly lower estimated values of diffusivity for Model 5 versus Model 1.

The parameter estimate for penetration depth is fairly uniform among the thinner samples but increases for the thicker samples, particularly the 1.7mm samples. An important point to make about the penetration depth parameter is that the sensitivity coefficients for this parameter become smaller as the sample becomes thicker. This is due to the increased time required, during the diffusive heat conduction process, for information related to the penetration to reach the temperature measurement surface. As this length of time increases, the accuracy of the flash penetration information transmitted through the temperature rise profile with respect to time, becomes diminished. Due to the L^2 dependency of this transmission time, the thicker samples are at a significant disadvantage in accurately estimating this parameter. The 1.7mm thick specimen, for example, requires a transmission time of 2.89 times that of the 1.0mm sample. This results in a significant amount of accuracy degradation.

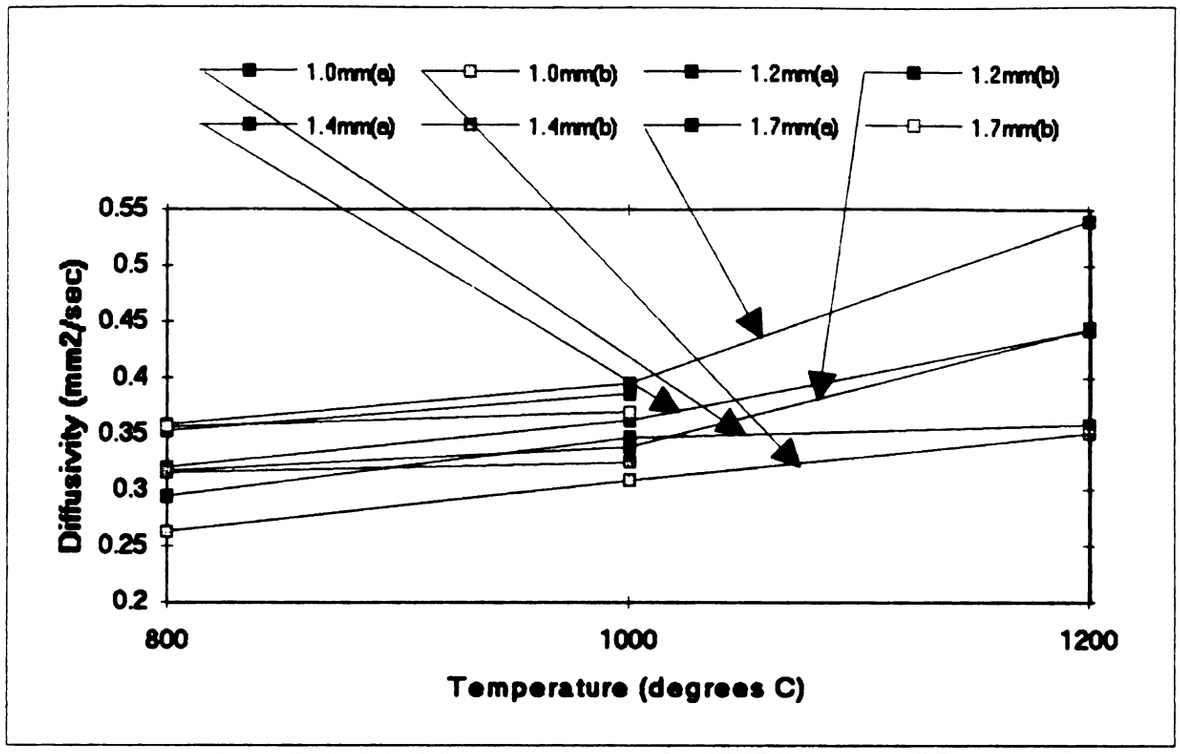

Figure 6-16 Diffusivity vs Temperature for CBCF Samples at ORNL Using Model 1

Another factor which can result in degradation of accuracy in the thicker samples is the added surface area for heat transfer at the edges. As heat loss at the edges becomes more significant, the one-dimensional assumption on which the models are built loses some validity which makes the results less reliable. This is why samples are normally used which are as thin as possible when analyzing the material for parameter estimation. The thicker samples shown here were prepared and tested specifically to investigate the effect of thickness on the flash penetration models.

Figures 6-16 and 6-17 provide a graphical portrayal of

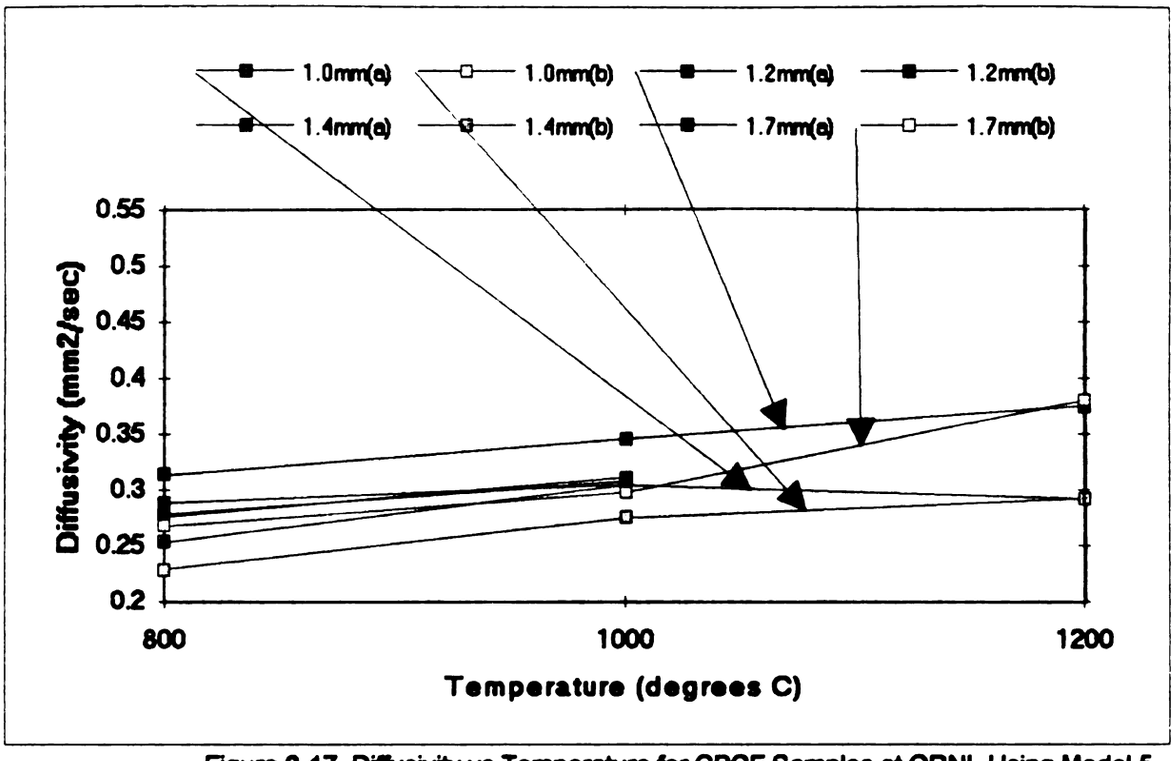

Figure 6-17 Diffusivity vs Temperature for CBCF Samples at ORNL Using Model 5

the estimated diffusivities for the four sample thicknesses using both of the models of analysis. Figure 6-16 provides results from using Model 1 as a method of analysis and Figure 6-17 presents Model 5 results. As shown in the tables, many of the samples did not produce measurements at 1200 degrees for which convergence was obtained when analyzed. Since both figures have the same scale on the vertical axis, the figures provide a visual comparison of the range of the estimated diffusivities using both models. As discussed above, the Model 5 diffusivity values are uniformly lower than those estimated using Model 1. Once again, the general trend of higher diffusivities at higher

temperatures can be clearly seen in the graphs. Another conclusion which is clearly evident in the graphs is the closer agreement between diffusivity values among all samples using Model 5. Accounting for the flash penetration in this model seems to reduce the variance of estimated values between samples, independent of the sample thicknesses. The closer agreement between samples can be taken as another validating factor for Model 5 and the concept of accounting for flash penetration.

CHAPTER 7

SUMMARY AND RECOMMENDATIONS

7.1 SUMMARY

As outlined in Chapter 1, the goals of this research were

1. To determine thermal properties of the materials, specifically thermal diffusivity, from transient temperature measurements.
2. To investigate the possibility of internal radiation as an ancillary means of heat transfer to Fourier conduction and to investigate penetration of the laser flash beyond the surface of the specimen.
3. To investigate non-radiative effects which may have been responsible for systematic disparities between the measured data and the mathematical model.

The common underlying motivation behind each of the above objectives was to develop and utilize a heat transfer model for flash diffusivity experiments which would more accurately conform to the physical phenomenon observed, thereby giving greater confidence in the parameter values reported. The primary means of evaluating the degree of success achieved in this endeavor, was the extent to which reductions were achieved in the residual signatures, evident in previous analyses. These signatures indicated an inadequacy in the models used previously which, in turn,

implied some unreliability in the estimated parameters. Other measurement methods of model adequacy used in the evaluation of the models developed in this research, included a reduction of the standard deviation of the residuals, a reduction of the confidence region, and the reduction in the variation of the sequential estimates.

In the process of achieving these desired goals, this research investigated several areas which have not been examined previously: simultaneous estimation of internal radiation parameters in flash diffusivity measurement experiments, development of a numerical means for stabilizing equations used in extracting radiation heat transfer parameters from experimental data, and modeling of laser flash penetration into the samples. From these new models, the magnitude of the extinction coefficient for the laser flash has been estimated in concert with the other thermal parameters. Even more important is that the analysis of actual laboratory data has given validation to these models and has provided explanations for the inadequacies in previously used models.

The success of the higher order models developed as part of this research has been validated in several ways. Model 5, as presented in Chapter 4, achieved a higher level of agreement between samples when comparing the estimated parameters measured at one temperature. By contrast, the results obtained using the simpler model described in

Chapter 2 produced a wider range of values under the same conditions. The observed reduction in the magnitude of the residuals, the reduction of the residual signature, the reduction of the confidence region, and the reduction in the straying of the sequential estimates, are all validations of the higher order models.

Not all types of materials were found to have benefitted from the use of the additional parameters of the higher order models. Materials which are totally opaque or are coated with a gold film are not susceptible to laser flash penetration. Additionally, flash diffusivity laboratory systems which do not allow laser leakage within the sample enclosure do not benefit from the back-side flash parameter model described in Chapter 4. The samples which benefit the most from the higher order models are those that have permeable or semi-permeable surfaces with respect to the laser flash.

The value of the main parameter of interest, thermal diffusivity, can be sensitive to the type of model used, affecting the magnitude of the estimated value by as much as 20 percent. The results generated by the refined models can be reported with greater confidence, as demonstrated by the improvements noted above, and are therefore more reliable for use in subsequent work with these materials. Since the differences in estimated diffusivity, the parameter of interest, can be significant when accounting for flash

penetration, the results from this research can have an impact on other aspects of engineering. From a design aspect, this ultimately leads to safer and higher performing equipment and products designed using the published estimated parameters obtained using these improved methods.

7.2 RECOMMENDATIONS

For future work in this area, the following recommendations are offered

1. The internal radiation model should be utilized in analyzing experiments performed on samples which actually exhibit combined conduction and internal radiation.
2. Testing should be continued on materials which are subject to surface penetration of flash heating. Testing identical materials at varying thicknesses will provide additional confirmation of the penetration models, since estimated diffusivity for thick samples using Model 1 should approach those of Model 5 for thin samples.
3. The models presented in this research, particularly Model 5, should be incorporated in the software packages provided with flash diffusivity testing equipment.

APPENDIX

DATA FILE (A_R1)

Palaiseau, France

Ambient Temperature: 20°C
Sample Thickness: L=3.0mm
Maximum measured Reading: 856.9746
Anticipated Residual Std Dev: σ=0.7955155
Applied Null Value: 0

Model Nmbr.	Diff. (α)	Heat Flux	Biot Number	β_4	β_5	β_6	Resid. (s)
1	1.2813	2920	.08633				4.811
4	1.1190	3325	.20423	.06850			2.416
5	1.1344	3236	.19432	.26207			1.945
17	1.1673	1057	.16894	.2782	.63479	1.4243	1.0417

	95% Confidence Interval	Correlation Coefficient
1	.005776	.940228
4	.010879	.806608
5	.006361	.709900
17	.006128	.515124

DATA FILE A_R2

Palaiseau, France

Ambient Temperature: 980°C
Sample Thickness: L=3.05mm
Maximum measured Reading: 462.1537
Anticipated Residual Std Dev: σ=.615957
Applied Null Value: 0

Model Nmbr.	Diff. (α)	Heat Flux	Biot Number	β_4	β_5	β_6	Resid. (s)
1	1.23366	1587	.08165				.74589
4	1.22658	1594	.08490	.00344			.73553
5	1.22665	1591	.08487	.06462			.73579
17	1.23182	1521	.08268	.0112	.33750	.19175	.70865

	95% Confidence Interval	Correlation Coefficient
1	.001490	.42142
4	.004653	.458935
5	.004571	.458409
17	.004606	.491917

DATA FILE (C_R1)

West Lafayette, Indiana

Ambient Temperature: 400°C
Sample Thickness: L=1.9685mm
Maximum measured Reading: 2.718663
Anticipated Residual Std Dev: σ=.0047949
Applied Null Value: 0

Model Nmbr.	Diff. (α)	Heat Flux	Biot Number	β_4	β_5	β_6	Resid. (s)
1	.33181	6.388	.12974				.01492
4	.29947	7.019	.21629	.08770			.01032
5	.29932	6.916	.21927	.16159			.00910
17	.31533	3.406	.17602	.10176	.3603	.0033	.00293

95% Confidence Interval	Correlation Coefficient
1 .005376	.947993
4 .013411	.885454
5 .008977	.855693
17 .003420	.558632

DATA FILE (E_R1)

Vandoeuvre les Nancy, France

Ambient Temperature: 20°C
Sample Thickness: L=10.34mm
Maximum measured Reading: -0.0356
Anticipated Residual Std Dev: σ=.00018395
Applied Null Value: -0.1631

Model Nmbr.	Diff. (α)	Heat Flux	Biot Number	β_4	β_5	β_6	Resid. (s)
1	2.13194	1.3764	.02821				.00040
4	2.12487	1.3772	.02849	.02114			.00040
5	2.13169	1.3758	.02807	.07265			.00040
17	2.13074	1.1331	.02819	.03750	.02194	.00004	.00040

95% Confidence Interval	Correlation Coefficient
1 .002399	.585307
4 .002540	.603788
5 .002399	.589470
17 .014275	.911547

DATA FILE (E_R2)

Vandoeuvre les Nancy, France

Ambient Temperature: 20°C
Sample Thickness: L=4.6mm
Maximum measured Reading: 0.3346
Anticipated Residual Std Dev: σ=.0039249
Applied Null Value: -0.3453

Model Nmbr.	Diff. (α)	Heat Flux	Biot Number	β_4	β_5	β_6	Resid. (s)
1	2.08497	3.431	.06287				.00550
4	2.08470	3.431	.06292	.00003			.00550
5	2.08489	3.431	.06290	.00098			.00550
17	Unstable						

95% Confidence Interval	Correlation Coefficient
1 .006296	.962768
4 .006296	.962727
5 .006280	.953760
17 Unstable	

DATA FILE (G_R1)

Bombay India

Ambient Temperature: 1403°C
Sample Thickness: L=1.0872mm
Maximum measured Reading: 496
Anticipated Residual Std Dev: σ=.3709797
Applied Null Value: 222

Model Nmbr.	Diff. (α)	Heat Flux	Biot Number	β_4	β_5	β_6	Resid. (s)
1	11.260	350.0	.10934				2.9527
4	11.260	350.0	.10934	9.76E-10			2.9527
5	11.284	348.6	.10626	.00076			2.9527
17	11.259	321.9	.10934	.00005	.01250	.00025	2.9527

95% Confidence Interval	Correlation Coefficient
1 .008716	.956708
4 .008732	.956708
5 .015172	.593499
17 .013529	.956886

DATA FILE (H_R1)

Trappes, France

Ambient Temperature: 300°C
Sample Thickness: L=3mm
Maximum measured Reading: 3.118764
Anticipated Residual Std Dev: σ=.00786077
Applied Null Value: 0

Model Nmbr.	Diff. (α)	Heat Flux	Biot Number	β_4	β_5	β_6	Resid. (s)
1	14.8448	11.09	.14804				.30019
4	11.2068	13.92	.36753	.01475			.29742
5	12.3922	12.40	.27802	.33994			.29801
17	Unstable						

Model Nmbr.	95% Confidence Interval	Correlation Coefficient
1	.084077	.001804
4	.293294	.002279
5	.198615	.003849
17	Unstable	

DATA FILE (I_R1)

Buenos Aires, Argentina

Ambient Temperature: 20°C
Sample Thickness: L=3.895mm
Maximum measured Reading: 1.85
Anticipated Residual Std Dev: σ=.0178227
Applied Null Value: -2.8656

Model Nmbr.	Diff. (α)	Heat Flux	Biot Number	β_4	β_5	β_6	Resid. (s)
1	3.65094	18.11	.00001				.02405
4	3.57298	18.14	.00001	.01195			.02141
5	3.57561	18.14	.00001	.20357			.02136
17	Unstable						

Model Nmbr.	95% Confidence Interval	Correlation Coefficient
1	.002649	.343374
4	.005880	.169516
5	.005509	.166428
17	Unstable	

DATA FILE (J_R1)

Talence, France

Ambient Temperature: 20°C
Sample Thickness: L=18.05mm
Maximum measured Reading: 167
Anticipated Residual Std Dev: σ=1.043377
Applied Null Value: 0

Model Nmbr.	Diff. (α)	Heat Flux	Biot Number	β_4	β_5	β_6	Resid. (s)
1	.59017	5801	.49238				1.0452
4	.59017	5801	.49237	.00001			1.0452
5	.59057	5787	.48915	.00563			1.0464
17	Unstable						

	95% Confidence Interval	Correlation Coefficient
1	.011383	.896098
4	.011484	.896099
5	.013807	.630977
17	Unstable	

DATA FILE (K_R1)

Belgrade, Yugoslavia

Ambient Temperature: 20°C
Sample Thickness: L=2.48mm
Maximum measured Reading: 27.74
Anticipated Residual Std Dev: σ=.4293872
Applied Null Value: -1.319

Model Nmbr.	Diff. (α)	Heat Flux	Biot Number	β_4	β_5	β_6	Resid. (s)
1	6.46155	75.89	.02915				1.0666
4	6.46109	75.89	.02915	.00001			1.0667
5	6.48789	75.75	.02838	.00035			0.9894
17	Unstable						

	95% Confidence Interval	Correlation Coefficient
1	.029238	.078318
4	.060280	.078370
5	.029554	.080687
17	Unstable	

DATA FILE (L_R1)

Poitiers, France

Ambient Temperature: 20°C
Sample Thickness: L=2mm
Maximum measured Reading: 1.32574
Anticipated Residual Std Dev: σ=.004954192
Applied Null Value: 0

Model Nmbr.	Diff. (α)	Heat Flux	Biot Number	β_4	β_5	β_6	Resid. (s)
1	3.81851	2.826	.04433				.12607
4	3.49869	2.885	.05648	.01103			.12588
5	3.58016	2.856	.05308	.17115			.12591
17	3.96091	1.358	.02624	.00154	1.0000	.00050	.00689

95% Confidence Interval	Correlation Coefficient
1 .074467	.006850
4 .187615	.005592
5 .162719	.006211
17 .006300	.335489

DATA FILE (M_R1)

Hunan, China

Ambient Temperature: 23°C
Sample Thickness: L=2.55mm
Maximum measured Reading: 3048
Anticipated Residual Std Dev: σ=5.4985
Applied Null Value: 0

Model Nmbr.	Diff. (α)	Heat Flux	Biot Number	β_4	β_5	β_6	Resid. (s)
1	20.307	8596	.06568				17.732
4	19.654	8788	.08269	.00087			17.094
5	19.487	8800	.08762	.14639			16.859
17	19.927	3423	.07764	.00420	1.000	2210	7.255

95% Confidence Interval	Correlation Coefficient
1 .005280	.847107
4 .015978	.831695
5 .014074	.825329
17 .003583	.899414

DATA FILE (N_R1)

Stuttgart, Germany

Ambient Temperature: 366°C
Sample Thickness: L=1.86mm
Maximum measured Reading: 8.046875
Anticipated Residual Std Dev: σ=.0079494
Applied Null Value: 1.1152338

Model Nmbr.	Diff. (α)	Heat Flux	Biot Number	β_4	β_5	β_6	Resid. (s)
1	79.7225	17.58	.28631				.04862
4	79.7214	17.58	.28633	.00001			.04862
5	79.7793	17.54	.28443	.00500			.04887
17	Unstable						

95% Confidence Interval	Correlation Coefficient
1 .008504	.939483
4 .009221	.939475
5 .013585	.644702
17 Unstable	

DATA FILE (O_R1)

Le Barp, France

Ambient Temperature: 20°C
Sample Thickness: L=9.85mm
Maximum measured Reading: 0.63672
Anticipated Residual Std Dev: σ=.00514629
Applied Null Value: 0

Model Nmbr.	Diff. (α)	Heat Flux	Biot Number	β_4	β_5	β_6	Resid. (s)
1	71.8983	6.182	.00001				.00476
4	71.8947	6.183	.00001	.00001			.00476
5	71.9000	6.183	.00001	.02500			.00476
17	71.8942	6.276	.00001	.01055	.00006	.00475	.00476

95% Confidence Interval	Correlation Coefficient
1 .003925	.314520
4 .012128	.316054
5 .010506	.028702
17 .008678	.323732

DATA FILE (Q_R1)

Manchester, United Kingdom

Ambient Temperature: 327°C
Sample Thickness: L=3.24mm
Maximum measured Reading: 2156.688
Anticipated Residual Std Dev: σ=15.11283
Applied Null Value: 557.8

Model Nmbr.	Diff. (α)	Heat Flux	Biot Number	β_4	β_5	β_6	Resid. (s)
1	12.248	5102	.00767				22.909
4	10.571	5466	.05176	.01313			18.798
5	10.639	5430	.05113	.36818			17.939
17	11.093	1647	.03781	.27186	1.0000	12.253	16.155

	95% Confidence Interval	Correlation Coefficient
1	.012323	.492996
4	.029308	.247158
5	.021646	.182597
17	.022393	.078951

DATA FILE (S_R1)

Ardmore, Pennsylvania

Ambient Temperature: Unknown
Sample Thickness: L=2.9mm
Maximum measured Reading: 6.39961
Anticipated Residual Std Dev: σ=0.1028782
Applied Null Value: 0

Model Nmbr.	Diff. (α)	Heat Flux	Biot Number	β_4	β_5	β_6	Resid. (s)
1	3.50009	45.05	1.0234				.90882
4	2.43694	79.74	2.1573	.05063			.89569
5	2.24625	79.63	2.8976	.36752			.89200
17	2.23109	27.72	2.9401	.37014	1.00000	.00000	.89200

	95% Confidence Interval	Correlation Coefficient
1	.196966	.008036
4	1.04830	.016209
5	.490873	.017972
17	.500564	.017879

CBCF DATA (Holometrix)

Oak Ridge, Tennessee

Ambient Temperature: 100°C
Sample Thickness: L=1.0mm
Maximum measured Reading: 3.4817
Anticipated Residual Std Dev: 0.002629
Applied Null Value: 0

Model Nmbr.	Diff. (α)	Heat Flux	Biot Number	β_4	β_5	β_6	Resid. (s)
1	.32426	4.231	.14654				.01726
4	.29172	4.627	.22840	.02521			.00609
5	.29514	4.508	.22029	.08099			.00495
17	.29772	4.488	.21352	.08200	.85912	.00271	.00414

	95% Confidence Interval	Correlation Coefficient
1	.00457	.959097
4	.00556	.794955
5	.003523	.688726
17	.005083	.690548

CBCF DATA (Holometrix)

Oak Ridge, Tennessee

Ambient Temperature: 400°C
Sample Thickness: L=0.96mm
Maximum measured Reading: 7.762737
Anticipated Residual Std Dev: 0.005604
Applied Null Value: 0

Model Nmbr.	Diff. (α)	Heat Flux	Biot Number	β_4	β_5	β_6	Resid. (s)
1	.31351	13.45	.53483				.03657
4	.28644	14.77	.65473	.02034			.01694
5	.28858	14.01	.64592	.07311			.01485
17	.29210	13.92	.62951	.06521	1.0000	.01561	.00419

	95% Confidence Interval	Correlation Coefficient
1	.003946	.934237
4	.006498	.751121
5	.004486	.672286
17	.001371	.289023

CBCF DATA (Holometrix)

Oak Ridge, Tennessee

Ambient Temperature: 500°C
Sample Thickness: L=1.0mm
Maximum measured Reading: 9.217506
Anticipated Residual Std Dev: 0.007871
Applied Null Value: 0

Model Nmbr.	Diff. (α)	Heat Flux	Biot Number	β_4	β_5	β_6	Resid. (s)
1	.31217	18.52	.73590				.04472
4	.28552	20.47	.88173	.01950			.02274
5	.28757	19.14	.87119	.07156			.02040
17	.29142	19.01	.84896	.06304	1.000	.02182	.00629

	95% Confidence Interval	Correlation Coefficient
1	.003949	.910976
4	.007236	.703975
5	.005090	.627923
17	.001694	.059215

CBCF DATA (Holometrix)

Oak Ridge, Tennessee

Ambient Temperature: 600°C
Sample Thickness: L=0.96mm
Maximum measured Reading: 8.549782
Anticipated Residual Std Dev: 0.007031
Applied Null Value: 0

Model Nmbr.	Diff. (α)	Heat Flux	Biot Number	β_4	β_5	β_6	Resid. (s)
1	.30868	18.02	.86752				.04093
4	.27930	20.50	1.07002	.01872			.01946
5	.28255	18.83	1.04763	.06800			.01790
17	.28620	19.46	1.02083	.06103	1.000	.01746	.00723

	95% Confidence Interval	Correlation Coefficient
1	.004041	.904892
4	.007416	.642220
5	.005177	.572979
17	.002255	.092708

CBCF DATA (Holometrix)

Oak Ridge, Tennessee

Ambient Temperature: 700°C
Sample Thickness: L=.956mm
Maximum measured Reading: 6.8258
Anticipated Residual Std Dev: 0.0091074
Applied Null Value: 0

Model Nmbr.	Diff. (α)	Heat Flux	Biot Number	β_4	β_5	β_6	Resid. (s)
1	.31136	17.85	1.23326				.03697
4	.27615	21.29	1.56101	.02107			.01250
5	.28193	18.64	1.50312	.06964			.01244
17	.28364	19.42	1.48574	.06681	1.00000	.00751	.01074

	95% Confidence Interval	Correlation Coefficient
1	.004431	.908390
4	.005980	.364464
5	.004338	.367844
17	.004025	.329394

REFERENCES

REFERENCES

[1] R. Siegel and J. Howell, Thermal Radiation Heat Transfer, Hemisphere Publishing Corp., New York (1981).

[2] A. Hazzah, Transient Heat Transfer by Simultaneous Conduction and Radiation in Absorbing, Emitting and Scattering Medium, Ph.D. Dissertation, Michigan State University (1968).

[3] W. Minkowycz, E. Sparrow, G. Schneider and R. Pletcher, Handbook of Numerical Heat Transfer, Wiley, New York, (1988).

[4] A. Hazzah and J. Beck, Unsteady Combined Conduction-Radiation Energy Transfer Using a Rigorous Differential Method, International Journal of Heat and Mass Transfer, Pergamon Press, (1970).

[5] A. Tuntomo and C.Tien, Transient Heat Transfer in a Conducting Particle With Internal Radiant Absorption, Journal of Heat Transfer, ASME, (1992).

[6] A. Helte, Radiative and Conductive Heat Transfer in Pourous Media: Estimation of the Effective Thermal Conductivity, Journal of Applied Physics, American Institute of Physics, (1993).

[7] P. Jones and Y. Bayazitoglu, Radiation, Conduction and Convection From a Sphere in an Absorbing, Emitting, Gray Medium, Journal of Heat Transfer, ASME, (1992).

[8] M. Brewster, Thermal Radiative Transfer and Properties,

Wiley, New York, (1992).

[9] E. Sparrow and R. Cess, Radiation Heat Transfer, Hemisphere, New York, (1978).

[10] M. Modest, Radiative Heat Transfer, McGraw-Hill, New York, (1993).

[11] D. Schwander, G. Flamant and G. Olalde, Effects of Boundary Properties on Transient Temperature Distributions in Condensed Semi-Transparent Media, International Journal of Heat And Mass Transfer, (1990).

[12] M. Naraghi and C. Saltiel, Combined Mode Heat Transfer in Radiatively Participating Media: Computational Considerations, ASME Heat Transfer Division, (1990).

[13] H. Chu and T. Chen, Transient Conduction and Radiation Heat Transfer in Ultra-Fine Powder Insulation, Hemisphere, New York, (1991).

[14] M. Goldstein and J. Howell, Boundary Conditions for the Diffusion Solution of Coupled Conduction-Radiation Problems, NASA TN D-4618, (1968).

[15] J. Beck, B. Blackwell, C. St Clair, Inverse Heat Conduction - Ill Posed Problems, Wiley, New York, (1985).

[16] J. Novotny and K. Yang, The Interaction of Thermal Radiation in Optically Thick Boundary Layers, ASME 67-HT-9, (1967).

[17] R. Edwards and R. Bobco, Radiant Heat Transfer From Isothermal Dispersions With Isotropic Scattering, ASME 67-HT-8, (1967).

[18] W. Dalzell and A. Sarofim, Optical Constants of Soot and Their Application to Heat Flux Calculations, ASME 68-HT-13, (1968).

[19] J. Schornhorst and R. Viscanta, An Experimental Examination of the Validity of the Commonly Used Methods of Heat Transfer Analysis, ASME 68-HT-42, (1968).

[20] A Sarofim, I. Vasalos and A. Jeje, Experimental and Theoretical Study of Absorption in an Anisotropically Scattering Medium, ASME 71-HT-20, (1972).

[21] R. Bobco, Directional Emissivities From a Two Dimensional Absorbing Scattering Medium: The Semi-Infinite Slab, ASME 67-HT-12, (1967).

[22] L. Matthews, R. Viscanta, and F. Incropera, Development of Inverse Methods for Determining Thermophysical and Radiative Properties of High-Temperature Fibrous Materials, International Journal of Heat and Mass Transfer, (1984).

[23] A. Neto and M. Ozisik, An Inverse Analysis of Simultaneously Estimating Phase Function, Albedo and Optical Thickness, Developments in Radiative Heat Transfer, ASME, (1992).

[24] G. Forsyth and W. Wasow, Finite Difference Methods for Partial Differential Equations, Wiley, New York, (1960).

[25] J. Beck and K. Arnold, Parameter Estimation, Wiley, New York, (1977).

[26] S. Conte and C. de Boor, Elementary Numerical Analysis, McGraw-Hill, New York, (1980).

[27] D. Murio, The Mollification Method and the Numerical Solution of Ill posed Problems, Wiley-Interscience, New York, (1993).

[28] S. Chandrasekhar, Radiative Transfer, Dover Publications, New York, (1960).

[29] N. Ruperti, M. Raynaud and J.Sacadura, The Method for the Solution of the Coupled Inverse Heat Conduction-Radiation Problem, ASME Journal of Heat Transfer, Vol 118, (1996).

[30] U. Koylu and G. Faeth, Spectral Extinction Coefficients of Soot Aggregates From Turbulent Diffusion Flames, ASME Journal of Heat Transfer, Vol 118, (1996).

[31] T. Hendricks and J. Howell, Absorption/Scattering Coefficients and Scattering Phase Functions in Reticulated Porous Ceramics, ASME Journal of Heat Transfer, Vol 118, (1996).

[32] T. Ito and S. Fujimura, Simultaneous Measurement of Temperature and Absorption of Distributed Medium by Using Infrared Emmission CT, IEEE Transactions on Instrumentation and Measurement, Vol 44 No 3 (1995).

[33] J. Longtin, T Qiu, and C. Tien, Pulsed Laser Heating of Highly Absorbing Particles, ASME Journal of Heat Transfer, Vol 117, (1995).

[34] Y. Sakamoto, M. Ishiguro and G. Ktagawa, Akaike Information Criterion Statistics, Reidel Publishing, Tokyo, (1986).

[35] J. Beck and A. Osman, Sequential Estimation of Temperature-Dependent Thermal Properties, High Temperatures-High Pressures, Vol 23, (1991).

[36] O. Hahn, F. Raether, M. Arduini-Schuster, and J. Fricke Transient Coupled Conductive/Radiative Heat Transfer in Absorbing, emitting and Scattering Media: Application to Laser Flash Methods on Ceramic Materials, International Journal of Heat and Mass Transfer, Vol 40 No 3, (1996).

[37] J. Beck and R. Dinwiddie, Parameter Estimation Method for Flash Thermal Diffusivity with Two Different Heat Transfer Coefficients, Proceedings from 23rd Thermal Conductivity Conference, Technomic Publishing, Lancaster, Pa. (1996).

[38] Y. Gu, D. Zhu, L. Zhu, J.Ye, Thermal Diffusivity Measurement of Thin Films by the Periodic Heat Flow Method with Laser Heating, High Temperatures-High Pressures, Vol 25, (1993).

[39] P. Boulet, G.Jeandel, P. De Dianous and F. Pincemin, Combined Radiation and Conduction in Fiberous Insulation, Proceedings from 23rd Thermal Conductivity Conference, Technomic Publishing, Lancaster, Pa. (1996).

[40] American Society for Testing and Materials, Standard Test Method for Thermal Diffusivity of Solids by the Flash Method,
E 1461-92 ASTM Committe on Standards, Philadelphia, Pa. (1992).

[41] H. Wang, R. Dinwiddie and P. Gaal, Multiple Station Thermal Diffusivity Instrument, Proceedings from 23rd Thermal Conductivity Conference pp 120-125, Technomic Publishing, Lancaster, Pa. (1996).

[42] J. Koski, Improved Data Reduction Methods for Laser Pulse Diffusivity Determination with the use of Minicomputers, National Technical Information Service, Springfield Va.(1981).

[43] R. Cowan, Pulse Method of Measuring Thermal Diffusivity at High Temperature, Journal of Applied Physics, Vol. 34, No. 4, pp. 926-927, (1963).

[44] L. Clark, R. Taylor, Radiation Loss in the Flash Method for Thermal Difusivity, Journal of Applied Physics, Vol. 26, No .2, pp. 714-719, (1975).

[45] C. Strodtman, A Design Optimization Technique Applied to a Squeeze Film Gas Journal Bearing, Ph.D. Dissertation, Michigan State University, (1968).

[46] W. Parker, Jenkins, C. Butler and G. Abbott, Flash Method of Determining Thermal Diffusivity, Heat Capacity and Thermal Conductivity, Journal of Applied Physics, vol. 32(9), 1679-1684, (1961).

[47] R. Taylor, Heat Pulse Thermal Diffusivity Measurements, High Temperatures - High Pressures, vol. 11, pp. 43-58, (1979).

[48] M. Raynaud, J. Beck, R. Shoemaker and R. Taylor, Sequential Estimation of Thermal Diffusivity for Flash

Tests, Proceedings from 20th Thermal Conductivity Conference pp 305-321, Plenum Publishing, (1989).

[49] C. Lin, C. Hwang, and Y. Chang, The Unsteady Solutions of a Unified Heat Conduction Equation, International Journal of Heat and Mass Transfer, Vol. 40, No. 7, pp. 1716-1719, (1997).

[50] L. Vozar and T. Sramkova, Two Data Reduction Methods for Evaluation of Thermal Diffusivity from Step-Heating Measurements, International Journal of Heat and Mass Transfer, Vol. 40, No. 7, pp. 1647-1655, (1997).

[51] J. Beck, K. Cole, A. Haji-Sheikh, and B. Litkouhi, Heat Conduction Using Green's Functions, Hemisphere Publishing, Washington D.C., (1992).

[52] S. Andre and A. Degiovanni, Experimental Measurements of the Phonic Diffusivity of Semi-Transparent Materials up to 800K, Glastechnische Berichte, Vol. 66, No. 11, pp. 291-298, (1993).

[53] H. Ohta, M. Masuda, K. Watanabe, K. Nakajima, H. Shibata, and Y. Waseda, Determination of Thermal Diffusivities of Continuous Casting Powders for Steel by Precicely Excluding the Contribution of the Radiative Component at High Temperature, Journal of the Iron and Steel Institute of Japan, Vol 80, No. 6, pp. 33-38, (1994).

[54] C. Moreau, P. Fargier-Richard, R. St. Jacques, G. Robert, and P.Cielo, Thermal Diffusivity of Plasma Sprayed Tungsten Coatings, Surface and Coatings Technology, Vol. 61,

No. 1-3, Part 1, pp. 67-71, Dec (1993).

[55] K. Yamamoto, T. Hirosawa, K. Yoshikawa, K. Morozumi, ans S. Nomura, Melting Temperature and Thermal Conductivity of Irradiated Mixed Oxide Fuel, Journal of Nuclear Materials, Vol. 204, pp. 85-92, (1993).

[56] R. Bailey, F. Cruickshank, P. Kerkoc, D. Pugh and J. Sherwood, Thermal Conductivity of the Molecular Crystal (-)2-(alpha-methylbenzylamino)-5-Nitropyridine, Journal of Applied Physics, Vol. 74, Part 5, pp. 3047-3051, (1993).

[57] L. Kehoe, P. Kelly, G. O'Connor, M. O'Reilly and G. Crean, A Methodology for Laser-Based Thermal Diffusivity Measurenment of Advanced Multi-Chip Module Ceramic Materials, IEEE Transactions on Components, Packaging and Manufacturing Technology, Part A, Vol. 18, No. 4, December, (1995).

[58] H. Maleki and L. Holland, Thermal Diffusivity Measurement of Near-Pseudobinary HgCdTe Solid and Melt, Te-Rich HgCdTe and HgZnTe melts and Pure Te Solid and Melt by the Laser Flash Technique, Journal of Applied Physics, Vol. 76, Part 7, October (1994).

[59] R. Heckman, Error Analysis of the Flash Thermal Diffusivity Technique, Proceedings of the 14th Thermal Conductivity Conference, pp. 491-498, Plenum Publishing, New York, (1974).

[60] R. Taylor, T. Lee and A. Donaldson, Determination of Thermal Physical Properties of Layered Composites by the

Flash Method, Proceedings of the 15th Thermal Conductivity Conference, pp. 135-148, Plenum Publishing, New York, (1978).

[61] M. Yovanovich, Simple Explicit Expressions for Calculation of the Heisler-Grober Charts, Proceedings of the 1996 Heat Transfer Conference, American Institute of Aeronautics and Astronautics 96-3968, Reston Va., (1996).

[62] G. Golub, Matrix Computations, Johns Hopkins University Press, Baltimore Md, (1989).

[63] J. Beck, Sensitivity Coefficients Utilized in Non-Linear Estimation with Small Parameters in a Heat Transfer Problem, Jornal of Basic Engineering, (1970).